Hamburger Geophysikalische Einzelschriften

Herausgegeben von den Geophysikalischen Instituten der Universität Hamburg
und dem Max-Planck-Institut für Meteorologie
(Fachgebiete: Meteorologie, Ozeanographie, Physik des Erdkörpers)

Reihe A: Wissenschaftliche Abhandlungen

Heft 52

A symmetrical method of computing the nonlinear transfer in a gravity wave spectrum

Part I: Method
Part II: Results
Part III: Parameterization

von

S. Hasselmann
K. Hasselmann

Hamburg 1981

G. M. L. WITTENBORN SÖHNE
2000 HAMBURG 13

Preis 36,— DM

Aus dem MAX-PLANCK-INSTITUT für METEOROLOGIE, Hamburg

Hamburger Geophysikalische Einzelschriften

Herausgegeben von den Geophysikalischen Instituten der Universität Hamburg
und dem Max-Planck-Institut für Meteorologie
(Fachgebiete: Meteorologie, Ozeanographie, Physik des Erdkörpers)

Reihe A: Wissenschaftliche Abhandlungen

Heft 52

A symmetrical method of computing the nonlinear transfer in a gravity wave spectrum

Part I: Method
Part II: Results
Part III: Parameterization

von

S. Hasselmann
K. Hasselmann

Hamburg 1981

G. M. L. WITTENBORN SÖHNE
2000 HAMBURG 13

Preis 36,— DM

Contents

Part I : Method

1. Introduction

The principal goal of the first part of this investigation is to develop a fast, accurate method for integrating the Boltzmann integral expression

$$\frac{\partial n_4}{\partial t} = \int \sigma \delta(\underline{k}_1 + \underline{k}_2 - \underline{k}_3 - \underline{k}_4)\, \delta(\omega_1 + \omega_2 - \omega_3 - \omega_4) \cdot \left[n_1 n_2 (n_3 + n_4) - n_3 n_4 (n_1 + n_2) \right] d\underline{k}_1\, d\underline{k}_2\, d\underline{k}_3 \qquad (1.1)$$

representing the energy transfer within a surface gravity-wave spectrum due to resonant third-order interactions (Hasselmann, 1962). It is known that this process plays a key role in controlling the evolution of a wind sea (Hasselmann et al., 1975, Mitsuyasu, 1968, 1969, Hasselmann et al., 1976). In equation (1.1) $n(\underline{k}_j) = F(\underline{k}_j)/\omega_j$ represents the action (number) density, where $F(\underline{k}_j)$ is the two dimensional variance spectrum of the surface displacement at the interacting wavenumber $\underline{k}_j$, and ω_j is the wave frequency. The term σ represents a scattering cross section proportional to the square of a (rather complex) interaction coefficient (Hasselmann, 1962, 1963a).

Equation (1.1) has been integrated numerically by several workers using standard integration techniques (Hasselmann, 1963b, Cartwright, 1966, unpublished, Sell and Hasselmann, 1972, Webb, 1978). The δ-functions were eliminated by projection on to the three dimensional resonance subspace of the (formally) six dimensional integral. The integrable singularities which arise along the caustics of the resonance surfaces are normally removed by using stretched coordinates.

Because of the extensive computing time required in the past to evaluate (1.1), various approximations

of (1.1) for narrow-peak spectra have also been considered (Longuet-Higgins, 1976, Fox, 1976, Herterich and Hasselmann, 1980, Dungey and Hui (1980)). These reproduce many of the qualitative features of the exact expression, but are nevertheless not sufficiently good approximations for typical wind sea spectra to be applied in detailed quantitative investigations of the spectral energy balance. An accurate, fast technique for computing (1.1) thus remains an important requirement for systematic studies of the nonlinear transfer in a gravity wave spectrum.

In Sell and Hasselmann (1972), it was pointed out that the integration of (1.1) could be simplified by making use of the properties of detailed balance of the scattering process. If the change in energy of a wave component $\underline{k}_4$ (in the left-hand side of (1.1)) due to the interaction with three other components $\underline{k}_1$, $\underline{k}_2$, and $\underline{k}_3$ (represented by the integrand in the right-hand side of (1.1)) has been computed, application of the principle of detailed balance yields also the simultaneous change in the energy of the other components $\underline{k}_1$, $\underline{k}_2$, and $\underline{k}_3$, without additional computations. This property was only partially exploited by Sell and Hasselmann: the basic integration was still carried out in terms of the three wavenumbers $\underline{k}_1$, $\underline{k}_2$, and $\underline{k}_3$ for given $\underline{k}_4$, the principle of detailed balance being used only to obtain two additional estimates of the integral by suitable wavenumber permutations. Although the mean of all three estimates yielded a more accurate result than any of the individual estimates, the second two estimates obtained in this manner turned out to be less reliable than the original estimate. This shortcoming was due essentially to an asymmetrical treatment of the four components $\underline{k}_1$, $\underline{k}_2$, $\underline{k}_3$, and $\underline{k}_4$ involved in an elementary interaction.

The approach used here makes full use of the principal of

detailed balance by introducing symmetrical variables at the outset. A further advantage of this approach is that it enables the straightforward exploitation of additional symmetry properties of the integrand.

A technical feature of the present approach which yields a further significant saving in computing time for a series of case studies is the separation of the computation of the integration grid and scattering cross-sections from the actual integration of the transfer rate for a given spectrum. Apart from avoiding repeated calculations, this enables unimportant regions of the interaction grid to be filtered out empirically.

The final reduction in computing time of the present scattering calculations relative to previous computations is estimated to be of the order of a factor 30 - 100. This makes it feasible to carry out systematic investigations of the energy balance of a surface-wave spectrum under various conditions of evolution and decay, to develop simplified parametrical expressions for the transfer rate, or even to integrate the basic radiative transport equation for certain idealized situations using the exact expression for the nonlinear energy transfer (cf. parts II and III).

Another new aspect of the present work is the consideration of finite depth effects. It is found that the nonlinear energy-transfer rate is enhanced considerably when the wavenumber-depth product becomes of order unity (wavelength-to-depth ratios of the order 6). The exact computations for finite depth waves presented here agree fairly well with the transformation rules relating the nonlinear transfer to deep-water and finite-depth waves proposed by Herterich and Hasselmann (1980). The generalization of the transformation rules for narrow-peak spectra to typical wind-sea, in particular the preservation of the frequency distribution of the

nonlinear transfer, suggests that the inclusion of the finite-depth effects in the parameterization of the non-linear transfer in wave prediction models should present no basic difficulty.

In the following sections the various steps involved in a symmetrical treatment of the scattering integral are outlined in more detail. The results of the computations and the derivation of parameterizations for use in wave prediction models are then discussed in Parts II and III.

2. Symmetrical representation of the scattering integral using the principle of detailed balance.

Instead of considering the asymmetrical integral expression (1.1), which represents the change in energy of a fixed wave component $\underline{k}_4$ due to all resonant interactions involving three other wave components $\underline{k}_1$, $\underline{k}_2$, and $\underline{k}_3$, it is more convenient for the present purpose to chose as starting point the symmetrical representation of an elementary four-wave-component interaction.

According to the rules for the wave-particle analogy (cf. Hasselmann, 1966) one may regard the resonant interaction between four wave components as the sum of four "collision" processes between wave "pakets" or particles (Fig. 1). The probability of a collision, expressed in terms of a probability density in the 8-dimensional wavenumber phase space of the four interacting wave components, is given by

$$\left.\begin{array}{ll} \text{(i):} & n_1 n_2 n_3 \\ \text{(ii):} & n_1 n_2 n_4 \\ \text{(iii):} & n_1 n_3 n_4 \\ \text{(iv):} & n_2 n_3 n_4 \end{array}\right\} \frac{\sigma}{4}\delta(\underline{k}_1+\underline{k}_2-\underline{k}_3-\underline{k}_4)\,\delta(\omega_1+\omega_2-\omega_3-\omega_4)\,d\underline{k}_1\,d\underline{k}_2\,d\underline{k}_3\,d\underline{k}_4 \qquad (2.1)$$

with the same collision cross-section σ for all four processes (principle of detailed balance). In each collision the three ingoing particles or antiparticles are annihilated, and an outgoing particle is created. "Antiparticles" are denoted by cross bars in Fig. 1 and are associated with negative energy, momentum and number density n. The annihilation of an antiparticle is thus equivalent to the creation of a particle. (Note that the particularly simple rules given here for interpreting classical wave-wave interaction processes in a particle picture differ in some important details from the particle interpretation of quantum field theory - cf. Hasselmann, 1966). Applying these rules, the sum of the four collision processes of Fig. 1 produces a change Δn in the particle number (i.e. wave action) density, per unit time, which is the same, except for a sign, for each of the four wavenumbers involved in the interaction,

$$\left.\begin{array}{l}\Delta n_1 \\ \Delta n_2 \\ \Delta n_3 \\ \Delta n_4\end{array}\right\} = \left.\begin{array}{r}-1 \\ -1 \\ +1 \\ +1\end{array}\right\} \cdot dW \qquad (2.2)$$

where $$dW = \tilde{\sigma} \cdot \frac{P}{4} \cdot d\underline{k}_1 \cdot d\underline{k}_2 \cdot d\underline{k}_3 \cdot d\underline{k}_4 \qquad (2.3)$$

and $$\tilde{\sigma} = \sigma \delta(\underline{k}_1 + \underline{k}_2 - \underline{k}_3 - \underline{k}_4)\, \delta(\omega_1 + \omega_2 - \omega_3 - \omega_4) \qquad (2.4)$$

$$P = n_1 n_2 (n_3 + n_4) - n_3 n_4 (n_1 + n_2) \qquad (2.5)$$

The integral (1.1) follows from (2.2) - (2.5) by integrating equation (2.2) under the side condition that one of the four wavenumbers is fixed. (A factor 1/4 arises in (2.1) because each of the four interacting wavenumbers can be chosen in turn as the fixed wavenumber). However, if one simply

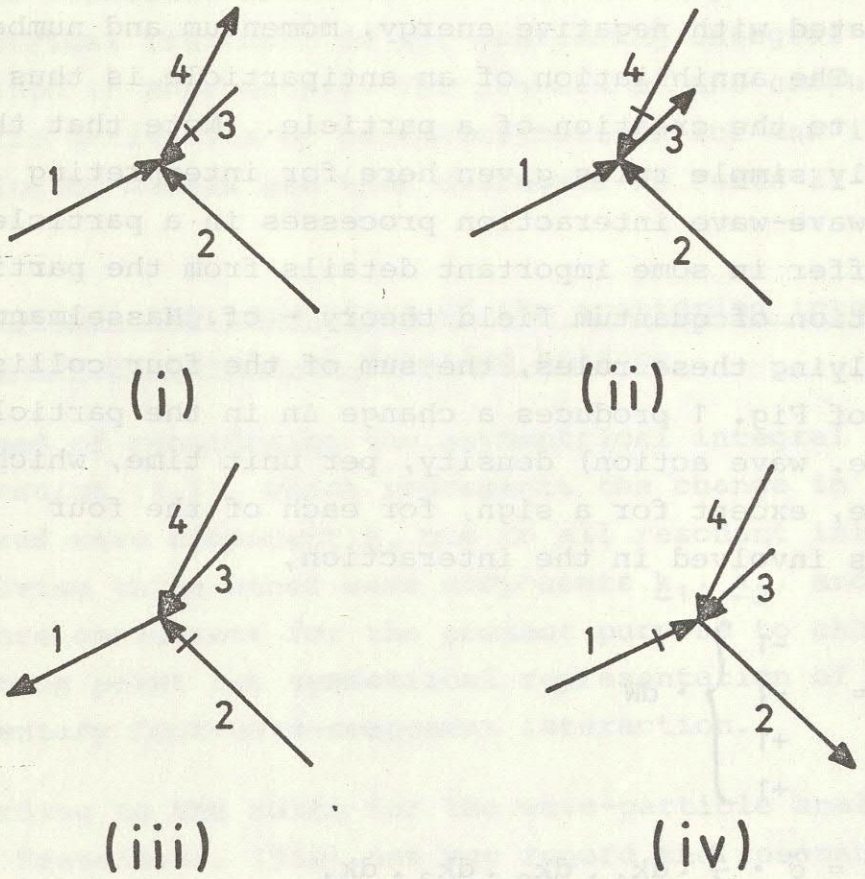

Fig. 1 Elementary collision processes in a particle picture corresponding to third order resonant wave-wave interactions. Antiparticles are denoted by cross bars.

integrates (1.1) one makes no use of the fact that the same elementary process which determines the change of the spectrum at the wavenumber $\underline{k}_4$ also determines the change of the spectrum at the remaining three wavenumbers of the interaction.

To exploit this additional information, the expression (2.2) may be integrated over the full phase space dW of all possible interactions. During the integration, one then keeps track of the change in the wavenumber density occurring not only at the wavenumber $\underline{k}_4$, say, but also at the associated wavenumbers $\underline{k}_1$, $\underline{k}_2$ and $\underline{k}_3$. Basically, the number of integrations involved must of course be the same in either method. Equation (1.1) represents a three-dimensional integral, which has to be computed for a two-dimensional array of wavenumbers $\underline{k}_4$, whereas dW represents a five-dimensional differential expression (allowing for the δ-functions in $\tilde{\sigma}$). However, the form (2.2) - (2.5) makes four-fold use of the calculation of each interaction and is also more convenient for exploiting the various symmetry properties of the interaction. It is shown in the following section that this reduces the effective phase space required for the integration of dW by a factor of 8 (or 16, for the cross-section calculations). A valuable additional feature of the symmetrical integration technique is that it automatically conserves energy, momentum and action, as these quantities are already conserved in the elementary collision processes (cf. (2.2)).

3. Transformation of variables

Because of the presence of the frequency δ-function in $\tilde{\sigma}$ it is not convenient to carry out the integration of dW with respect to the original wavenumbers $\underline{k}_1$, $\underline{k}_2$, $\underline{k}_3$, $\underline{k}_4$. Instead, the following variables were used:

$$
\begin{aligned}
\lambda_1 &= \omega_1 \\
\lambda_2 &= \omega_3 \\
\lambda_3 \equiv \hat{\omega} &= \omega_1 + \omega_2 \\
\lambda_4 \equiv \omega_s &= \omega_1 + \omega_2 - \omega_3 - \omega_4 \\
\lambda_5 \equiv \hat{k} &= |\underline{k}_1 + \underline{k}_2| = \{(k_1 \cos\alpha_1 + k_2 \cos\alpha_2)^2 + (k_1 \sin\alpha_1 + k_2 \sin\alpha_2)^2\}^{1/2} \\
\lambda_6 \equiv \hat{\alpha} &= \cos^{-1}\left\{ \frac{k_1 \cos\alpha_1 + k_2 \cos\alpha_2}{\hat{k}} \right\} \\
\left.\begin{matrix}\lambda_7 \\ \lambda_8\end{matrix}\right\} &\equiv \underline{k}_s = \underline{k}_1 + \underline{k}_2 - \underline{k}_3 - \underline{k}_4
\end{aligned}
\tag{3.1}
$$

Here (k_j, α_j) and $(\hat{k}, \hat{\alpha})$ represent the polar coordinates of the wavenumber vectors $\underline{k}_j$ and $\underline{\hat{k}} = \underline{k}_1 + \underline{k}_2$.

It is simpler to relate the new variables $\lambda_1, \ldots \lambda_8$ to the frequency and direction variables ω_j, α_j of the interacting components than to the wavenumber vectors $\underline{k}_j$. The Jacobian for the transformation from $\underline{k}$ to (ω, α) is $\left|\frac{\partial \underline{k}}{\partial(\omega,\alpha)}\right| = \frac{k}{v}$, where $v = \frac{d\omega}{dk}$ is the group velocity. The Jacobian for the further transformation from the variables (ω,α) to the variable set $\lambda_1, \ldots \lambda_8$ is readily computed from the (almost triangular) transformation matrix. One obtains finally

$$
\left|\frac{\partial(\underline{k}_1, \underline{k}_2, \underline{k}_3, \partial\underline{k}_4)}{\partial(\lambda_1, \ldots \lambda_8)}\right| = \hat{k}(v_1 . v_2 . v_3 . v_4 . k_1 . k_2 . k_3 . k_4 . \sin(\alpha_2 - \alpha_1)\sin(\alpha_4 - \alpha_3))^{-1} \tag{3.2}
$$

where v_j denotes the group velocity at the wavenumber $\underline{k}_j$.

Substituting the variables $\lambda_1, \ldots \lambda_8$ into equations (2.2) - (2.5) the two δ-functions are immediately eliminated upon integration with respect to ω_s $(= \lambda_4)$ and $\underline{k}_s$ $(= \lambda_7, \lambda_8)$.

The remaining integrations can be further simplified by replacing the integration variables ω_1 $(= \lambda_1)$ and ω_3 $(= \lambda_2)$ by the angles $\tilde{\alpha}_1$ and $\tilde{\alpha}_3$ subtended by the wavenumbers $\underline{k}_1$, $\underline{k}_3$ relative to the wavenumber $\hat{\underline{k}}$ (cf. Fig. 2). This avoids caustic-type singularities arising from the elimination of the frequency δ-function. For fixed $\hat{\underline{k}}$ and $\hat{\omega}$, the angles $\tilde{\alpha}_1$ and $\tilde{\alpha}_3$ are determined through the relations

$$\cos \tilde{\alpha}_1 = \frac{\hat{k}^2 + k_1^2 - k_2^2}{2\hat{k}\, k_1} \tag{3.3}$$

$$\cos \tilde{\alpha}_3 = \frac{\hat{k}^2 + k_3^2 - k_4^2}{2\hat{k}\, k_3} \tag{3.4}$$

where $k_1 = k_1(\omega_1)$, $k_3 = k_3(\omega_3)$ and similarly $k_2(\omega_2) = k_2(\hat{\omega}-\omega_1(k_1))$, $k_4(\omega_4) = k_4(\hat{\omega}-\omega_3\ (k_3))$ can be expressed, with the aid of the dispersion relation, in terms of the given frequencies ω_1, ω_3, and $\hat{\omega}$.

After introducing the Jacobian for this additional transformation the final differential form for the probability of a collision becomes

$$dW = \frac{\sigma}{4} P.\, k_1\, k_3\, \hat{k} \left[(v_2 \cos(\tilde{\alpha}_1-\tilde{\alpha}_2)-v_1)(v_4\cos(\tilde{\alpha}_3-\tilde{\alpha}_4)-v_3) \right]^{-1} d\hat{k}\, d\hat{\alpha}\, d\hat{\omega}\, d\tilde{\alpha}_1\, d\tilde{\alpha}_3 \tag{3.5}$$

The integration limits for the integral over all possible collisions follow from the structure of the resonant interaction diagram (cf. Fig. 2). The diagram applies for a particular sum wavenumber $\hat{k}$, each curve on the diagram representing the interaction for a fixed sum frequency $\hat{\omega}$. For infinite depth waves the diagrams for each $\hat{k}$ differ only by a scale factor, but for finite depth waves the forms of

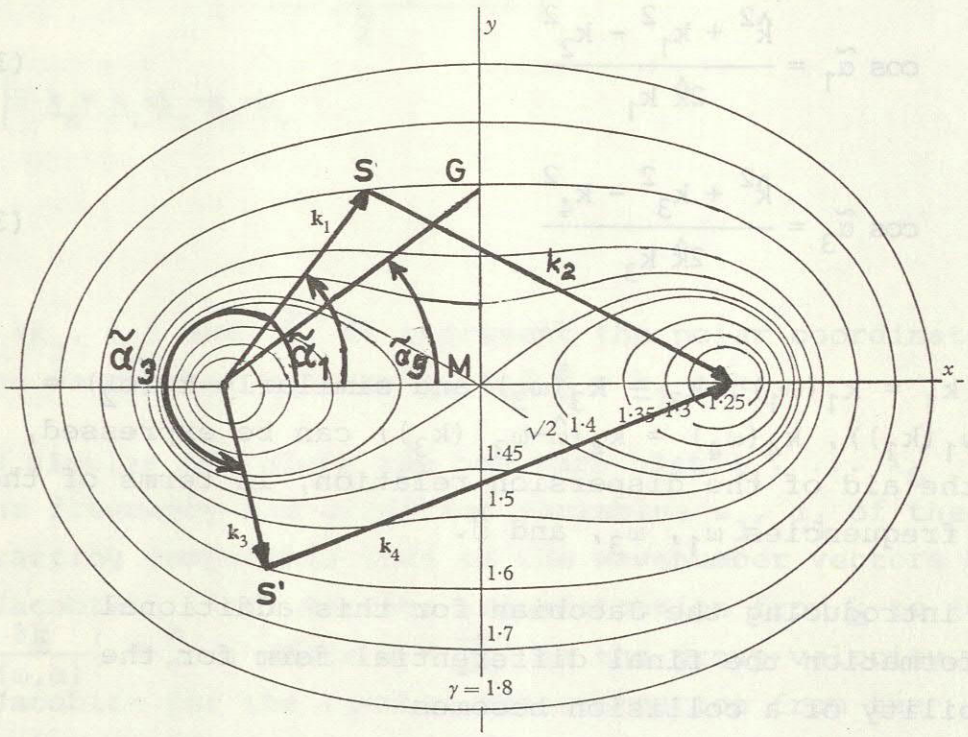

Fig. 2 Interaction diagram for third order resonant wave-wave interactions for deep-water waves (after Hasselmann, 1963b). The diagram applies for given $\hat{k}$, with each curve corresponding to fixed $\hat{\omega}$. The parameter γ is defined as $\hat{\omega} = \gamma\sqrt{g\hat{k}}$.

the interaction curves depend also on the parameter $\hat{k}\,h$, where h is the water depth. The variables $\hat{k}$ and $\hat{\omega}$ vary between 0 and ∞, the angle $\hat{\alpha}$ between 0 and 2π. The angles $\tilde{\alpha}_1$ and $\tilde{\alpha}_3$ vary between a lower limit $\tilde{\alpha}_o$ and an upper limit $2\pi-\tilde{\alpha}_o$, where $\tilde{\alpha}_o = 0$ for $\hat{\omega} \leq \hat{\omega}_r$, $\tilde{\alpha}_o = \tilde{\alpha}_g$ for $\hat{\omega} > \hat{\omega}_r$, and $\hat{\omega} = \hat{\omega}_r = 2\,\omega(\hat{k}/2)$ corresponds to the central point M of the interaction diagram separating the single-curve region from the double-curve region. The angle $\tilde{\alpha}_g = \tilde{\alpha}_g(\hat{k},\hat{\omega})$ refers to the point G in the diagram and is determined by the relation

$$\cos\tilde{\alpha}_g = \frac{\hat{k}}{2\,k_g}\,, \text{ where } k_g = (k_1)_g = (k_2)_g \qquad (3.6)$$

is the wavenumber corresponding to the frequency $\hat{\omega}/2$. On the basis of the symmetry arguments discussed in the following section, the wavenumber vectors $\underline{k}_1$ and $\underline{k}_3$ may be restricted to the left-hand side of the interaction diagram, so that the points S and S' are uniquely determined by the angles $\tilde{\alpha}_1$ and $\tilde{\alpha}_3$.

To compute the net energy transfer rate associated with the differential form (3.5), one integrates over all interactions, storing the four incremental changes in the action (number) for each of the four wave components involved in an elementary interaction, as given by (2.2), in the appropriate "bins" of a two-dimensional wavenumber grid. The net rate of change of the action spectral density is then obtained by dividing the change in action (particle number) computed for each bin by the area of the bin. A useful feature of this technique is that the wavenumber resolution of the output of the integration can be chosen independently of the integration grid used for the 5 parameters describing the probability density dW in the inter-

action phase space.

4. Symmetry considerations.

The expressions dW, equation (2.3), and Δn_j, equation (2.2), are invariant with respect to the permutations T_a, T_b corresponding to an interchange of the wave components $\underline{k}_1$, $\underline{k}_2$ and $\underline{k}_3$, $\underline{k}_4$, respectively. In addition, the cross section $\tilde{\sigma}$ is invariant with respect to the permutation T_c corresponding to an interchange of the wave component pair ($\underline{k}_1$, $\underline{k}_2$) with the pair ($\underline{k}_3$, $\underline{k}_4$), while P, and therefore dW, changes sign under this permutation. However, the signs in (2.2) are also interchanged through the permutation T_c, so that the expressions Δn_j again remain invariant under the permutation T_c.

The invariance of Δn_j with respect to the permutations T_a, T_b implies that the points S and S' in Figure 2 can be restricted to the left-hand side of the interaction diagram; the additional invariance of Δn_j with respect to T_c implies that the integration region can be further restricted by the side condition $\tilde{\alpha}_1 \leq \tilde{\alpha}_3$. Denoting this restricted interaction region by G_S, the original complete integration region G can be recovered from G_S by the operation

$$G = (1 + T_a)(1 + T_b)(1 + T_c)\, G_S = (1 + T_a + T_b + T_c + T_a T_b + T_b T_c + T_c T_a + T_a T_b T_c)\, G_S \qquad (4.1)$$

The parentheses on the right-hand side of (4.1) contain the 8 members of the finite permutation group generated by the permutations T_a, T_b and T_c.

It follows that equation (3.5) may be replaced by the equation

$$\left.\begin{matrix}\Delta n_1 \\ \Delta n_2 \\ \Delta n_3 \\ \Delta n_4\end{matrix}\right\} = \left.\begin{matrix}-1 \\ -1 \\ +1 \\ +1\end{matrix}\right\} \cdot 2\tilde{\sigma}.P.\ k_1 k_3 \hat{k}\left[(v_2\cos(\tilde{\alpha}_1-\tilde{\alpha}_2)-v_1)(v_4\cos(\tilde{\alpha}_3-\tilde{\alpha}_4)-v_3)\right]^{-1} \quad (4.2)$$
$$d\hat{k}\ d\hat{\alpha}\ d\hat{\omega}(d\tilde{\alpha}_1\ d\tilde{\alpha}_3)_s$$

which is identical to (3.5) except for the additonal factor 8 and the restriction of the variables $\tilde{\alpha}_1$, $\tilde{\alpha}_3$ to the region G_S, indicated by an index s on the differentials.

A further reduction of the integration region by a factor of two may be achieved by noting that the cross section $\tilde{\sigma}$ and transformation Jacobian are invariant with respect to a change in sign of either the x or y components of the wavenumbers. (This follows from the invariance of the basic hydrodynamic equations to this transformation). The invariance with respect to a change of sign of the x component has already been made use of through the invariance of the expressions Δn_j with respect to the permutation $T_a\ T_b = T_x$, which is identical to this transformation. However, the invariance of $\tilde{\sigma}$ and the transformation Jacobian with respect to the transformation T_y, a change in sign of the y components, has not yet been exploited. The transformation can be invoked to require that the point S in Figure 2 lies in the upper half plane, which yields a reduction of the region G_S to the region G_{sy}: $\tilde{\alpha}_o \leq \tilde{\alpha}_1 \leq \pi$, $\tilde{\alpha}_1 \leq \tilde{\alpha}_3 \leq 2\pi - \tilde{\alpha}_1$. To maintain the condition $\tilde{\alpha}_3 \geq \tilde{\alpha}_1$ for both G_S and G_{sy}, the transformation T_y must be applied in conjunction with the transformation T_c, so that G_S is generated from G_{sy} through the operation

$$G_S = (1 + T_y\ T_c)\ G_{sy} \quad (4.3)$$

In contrast to the permutation transformations T_a, T_b, T_c

which leave the entire differential expressions Δn_j unchanged, the transformation T_y leaves only part of the differential expression (4.2) invariant. The spectral product P is not invariant and must therefore be calculated separately for the two sub-regions G_{sy} and $T_y\ T_c\ G_{sy}$ of G_S. Nevertheless, the time consuming calculation of the cross section $\tilde{\sigma}$ need be carried out only once. (This advantage, however, no longer comes to bear very strongly in the "production mode" described in the following section, in which the integration of (4.2) is divided into two separate steps).

5. Coordinate stretching at the central interaction point

In test computations it was found that a greater stability of the numerical integration could be achieved by introducing a modification of the integration variables to remove a singularity of the transformation Jacobian at the center point M of the interaction diagram, where $\underline{k}_1 = \underline{k}_2 = \underline{k}_3 = \underline{k}_4$. The denominator on the right hand side of (4.2) is seen to vanish at M. It has been pointed out in Hasselmann (1963b) that this singularity, arising from a stationary point in the argument of the frequency δ-function in (2.4), is integrable and is furthermore cancelled by a zero in the spectral product P. However, because of the strongly peaked form of most surface wave spectra, the region near M in which P is small can be rather limited and surrounded by a region of very strong changes in P (this property, in fact, forms the basis of the narrow peak expansion of Longuet-Higgins, 1978, and Fox, 1978). It thus appears advisable to stretch the integration variables in the vicinity of M. This was achieved by introducing the variable

$$\xi = \sqrt{2}\ \left| \frac{\hat{\omega}}{\omega_r} - 1 \right|^{1/2} \qquad (5.1)$$

in place of $\hat{\omega}$ and variables η_1, η_3 in place of $\tilde{\alpha}_1$, $\tilde{\alpha}_3$,

where

$$\eta_{1,3} = \begin{cases} A \ln \left\{ \left[\tilde{\alpha}_{1,3} + (\tilde{\alpha}_{1,3}^2 + \tilde{\alpha}_g^2) \right] / \tilde{\alpha}_g \right\} \text{ for } \hat{\omega} < \omega_r \quad (o \leq \tilde{\alpha}_{1,3} < \pi) & (5.2) \\ A \ln \left\{ \alpha_{1,3} + \left[\tilde{\alpha}_{1,3}^2 - \tilde{\alpha}_g^2 + B^2 \tilde{\alpha}_g^4 \right] / (\tilde{\alpha}_g + B\tilde{\alpha}_g^2) \right\} \text{for } \hat{\omega} > \omega_r & (5.3) \end{cases}$$

$$(\tilde{\alpha}_g < \tilde{\alpha}_{1,3} < \pi)$$

$$\text{with} \quad A = 6.(\tilde{\alpha}_g \, \omega_r / \hat{\omega})^{1/2}, \qquad (5.4)$$

$$B = \frac{c_1}{c_2} (2/c_3)^{1/2}, \qquad (5.5)$$

The angle $\tilde{\alpha}_g$ is defined for $\hat{\omega} > \omega_r$ by equation (2.10) and for $\hat{\omega} < \omega_r$ by the relation

$$\tilde{\alpha}_g^2 = \frac{(\omega_r - \hat{\omega}) \omega_r^3}{c_2 g^2 \hat{k}^2} \qquad (5.6)$$

The coefficients c_1, c_2 and c_3 are equal to unity for deep water and for waves of finite depth are functions of $\hat{k}h$ which are determined by the expansion of the resonance condition near M. They are given in Herterich and Hasselmann, 1980 (with $\hat{k}h$ replaced by $2 k_p h$).

For $\tilde{\alpha}_3 > \pi$ the transformations (5.2), (5.3) must be replaced by identical relations with $\tilde{\alpha}_3$ replaced by $(2\pi - \tilde{\alpha}_3)$. (The angle $\tilde{\alpha}_1$ remains smaller than π within the region G_{sy}).

The transformation Jacobian is given by

$$\left| \frac{\partial(\hat{\omega}, \tilde{\alpha}_1, \tilde{\alpha}_3)}{\partial(\xi, \eta_1, \eta_3)} \right| = \begin{cases} \omega_r \, \xi \, A^{-2} \left[(\tilde{\alpha}_1^2 + \tilde{\alpha}_g^2)(\tilde{\alpha}_3^2 + \tilde{\alpha}_g^2) \right]^{1/2} & (5.7) \\ \quad \text{for } \hat{\omega} < \omega_r \quad (o \leq \tilde{\alpha}_{1,3} < \pi) & \\ \omega_r \, \xi \, A^{-2} \left[(\tilde{\alpha}_1^2 - \tilde{\alpha}_g^2 + B^2 \tilde{\alpha}_g^4)(\tilde{\alpha}_3^2 - \tilde{\alpha}_g^2 + B^2 \tilde{\alpha}_g^4) \right]^{1/2} & (5.8) \\ \quad \text{for } \hat{\omega} > \omega_r \quad (\tilde{\alpha}_g < \tilde{\alpha}_{1,3} < \pi) & \end{cases}$$

(the angle $\tilde{\alpha}_3$ is replaced again by $(2\pi - \tilde{\alpha}_3)$ for $\tilde{\alpha}_3 > \pi$). The transformations (5.1) - (5.3) are chosen such that the singularity of the denominator in (4.2) cancels against a zero of the same form in the Jacobian (5.7) - (5.8).

6. Separation of cross section computations and numerical integration

If a large number of nonlinear transfer calculations are to be carried out - which is, of course, the main purpose of developing an efficient integration method - a considerable saving in computing time can be achieved by separating the computations of the cross section, transformation Jacobian and interaction wavenumbers for a given integration grid from the actual integration of the nonlinear transfer for a particular spectrum. The first computations need be carried out only once. The integrations themselves are then made by reading the results of the first computation from a memory file and computing new only the spectral product expressions P.

Another advantage of separating the integration into two steps is that it provides a simple mechanism for filtering out insignificant regions of the interaction phase space. Experience shows that for typical peaked wave spectra, often only 10% of the interaction phase space contributes more than 95% of the nonlinear transfer in the wavenumber regions of significant transfer. For a five dimensional integral it is difficult to determine these regions a priori and design the integration grid accordingly. Standard dynamical grid adaption schemes tend to become cumbersome and ineffective for multi-dimensional integrals. However, a straightforward dynamical method can be implemented by simply discarding all grid points whose incremental contribution to the integral fails to exceed some preset lower limit.

The flagged grid points are determined by a trial integration with a typical test spectrum, and all subsequent integrations with similar spectra are then carried out using the filtered grid.

To check on the validity of the filtering procedure, two filtered grids, representing two cut-off-levels differing by a factor of 10 were generated, and the results of the two calculations for the coarse and fine filtered integrations were routinely compared. Significant deviations between the coarse and fine filtered integrations indicate that the filtering technique is unreliable (for example, because the spectrum considered differs significantly from the test spectrum) and that a complete integration, or a redefinition of the filtered grid, is required.
As example, Figure 1 in part II compares the results for the complete integration with the fine filtered integration for a mean JONSWAP spectrum with a Mitsuyasu-type frequency-dependent spreading function. The integration times were approximately 18 mins. for the complete integration and 40 secs. for the fine and coarse filtered integration together on a CDC CYBER 175. The fine filtered integration shows good agreement with the complete integration, but the (10 sec.) integration using the coarse filtered grid was also acceptable. The filtering technique yields large relative errors, as to be expected, when the transfer rate becomes small (i.e. for large angles in the present example).

Part II: Results

1. Purpose of computations

A series of nonlinear transfer computations were carried out for various forms of spectra. The purpose of the calculations was

a) to produce a basic set of exact calculations for developing and testing different schemes for parameterising the nonlinear transfer in a form sufficiently simple for application in wave prediction models,

b) to evaluate finite-depth effects and test the Herterich-Hasselmann transformation rules for relating the nonlinear transfer for finite-depth spectra to the infinite-depth case.

In this part of the report we present only the results of the calculations. A discussion of parameterization schemes and general conclusions which where drawn from the results are given in part III.

Unless otherwise stated, all computations were made for deep-water spectra with a wind-sea peak frequency $f_m = 0.3$ Hz and a Phillips' constant $\alpha = 0.01$. The results for other values of f_m and α can be deduced from the results presented here using the general scaling relation (cf. Hasselmann, 1963b, or Hasselmann et al., 1973) that a spectrum of the form

$$F(f,\theta) = \alpha g^2 f_m^{-5} \varphi(f/f_m,\theta)$$

yields a nonlinear transfer of the form

$$S_{nl}(f,\theta) = \alpha^3 g^2 f_m^{-4} \psi(f/f_m,\theta)$$

where φ and ψ are nondimensional shape functions independent of the scales α and f_m.

2. Cases computed

The computations may be divided into the following classes:

2.1 Standard JONSWAP frequency spectrum

$$E(f) = \alpha g^2 (2\pi)^{-4} f^{-5} \exp\left\{-\frac{5}{4}\left(f/f_m\right)^4\right\} \exp\left\{\ln\gamma \exp\left[-\frac{(f-f_m)^2}{2\sigma^2 f_m^2}\right]\right\}$$

with mean JONSWAP shape parameters

$\gamma = 3.3$, $\sigma = \sigma_a = 0.07$ for $f < f_m$

$\sigma = \sigma_b = 0.09$ for $f > f_m$

and various spreading functions $S(f,\theta)$:

Case 1: $S(f,\theta) = I(p)^{-1} \cos^{2p}(\theta/2)$ with

$$p = 10.^{0.99} (f/f_m)^{\beta}$$

$$\text{where } \beta = \begin{cases} 4.06 & \text{for } f < f_m \\ -2.34 & \text{for } f \geq f_m \end{cases} \qquad (1)$$

and the normalisation factor $I(p) = 2^{(2p-1)} \cdot \pi \cdot \Gamma^2(p+1)/\Gamma(2p+1)$.

This case corresponds to the empirical spreading functions found for JONSWAP wind-sea spectra. (D. Hasselmann, 1980). It is similar to the form proposed by Mitsuyasu et al. (1975) except that the frequency dependence of the exponent p is normalized in (1) with respect to the peak frequency (as expected for an energy balance controlled primarily by non-linear interactions in the vicinity of the peak) rather than the frequency g/U defined in terms of the wind speed U.

Case 1 represents the "reference deep-water wind-sea spectrum" used later in various parameterization schemes (cf. Part III).

Case 2: $$S(f,\theta) = \begin{cases} \frac{2}{\pi} \cos^2\theta & \text{for } |\theta| \leq \pi/2 \\ 0 & \text{for } \pi/2 < |\theta| \leq \pi \end{cases} \qquad (2)$$

Case 3: $$S(f,\theta) = \begin{cases} \frac{8}{3\pi} \cos^4\theta & \text{for } |\theta| \leq \pi/2 \\ 0 & \text{for } \pi/2 < |\theta| \leq \pi \end{cases} \qquad (3)$$

Cases 4 - 6: $S(f,\theta) = I(p)^{-1} \cos^{2p}(\theta/2)$ with p = 2,5 and 10. (4)

2.2 JONSWAP frequency spectra with a $\cos^2\theta$ spreading function (eq. (2)) and 9 different combinations of shape parameters as listed in Table 1.

case	γ	σ_a	σ_b
7	3,3	0,07	0.07
8	3.3	0.07	0.11
9	3.3	0.05	0.09
10	3.3	0.09	0.09
11	2.7	0.07	0.09
12	3.9	0.07	0.09
13	1.	0.07	0.09
14	1.5	0.07	0.09
15	7	0.07	0.09

Table 1

2.3 The same case (1) but for finite depth waves at various depths h given by

$$k_m h = 0.35,\ 0.5,\ 0.65,\ 0.8,\ 1,\ 1.5,\ 2,\ 5,\ 10$$

where k_m denotes the wavenumber corresponding to the peak frequency f_m (cases 16 - 24).

2.4 Case 25. A directionally skewed spectrum in which the one-dimensional spectrum is the mean JONSWAP spectrum, as in case 1, and the spreading function relative to the mean propagation direction θ_o was also the same as in case 1, but θ_o is a function of frequency in accordance with the relation

$$\theta_o = \begin{cases} 0 \text{ for } f/f_m \leq 1 \\ \pi(f/f_m - 1) \text{ for } 1 < f/f_m \leq 2 \\ \pi \text{ for } 2 < f/f_m \end{cases} \qquad (5)$$

2.5 Various swell-wind sea interaction cases as listed in Table 2 in which the swell was represented as an "old" wind-sea spectrum. The swell spectrum has the same shape as the local wind-sea spectrum, as given in case 1, but generally has a lower peak frequency, less energy and a different mean propagation direction. The wind sea was the same as in case 1.

case	swell parameters			$\frac{(f_m)_{sw}}{(f_m)_{ws}}$	$\frac{E_{sw}}{E_{ws}}$
	$10^2 \cdot \alpha$	f_m(Hz)	θ_o(^{o})		
26	0.066	0.18	0	0.6	0.5
27	0.2	0.24	0	0.8	0.5
28	0.2	0.24	90	0.8	0.5
29	0.5	0.3	90	1	0.5

Table 2

Table 3 gives a brief summary of all computations made. The results are presented in Figs 1 - 29 (case numbers and figure numbers are identical). Units in all figures are in m, Hz and sec.

class	description		case numbers = figure numbers
1	JONSWAP spectrum with different spreading function	F	1 - 6
2	JONSWAP spectrum with $\cos^2\theta$ spreading function and different shape parameters	F	7 - 15
3	Finite depth influences for reference JONSWAP spectrum with frequency-dependent spreading function (cf. case 1)	C	16 - 24
4	Skew spectrum	C	25
5	Interaction between old and new wind sea	C	26 - 29

Table 3 $\left.\begin{matrix}F\\C\end{matrix}\right\}$ integrations performed with $\left\{\begin{matrix}\text{filtered}\\\text{complete}\end{matrix}\right\}$ grid (cf. part I

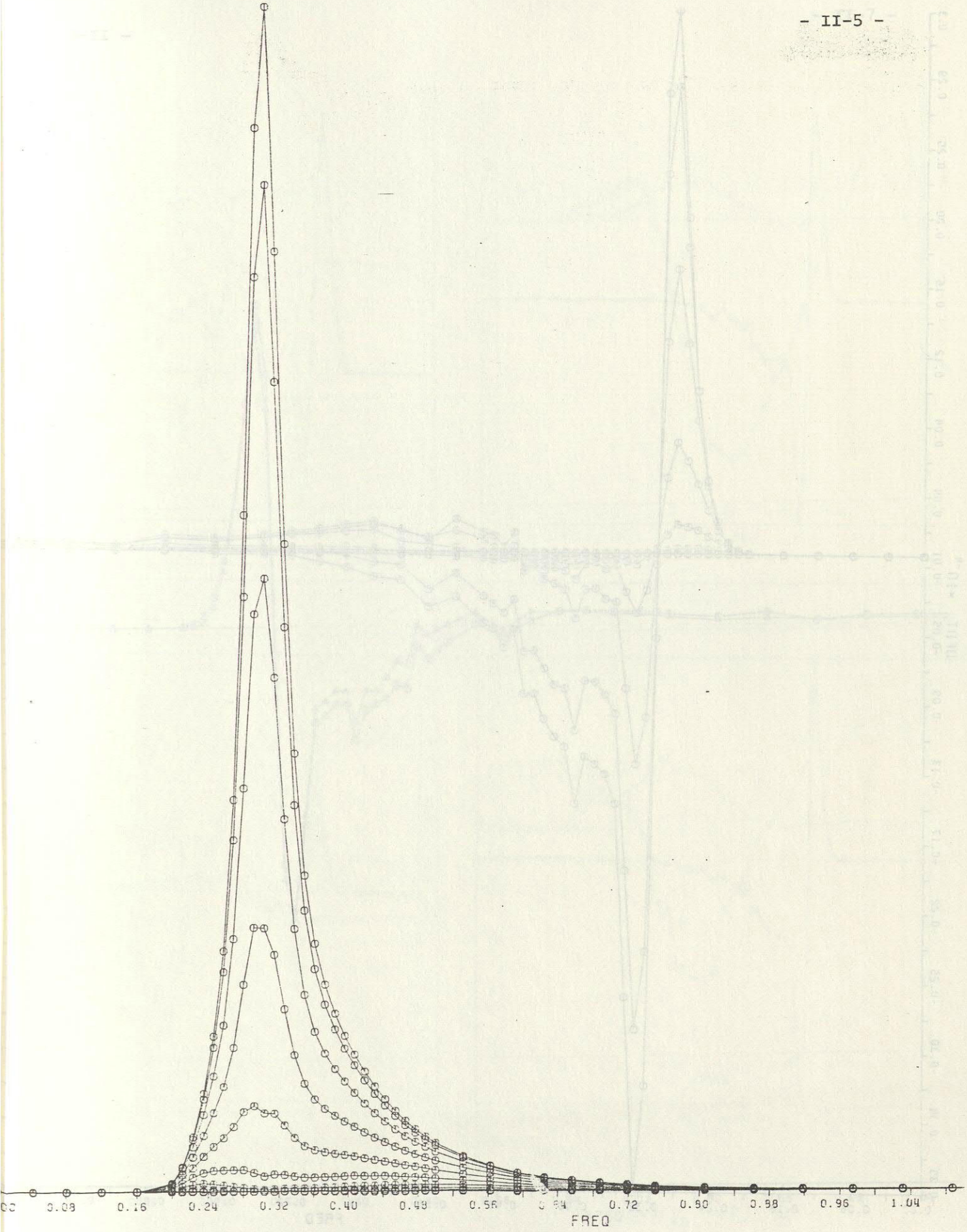

Fig. 1a Mean JONSWAP spectrum with $\cos^{2p}(\theta/2)$ spreading factor, where $p = p(f/f_m)$ in accordance with equation (1). Two-dimensional spectrum $E(f,\theta)$. Directional increments are 15^{o}.

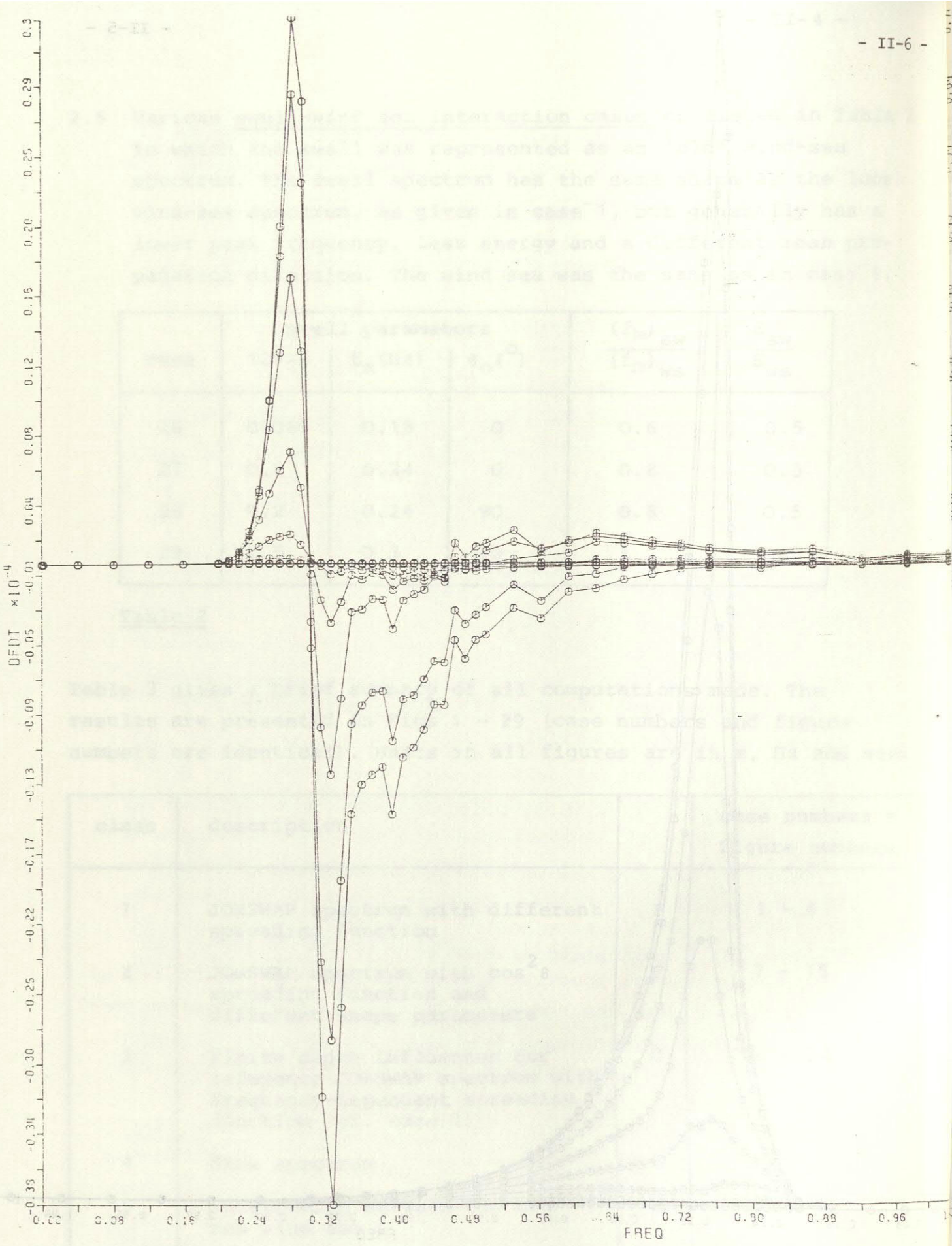

Fig. 1b Two-dimensional transfer rate $S_{nl}(f,\Theta)$. Directional increments are 15^{o}.

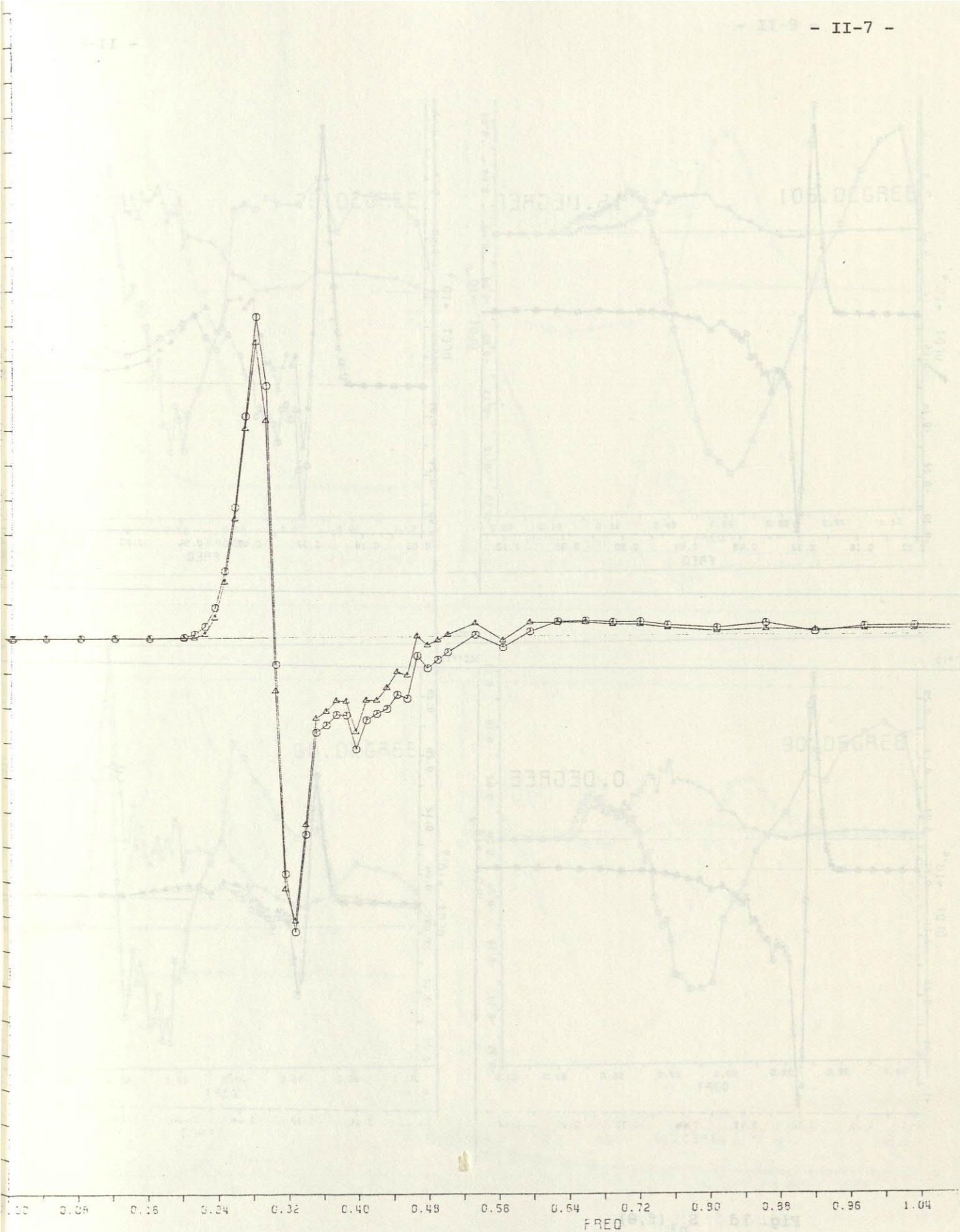

Fig. 1c One-dimensional transfer rate $S_{nl}(f) = \int S_{nl}(f,\theta)d\theta$.

Δ : filtered grid integration (standard integration method).

o : full integration.

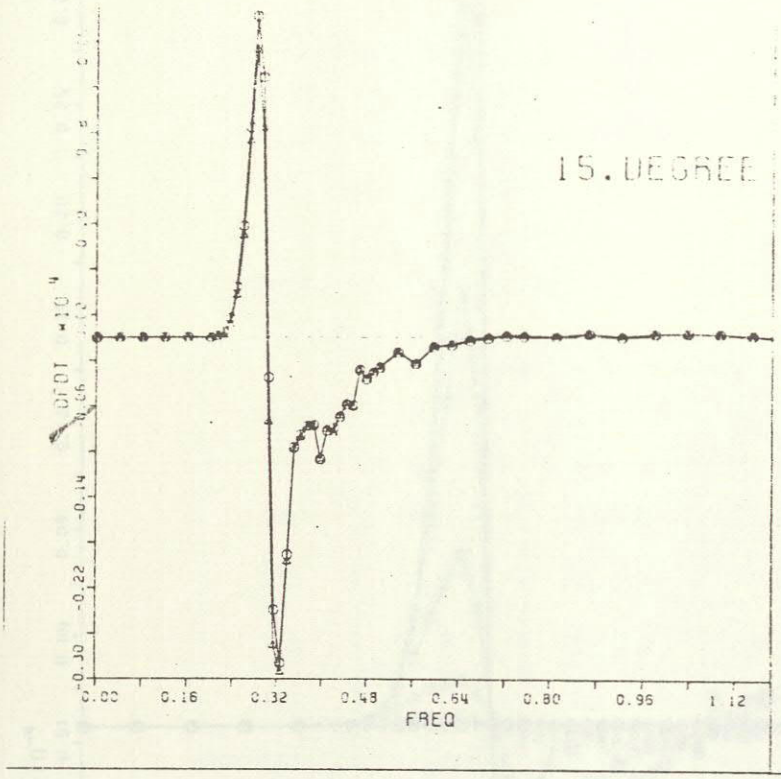

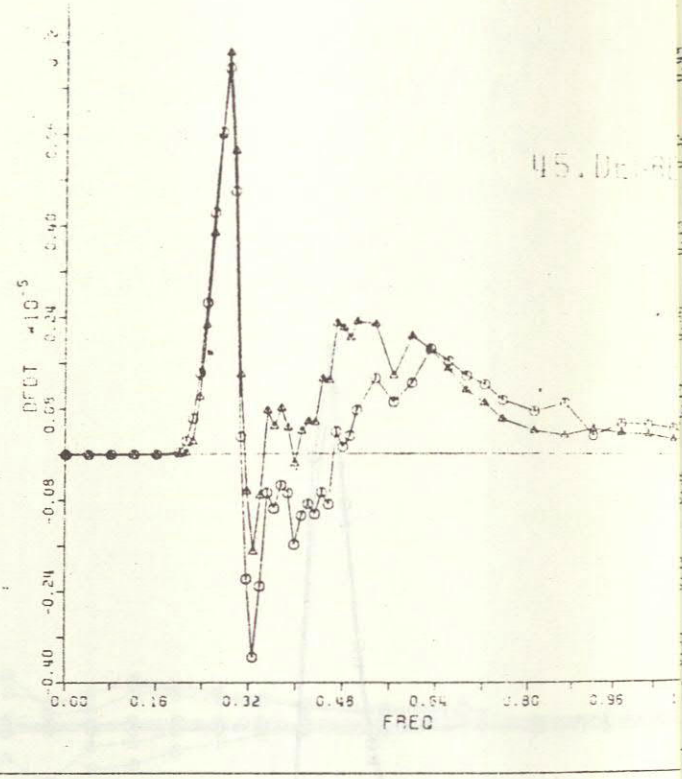

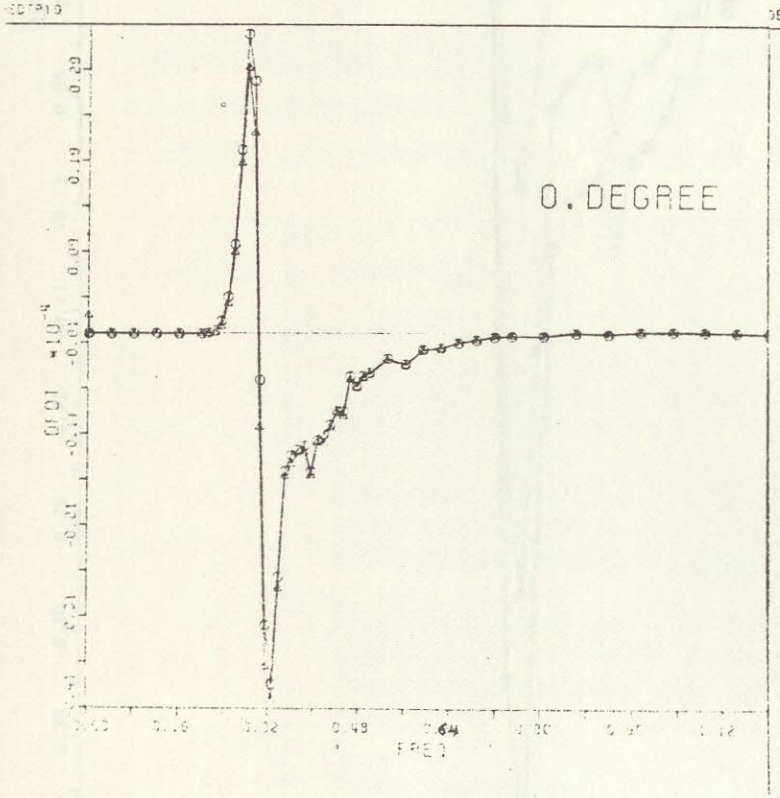

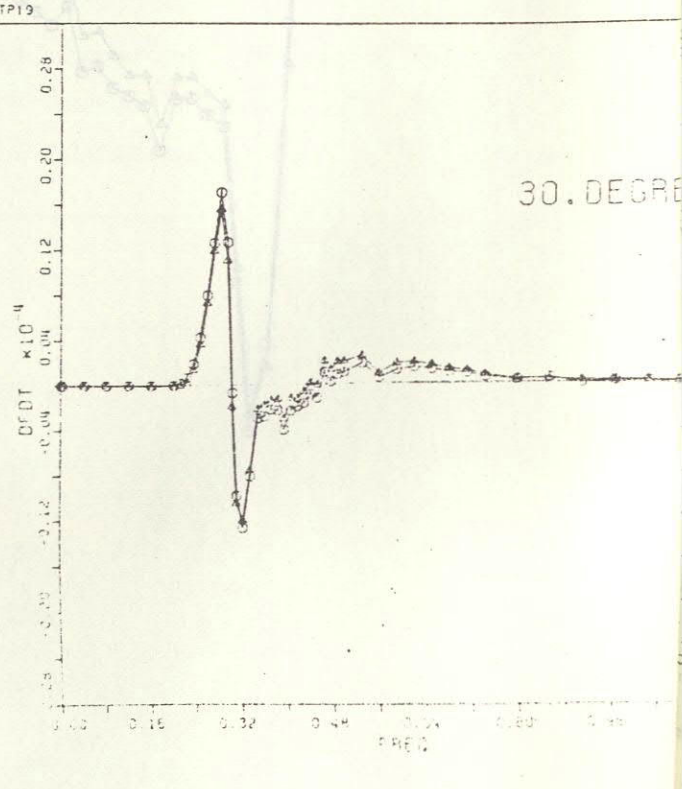

Fig. 1d $S_{nl}(f,\theta)$

Δ : filtered grid integration

o : full integration

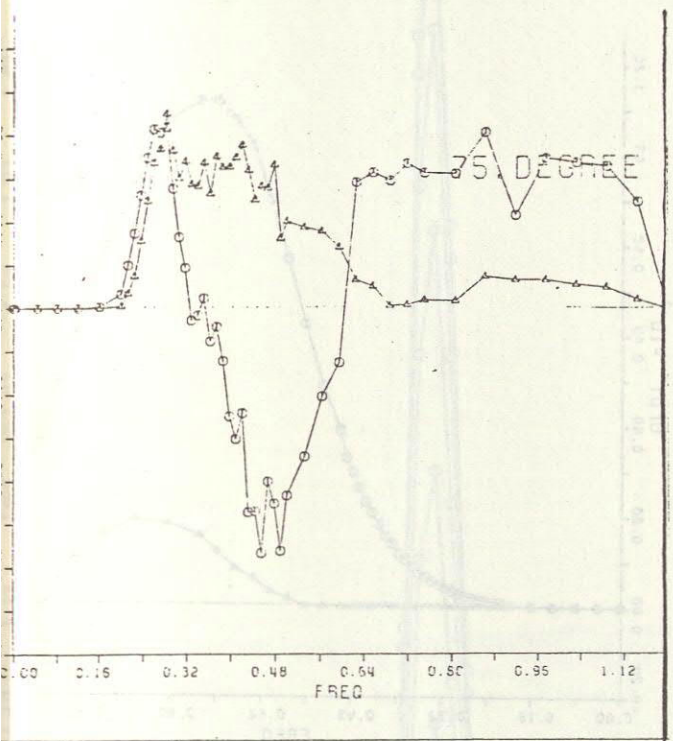

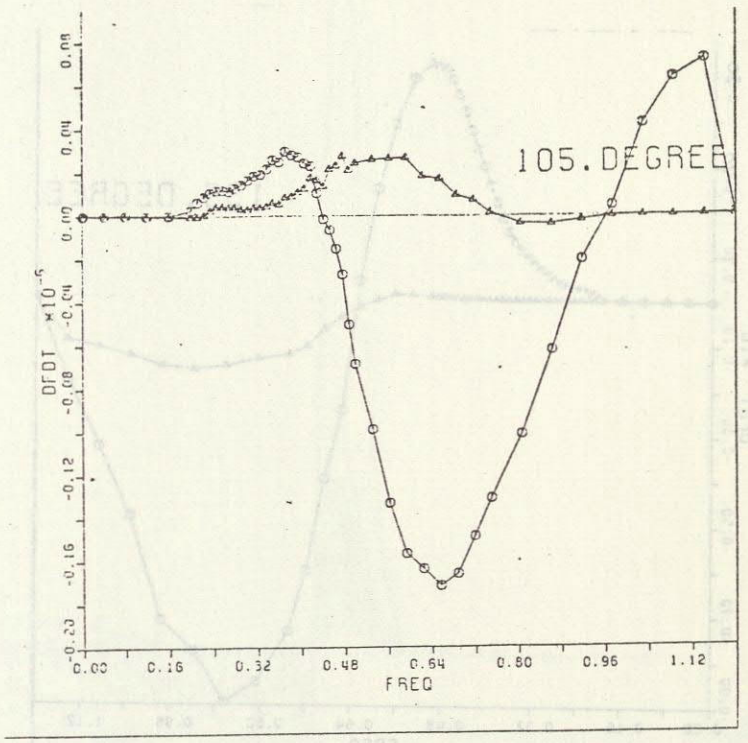

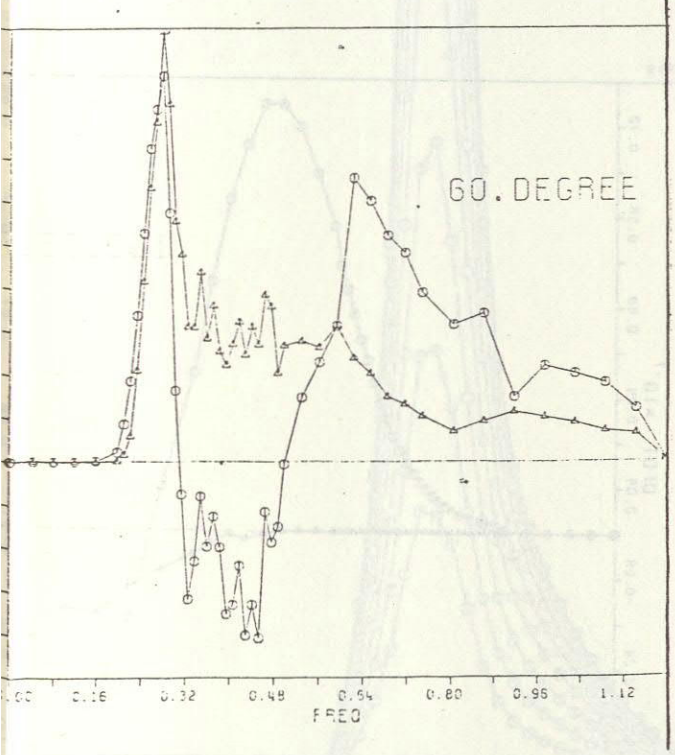

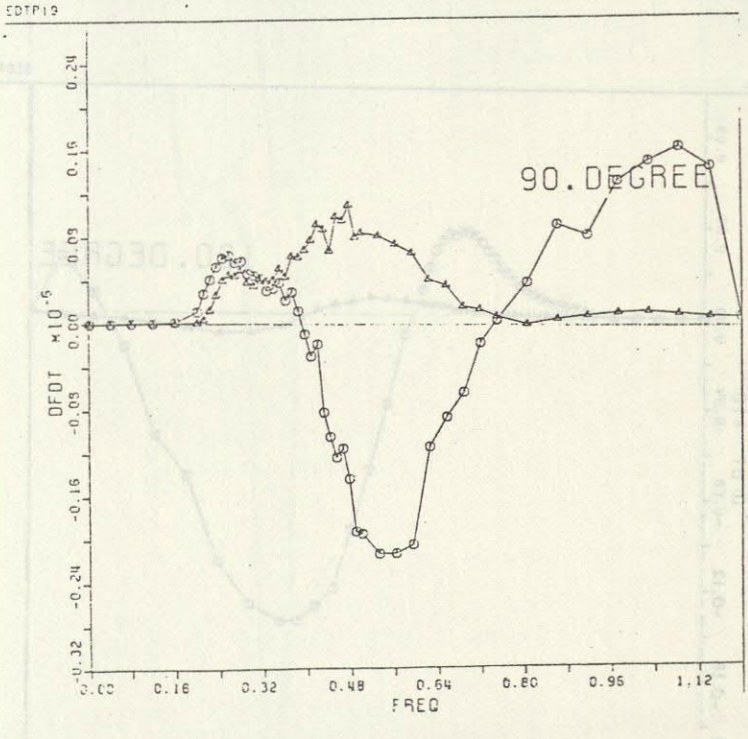

Fig. 1e $S_{nl}(f,\Theta)$

Δ : filtered grid integration

o : full integration

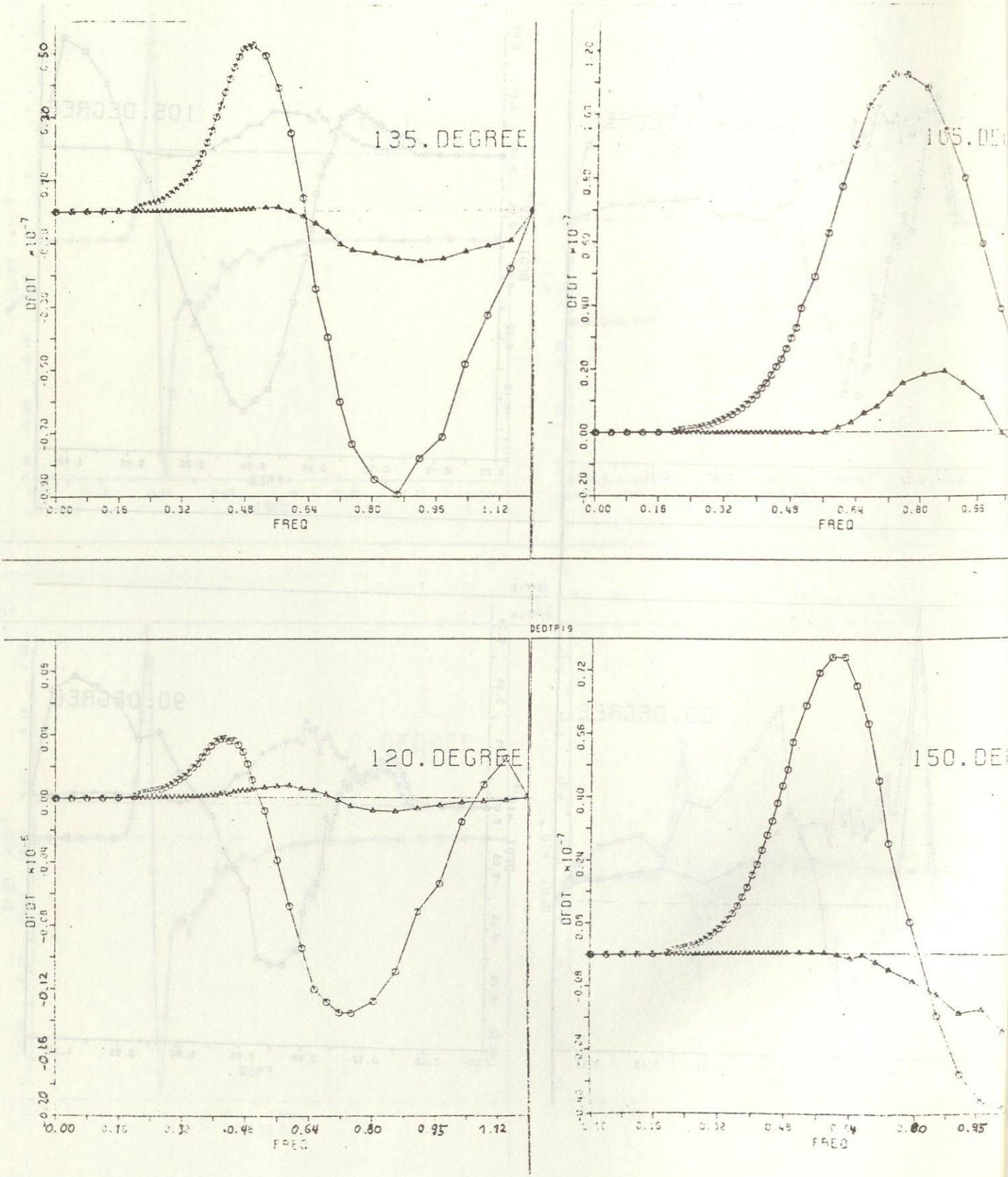

Fig. 1f $S_{nl}(f,\theta)$

Δ : filtered grid integration

o : full integration

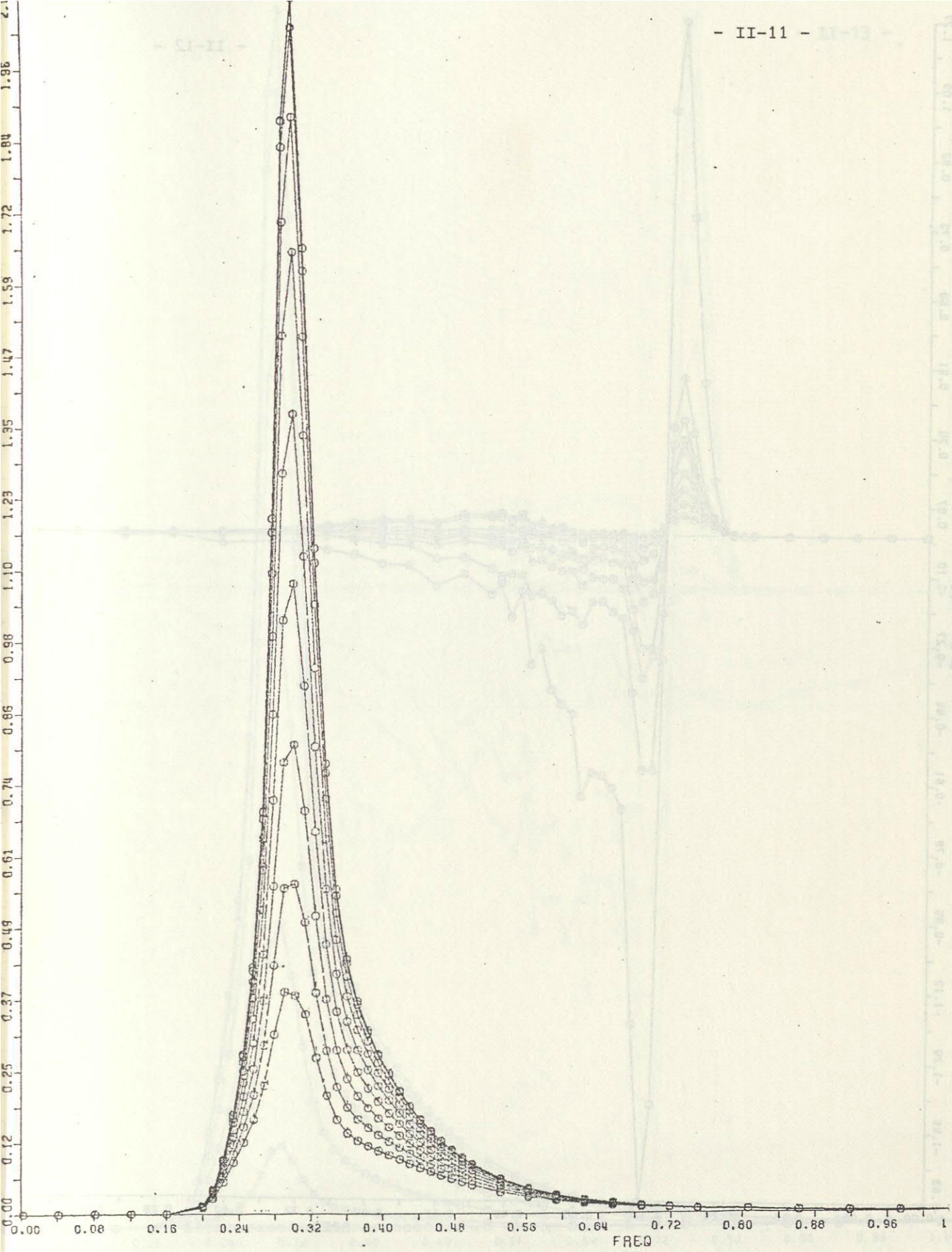

Fig. 1g JONSWAP spectrum, case 1, same as Fig. 1a, but with directional increment of 6^{o}

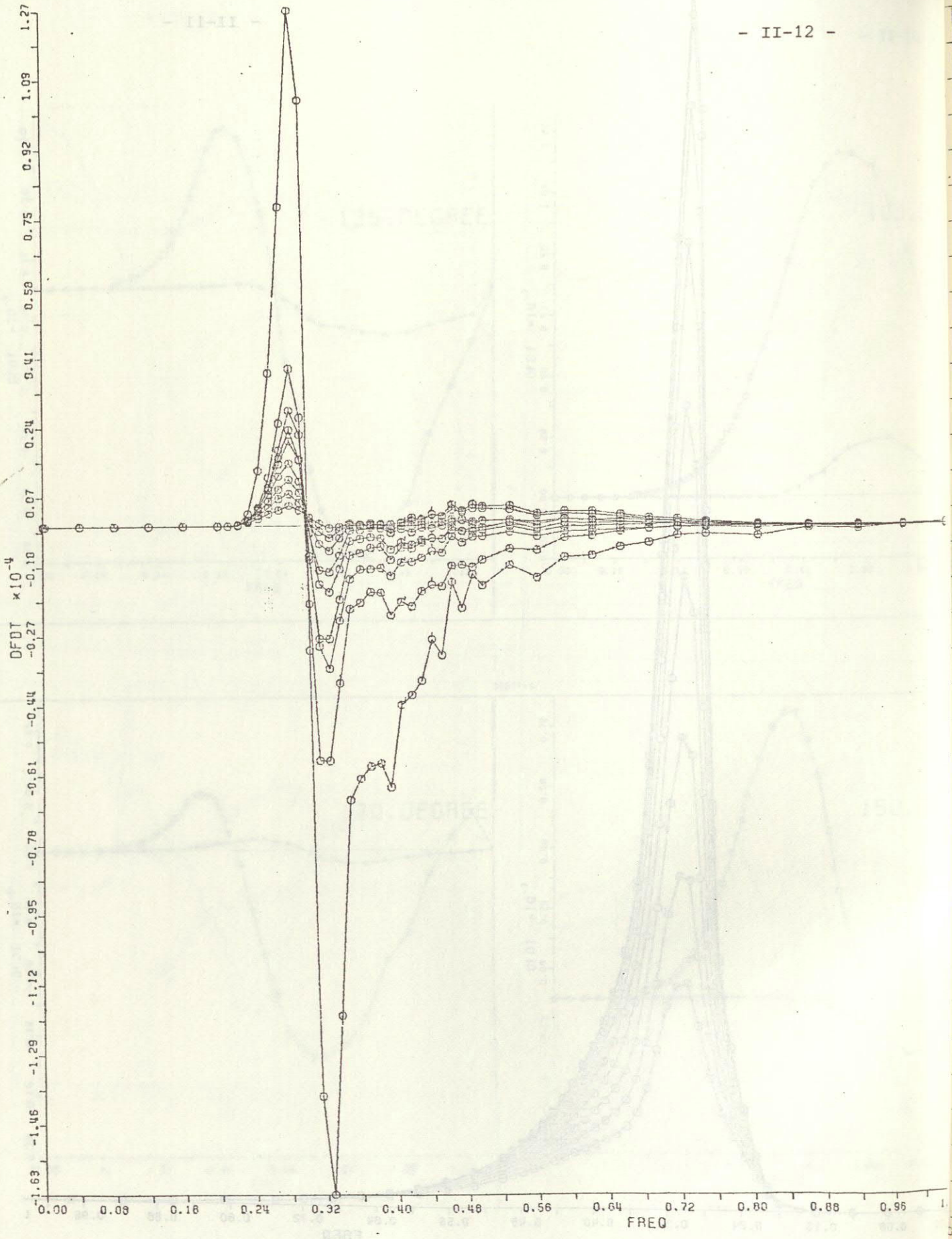

Fig. 1h Nonlinear transfer S_{nl}, same as Fig. 1b, but computed with directional increment of 6°

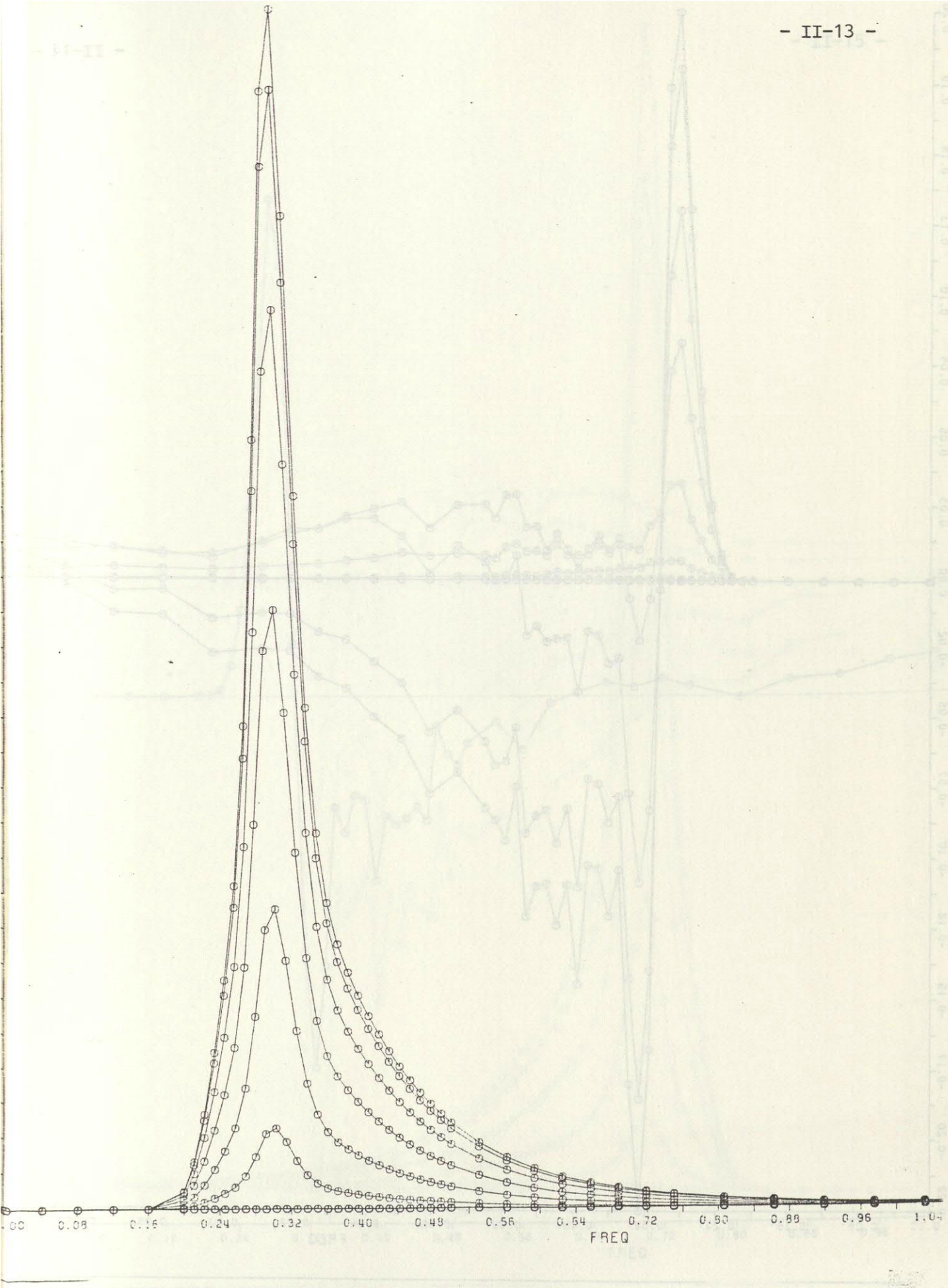

Fig. 2a Mean JONSWAP spectrum with $\cos^2\theta$ spreading factor. Two-dimensional spectrum $E(f,\theta)$. Directional increments are 15°.

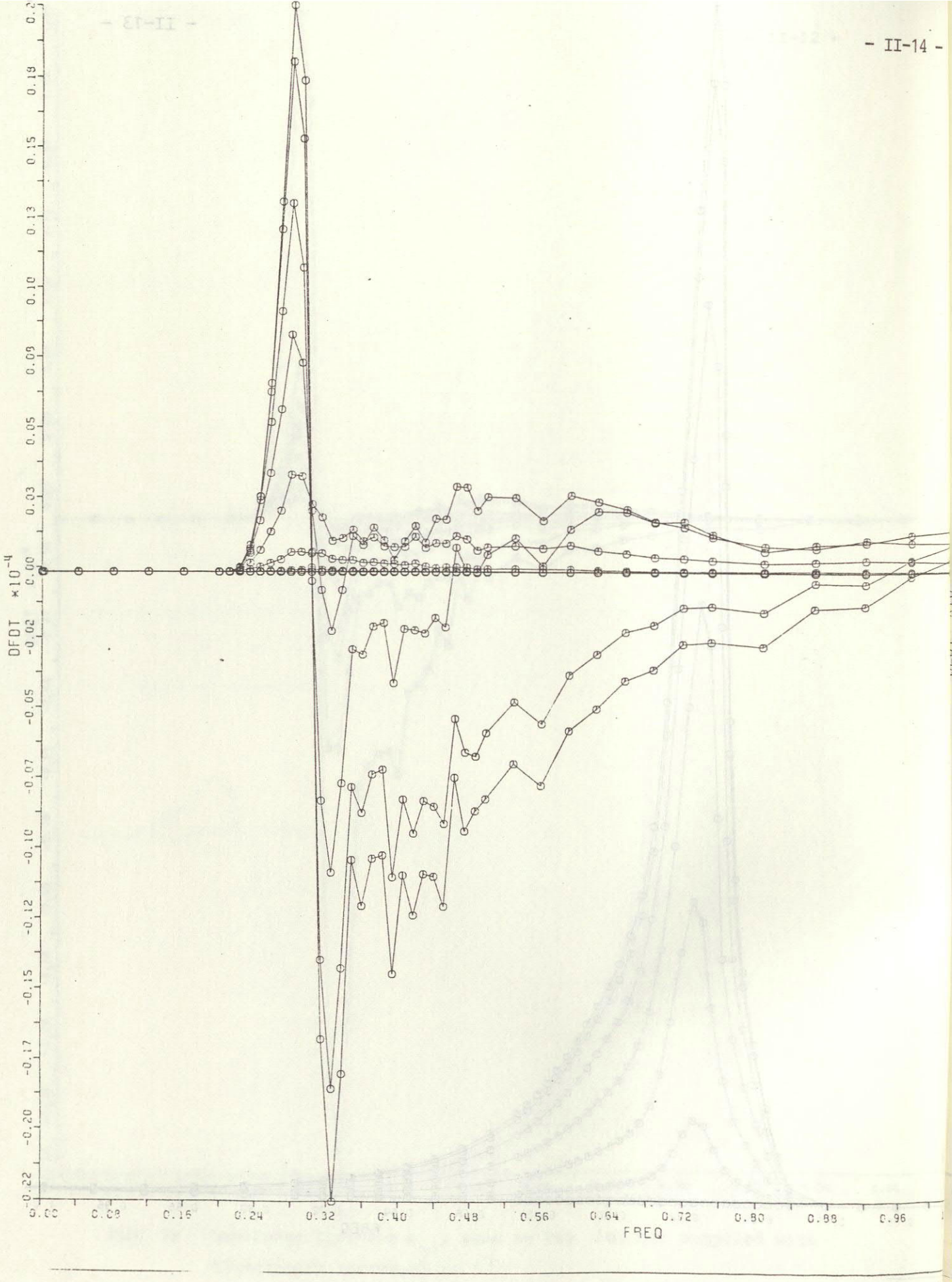

Fig. 2b Two-dimensional transfer rate $S_{nl}(f,\theta)$. Directional increments are 15^{o}.

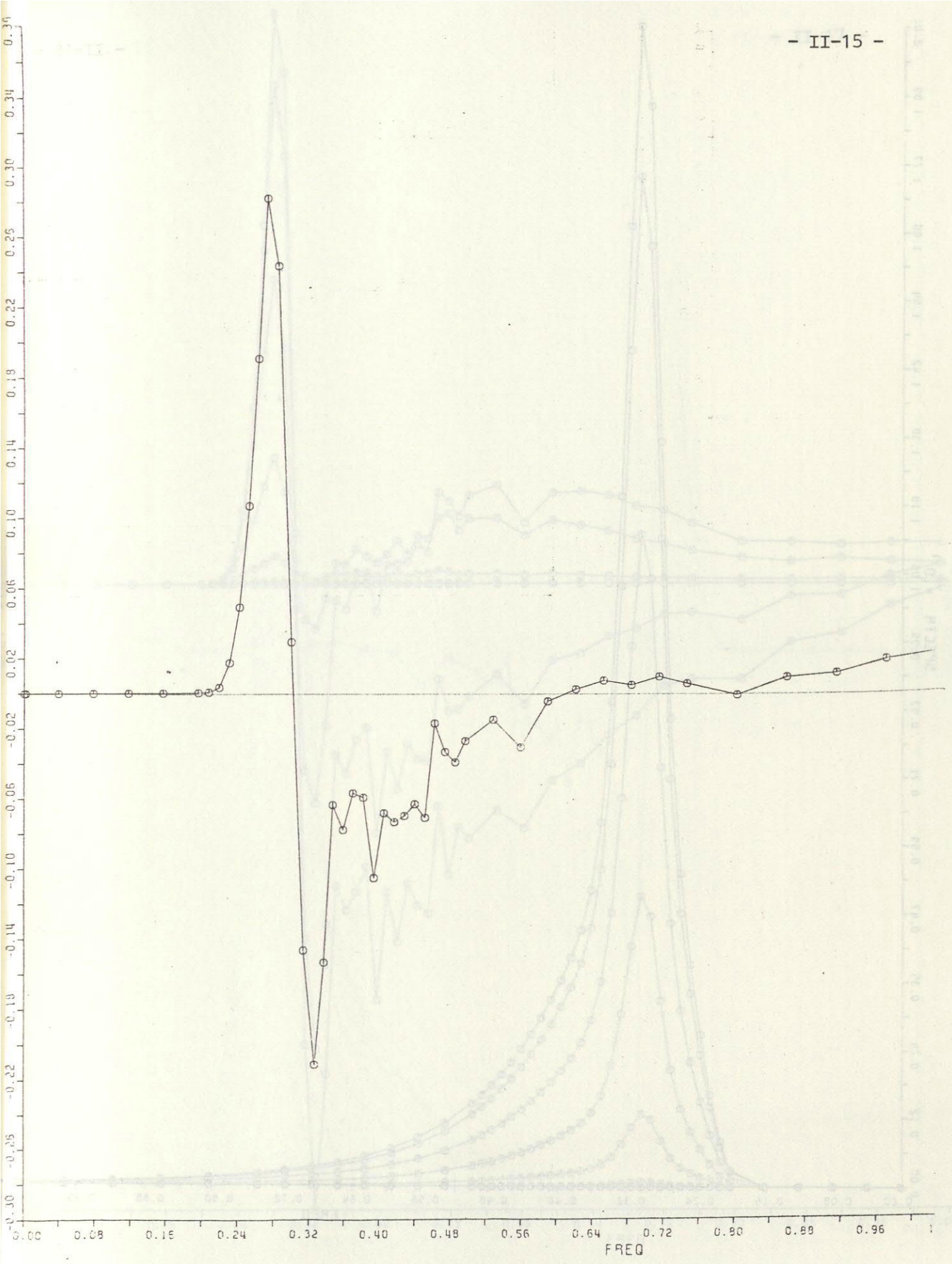

Fig. 2c One-dimensional transfer rate $S_{nl}(f) = \int S_{nl}(f,\theta)\,d\theta$.

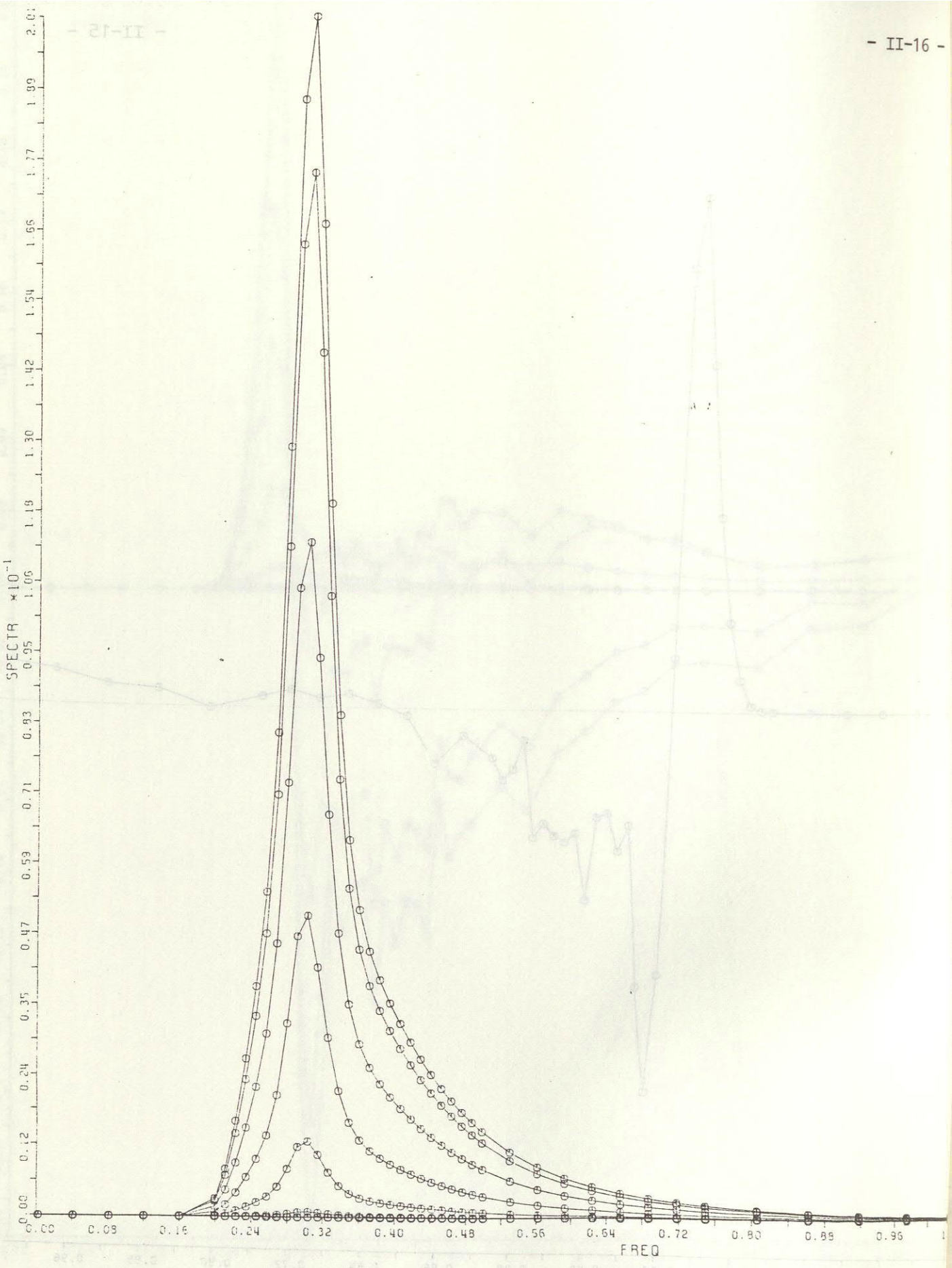

Fig.3a Mean JONSWAP spectrum with $\cos^4\theta$ spreading factor. Two-dimensional spectrum $E(f,\theta)$. Directional increments are 15°.

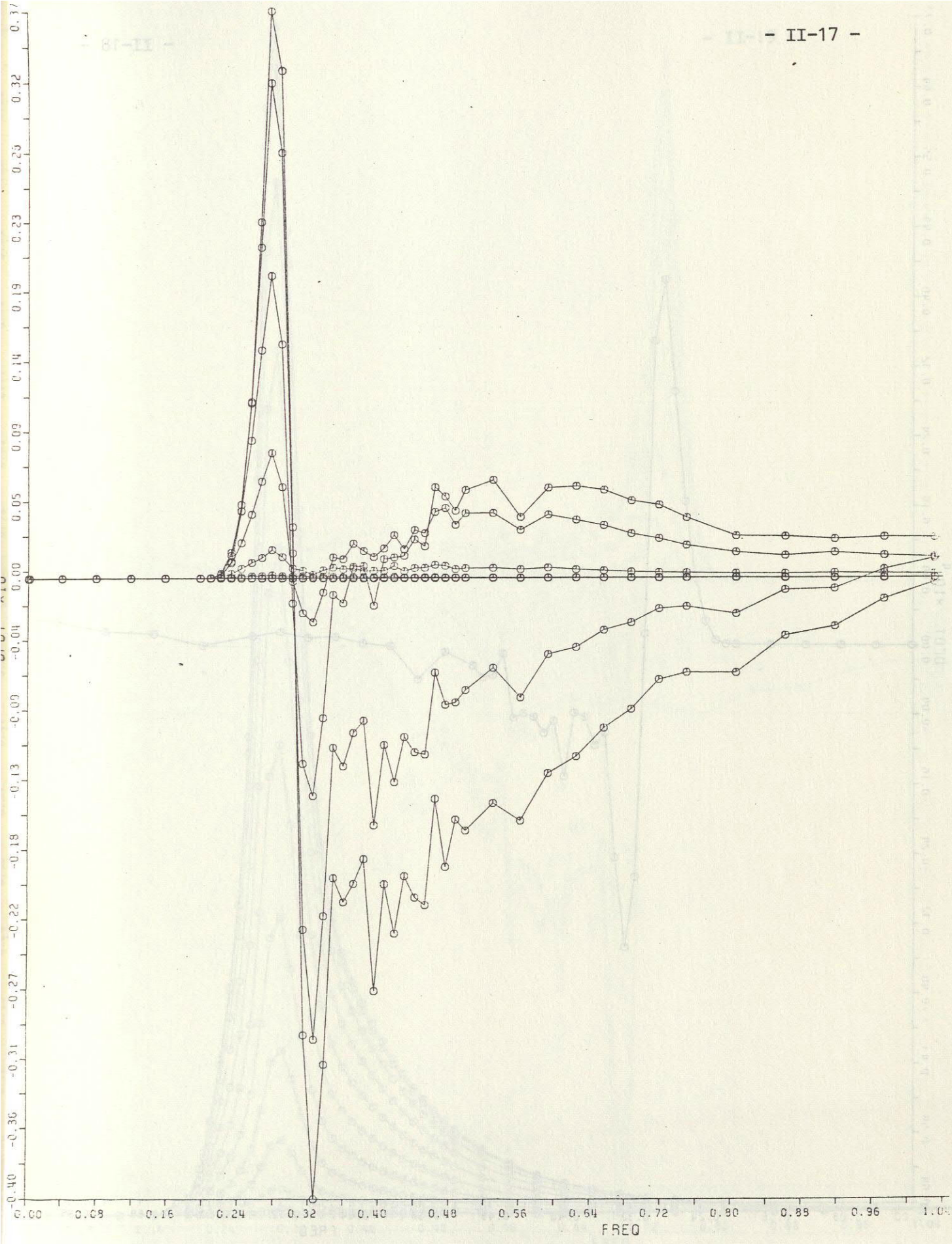

Fig. 3b Two-dimensional transfer rate $S_{nl}(f,\theta)$. Directional increments are 15^{o}.

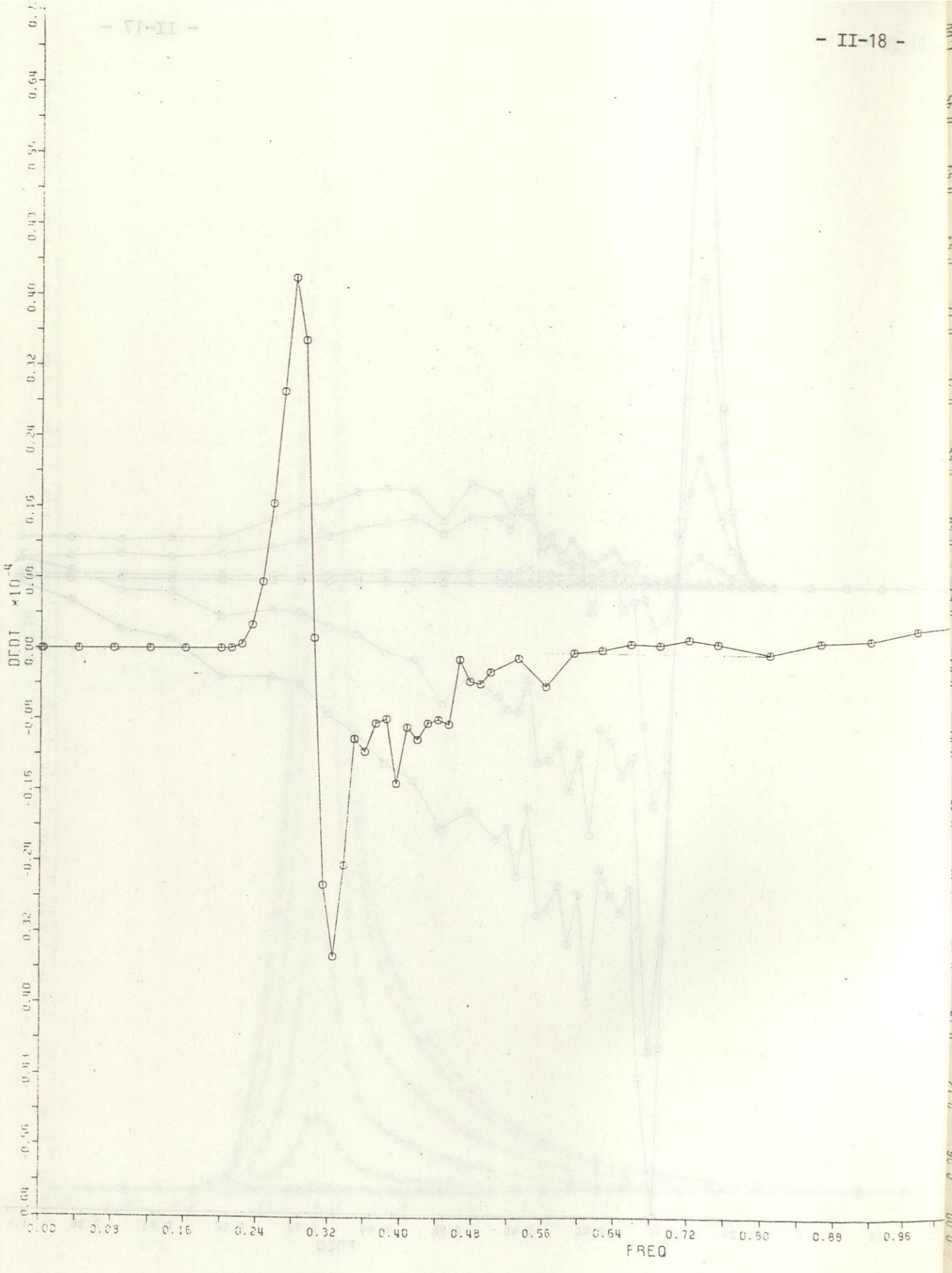

Fig. 3c One-dimensional transfer rate $S_{nl}(f) = \int S_{nl}(f,\theta)d\theta$.

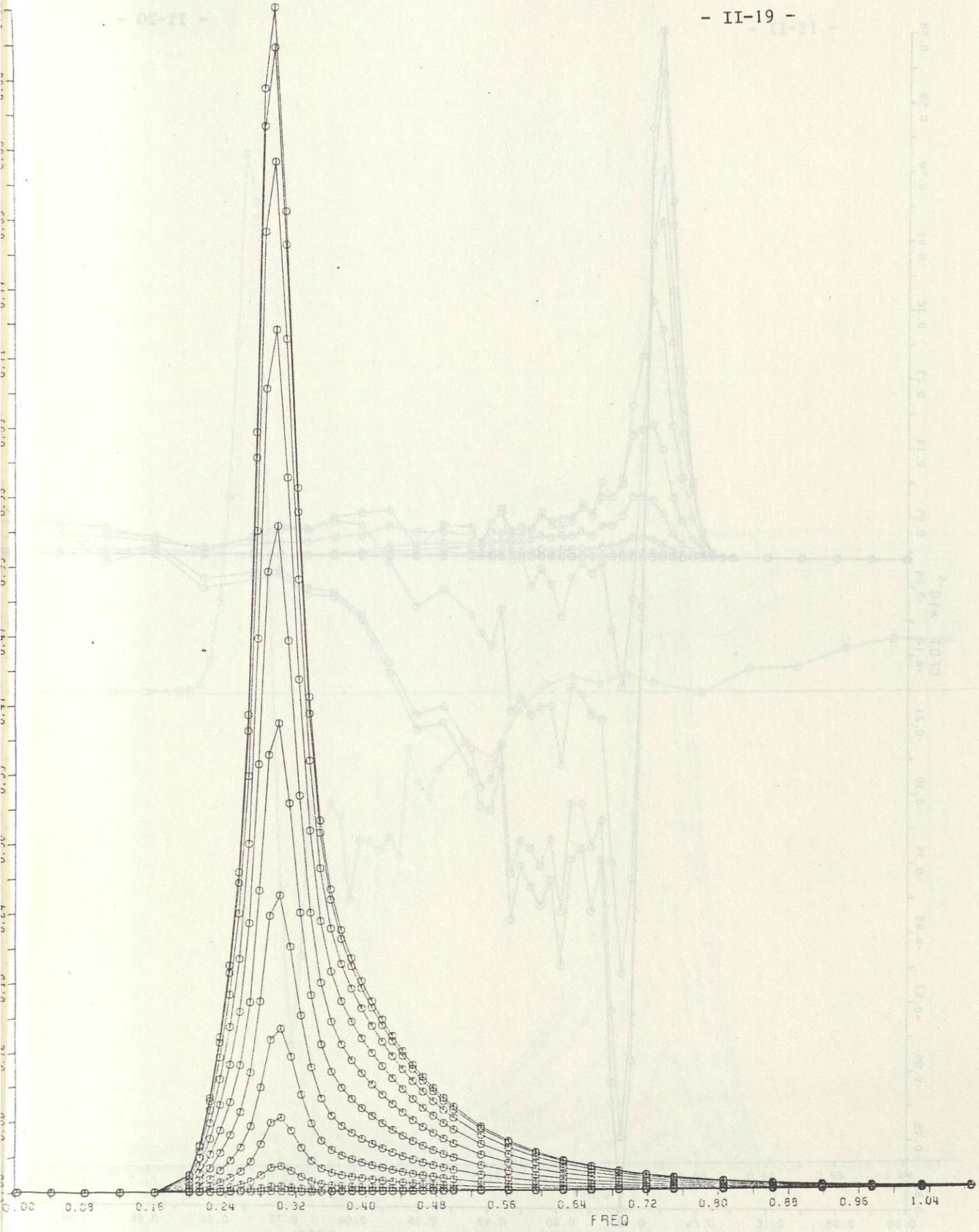

Fig. 4a Mean JONSWAP spectrum with $\cos^4(\theta/2)$ spreading factor. Two-dimensional spectrum $E(f,\theta)$. Directional increments are 15°.

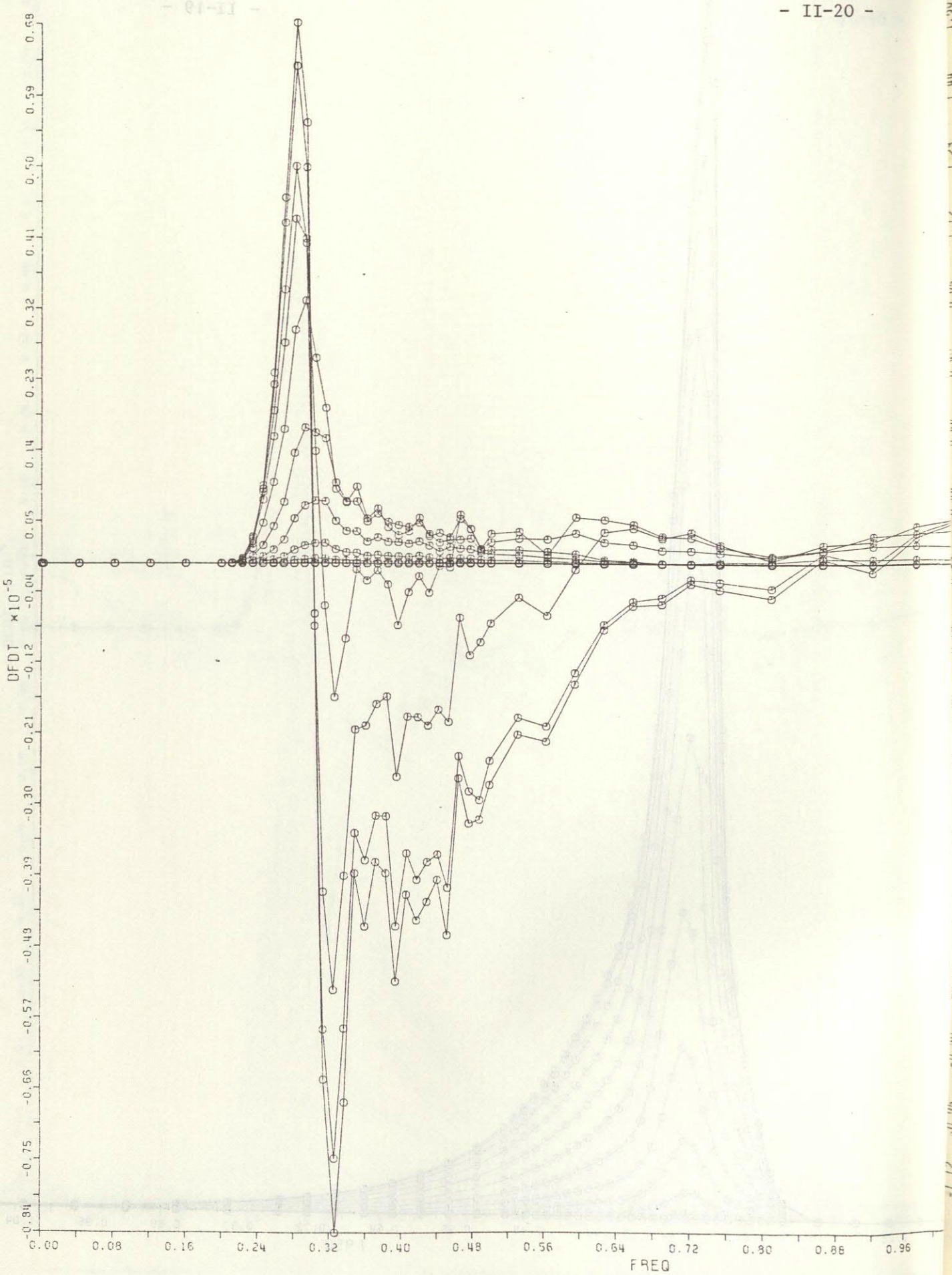

Fig. 4b Two-dimensional transfer rate $S_{nl}(f,\Theta)$. Directional increments are 15^{o}.

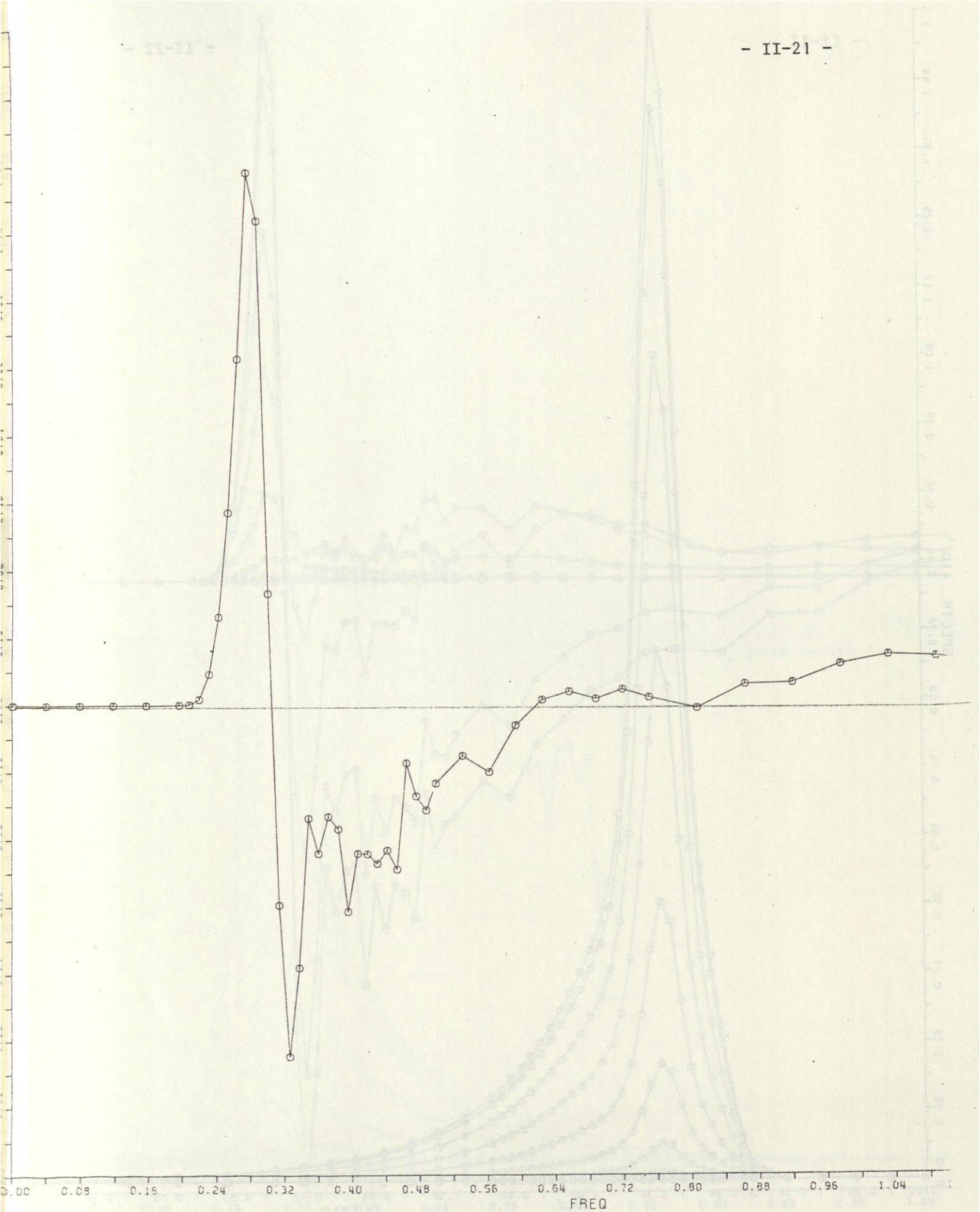

Fig. 4c One-dimensional transfer rate $S_{nl}(f) = \int S_{nl}(f,\theta)d\theta$.

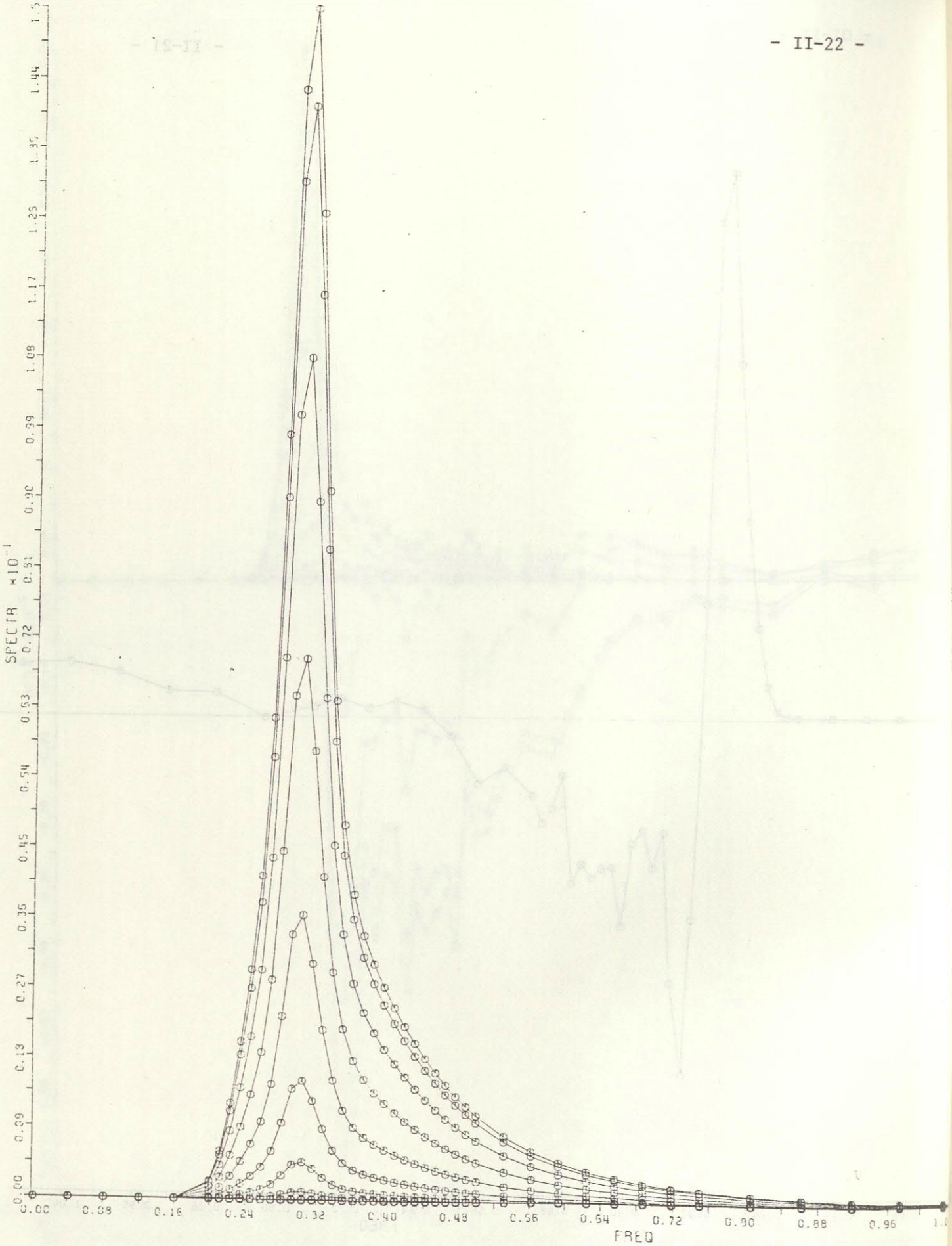

Fig. 5 a Mean JONSWAP spectrum with $\cos^{10}(\Theta/2)$ spreading factor. Two-dimensional spectrum $E(f,\Theta)$. Directional increments are 15^{o}.

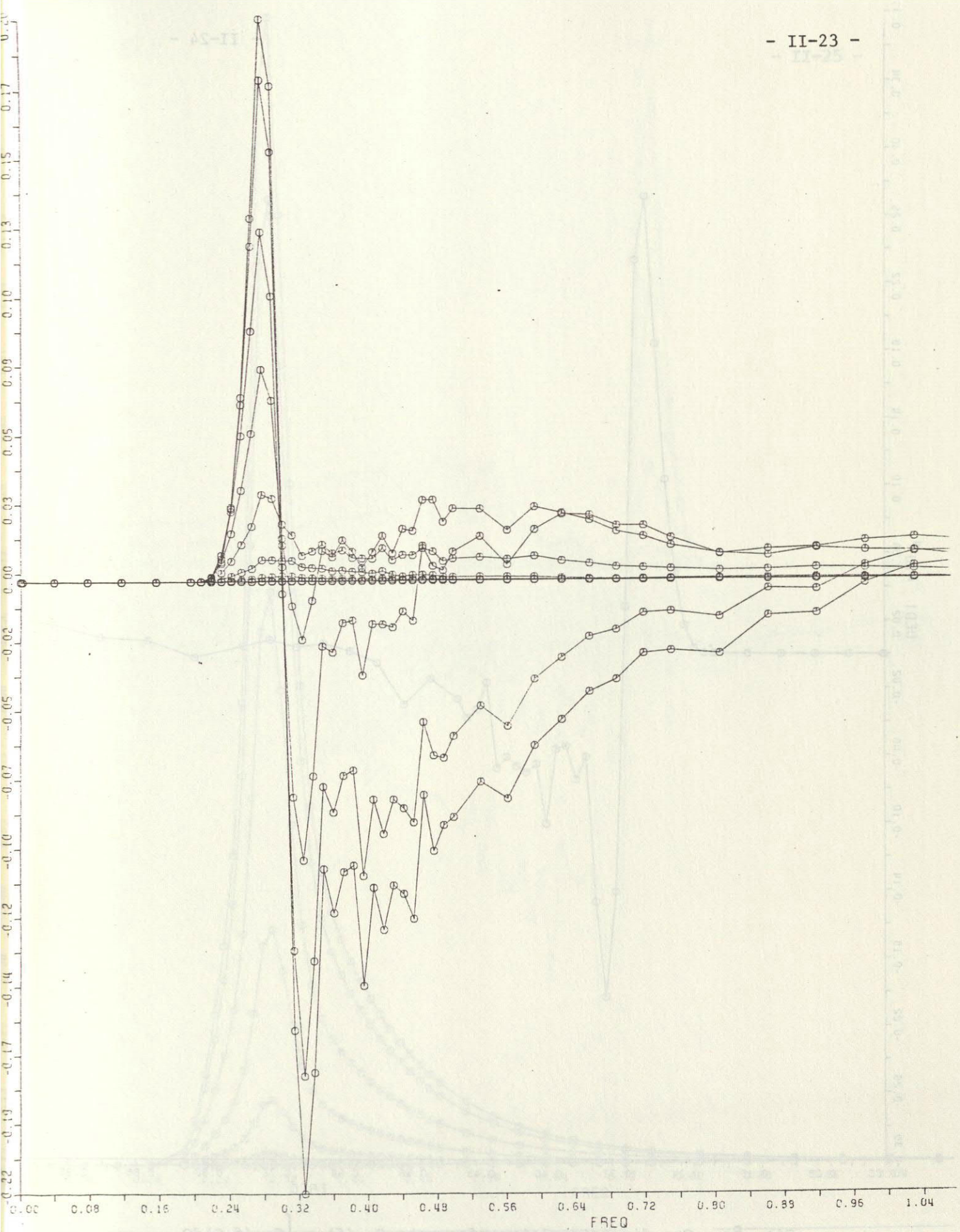

Fig. 5b Two-dimensional transfer rate $S_{nl}(f,\theta)$. Directional increments are 15^{o}.

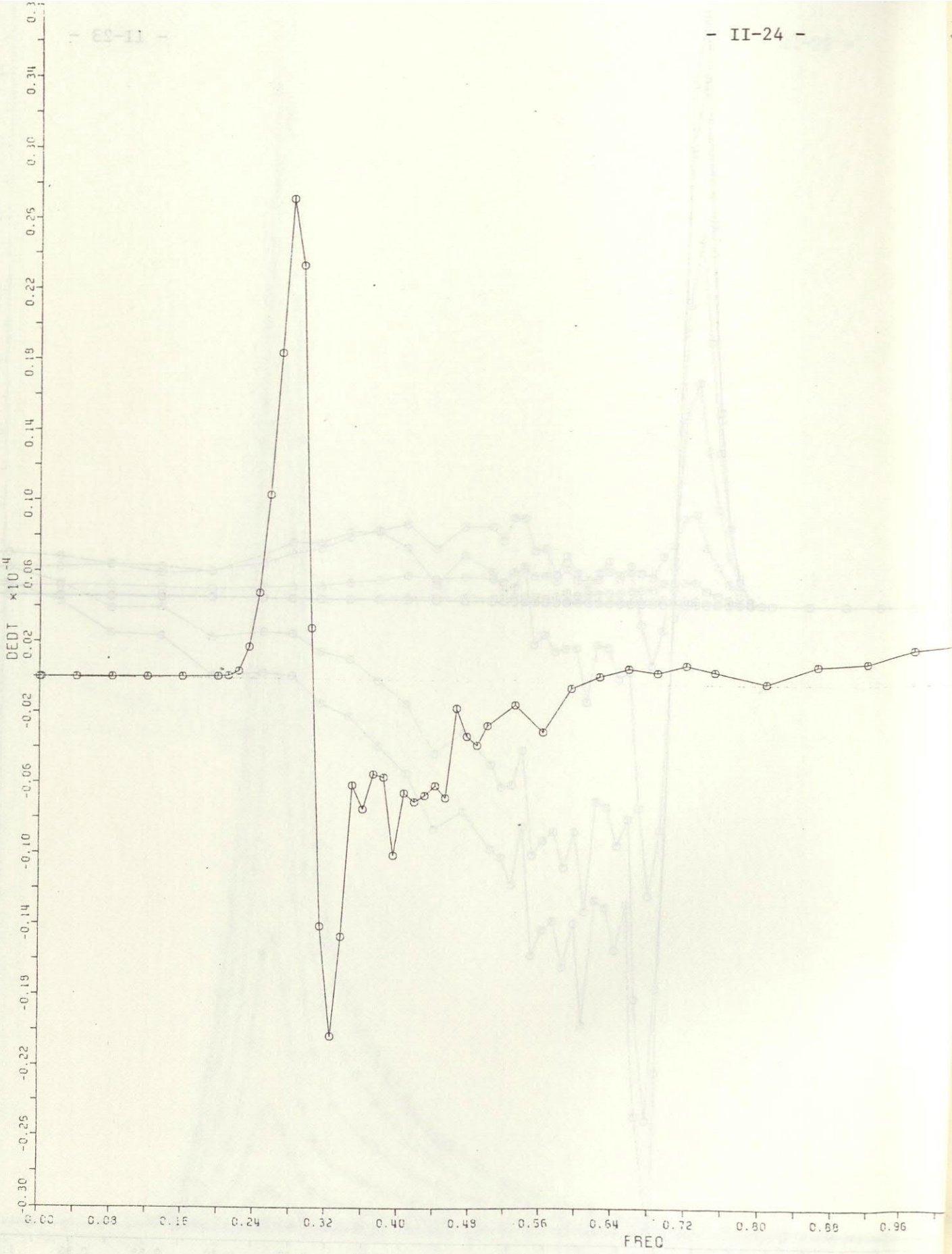

Fig. 5c One-dimensional transfer rate $S_{nl}(f) = \int S_{nl}(f,\theta)d\theta$.

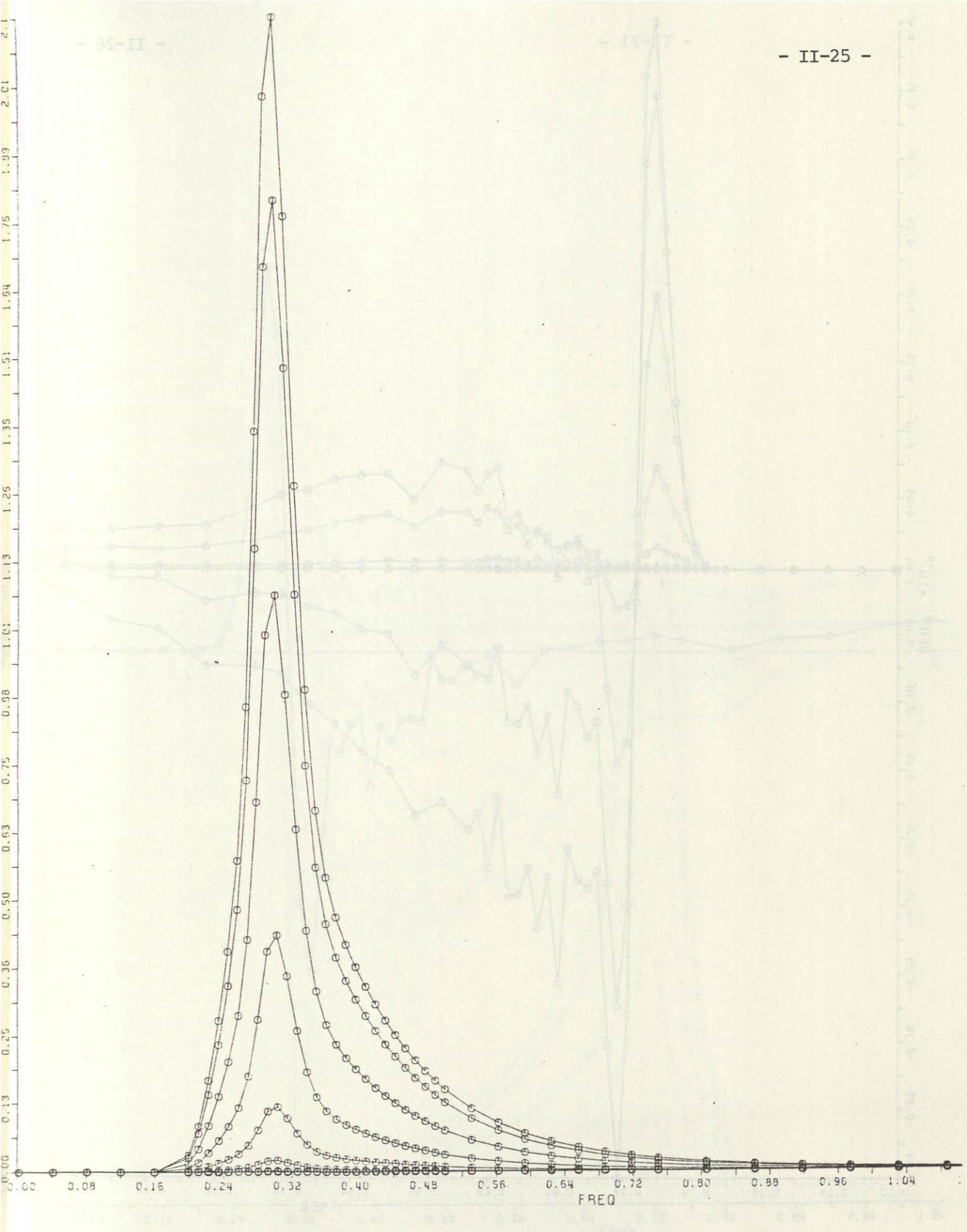

Fig. 6a Mean JONSWAP spectrum with $\cos^{20}(\theta/2)$ spreading factor. Two-dimensional spectrum $E(f,\theta)$. Directional increments are 15°.

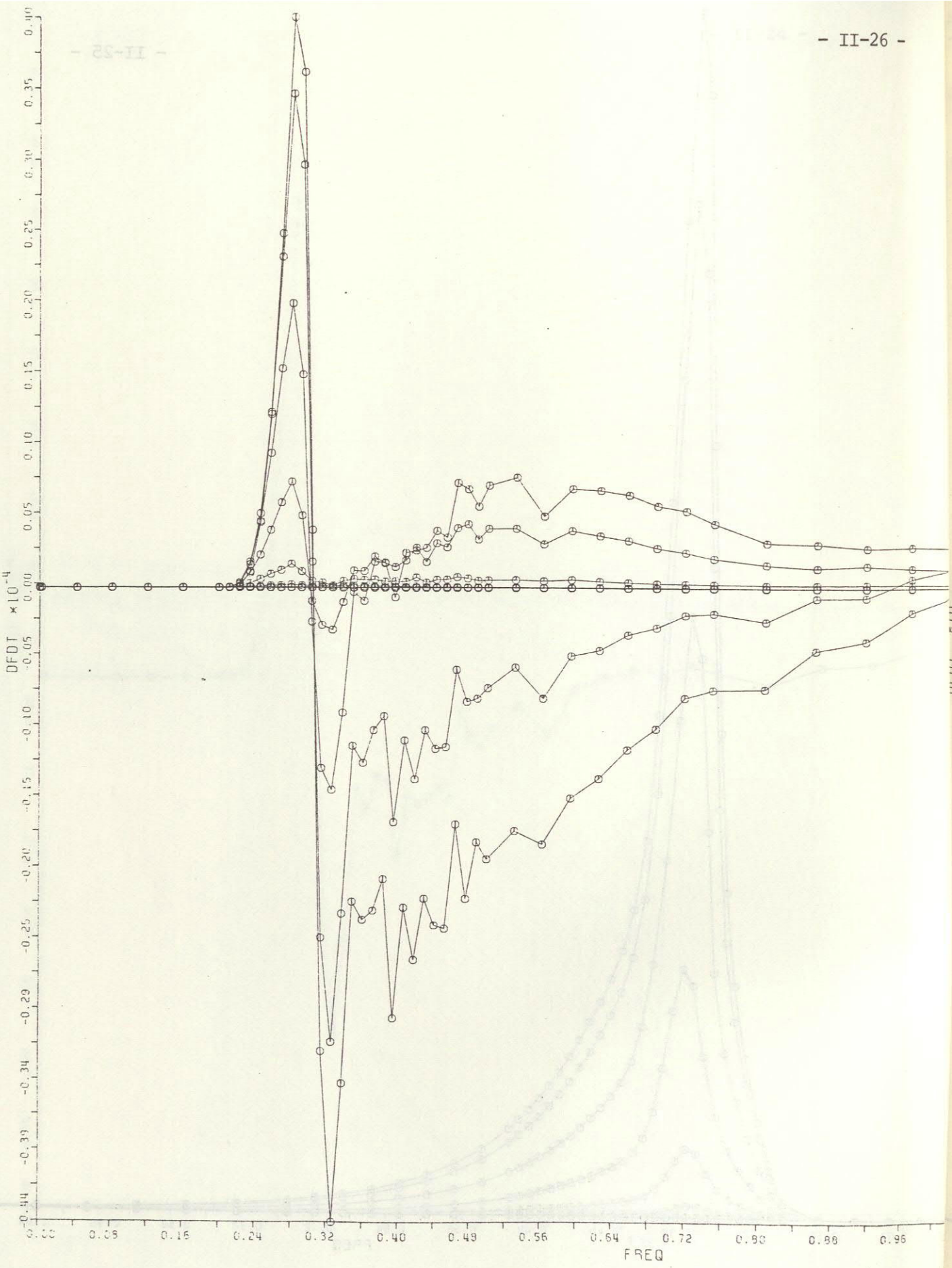

Fig. 6 b Two-dimensional transfer rate $S_{nl}(f,\Theta)$. Directional increments are 15°.

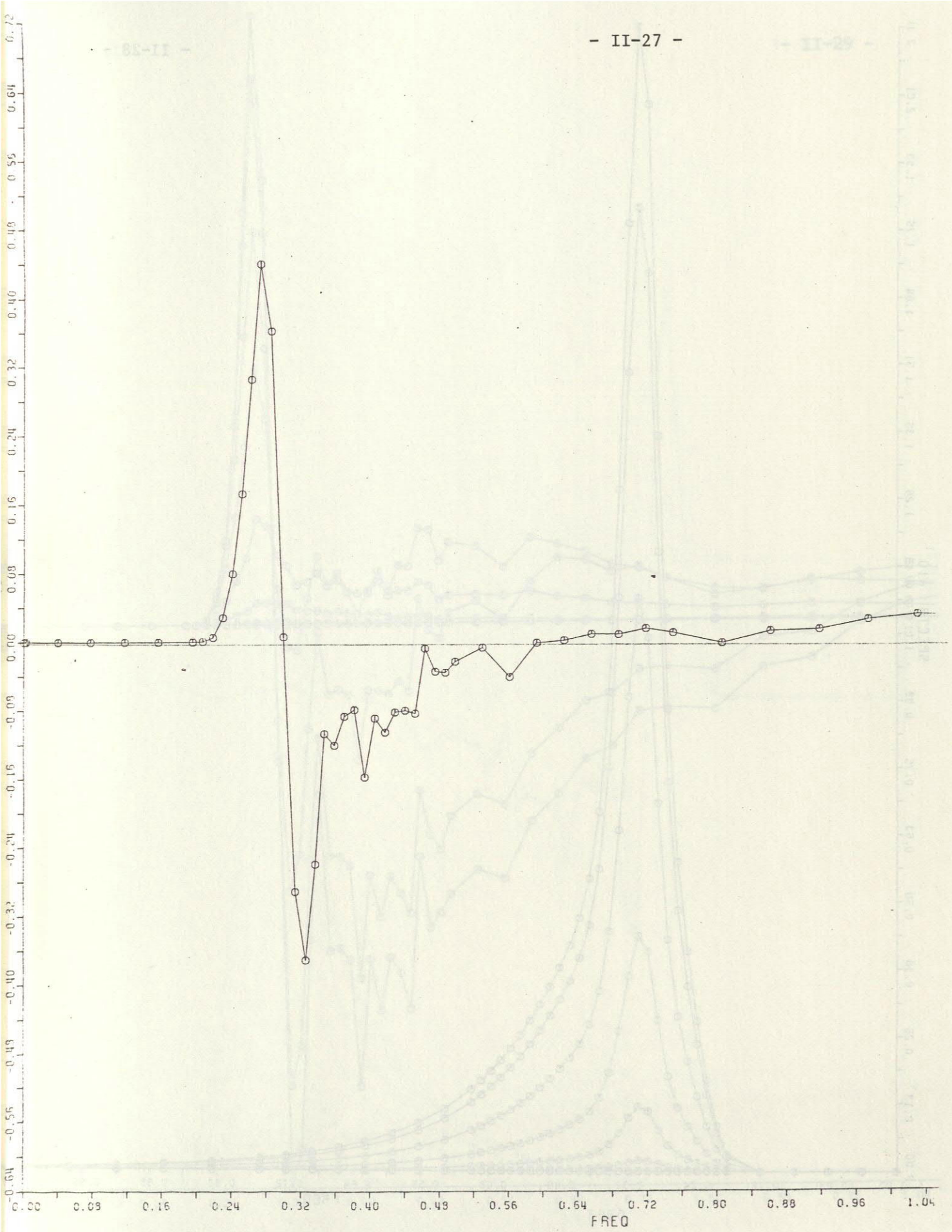

Fig. 6c One-dimensional transfer rate $S_{nl}(f) = \int S_{nl}(f,\theta)d\theta$.

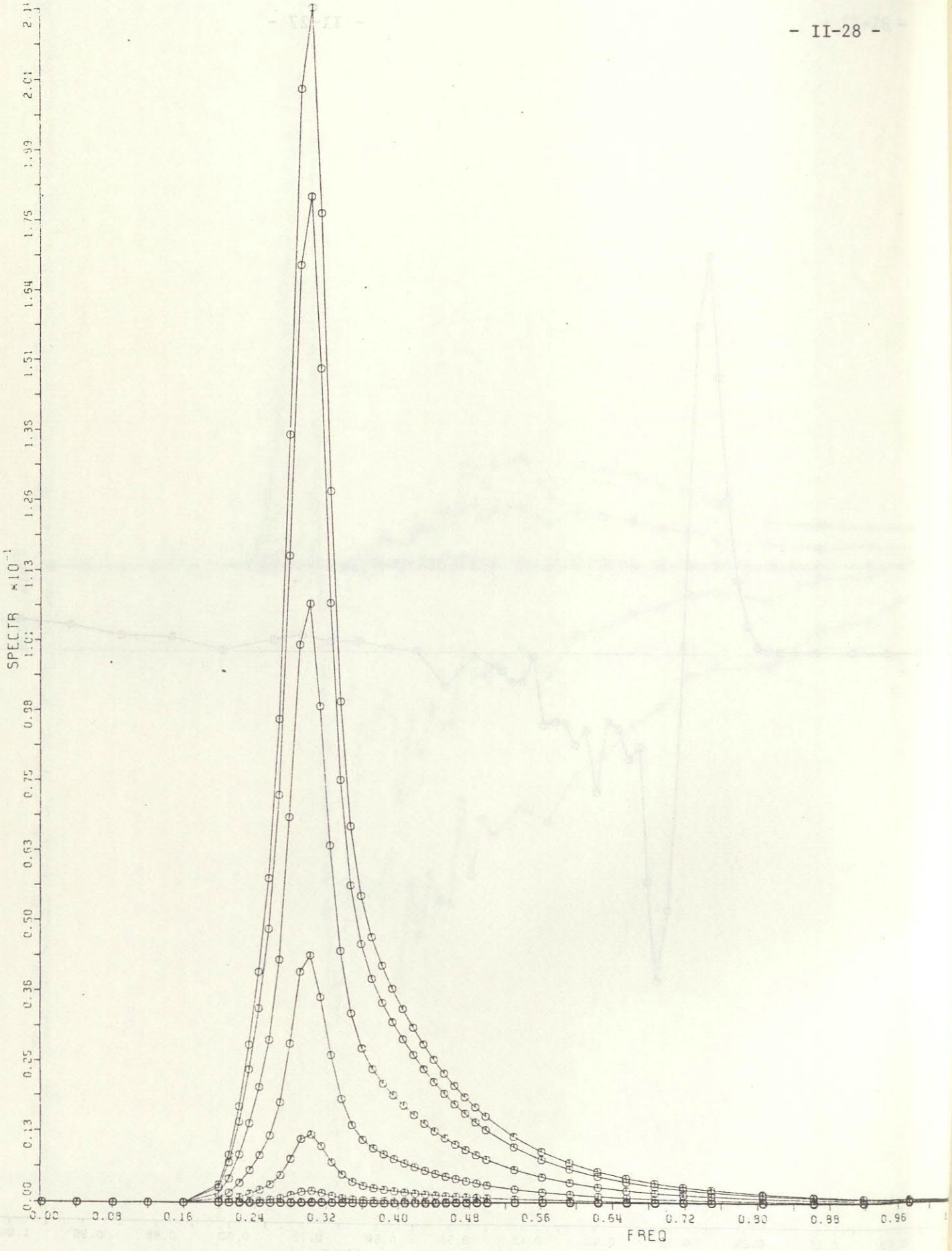

Fig. 7a Mean JONSWAP spectrum, but with σ_b = 0.07 instead of 0.09. Spreading function: $\cos^2\theta$. Two-dimensional spectrum $E(f,\theta)$. Directional increments are 15^o.

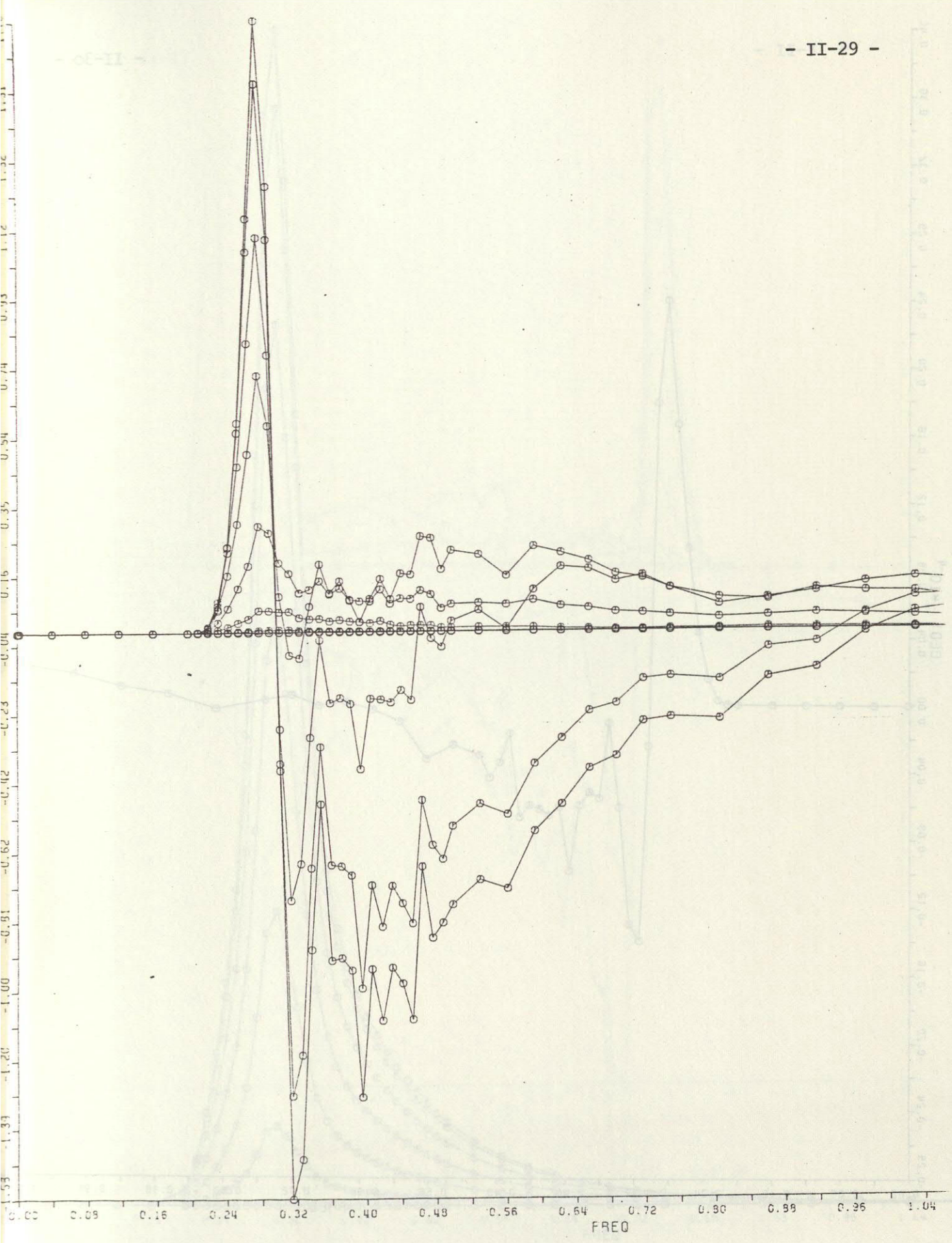

Fig. 7b Two-dimensional transfer rate $S_{nl}(f,\Theta)$. Directional increments are 15^{o}.

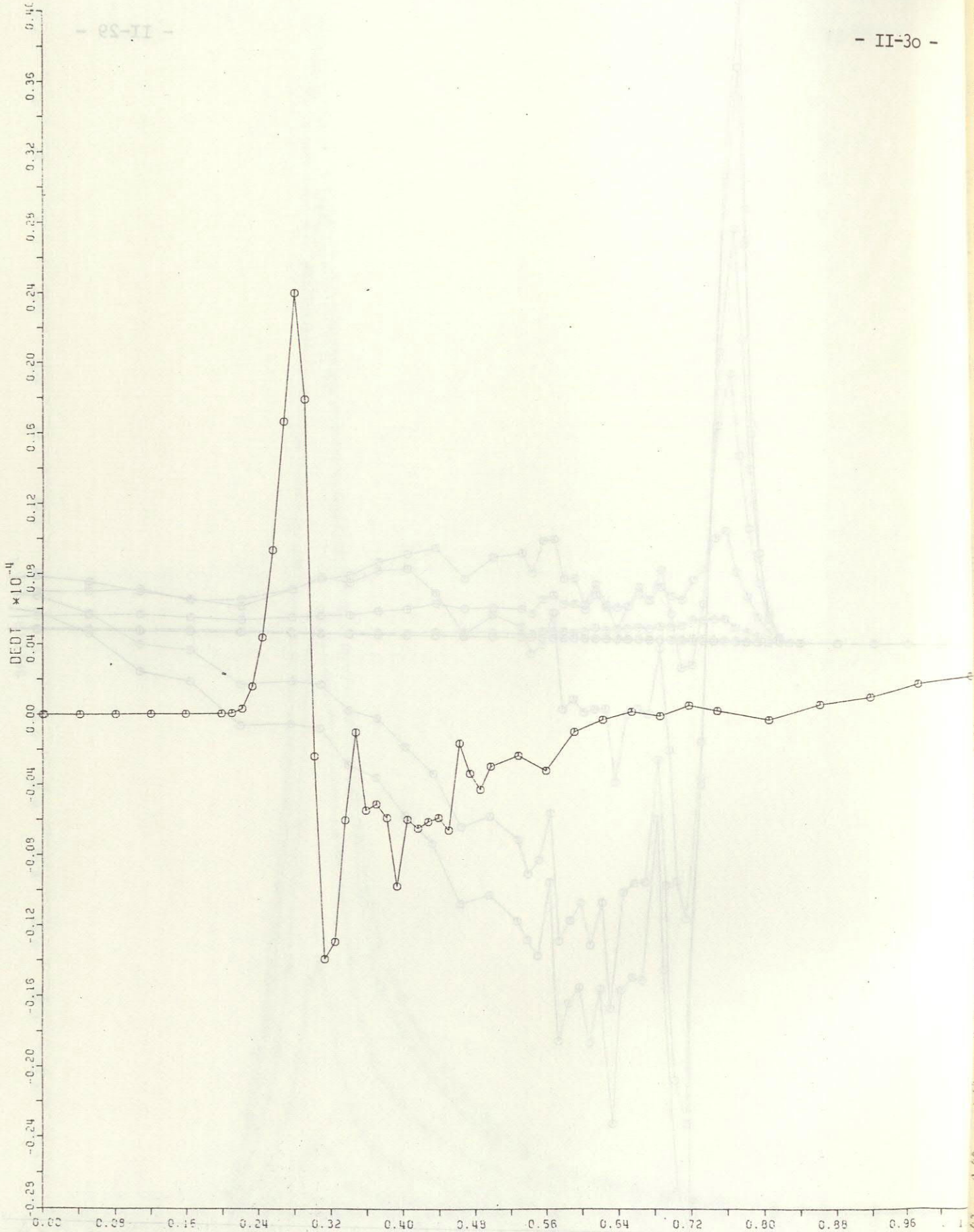

Fig. 7c One-dimensional transfer rate $S_{nl}(f) = \int S_{nl}(f,\theta)\,d\theta$.

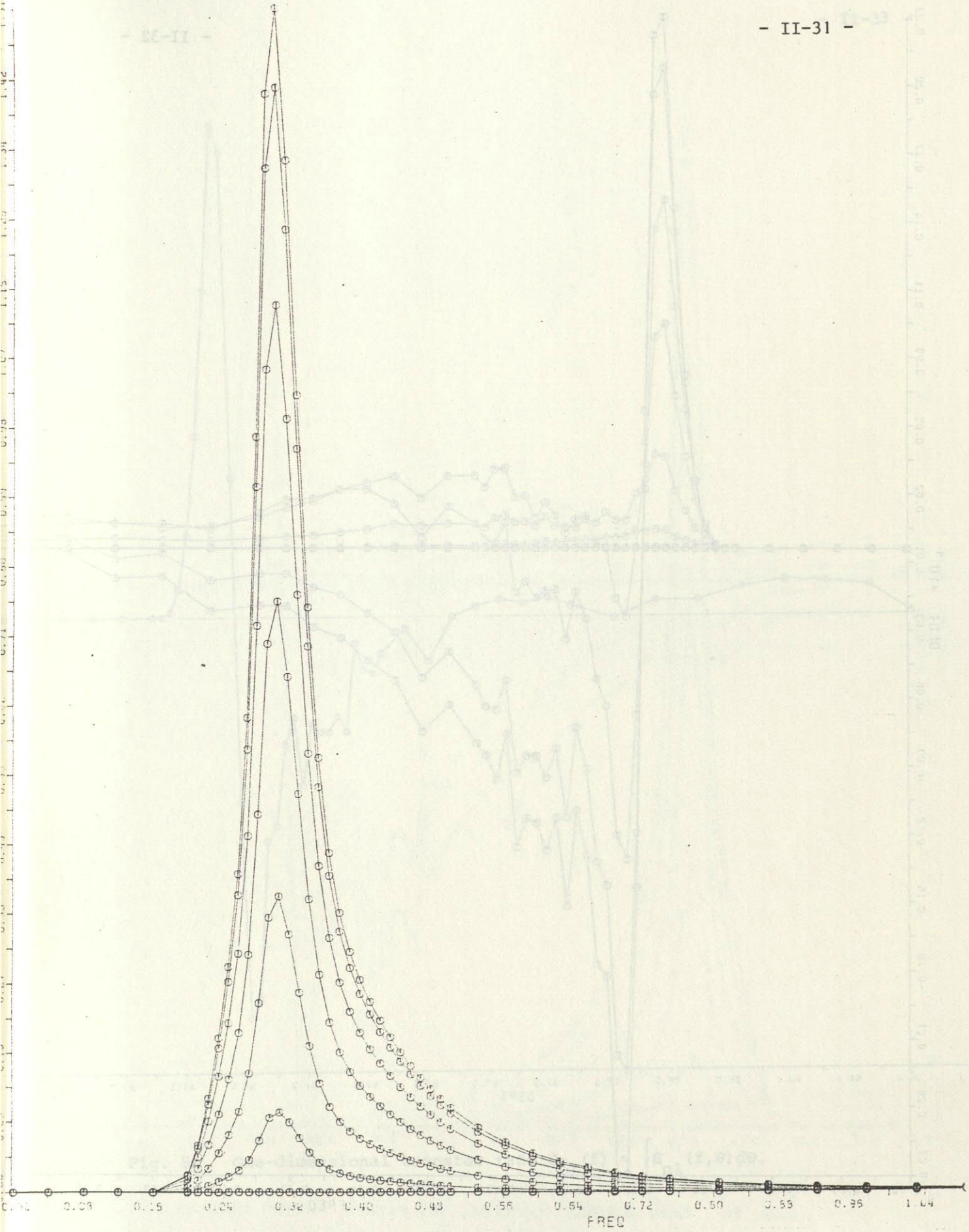

Fig. 8a Mean JONSWAP spectrum, but with σ_b = 0.11 instead of 0.09. Spreading function: $\cos^2\theta$. Two-dimensional spectrum $E(f,\theta)$. Directional increments are 15^o.

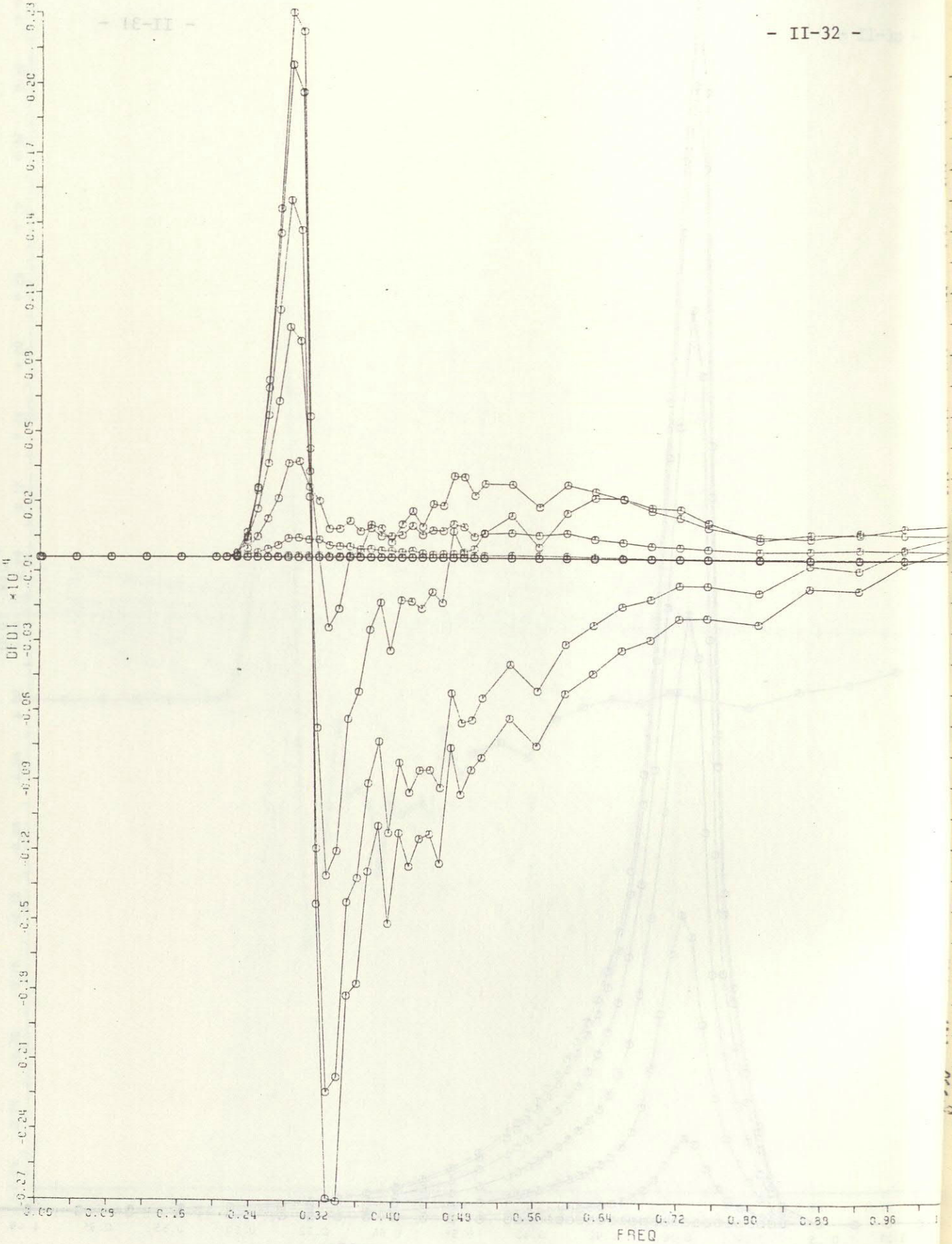

Fig. 8b Two-dimensional transfer rate $S_{nl}(f,\theta)$. Directional increments are 15^{o}.

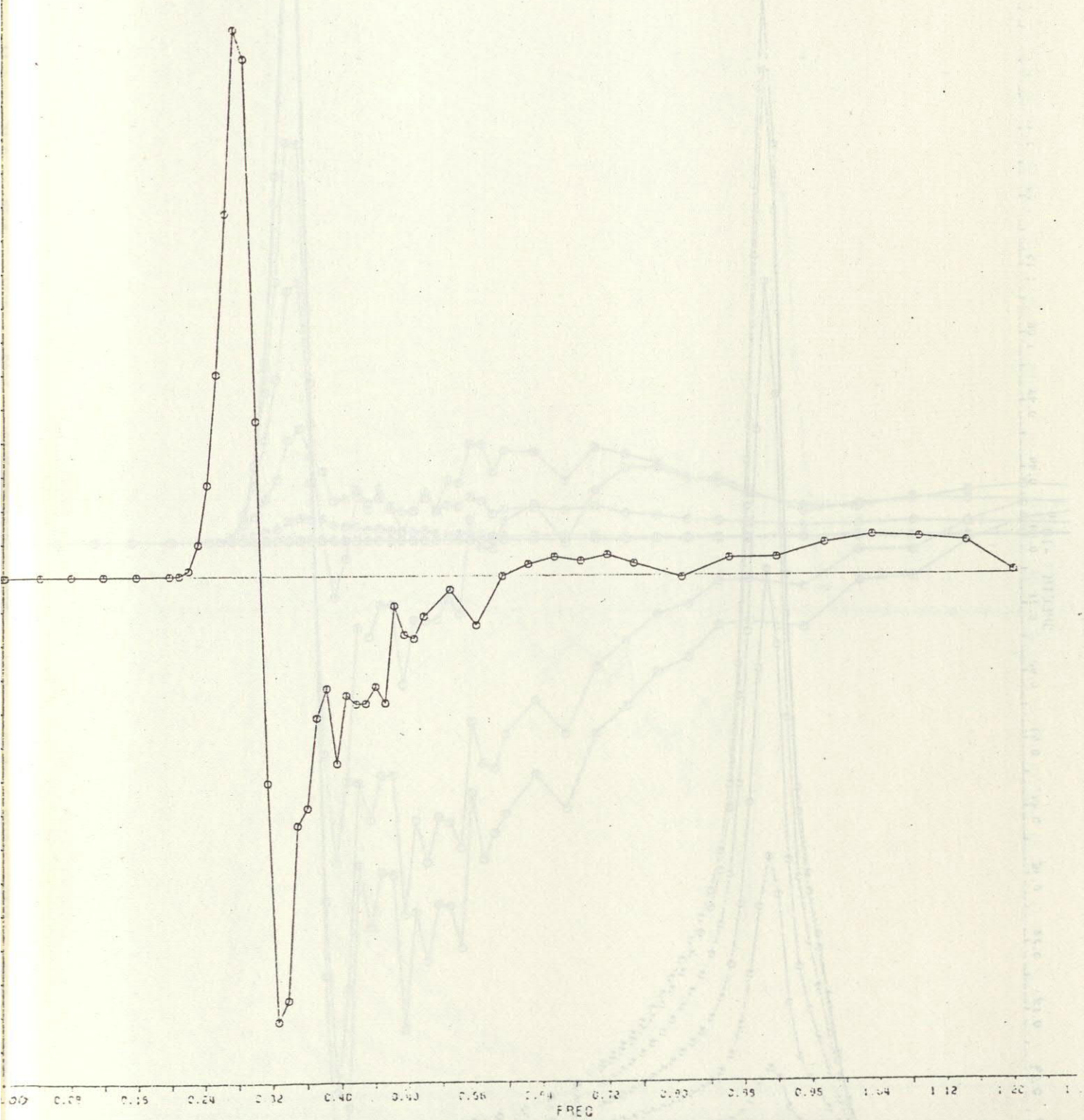

Fig. 8c One-dimensional transfer rate $S_{nl}(f) = \int S_{nl}(f,\Theta)d\Theta$.

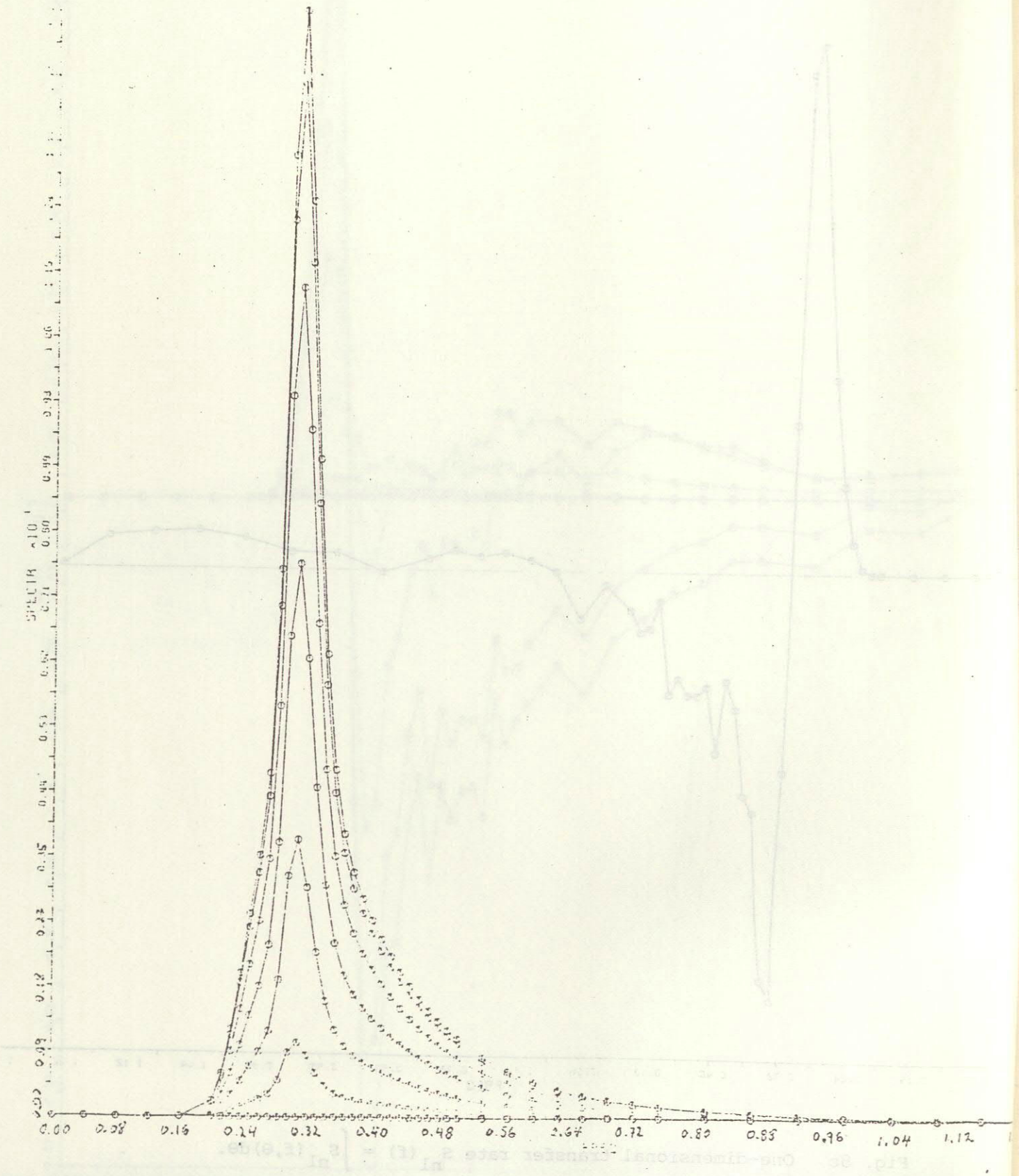

Fig. 9a Mean JONSWAP spectrum, but with σ_a = 0.05 instead of 0.07. Spreading function: $\cos^2\theta$. Two-dimensional spectrum $E(f,\theta)$. Directional increments are 15°.

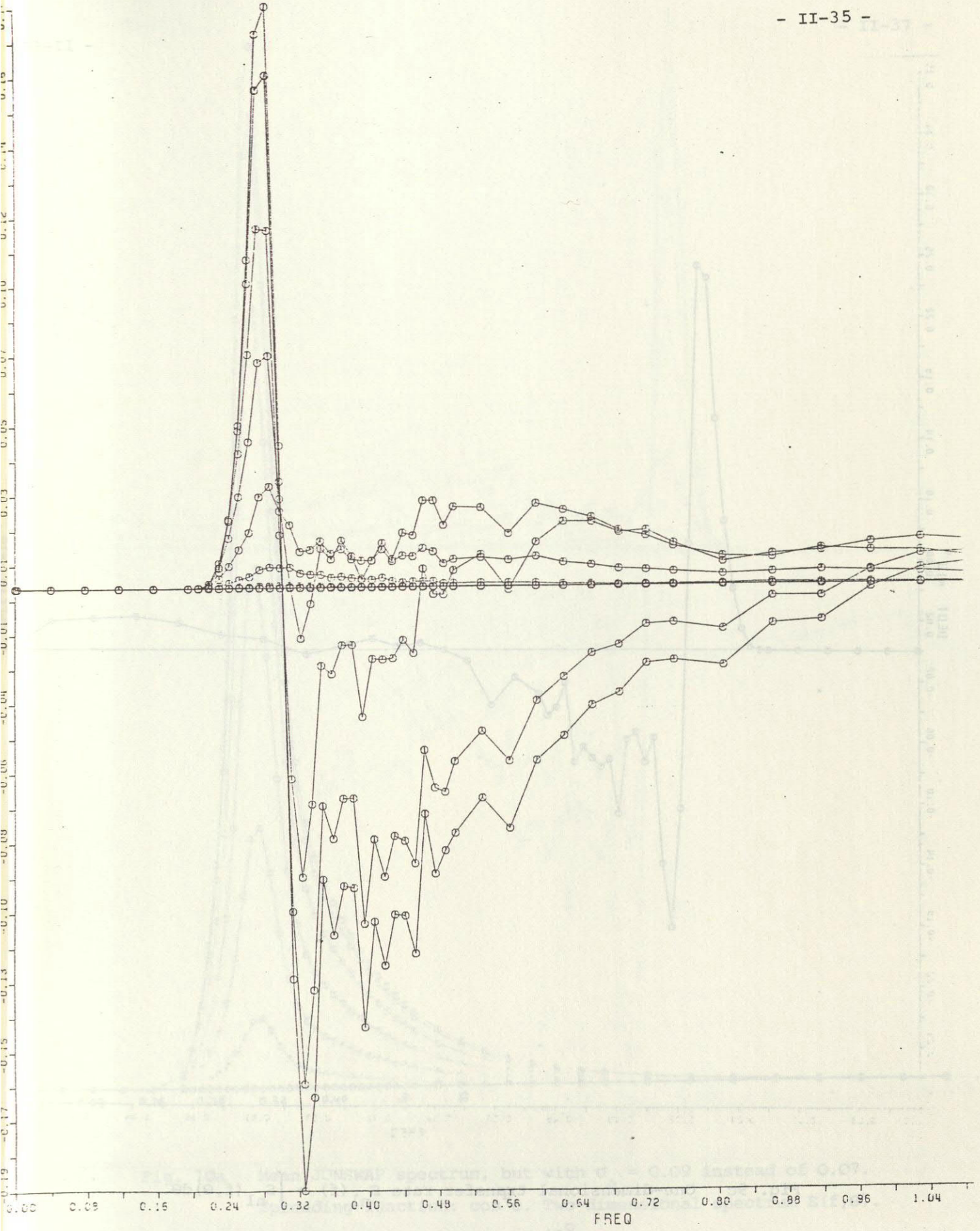

Fig. 9b Two-dimensional transfer rate $S_{nl}(f,\Theta)$. Directional increments are 15^{o}.

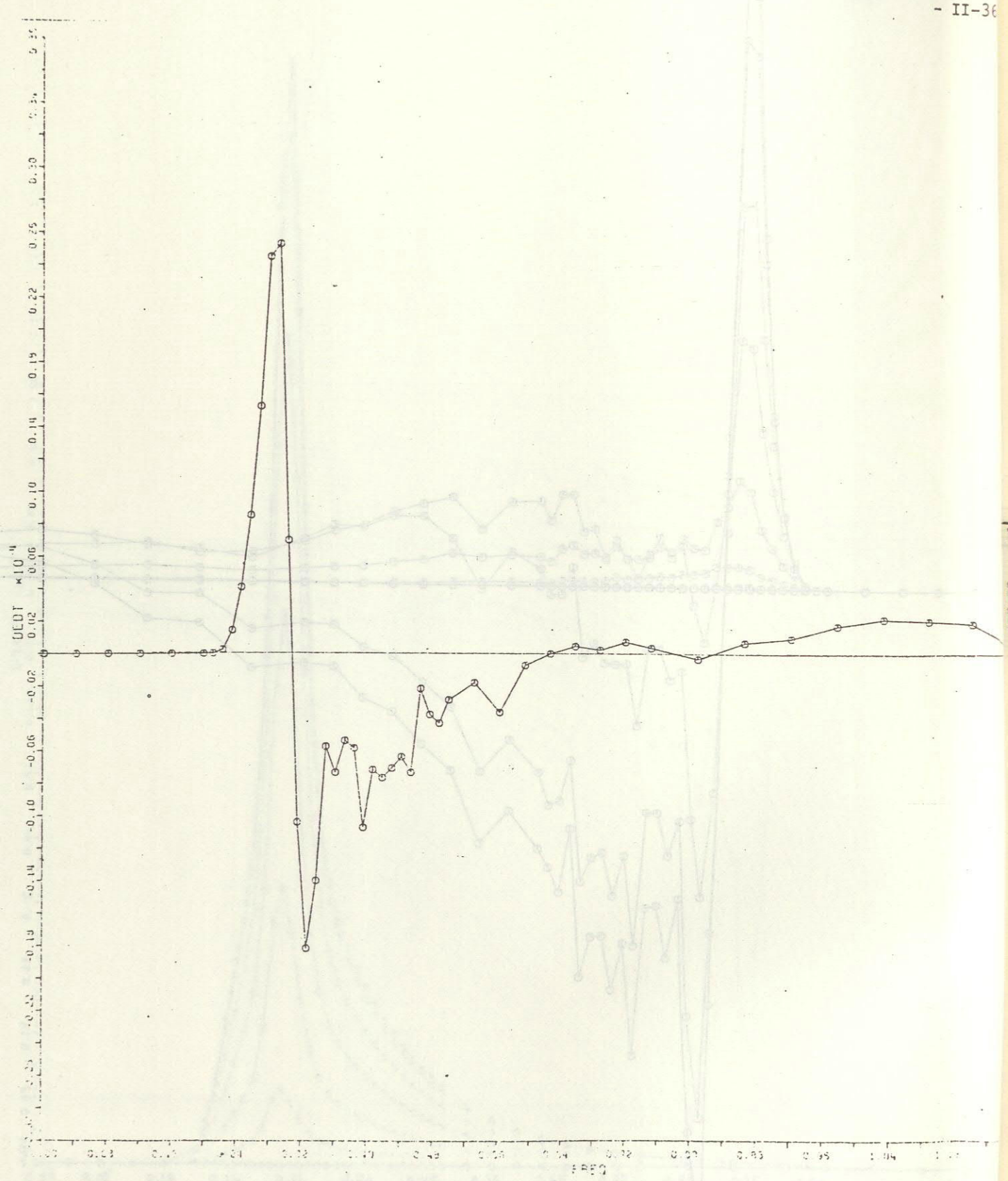

Fig. 9c One-dimensional transfer rate $S_{nl}(f) = \int S_{nl}(f,\theta)d\theta$.

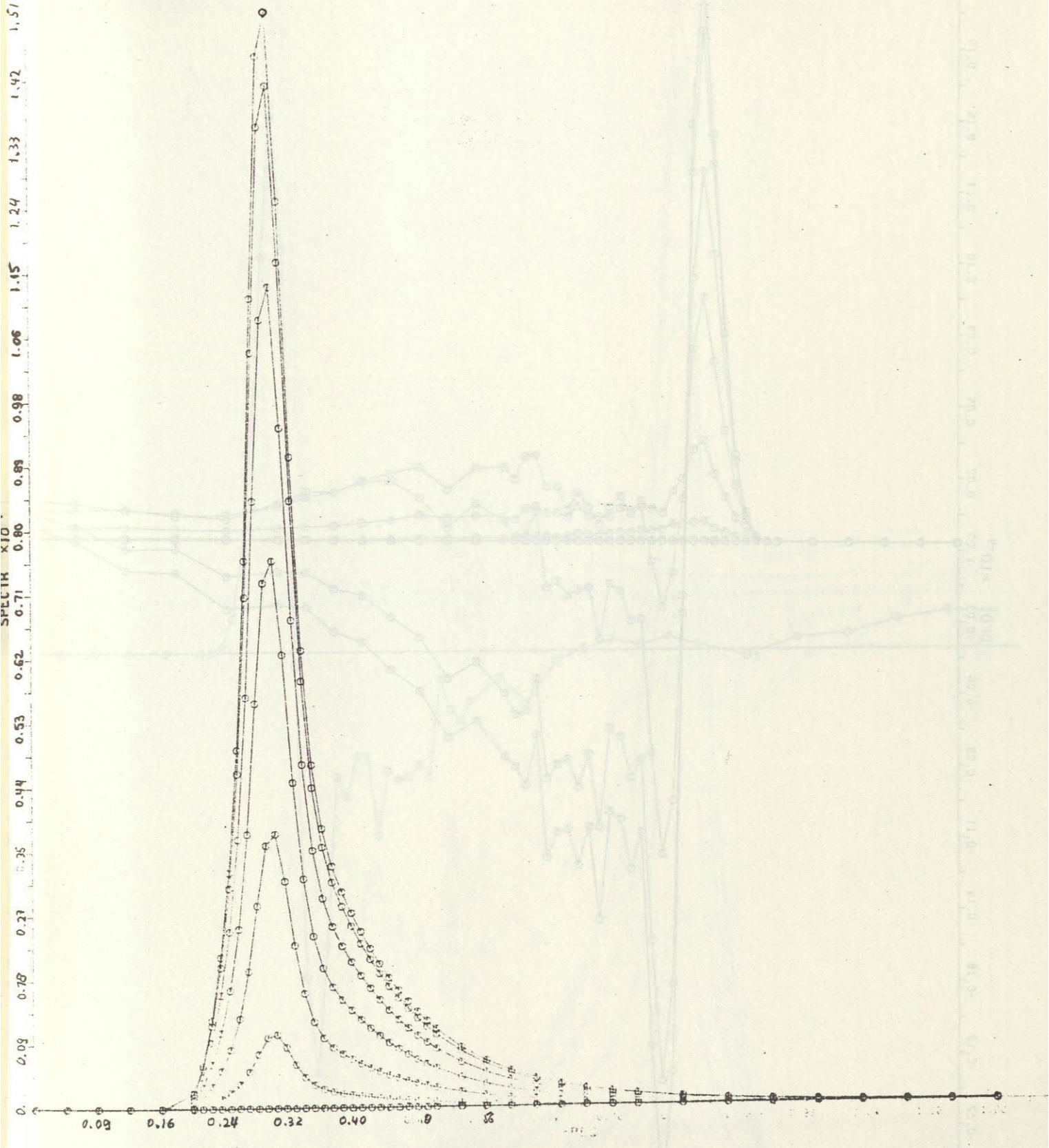

Fig. 10a Mean JONSWAP spectrum, but with σ_a = 0.09 instead of 0.07. Spreading function: $\cos^2\theta$. Two-dimensional spectrum $E(f,\theta)$. Directional increments are 15°.

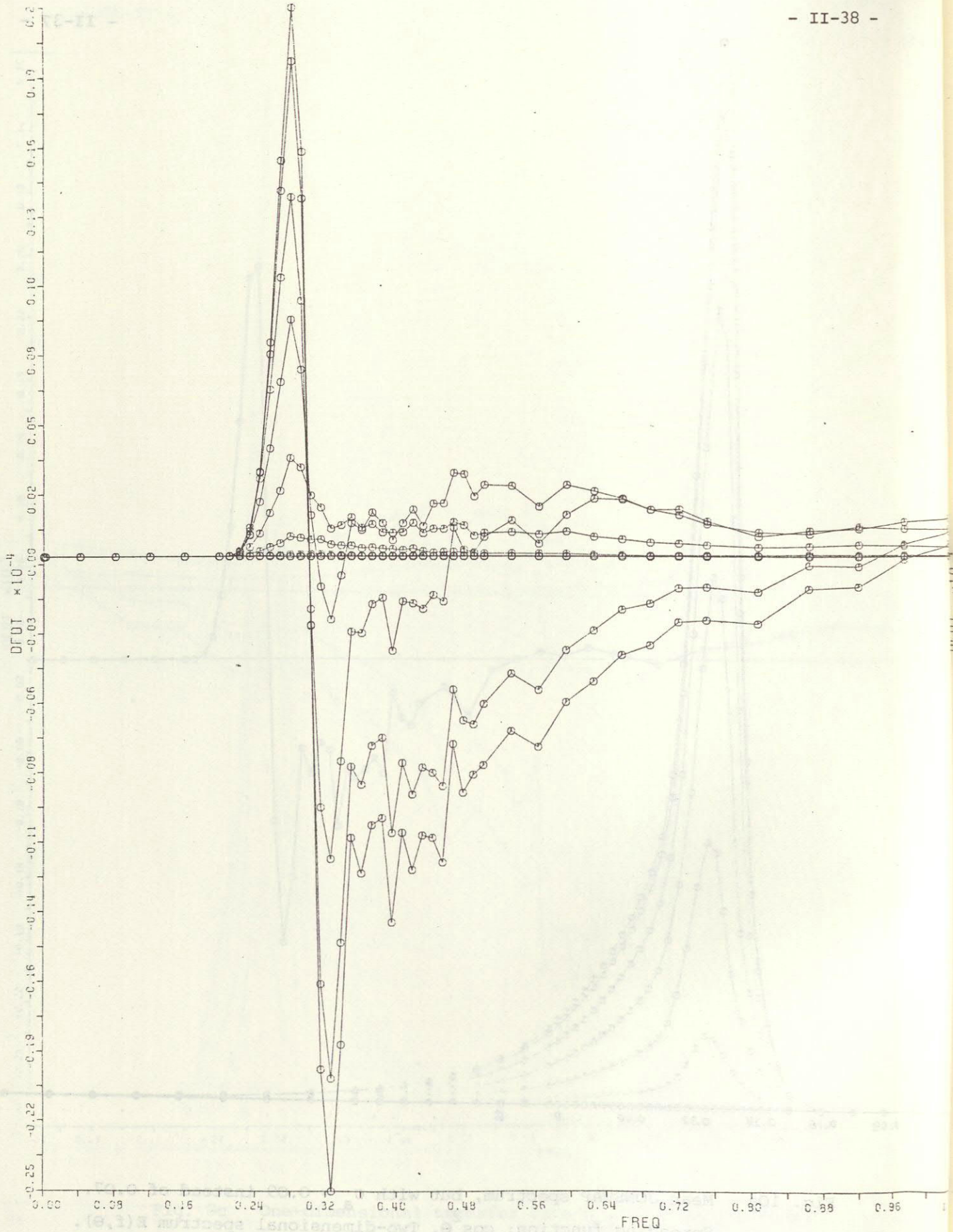

Fig. 10b Two-dimensional transfer rate $S_{nl}(f,\theta)$. Directional increments are 15^{o}.

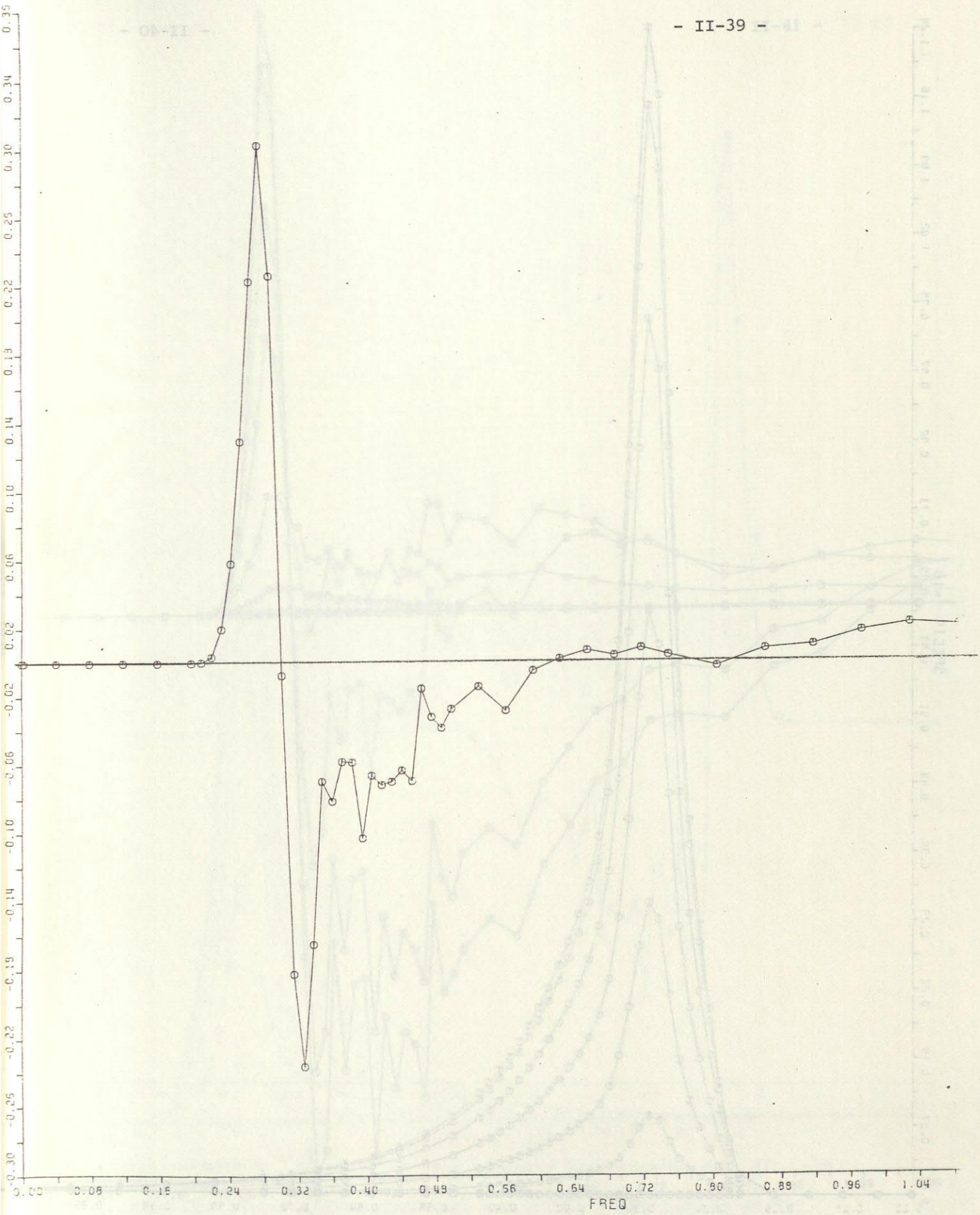

Fig. 10c One-dimensional transfer rate $S_{nl}(f) = \int S_{nl}(f,\theta)d\theta$.

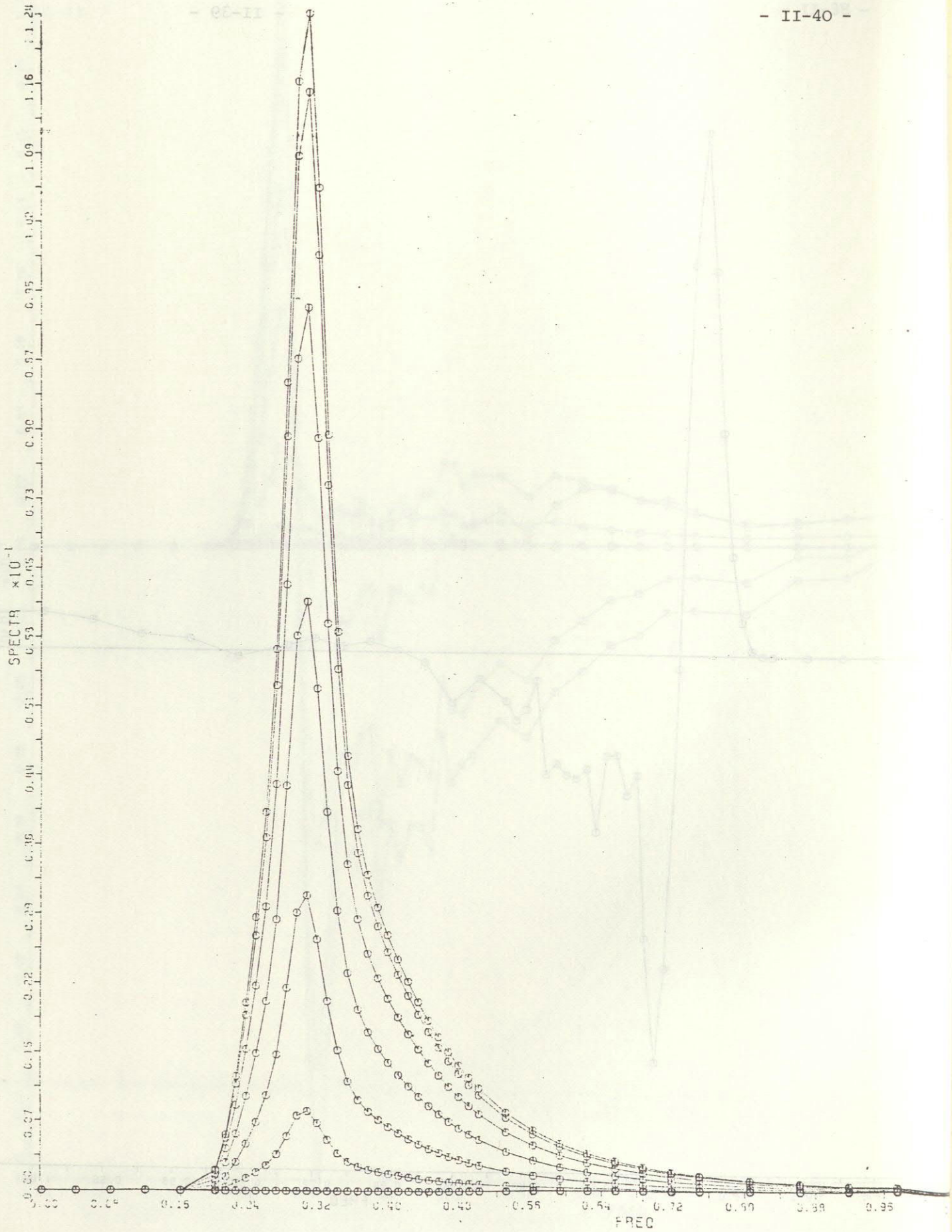

Fig. 11a Mean JONSWAP spectrum, but with $\gamma = 2.7$ instead of 3.3. Spreading function: $\cos^2\theta$. Two-dimensional spectrum $E(f,\theta)$. Directional increments are 15°.

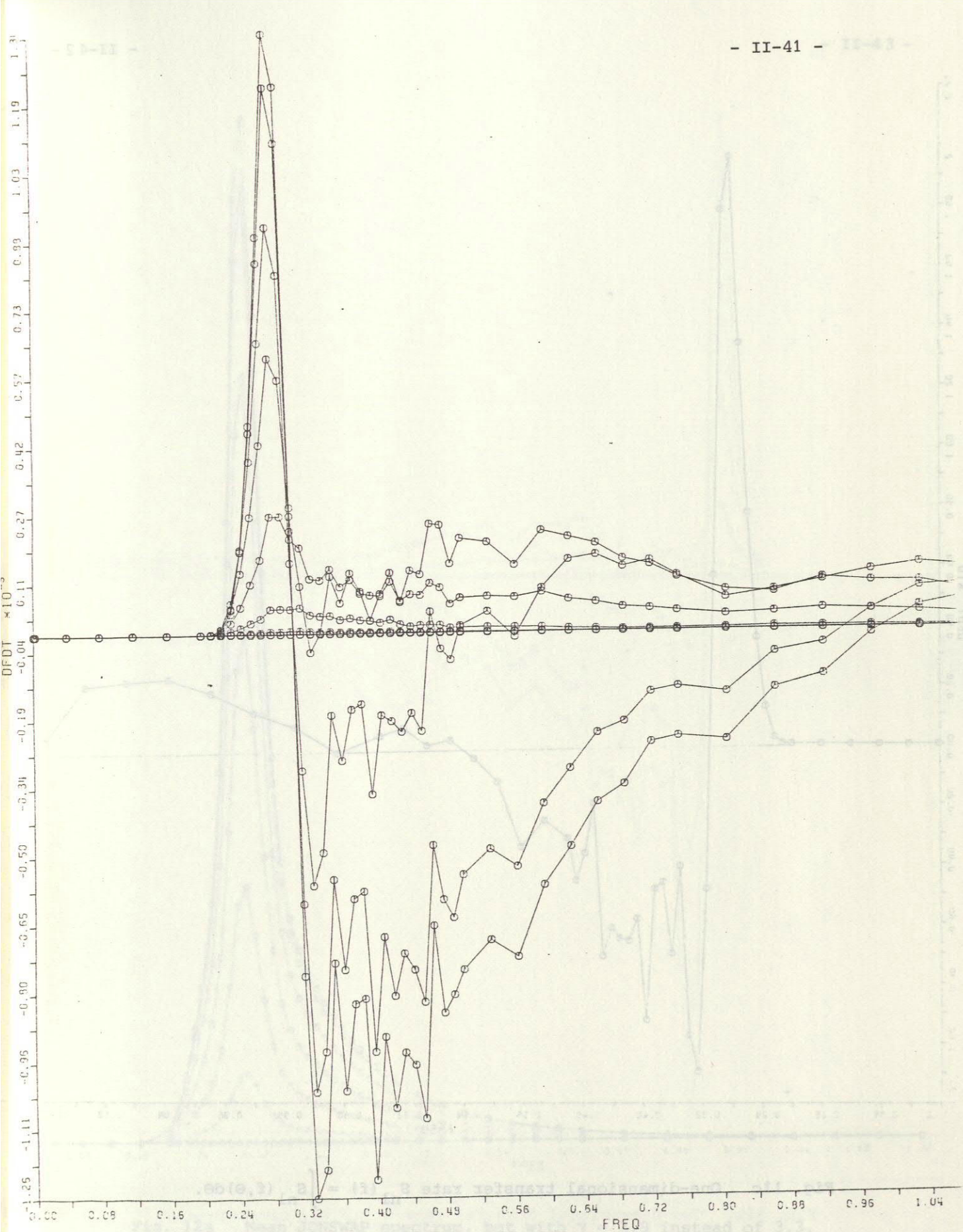

Fig. 11b Two-dimensional transfer rate $S_{nl}(f,\theta)$. Directional increments are 15^{o}.

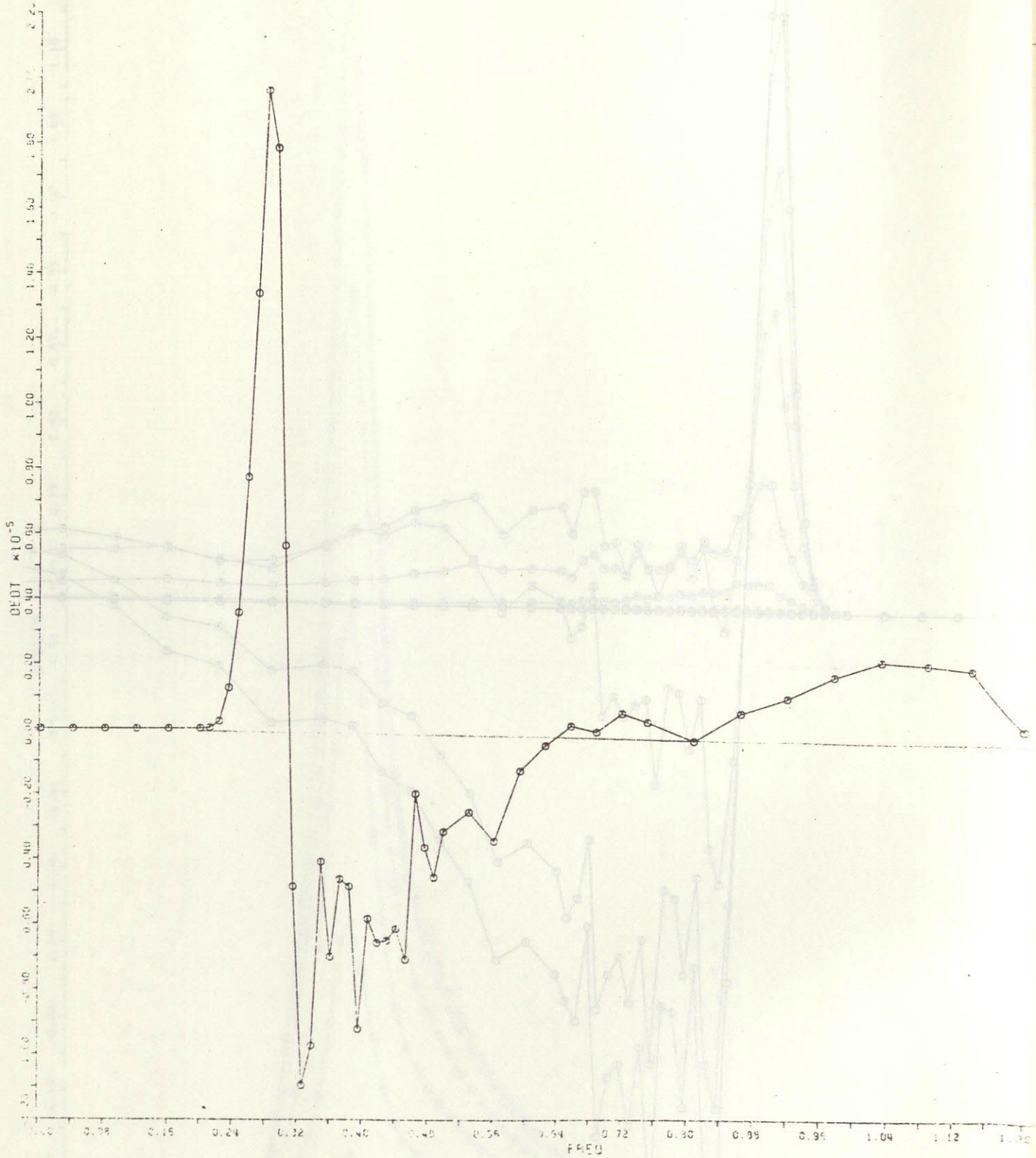

Fig. 11c One-dimensional transfer rate $S_{nl}(f) = \int S_{nl}(f,\theta)d\theta$.

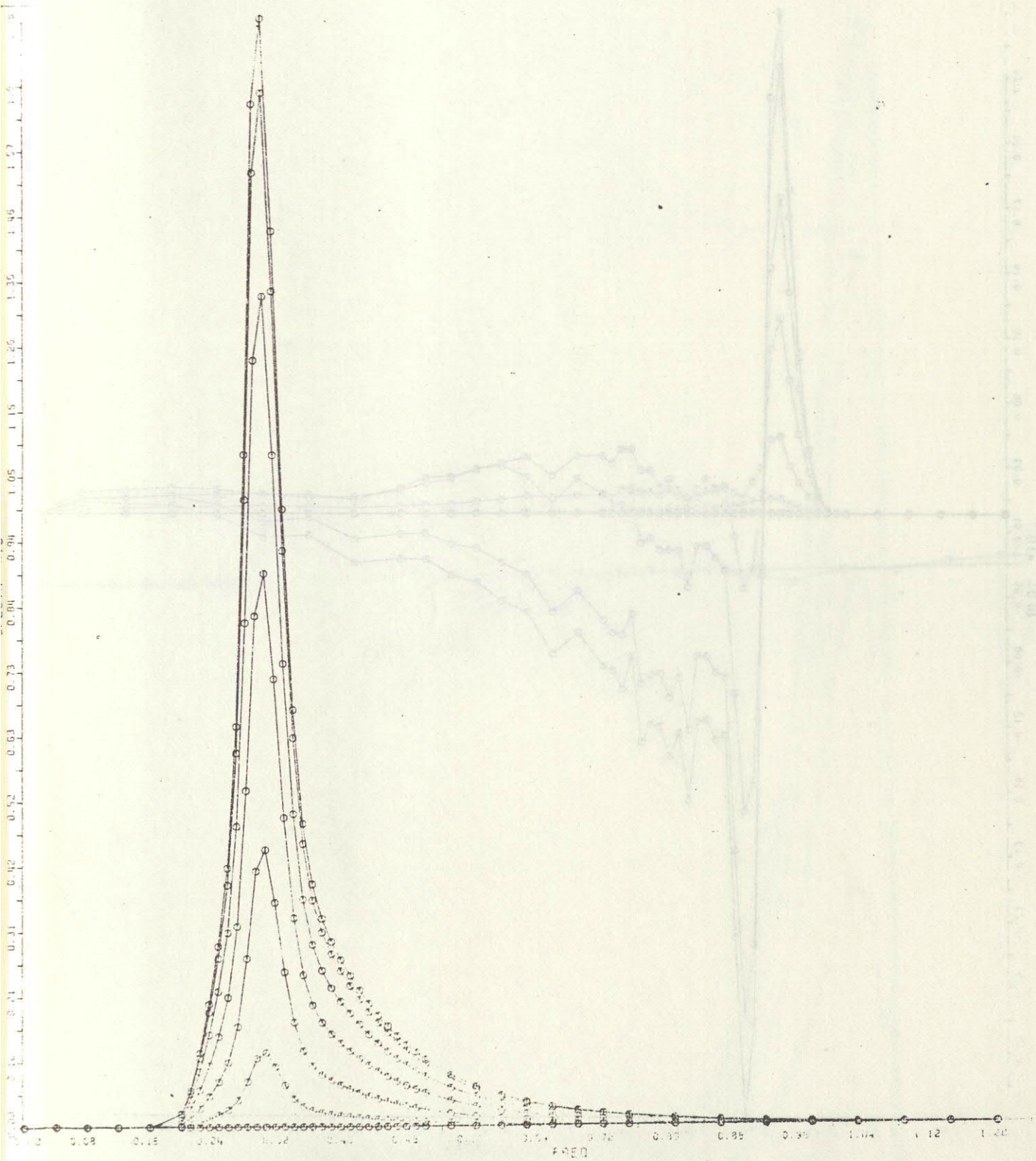

Fig. 12a Mean JONSWAP spectrum, but with $\gamma = 3.9$ instead of 3.3. Spreading function: $\cos^2\theta$. Two-dimensional spectrum $E(f,\theta)$. Directional increments are 15°.

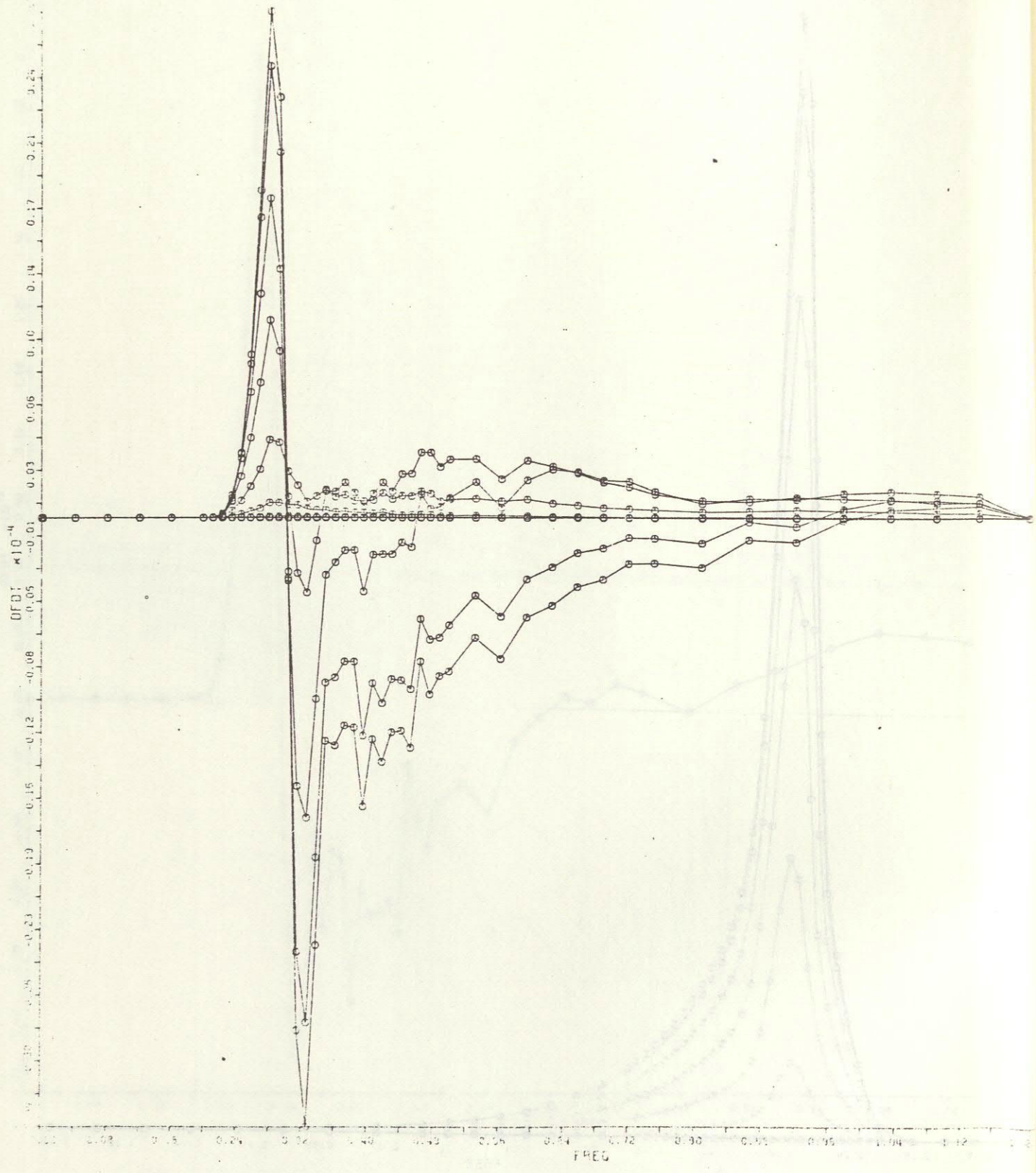

Fig. 12b Two-dimensional transfer rate $S_{nl}(f,\Theta)$. Directional increments are 15^{o}.

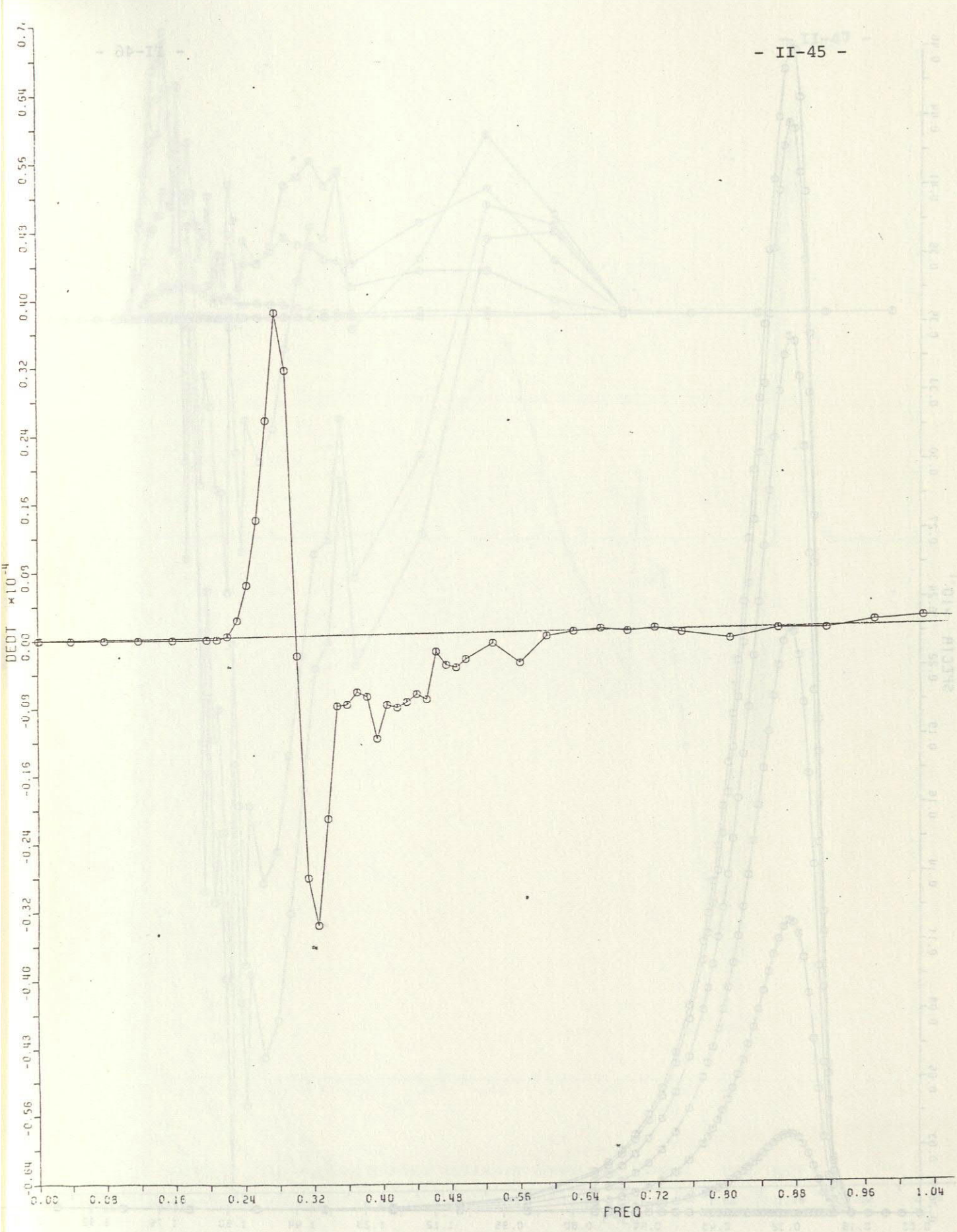

Fig. 12c One-dimensional transfer rate $S_{nl}(f) = \int S_{nl}(f,\theta)d\theta$.

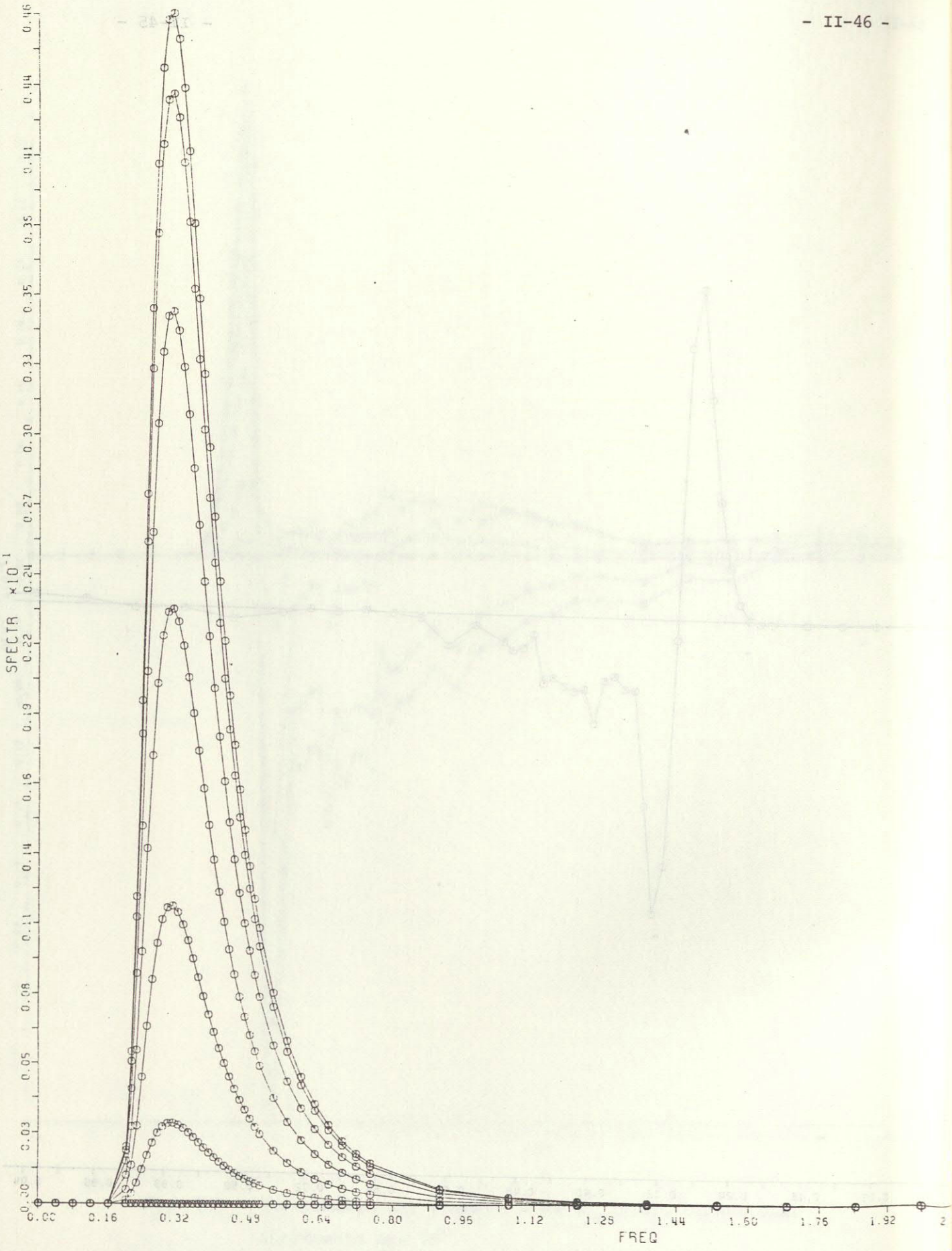

Fig. 13a Pierson-Moskowitz spectrum. Spreading function: $\cos^2\theta$.
Two-dimensional spectrum $E(f,\theta)$. Directional increments 15°.

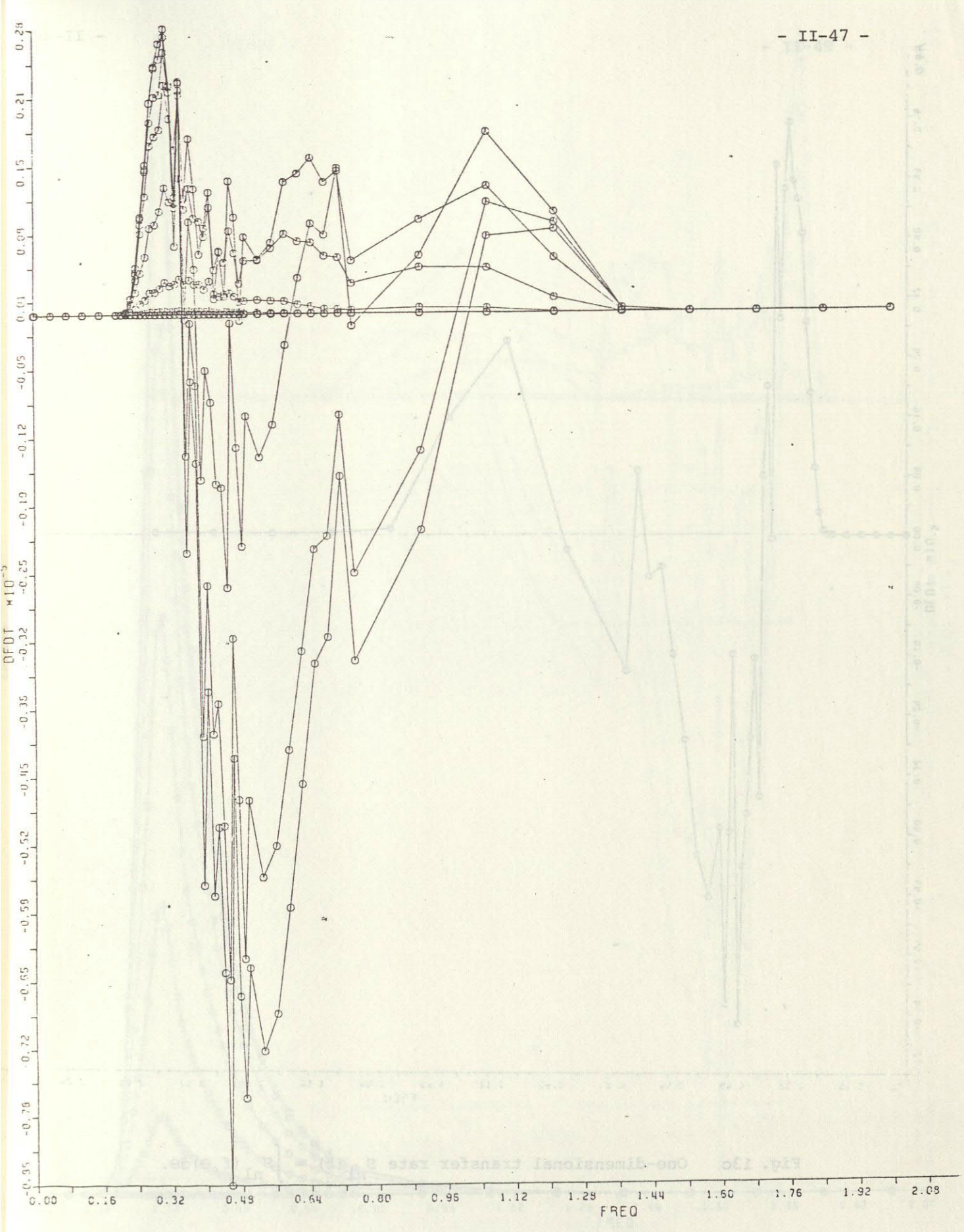

Fig. 13b Two-dimensional transfer rate $S_{nl}(f,\Theta)$. Directional increments are 15°.

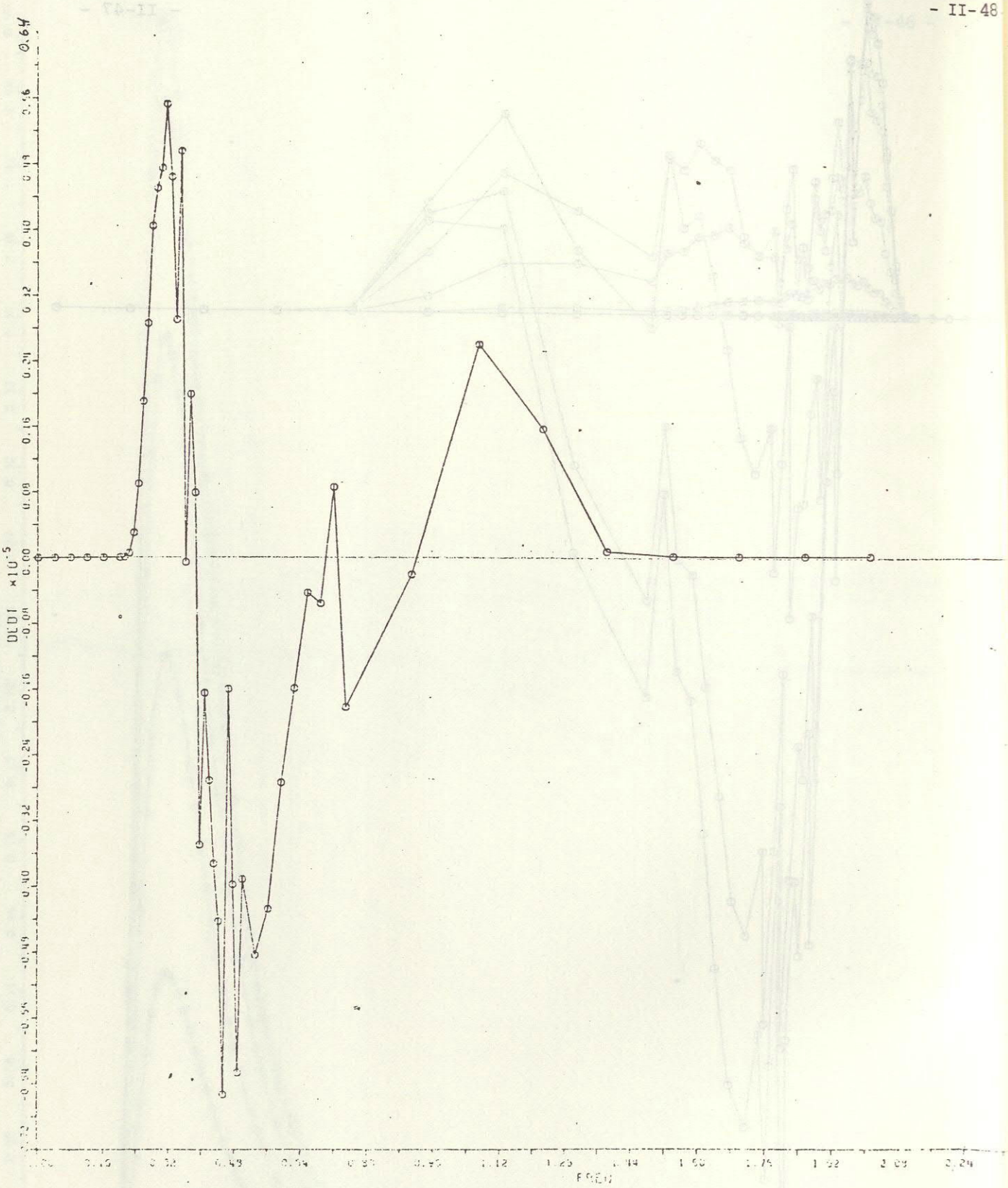

Fig. 13c One-dimensional transfer rate $S_{nl}(f) = \int S_{nl}(f,\theta)d\theta$.

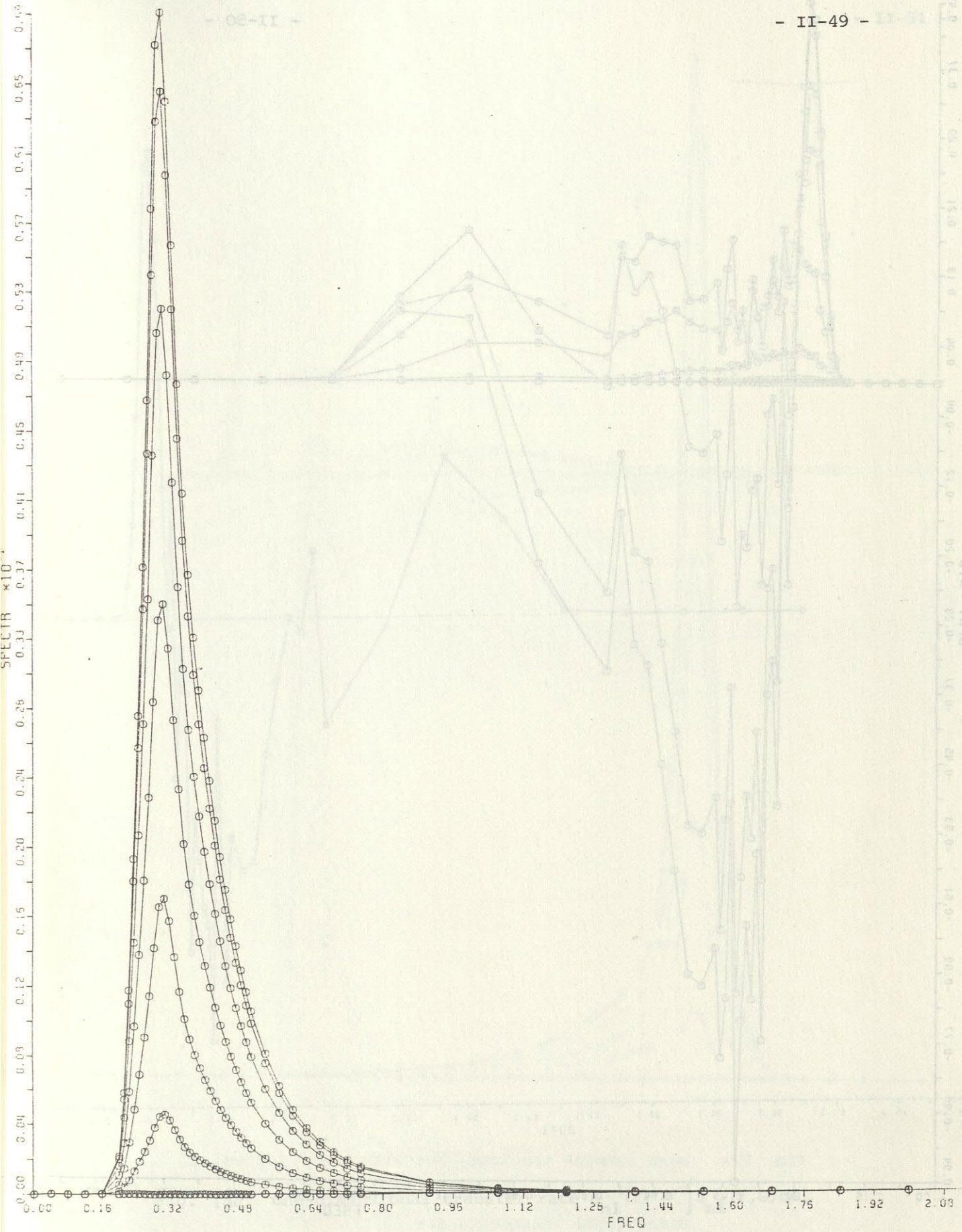

Fig. 14a Mean JONSWAP spectrum, but with $\gamma = 1.5$ instead of 3.3. Spreading function: $\cos^2\theta$. Two-dimensional spectrum $E(f,\theta)$. Directional increments are 15^o.

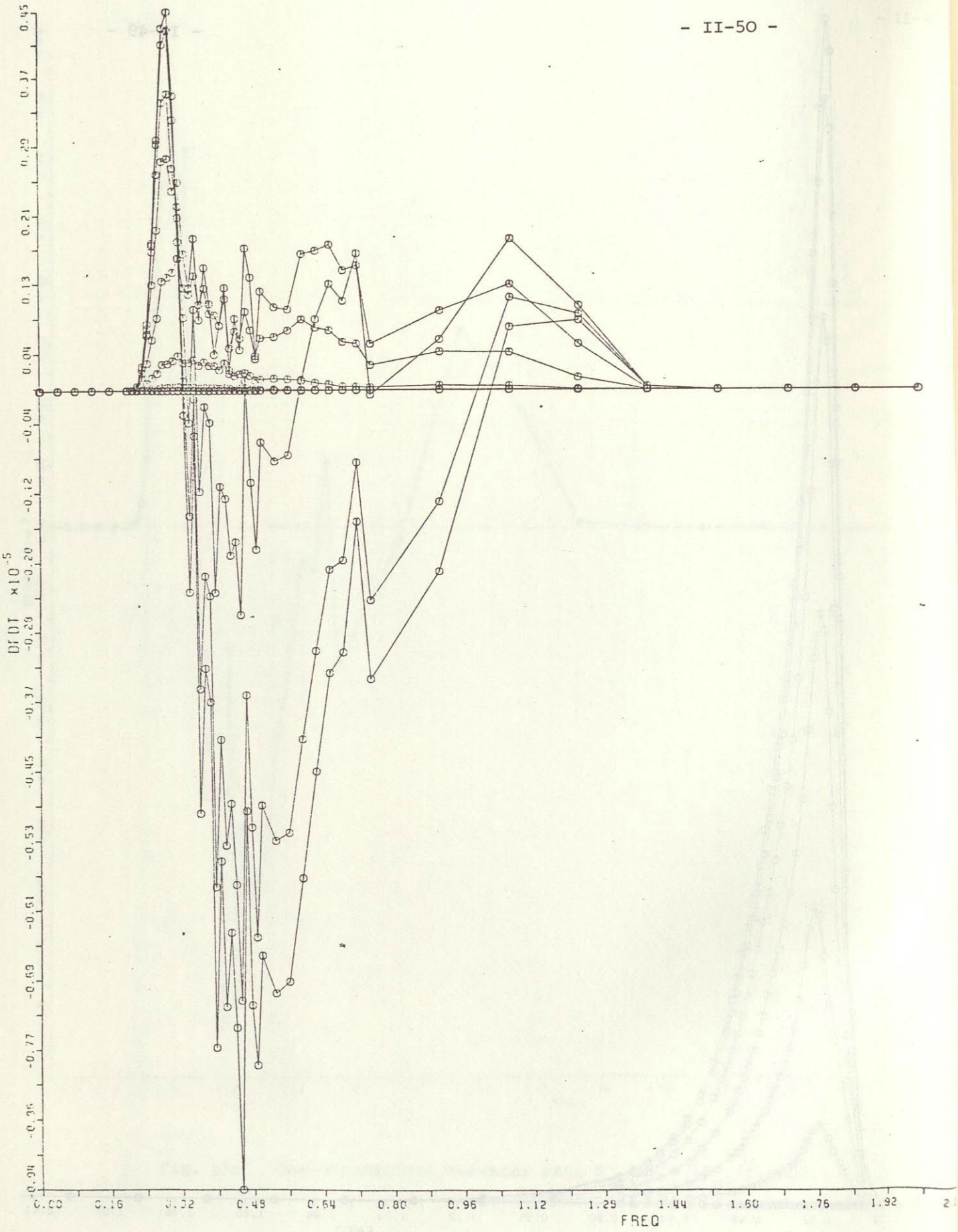

Fig. 14b Two-dimensional transfer rate $S_{nl}(f,\Theta)$. Directional increments are 15^{o}.

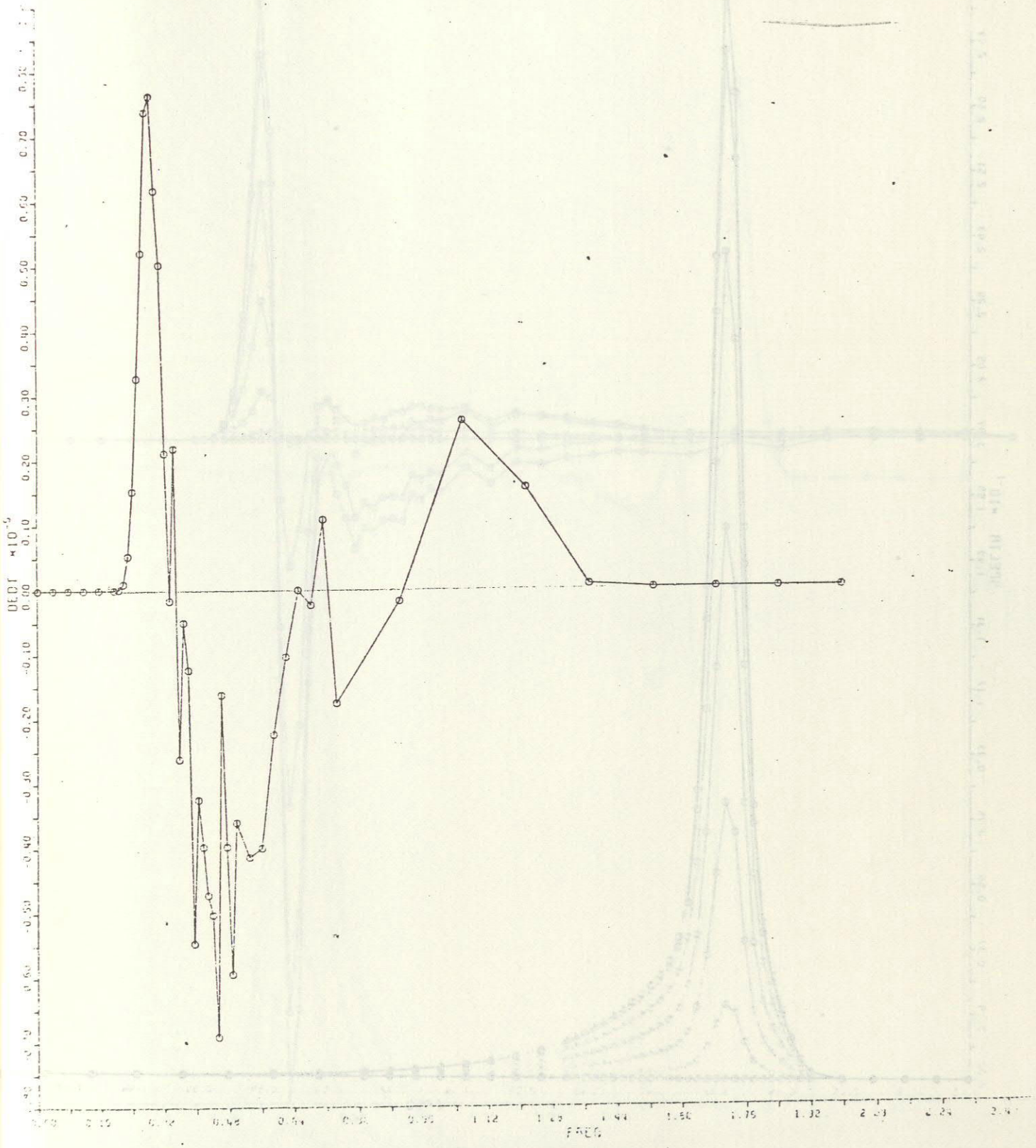

Fig. 14c One-dimensional transfer rate $S_{nl}(f) = \int S_{nl}(f,\Theta)d\Theta$.

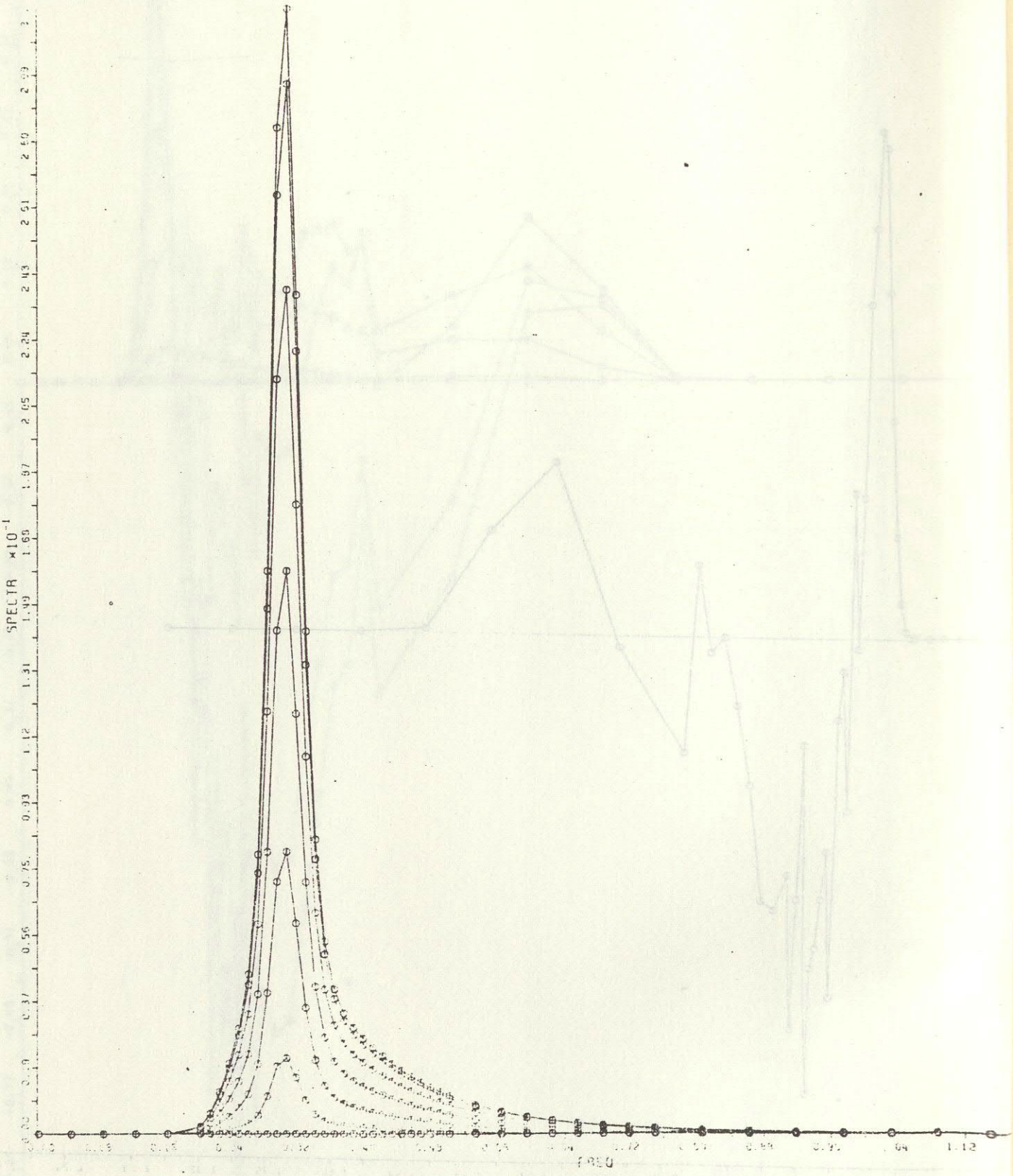

Fig. 15 a Mean JONSWAP spectrum, but with $\gamma = 7$ instead of 3.3. Spreading function: $\cos^2\theta$. Two-dimensional spectrum $E(f,\theta)$. Directional increments are 15°.

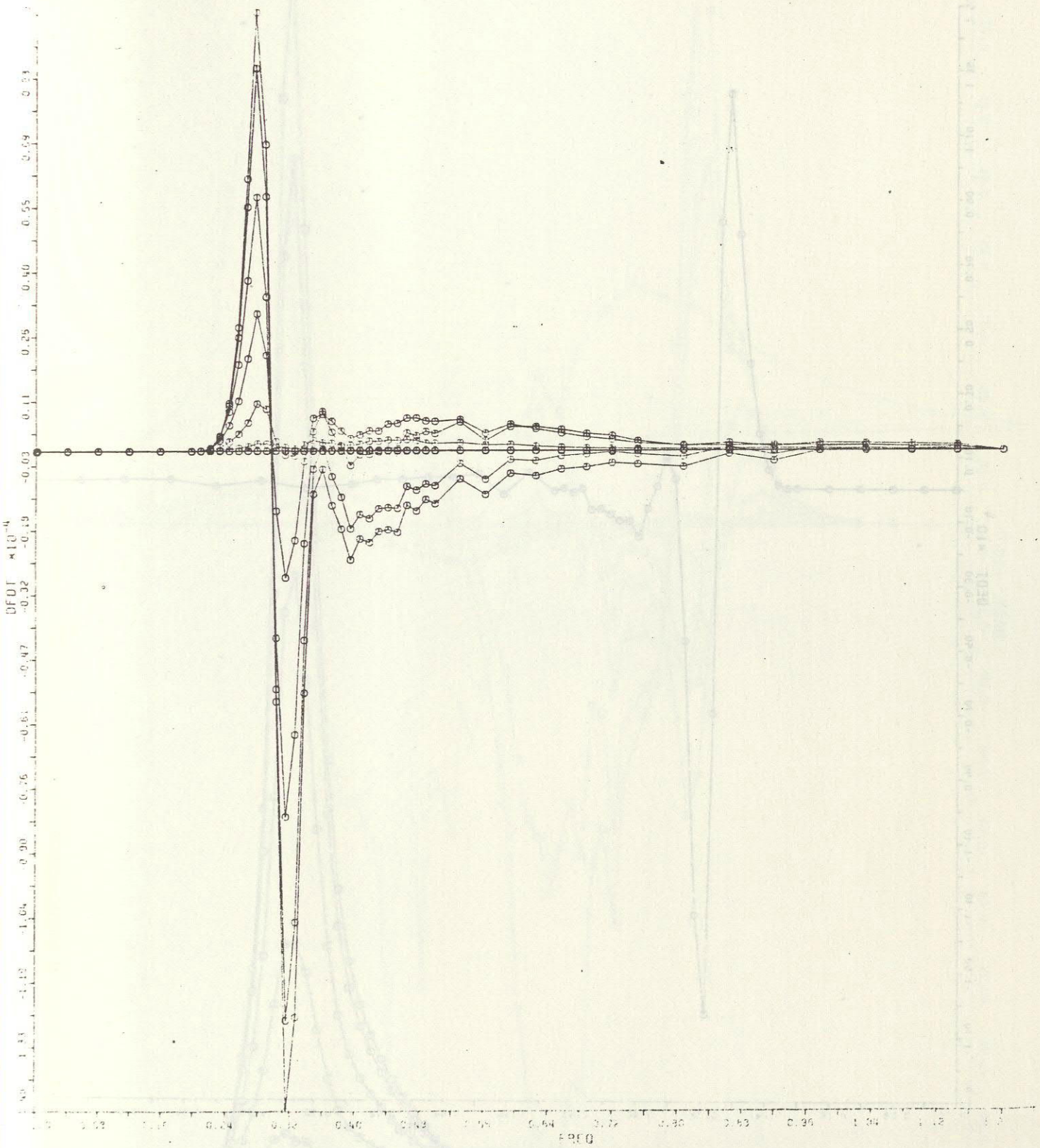

Fig. 15b Two-dimensional transfer rate $S_{nl}(f,\Theta)$. Directional increments are 15^{o}.

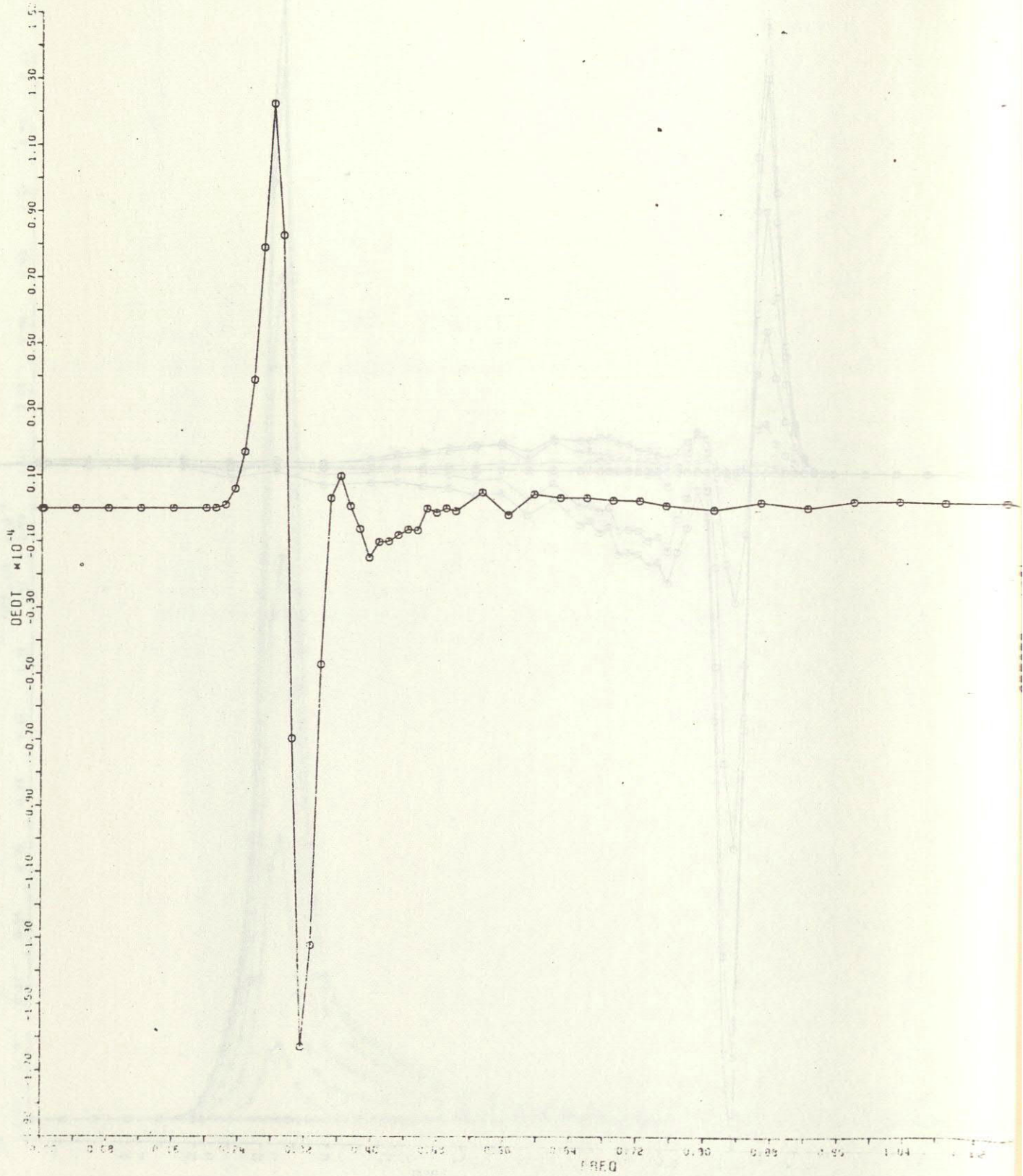

Fig. 15c One-dimensional transfer rate $S_{nl}(f) = \int S_{nl}(f,\theta)d\theta$.

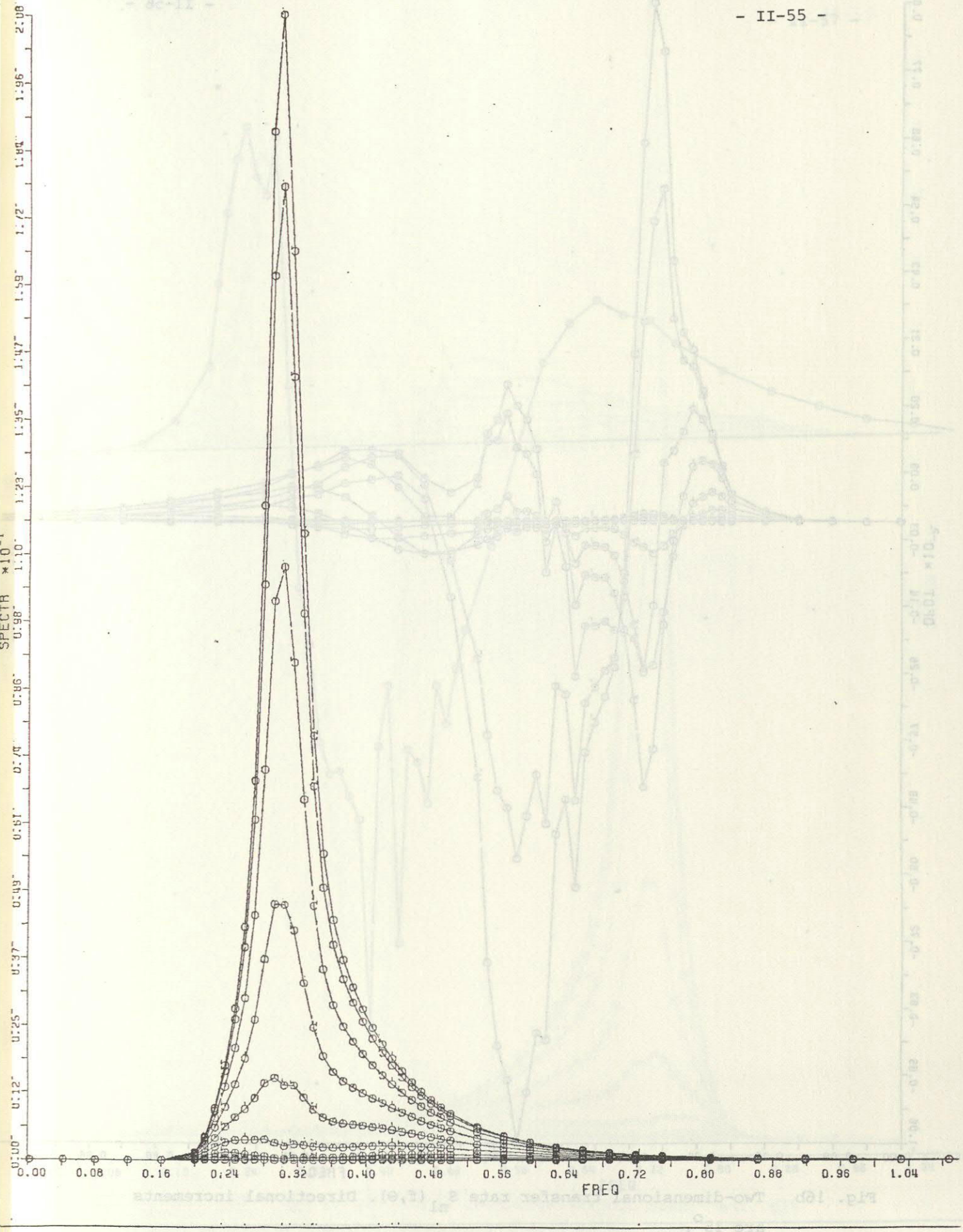

Fig. 16a Mean JONSWAP spectrum, finite depth, $k_m h = 0.35$ (essentially deep water) with a frequency-dependent spreading function given by (5). Two-dimensional spectrum $E(f,\Theta)$. Directional increments are 15°.

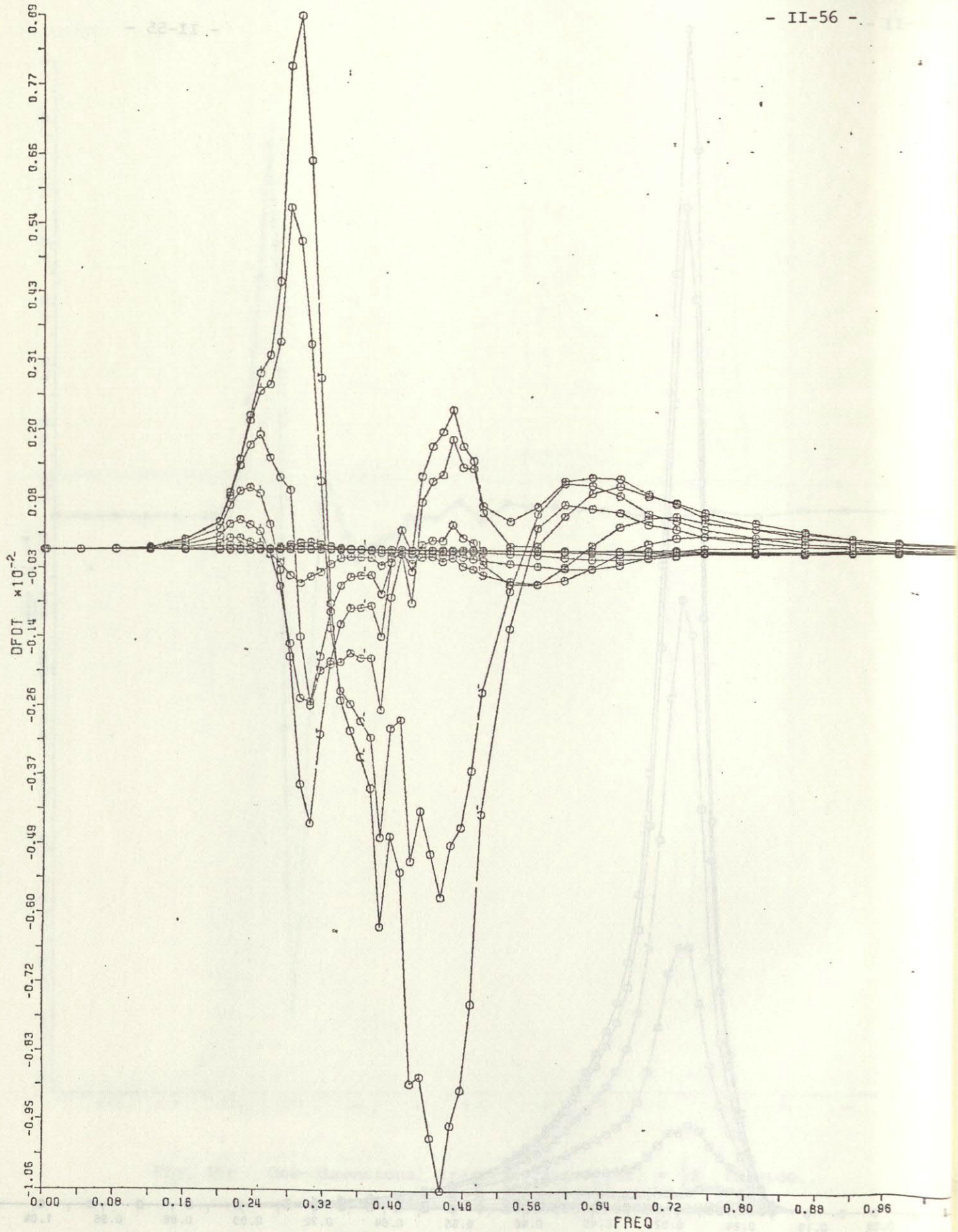

Fig. 16b Two-dimensional transfer rate $S_{nl}(f,\theta)$. Directional increments are 15^{o}.

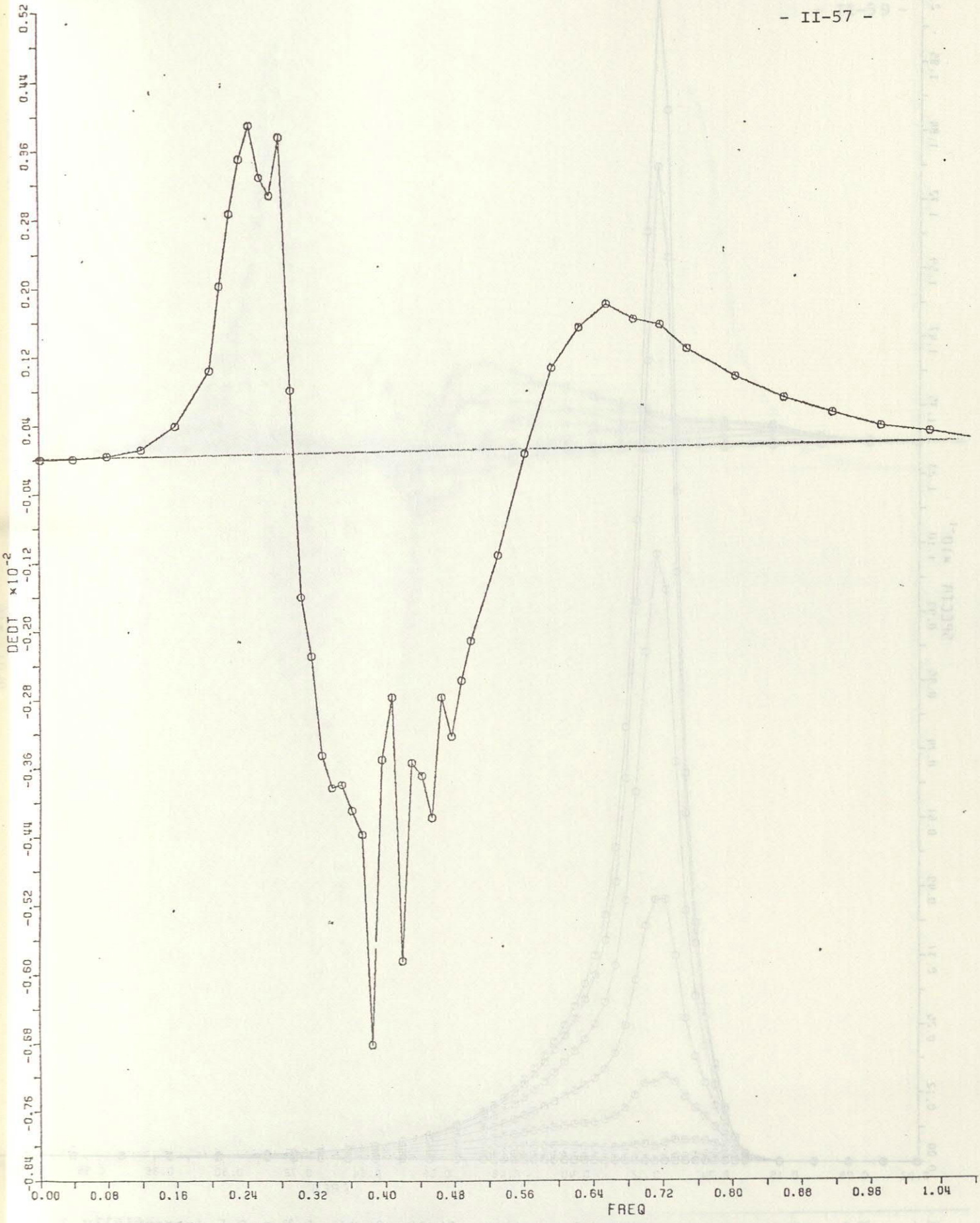

Fig. 16c One-dimensional transfer rate $S_{nl}(f) = \int S_{nl}(f,\Theta)d\Theta$.

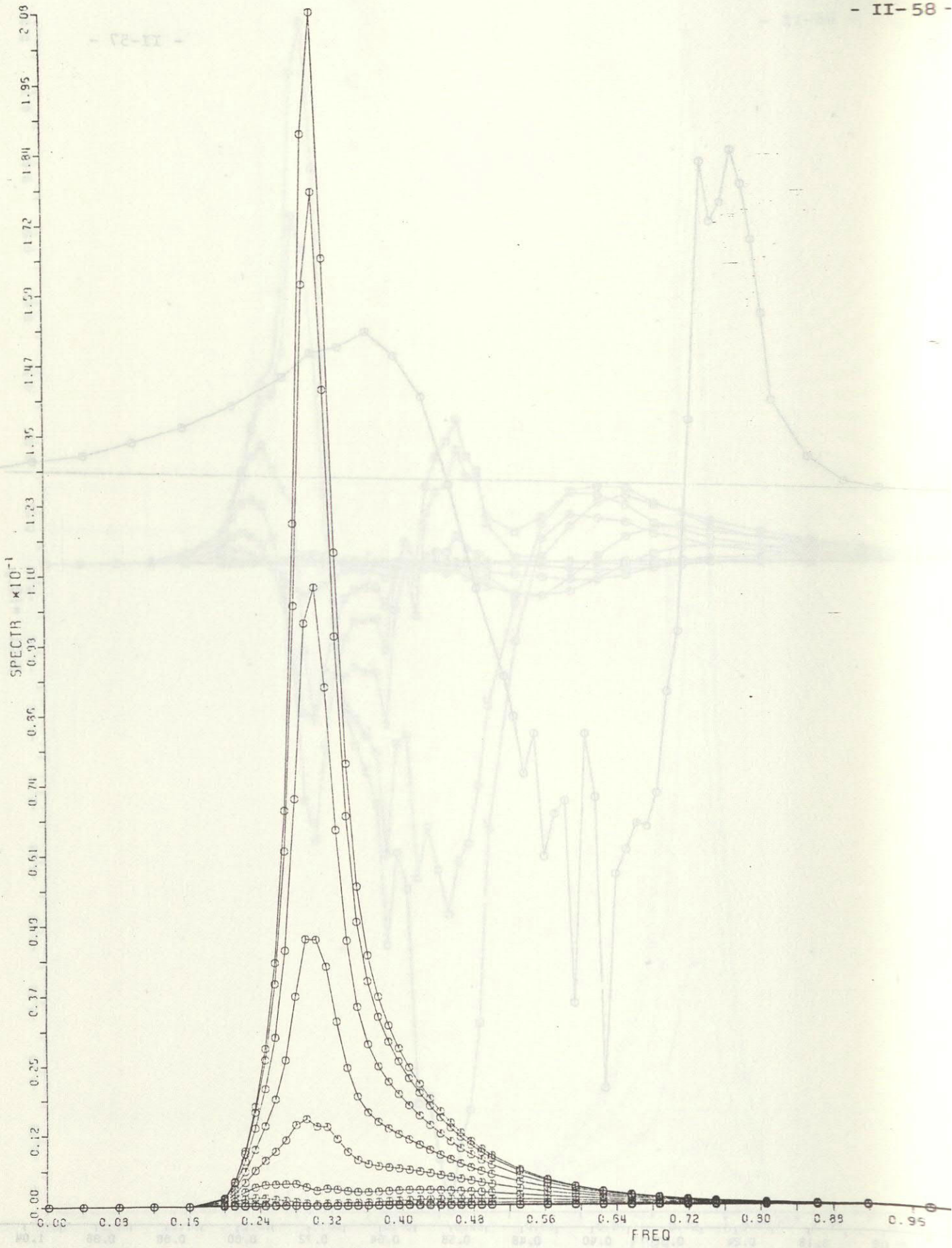

Fig. 17a Mean JONSWAP spectrum, finite depth, $k_m h = 0.5$ (essentially deep water) with a frequency-dependent spreading function given by (5). Two-dimensional spectrum $E(f,\Theta)$. Directional increments are 15°.

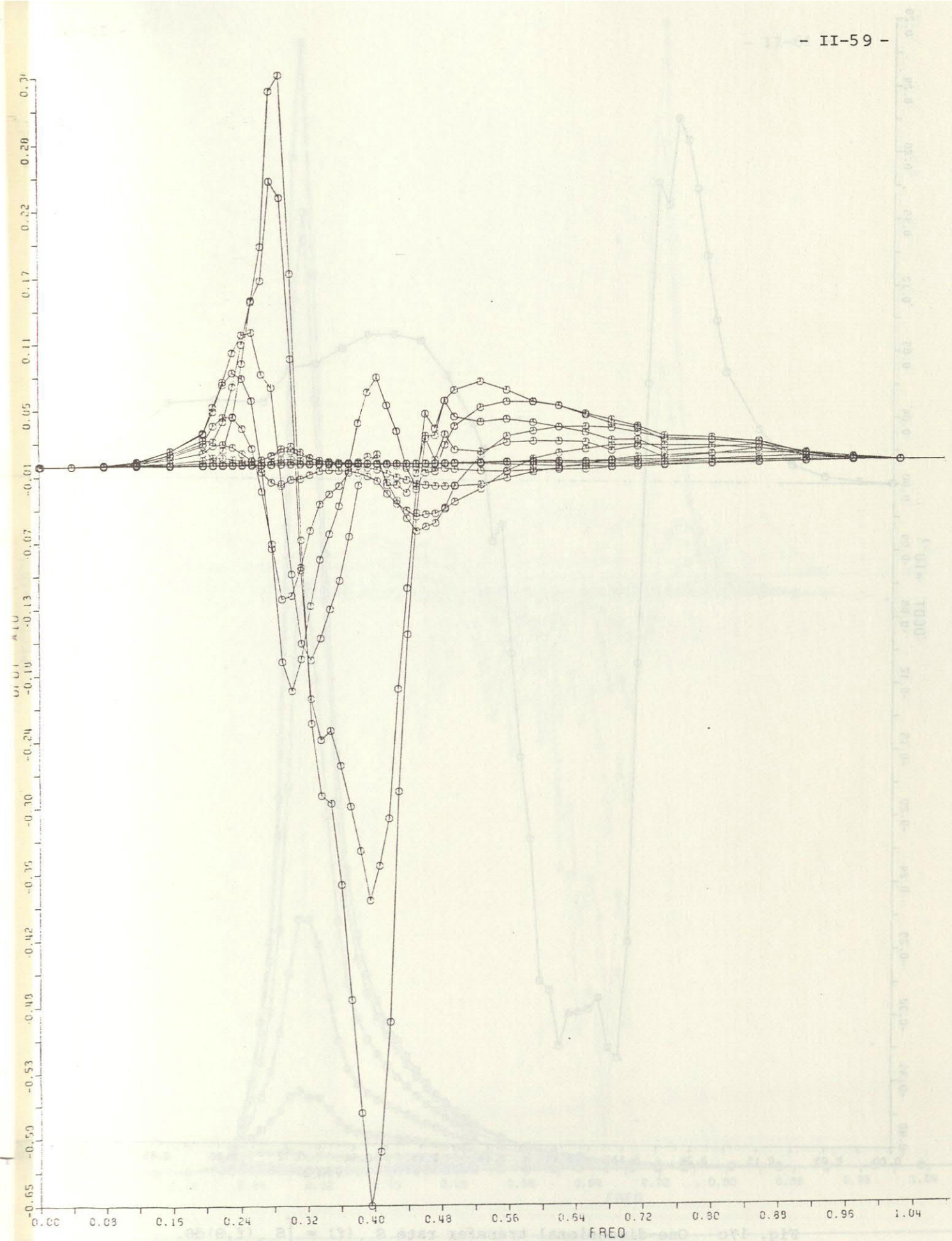

Fig. 17b Two-dimensional transfer rate $S_{nl}(f,\Theta)$. Directional increments are 15^{o}.

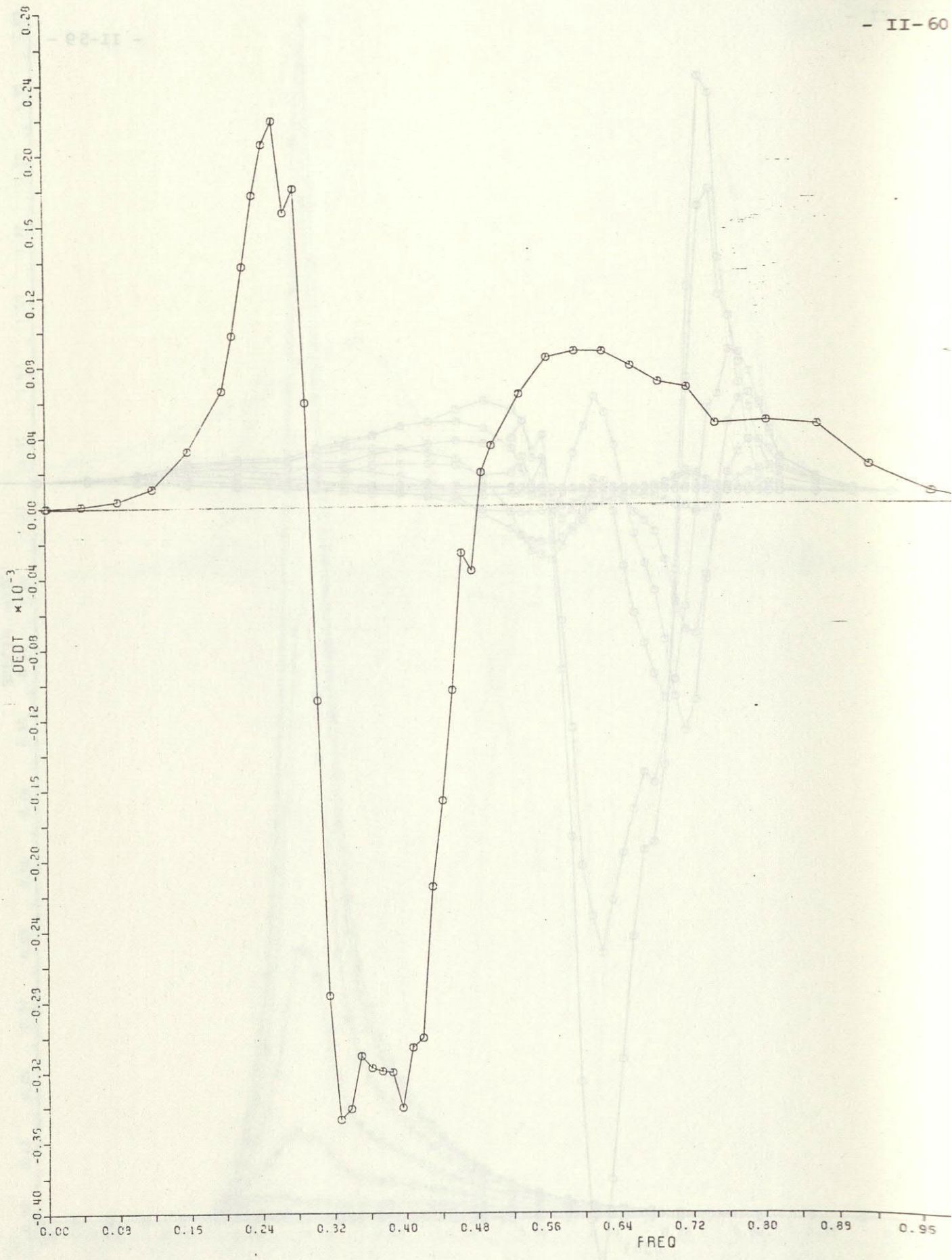

Fig. 17c One-dimensional transfer rate $S_{nl}(f) = \int S_{nl}(f,\theta)d\theta$.

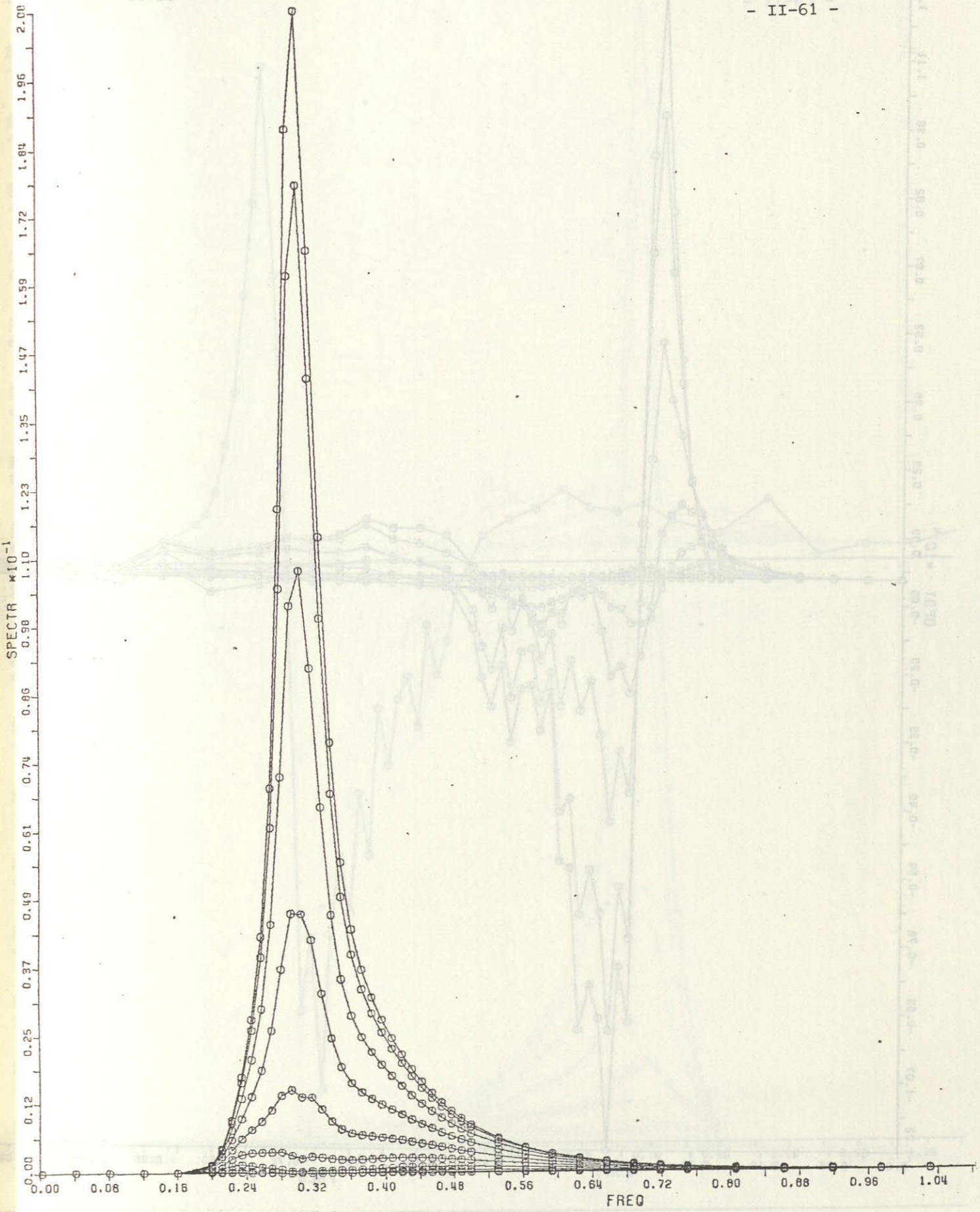

Fig. 18a Same as Fig. 16a with $k_m h = 0.65$.

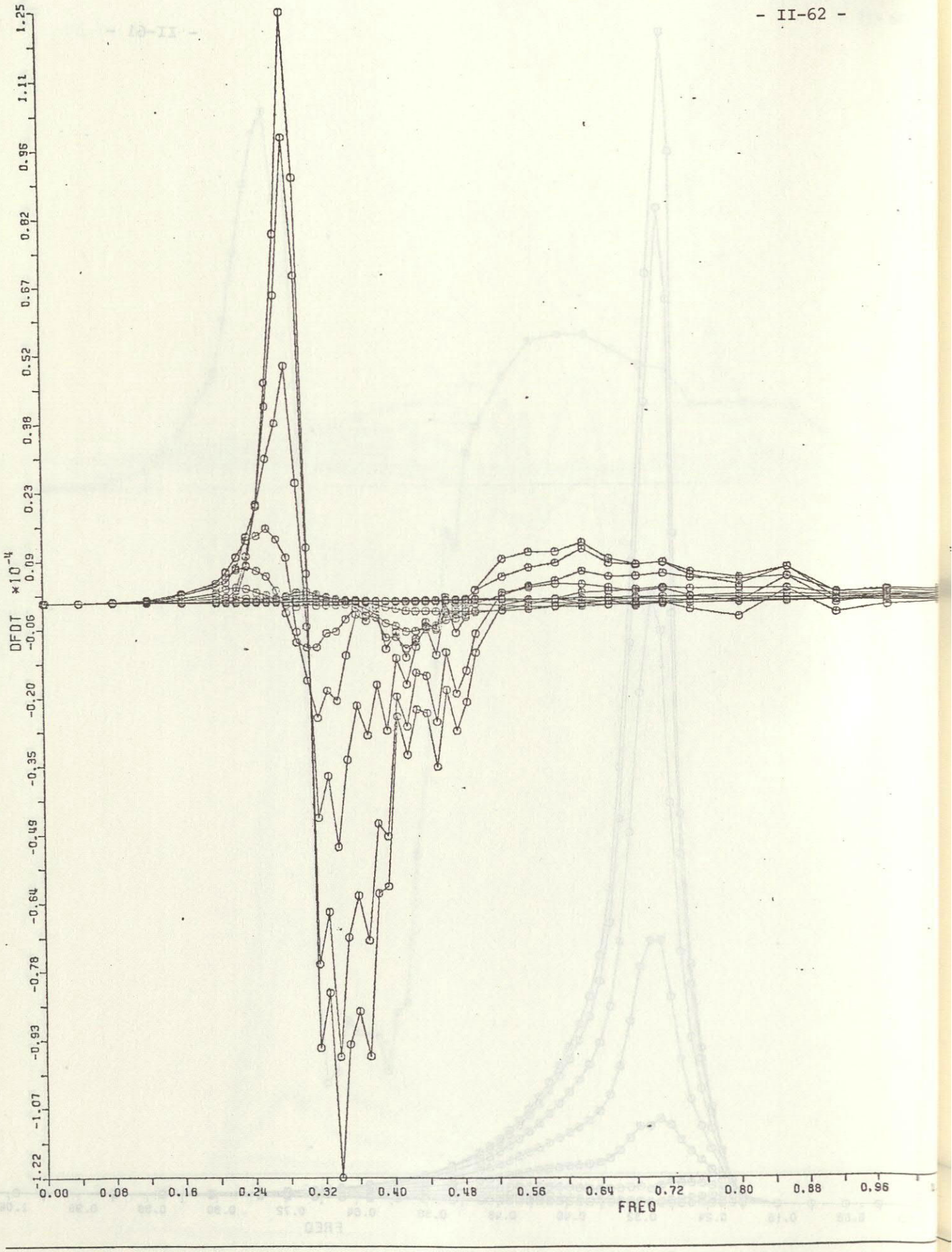

Fig. 18b Two-dimensional transfer rate $S_{nl}(f,\Theta)$. Directional increments are 15°.

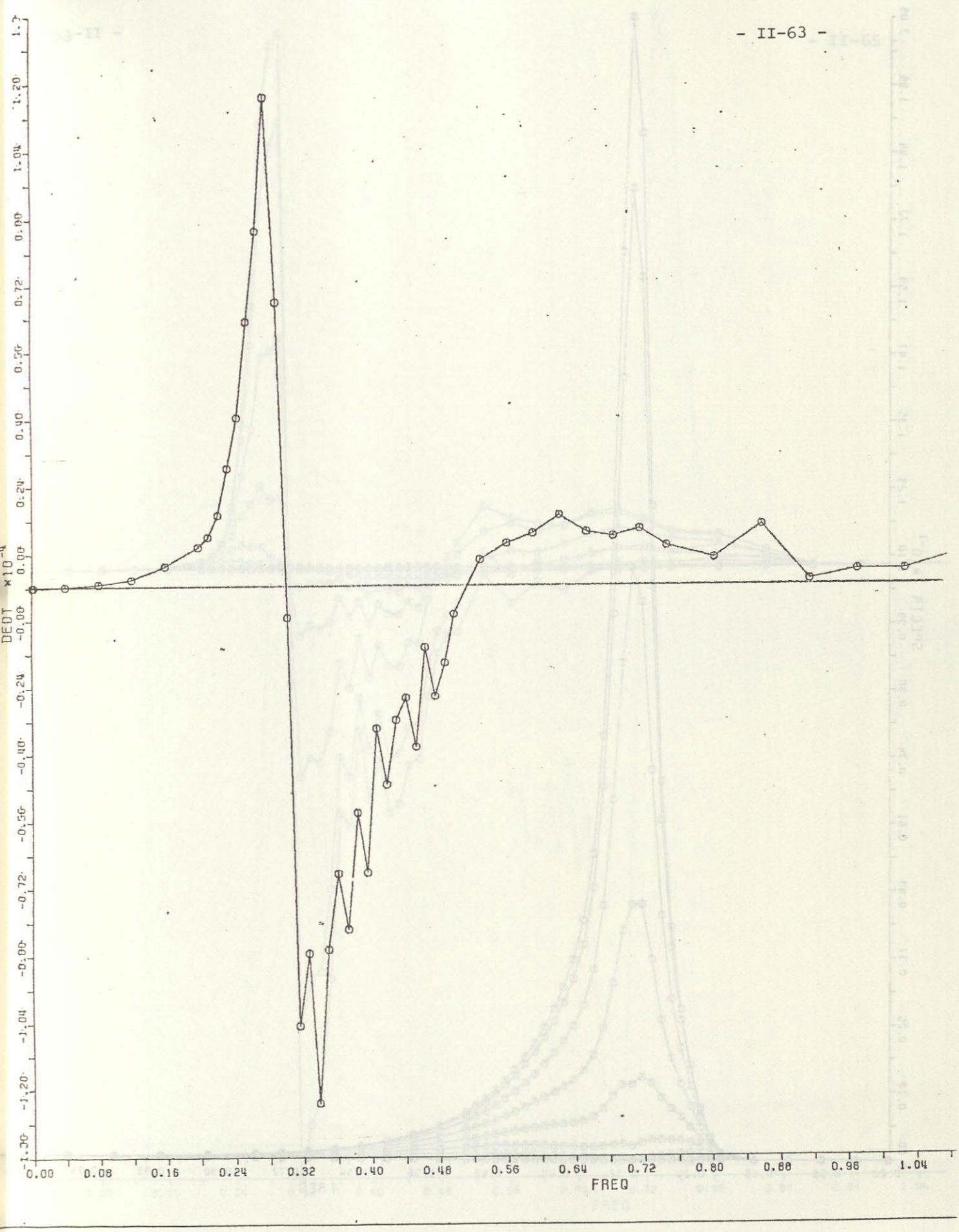

Fig. 18c One-dimensional transfer rate $S_{nl}(f) = \int S_{nl}(f,\theta)d\theta$.

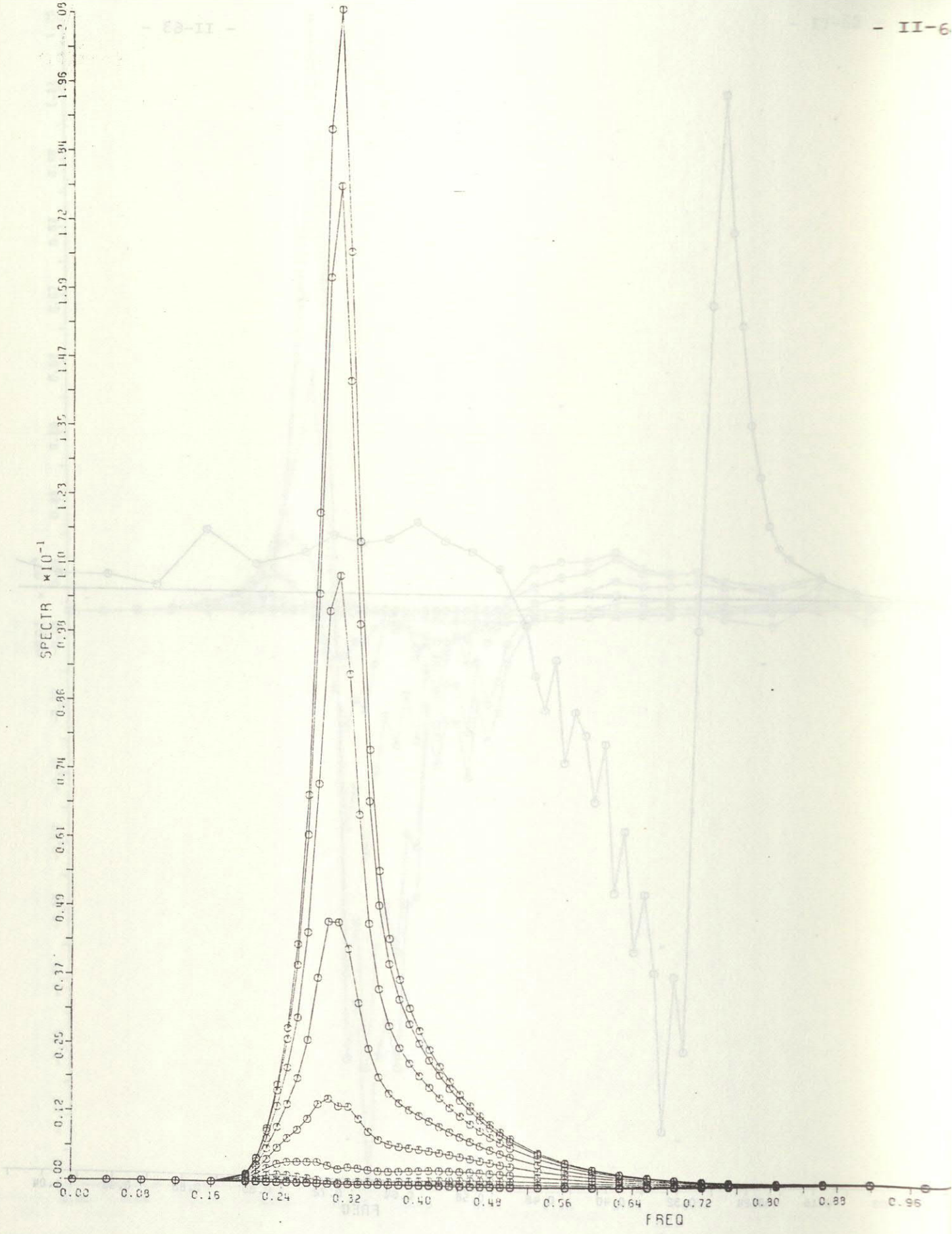

Fig. 19a Same as Fig. 16a with $k_m h = 1.5$.

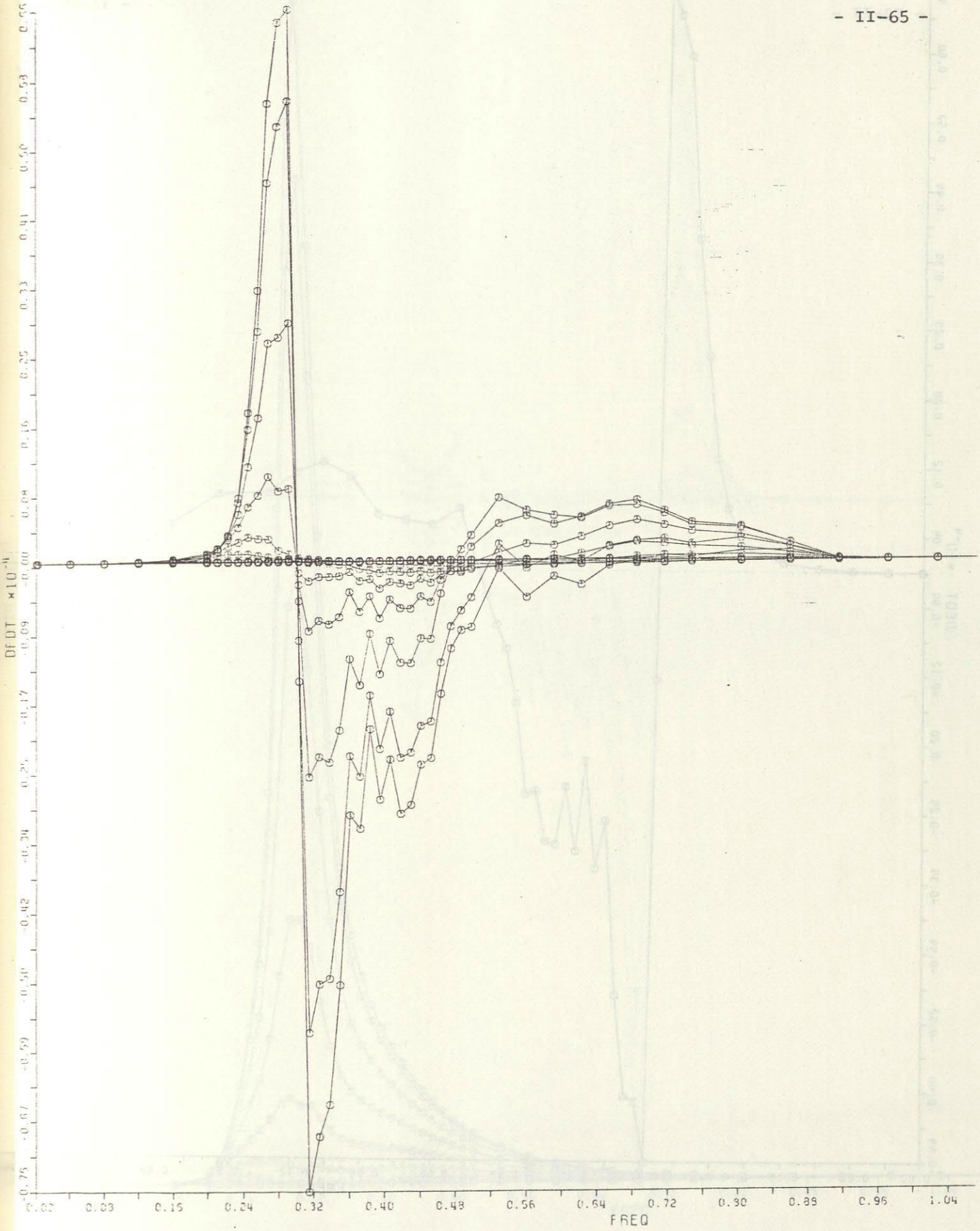

Fig. 19b Two-dimensional transfer rate $S_{nl}(f,\theta)$. Directional increments are 15^{o}.

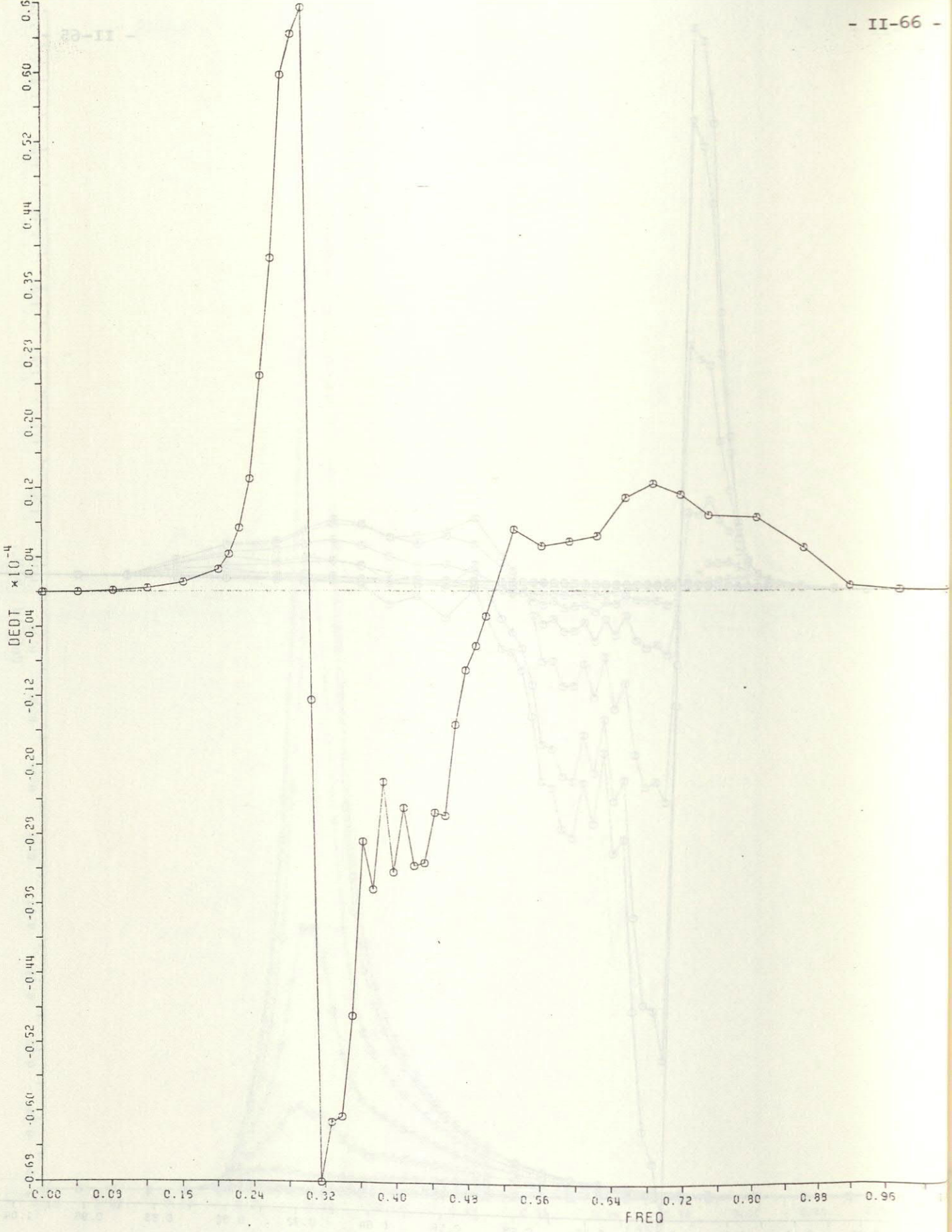

Fig. 19c One-dimensional transfer rate $S_{nl}(f) = \int S_{nl}(f,\theta)d\theta$.

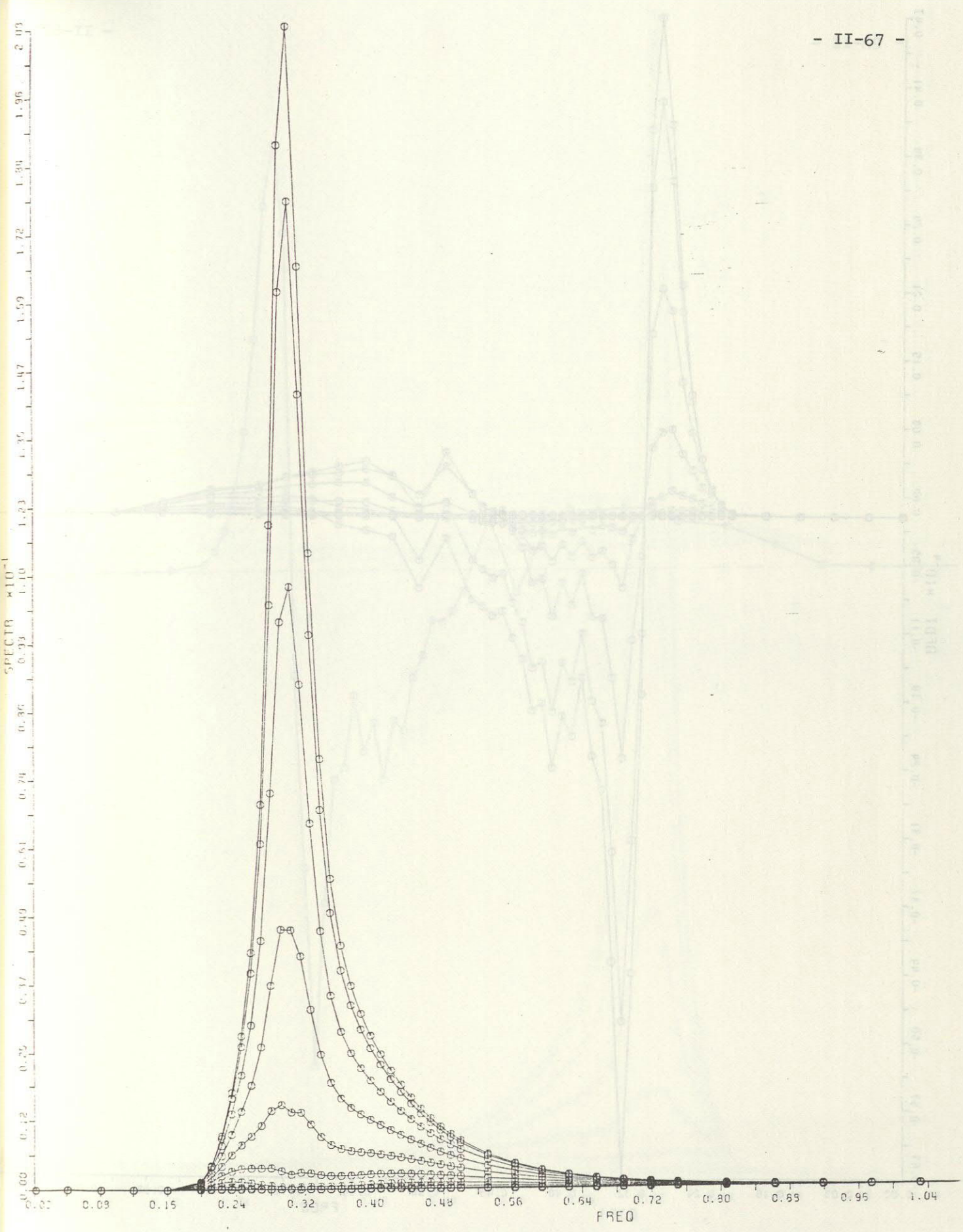

Fig. 20 a Same as Fig. 16a with $k_m h = 1.0$.

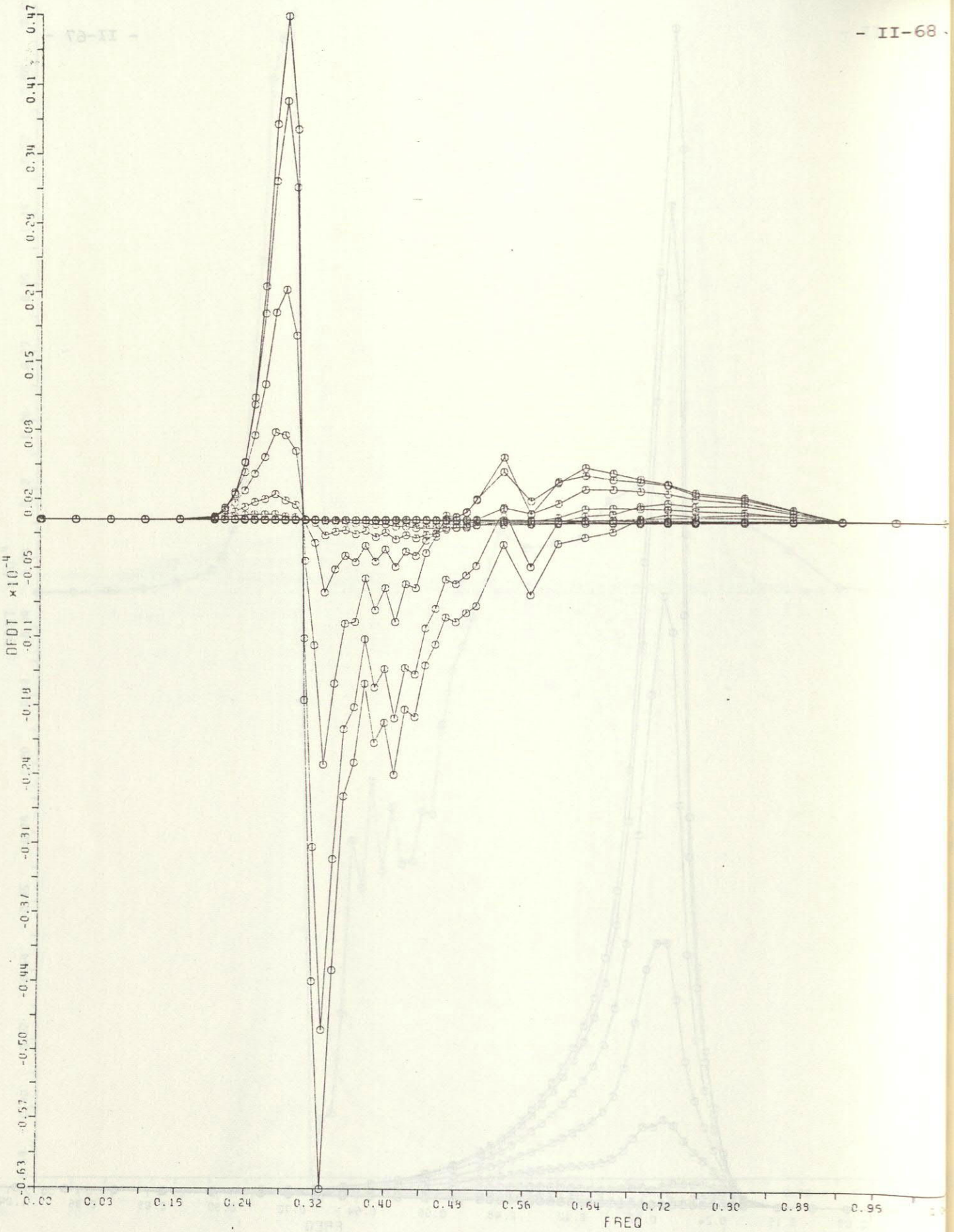

Fig. 20b Two-dimensional transfer rate $S_{nl}(f,\Theta)$. Directional increments are 15°.

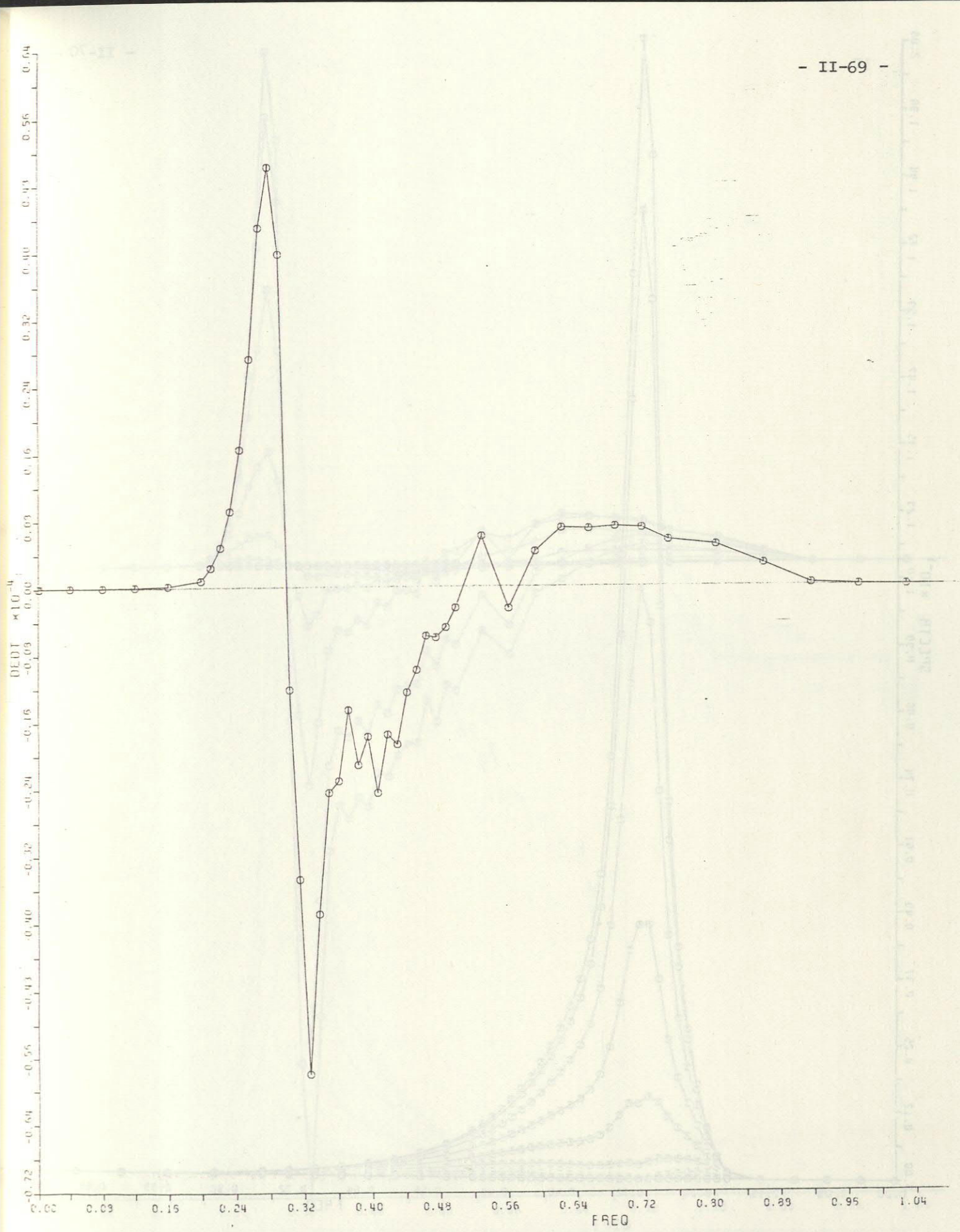

Fig. 20 c One-dimensional transfer rate $S_{nl}(f) = \int S_{nl}(f,\theta)d\theta$.

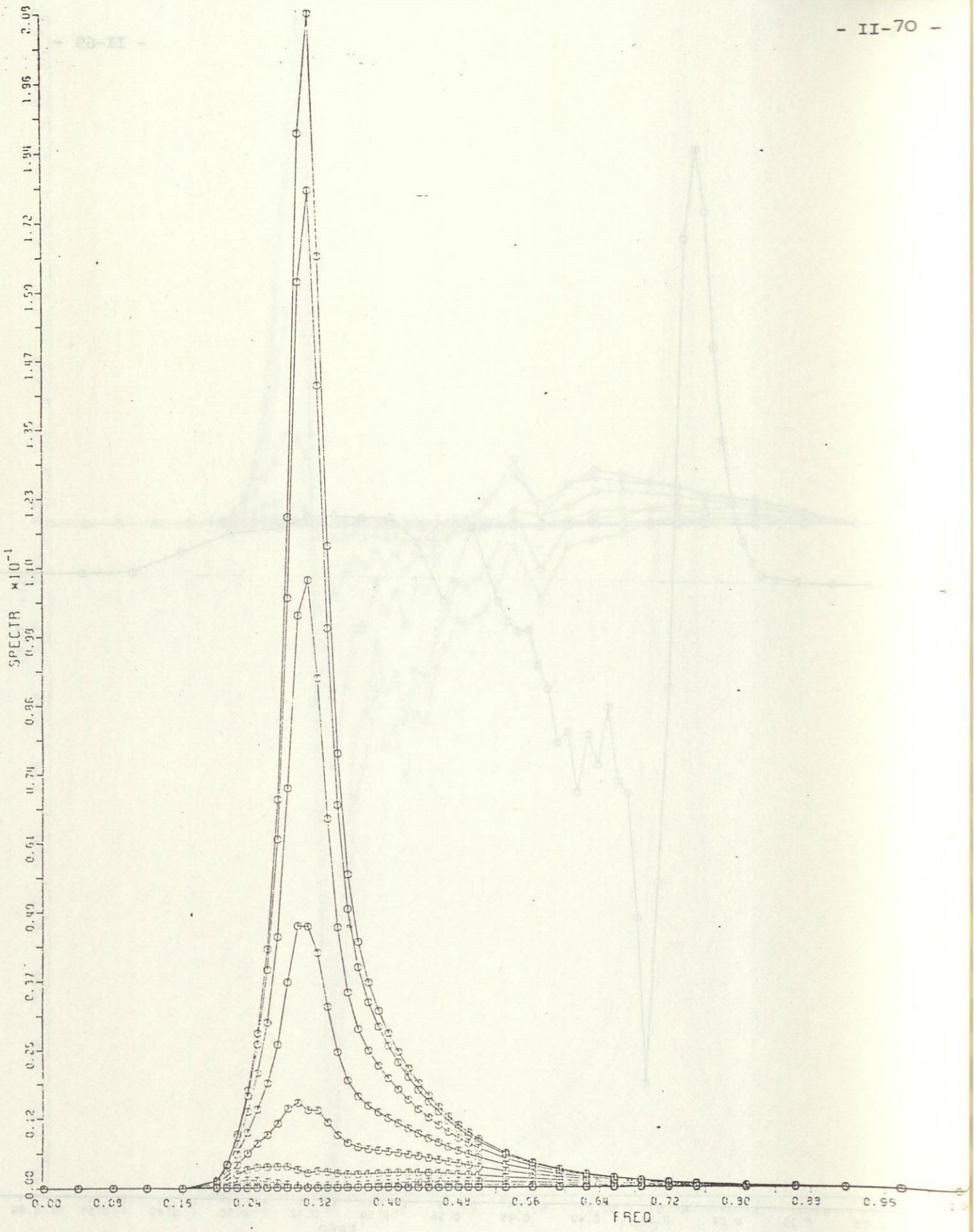

Fig. 21 a Same as Fig. 16a with $k_m h = 1.5$.

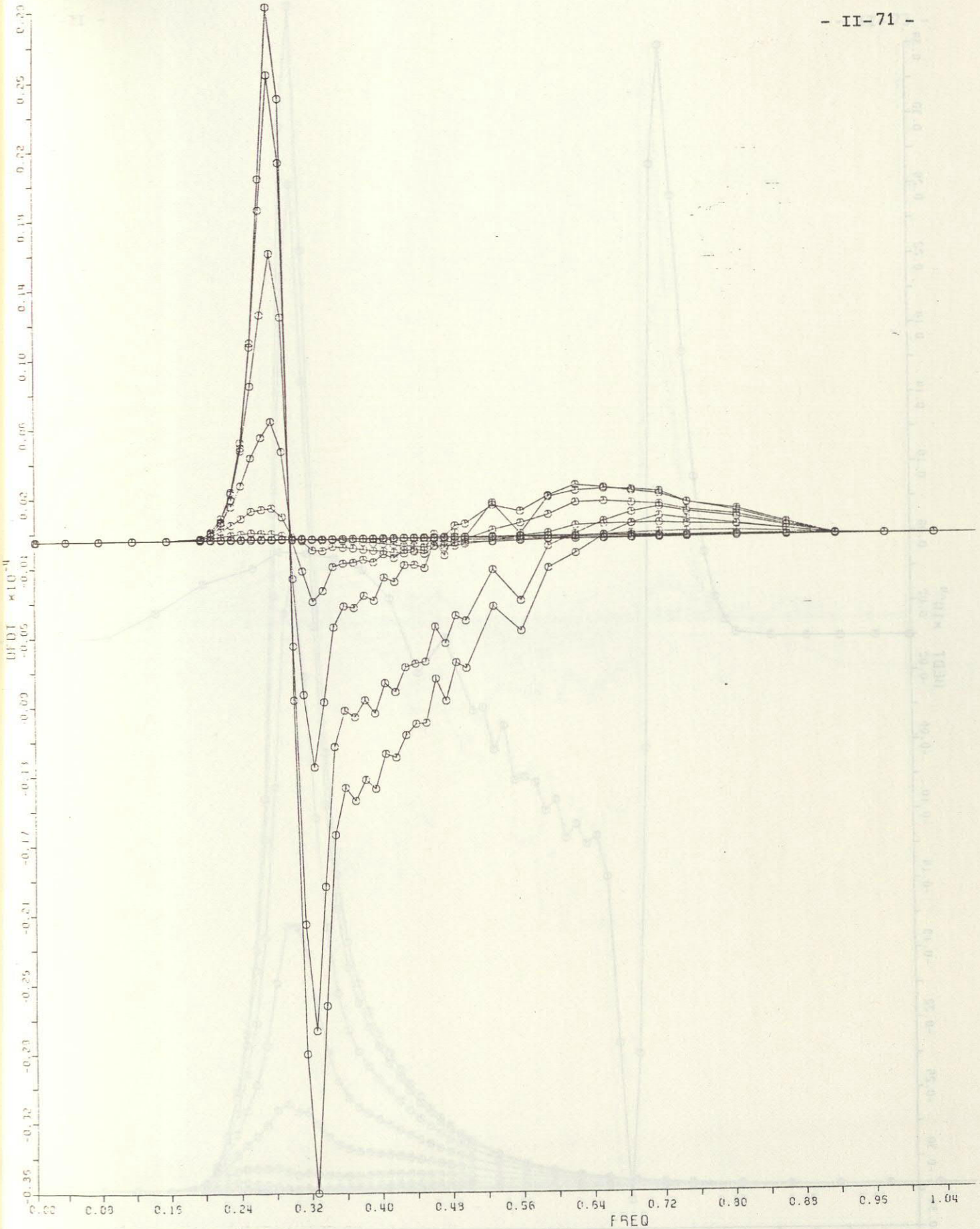

Fig. 21b Two-dimensional transfer rate $S_{nl}(f,\theta)$. Directional increments are 15^{o}.

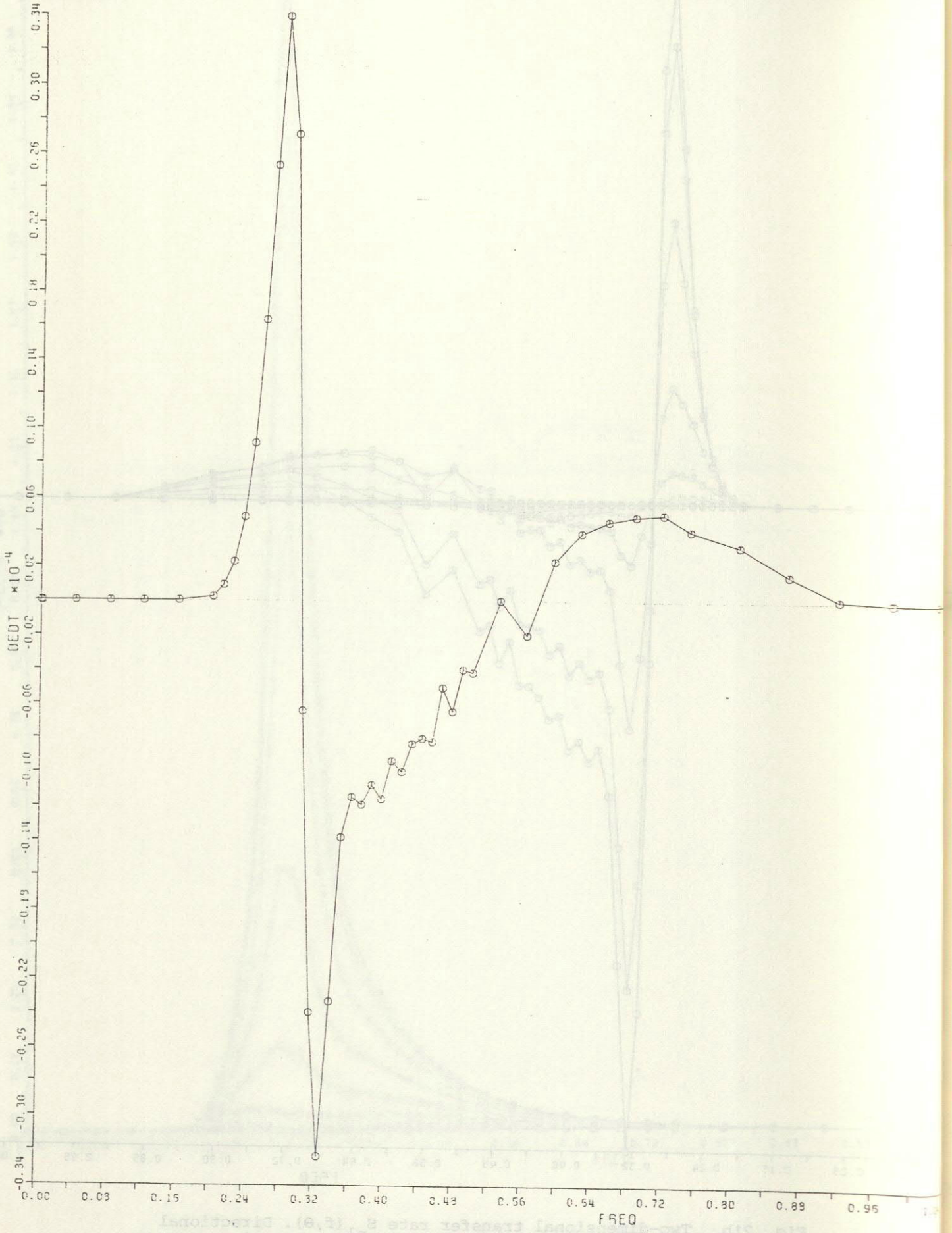

Fig. 21 c One-dimensional transfer rate $S_{nl}(f) = \int S_{nl}(f,\theta)\,d\theta$.

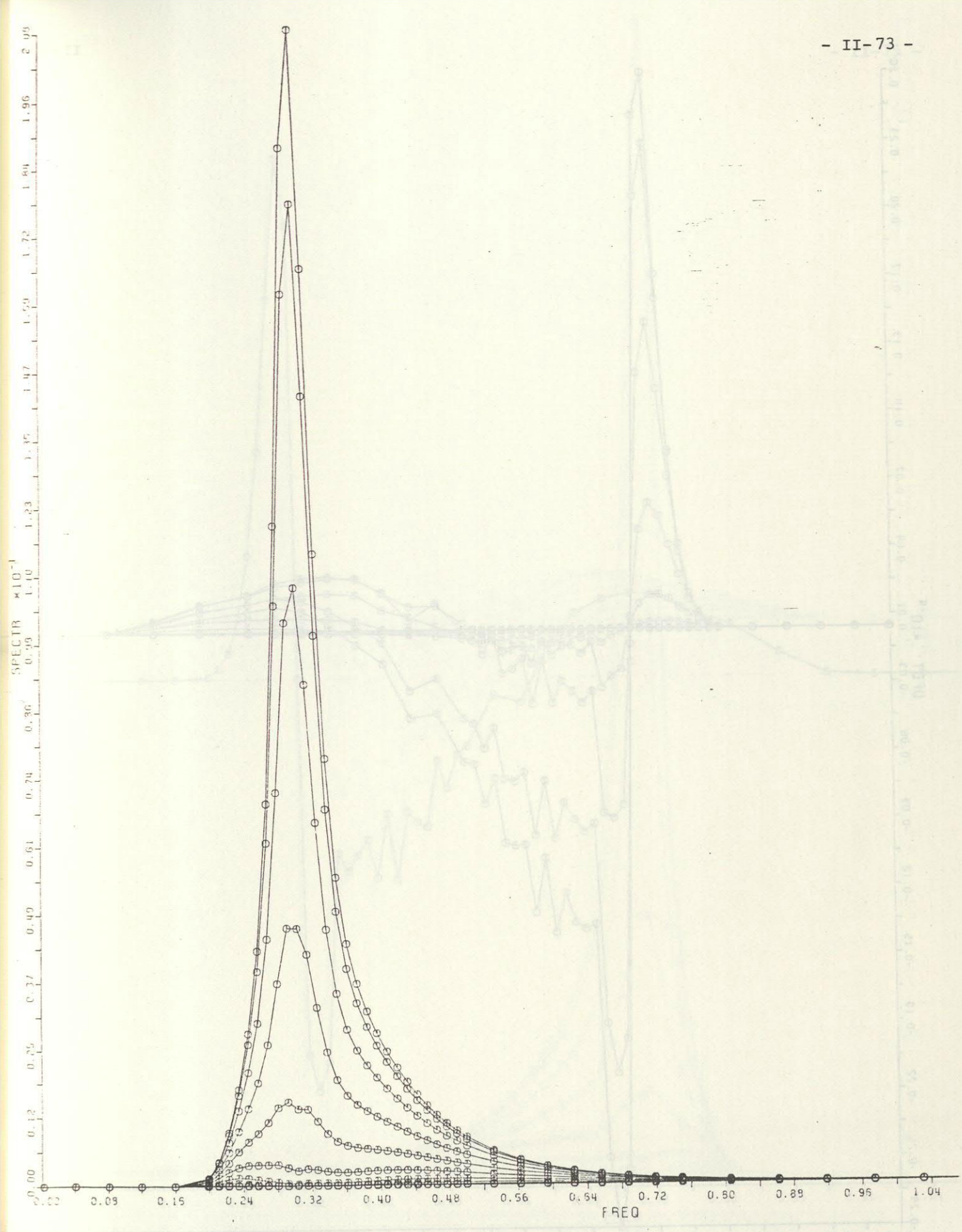

Fig. 22a Same as Fig. 16a with $k_m h = 2.0$.

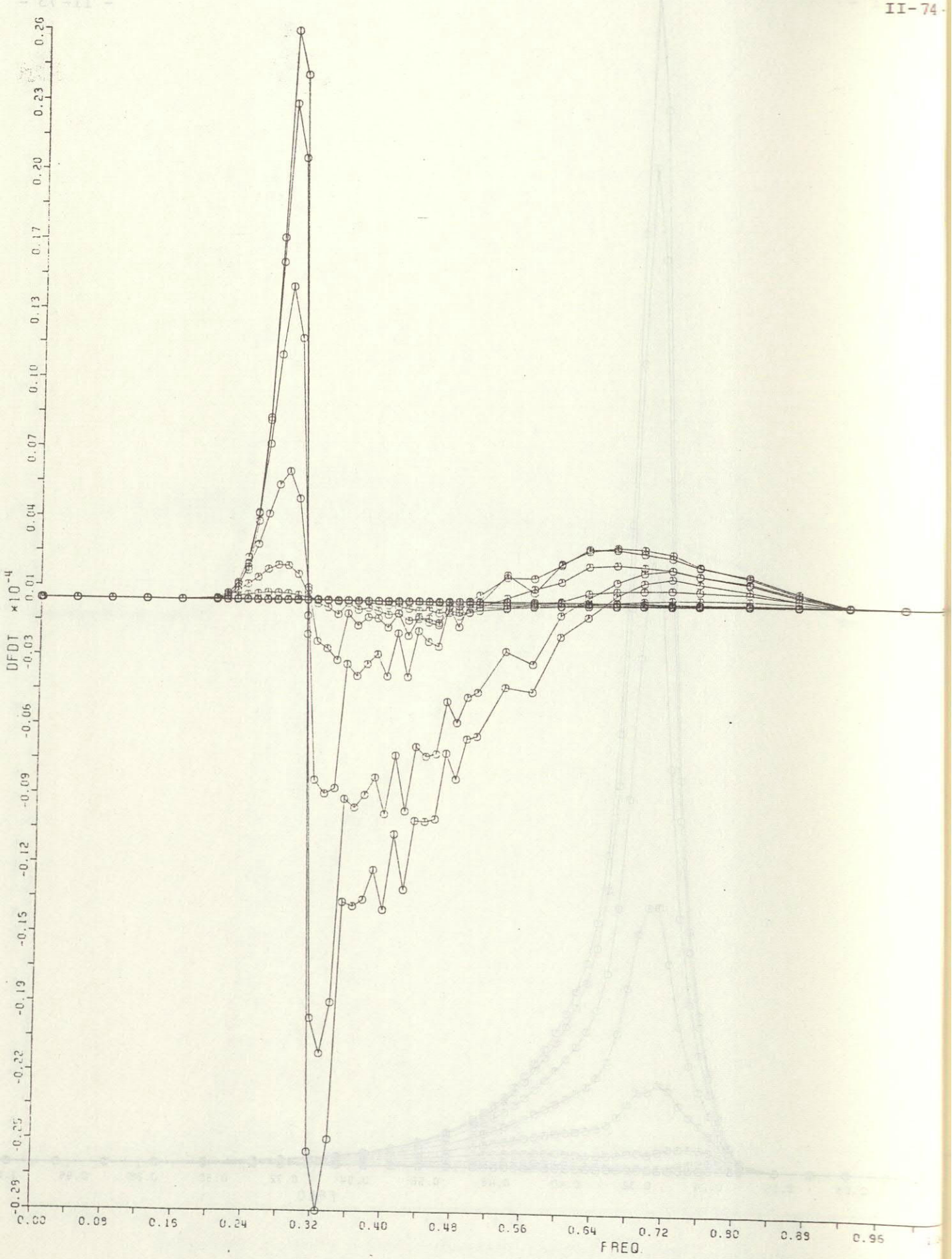

Fig. 22b Two-dimensional transfer rate $S_{nl}(f,\Theta)$. Directional increments are 15^{o}.

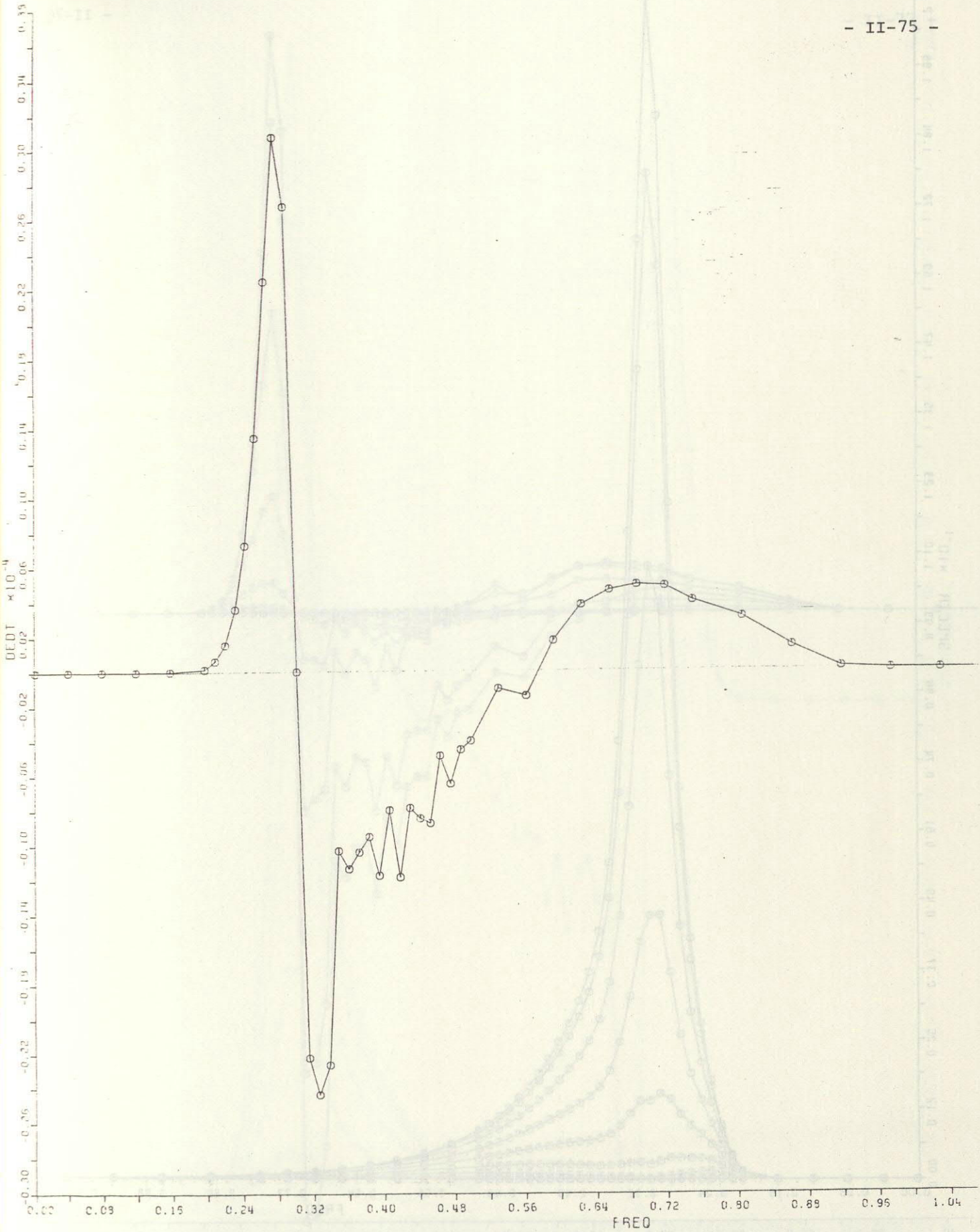

Fig. 22 c One-dimensional transfer rate $S_{nl}(f) = \int S_{nl}(f,\Theta)d\Theta$.

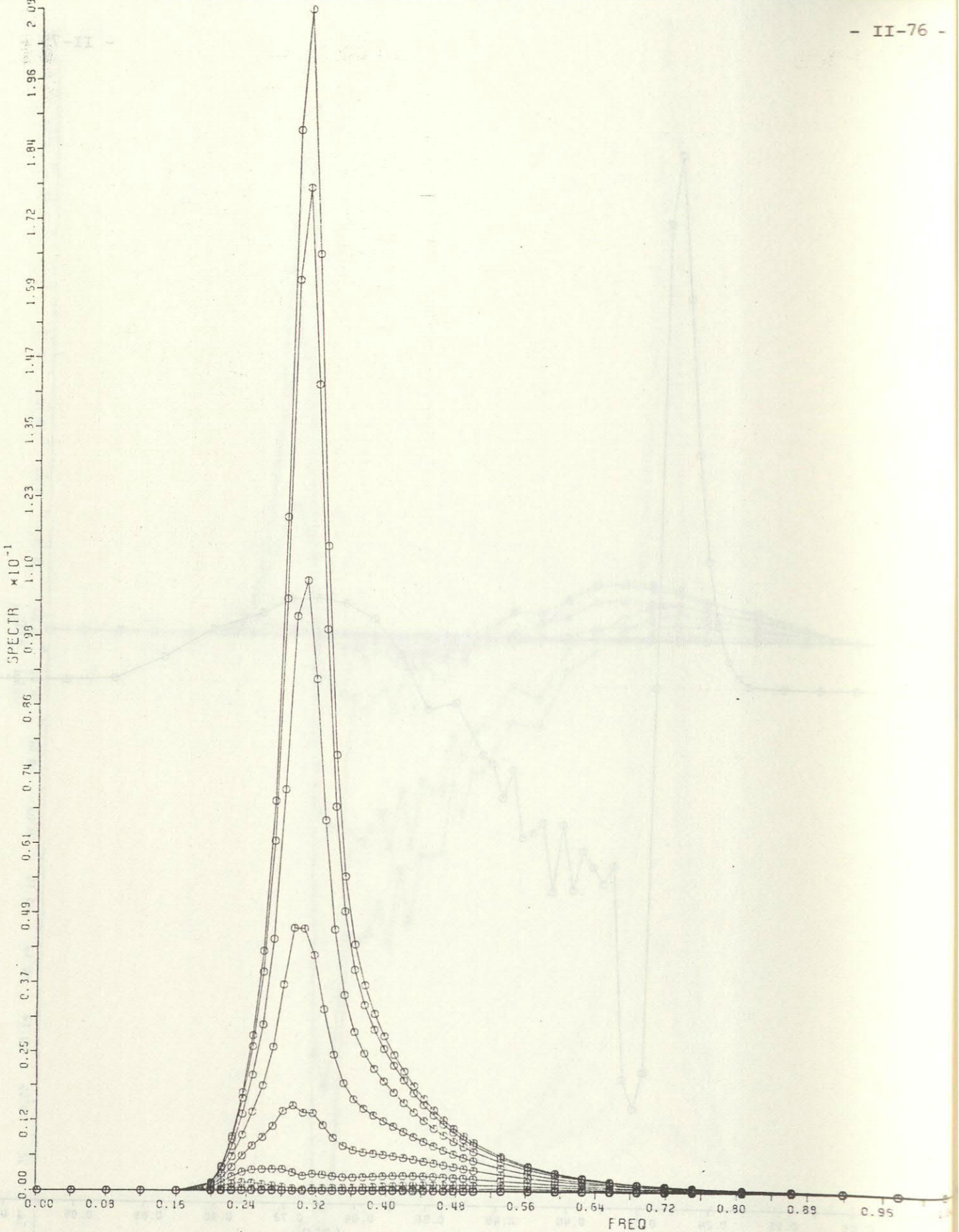

Fig. 23a Same as Fig. 16a with $k_m h = 5.0$.

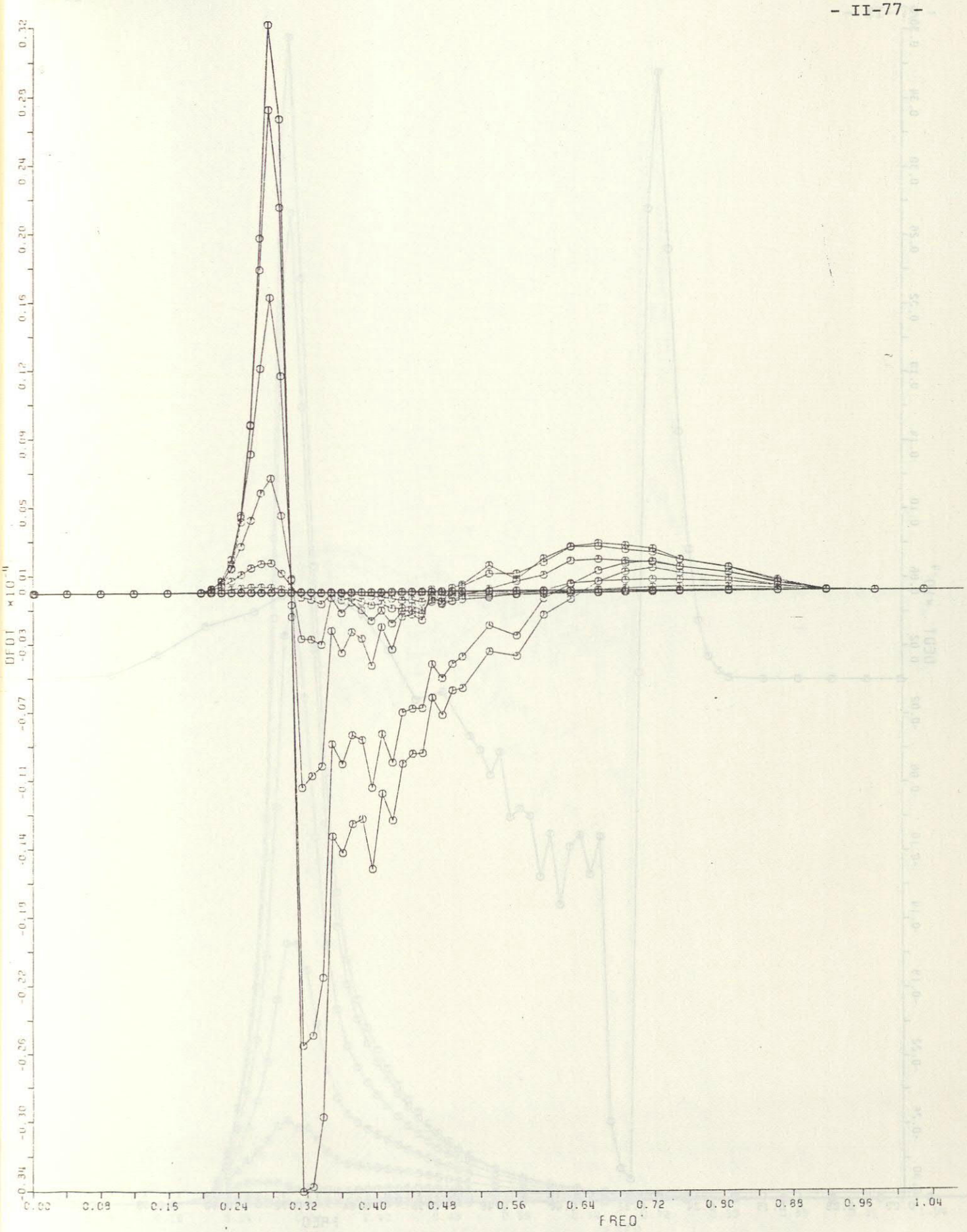

Fig. 23b Two-dimensional transfer rate $S_{nl}(f,\Theta)$. Directional increments are 15^{o}.

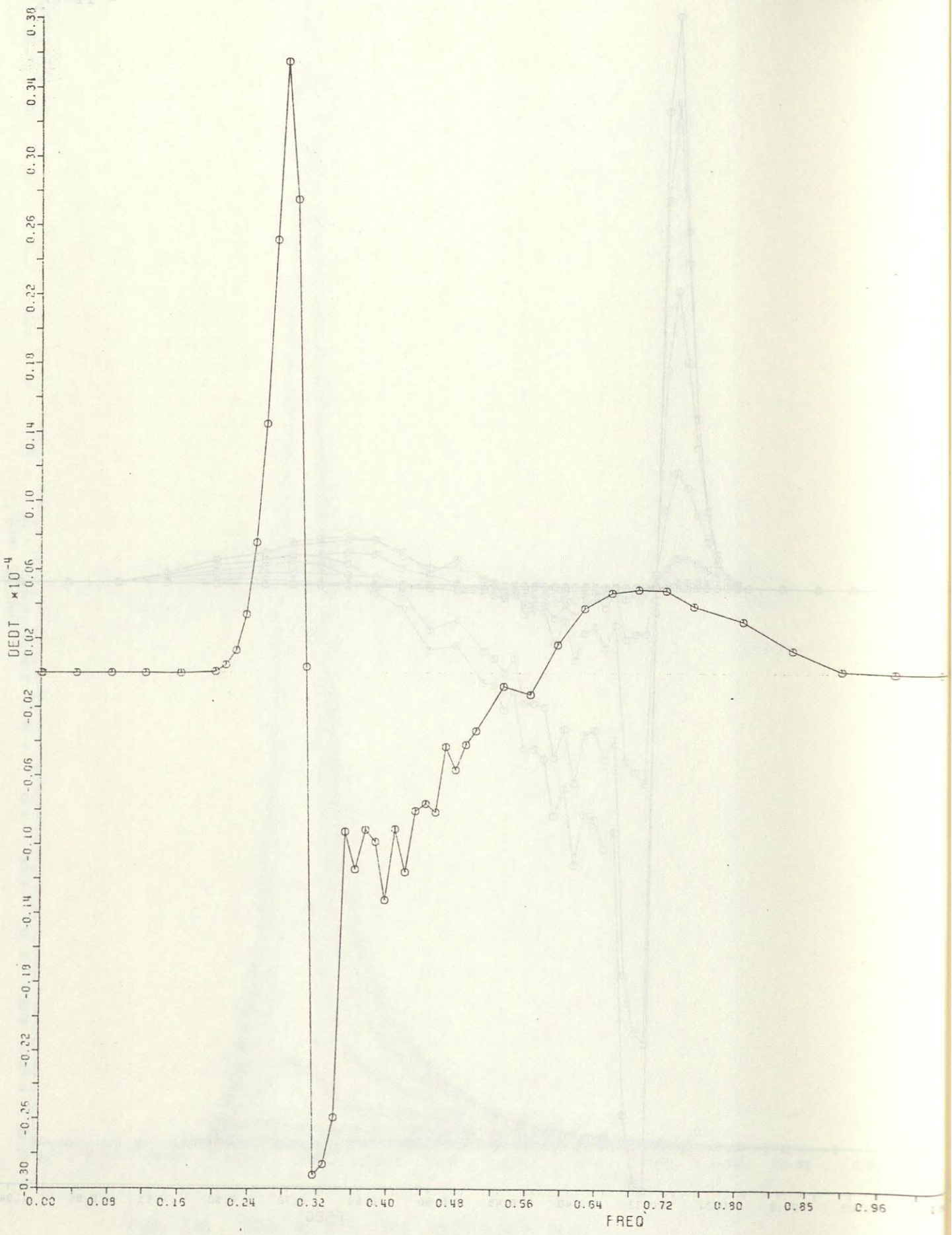

Fig. 23c One-dimensional transfer rate $S_{nl}(f) = \int S_{nl}(f,\theta)d\theta$.

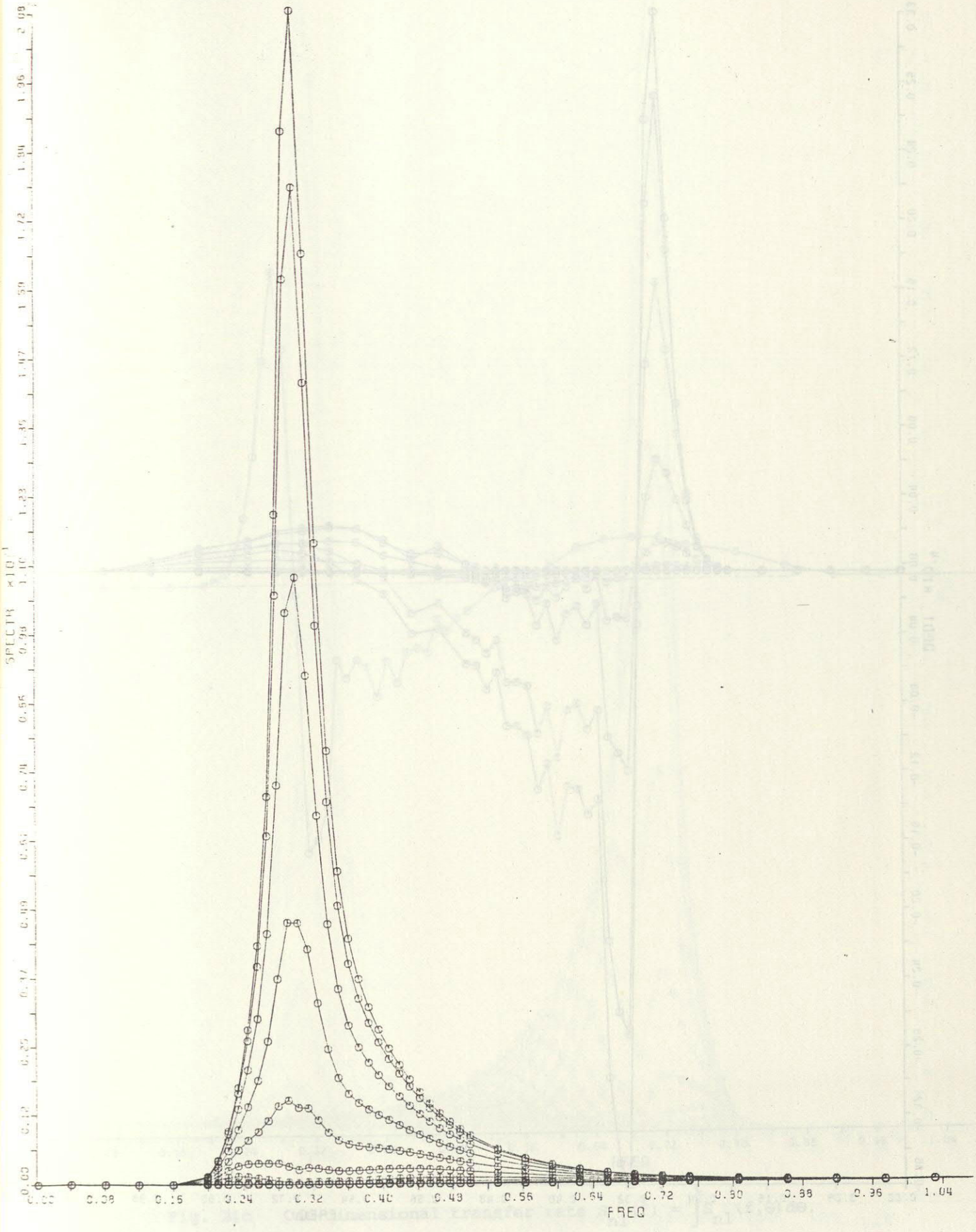

Fig. 24a Same as Fig. 16a with $k_m h$ = 10.0.

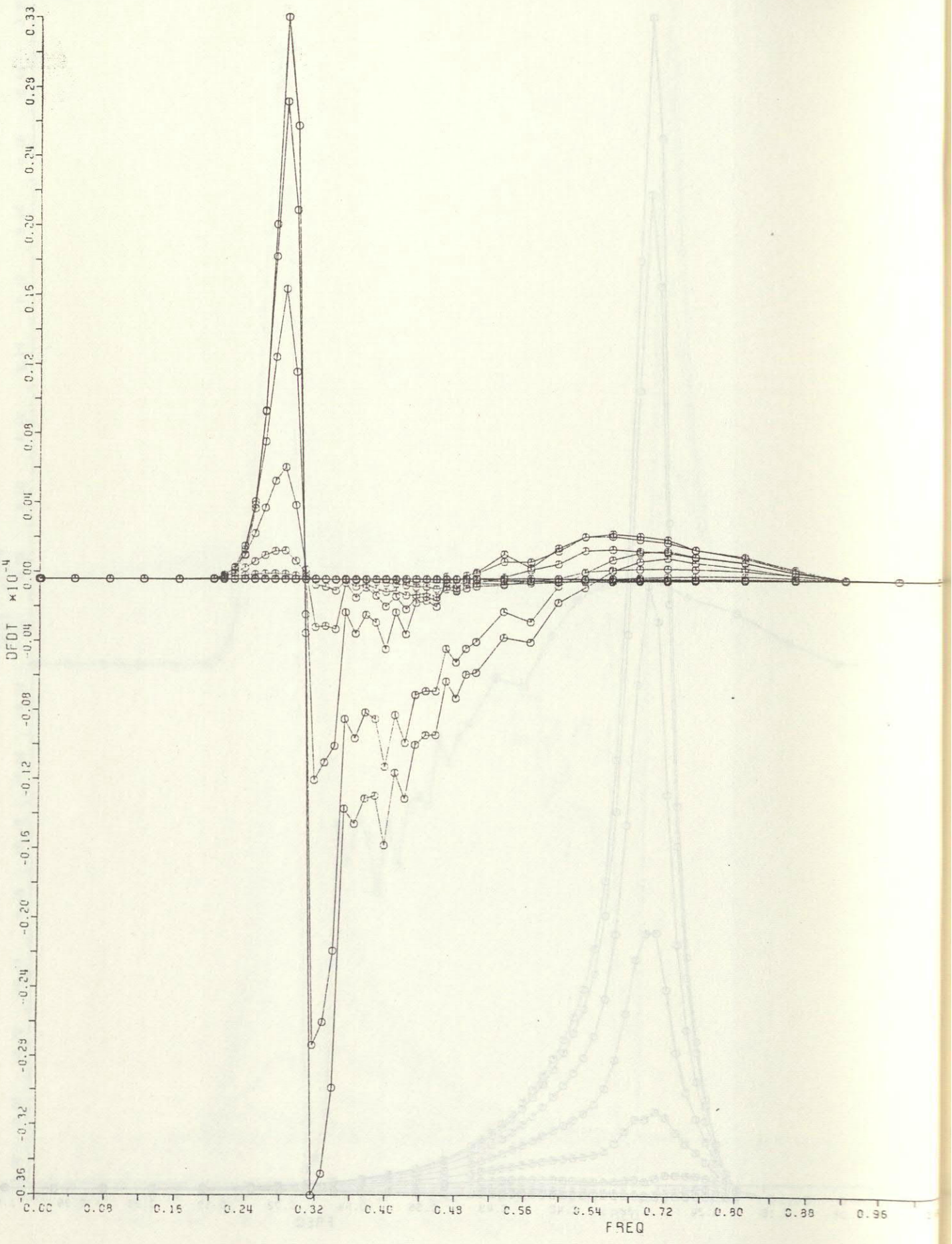

Fig. 24b Two-dimensional transfer rate $S_{nl}(f,\theta)$. Directional increments are 15^{o}.

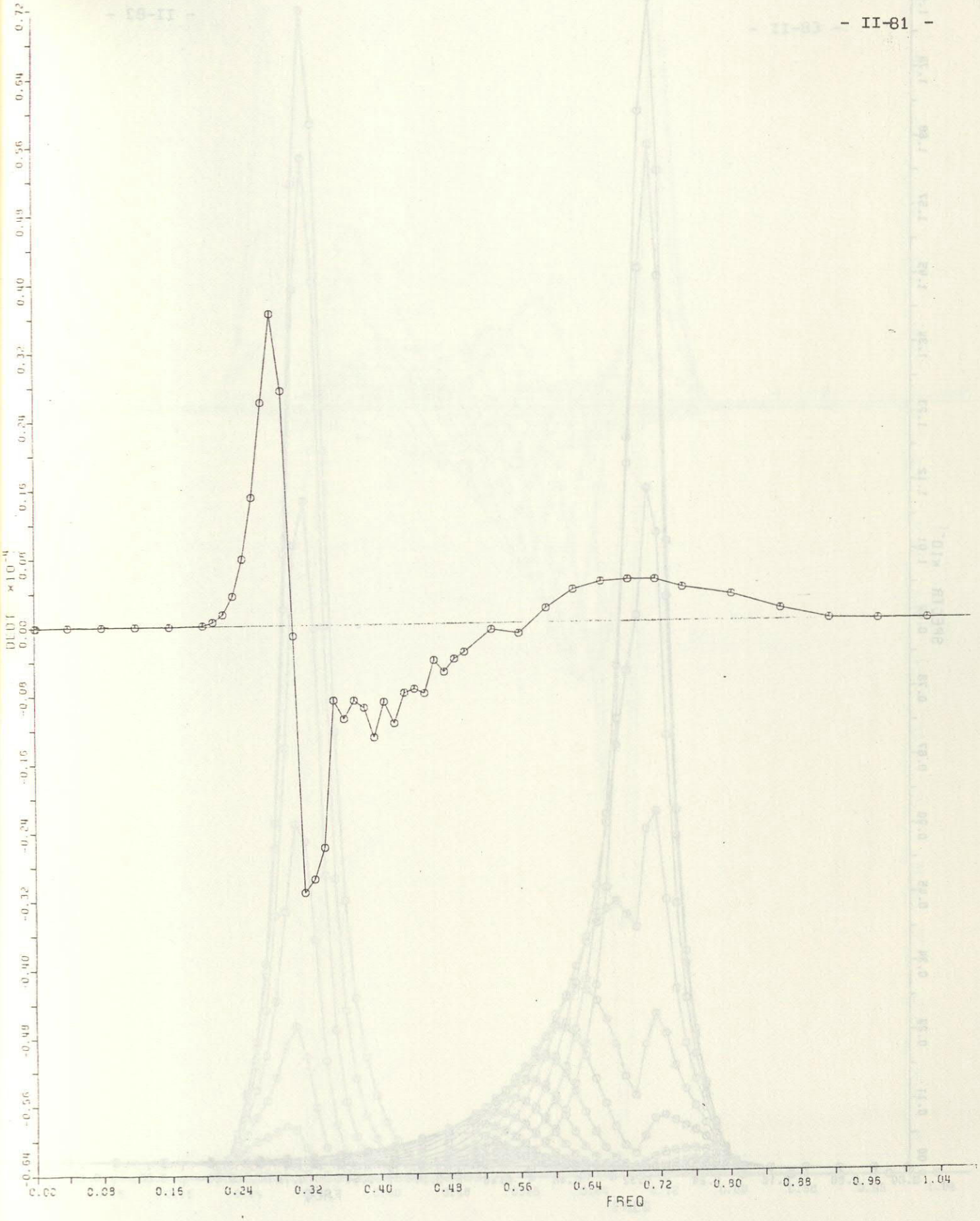

Fig. 24c One-dimensional transfer rate $S_{nl}(f) = \int S_{nl}(f,\theta)\,d\theta$.

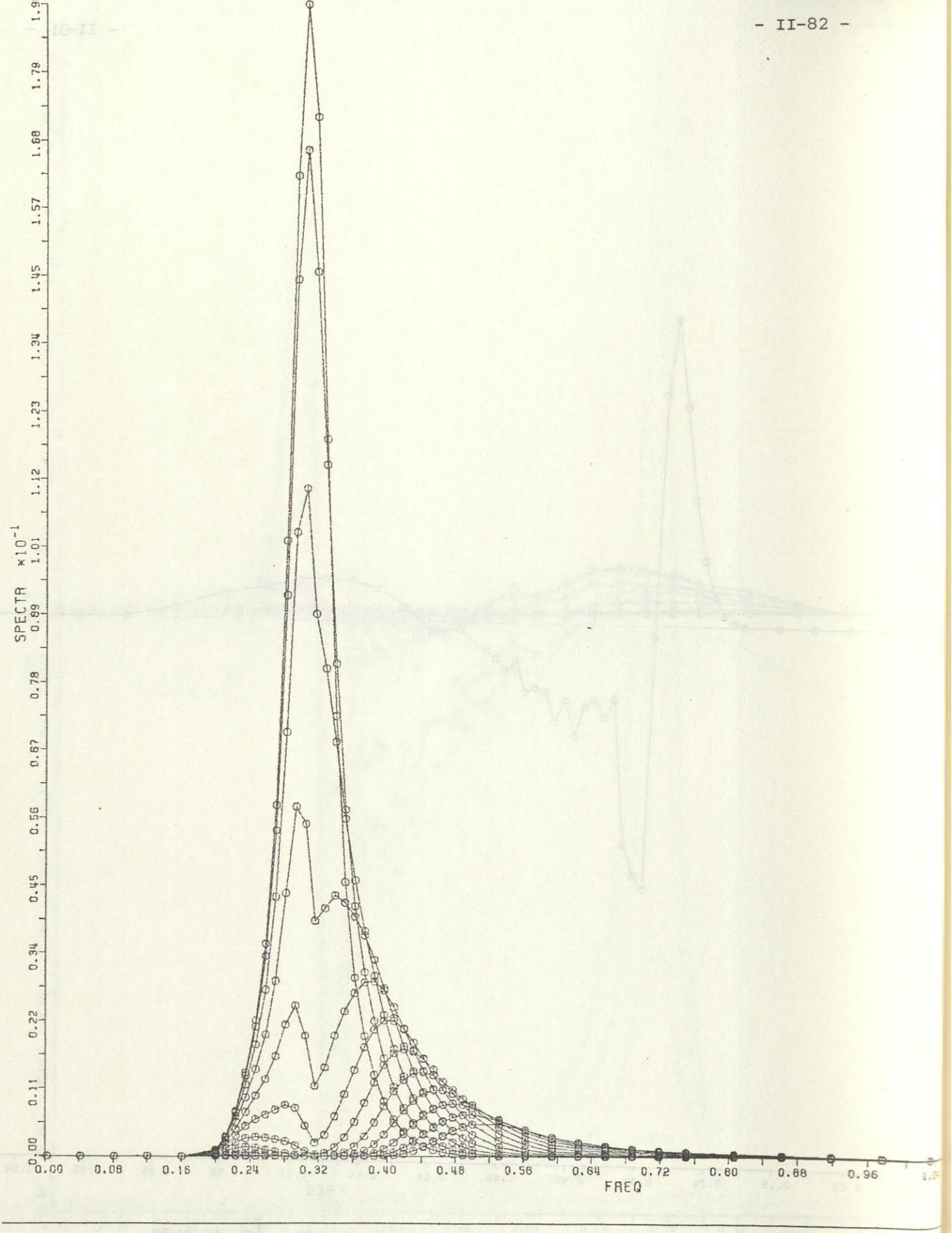

Fig. 25a Two-dimensional spectrum: mean JONSWAP frequency spectrum with $\cos^{2p}(\frac{\theta-\theta_o}{2})$ spreading factor as given by eqn (1), but with frequency dependent θ_o as given by eqn (5). Angular increments are 15^o, with angles from 0^o to 165^o

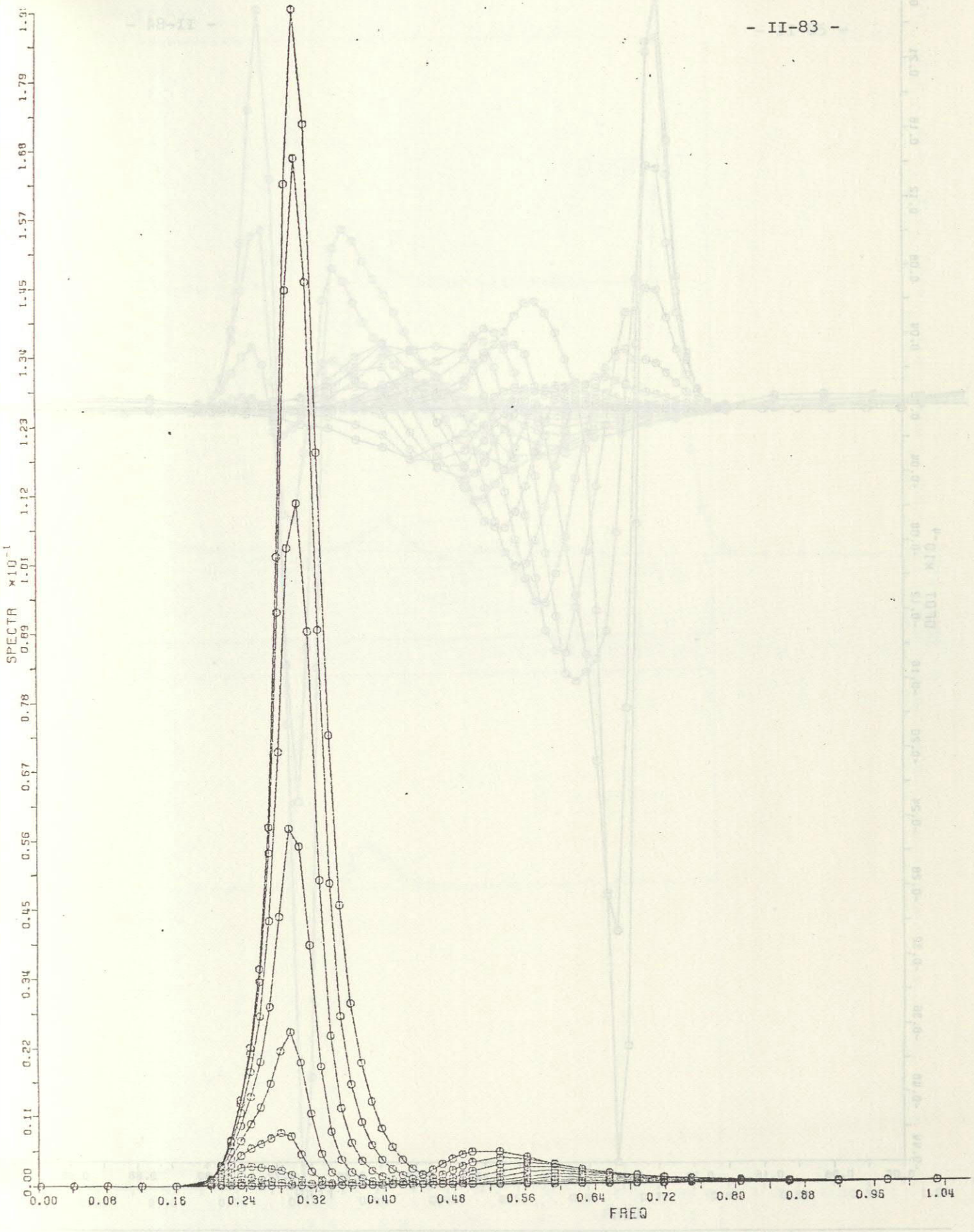

Fig. 25b Same as Fig. 25a, with angles from 0° to -180°.

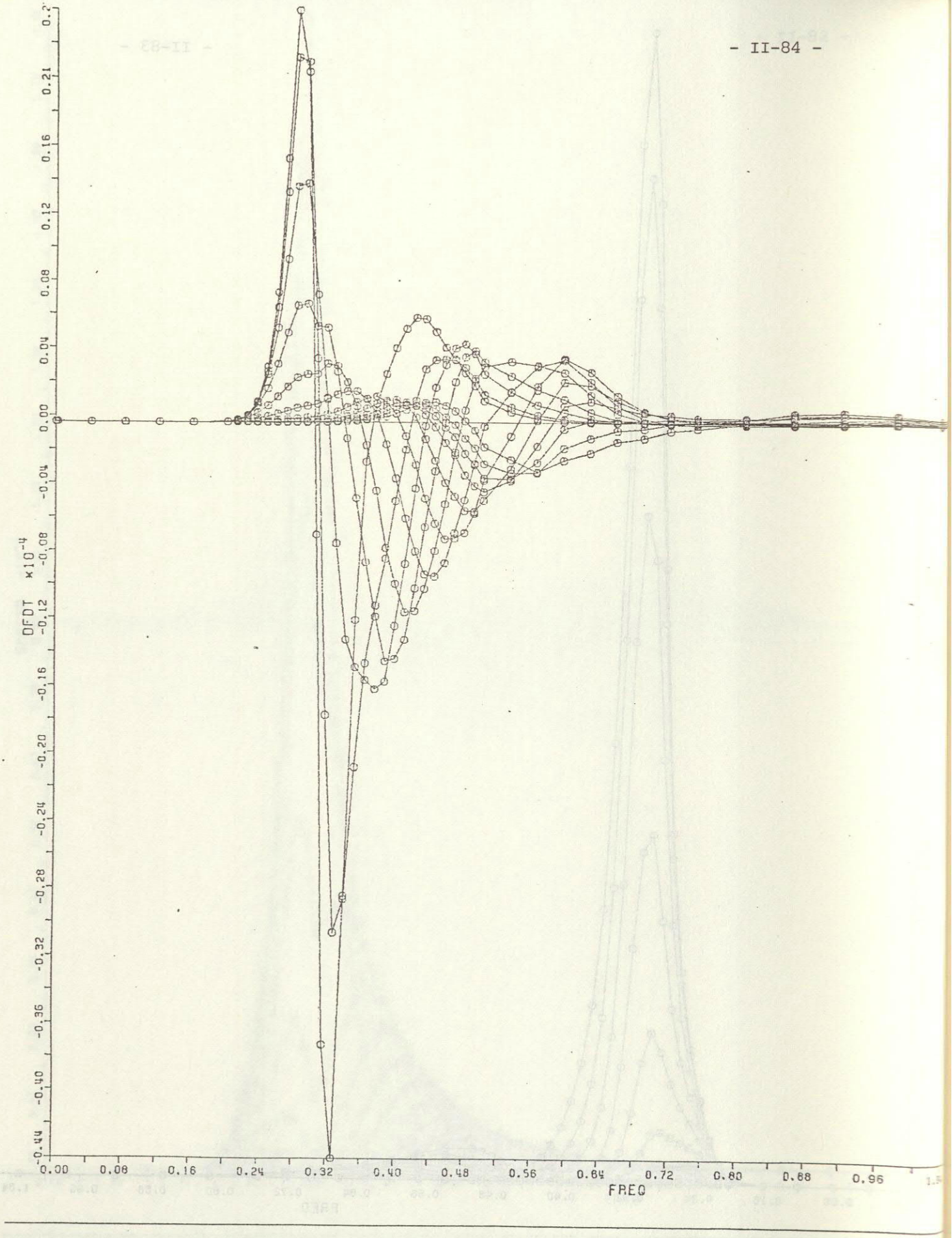

Fig. 25c Two-dimensional transfer rate S_{nl} from 0° to -165° in increments of 15°.

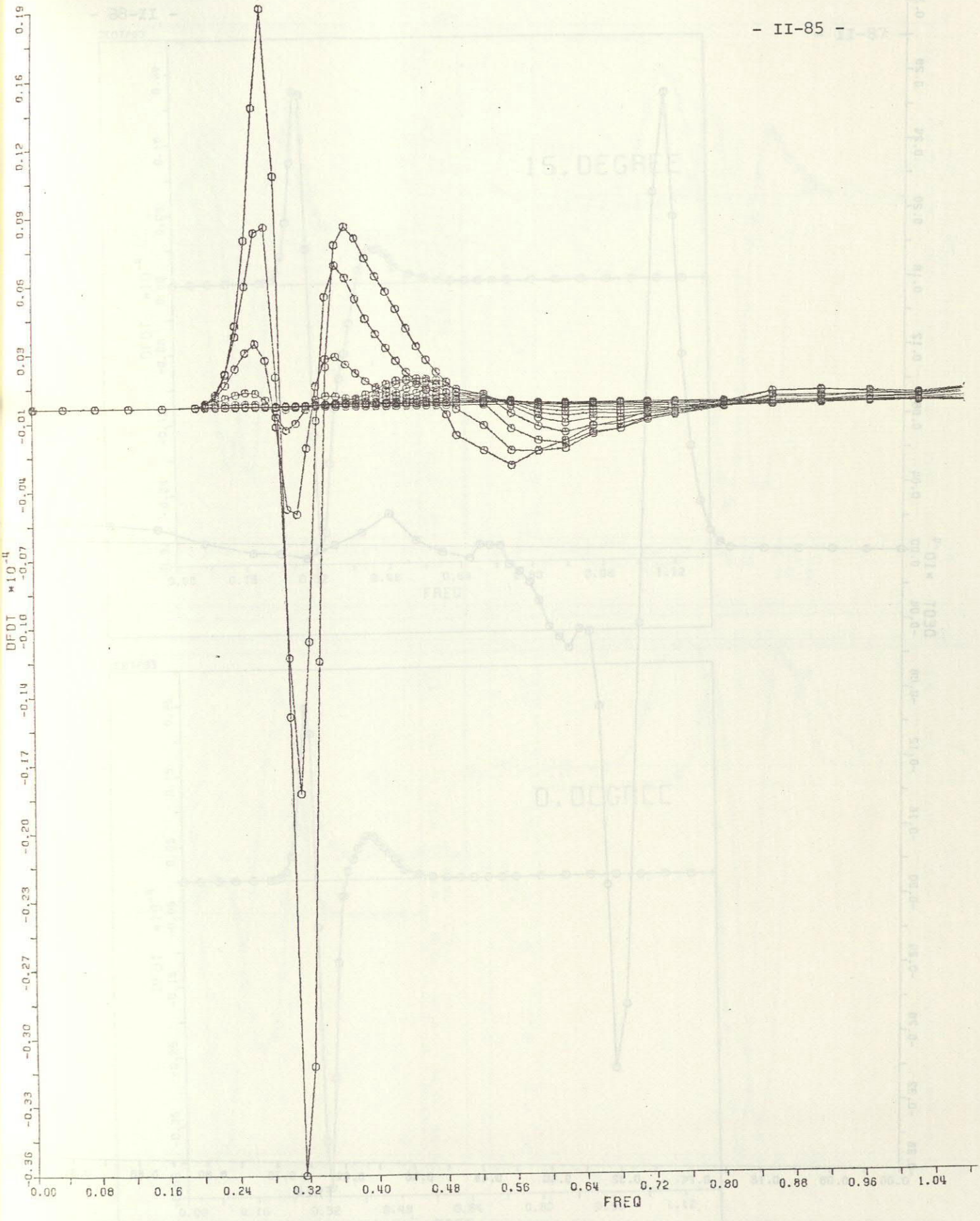

Fig. 25d Two-dimensional transfer rate S_{nl} from 180° - 345° in increments of 15°.

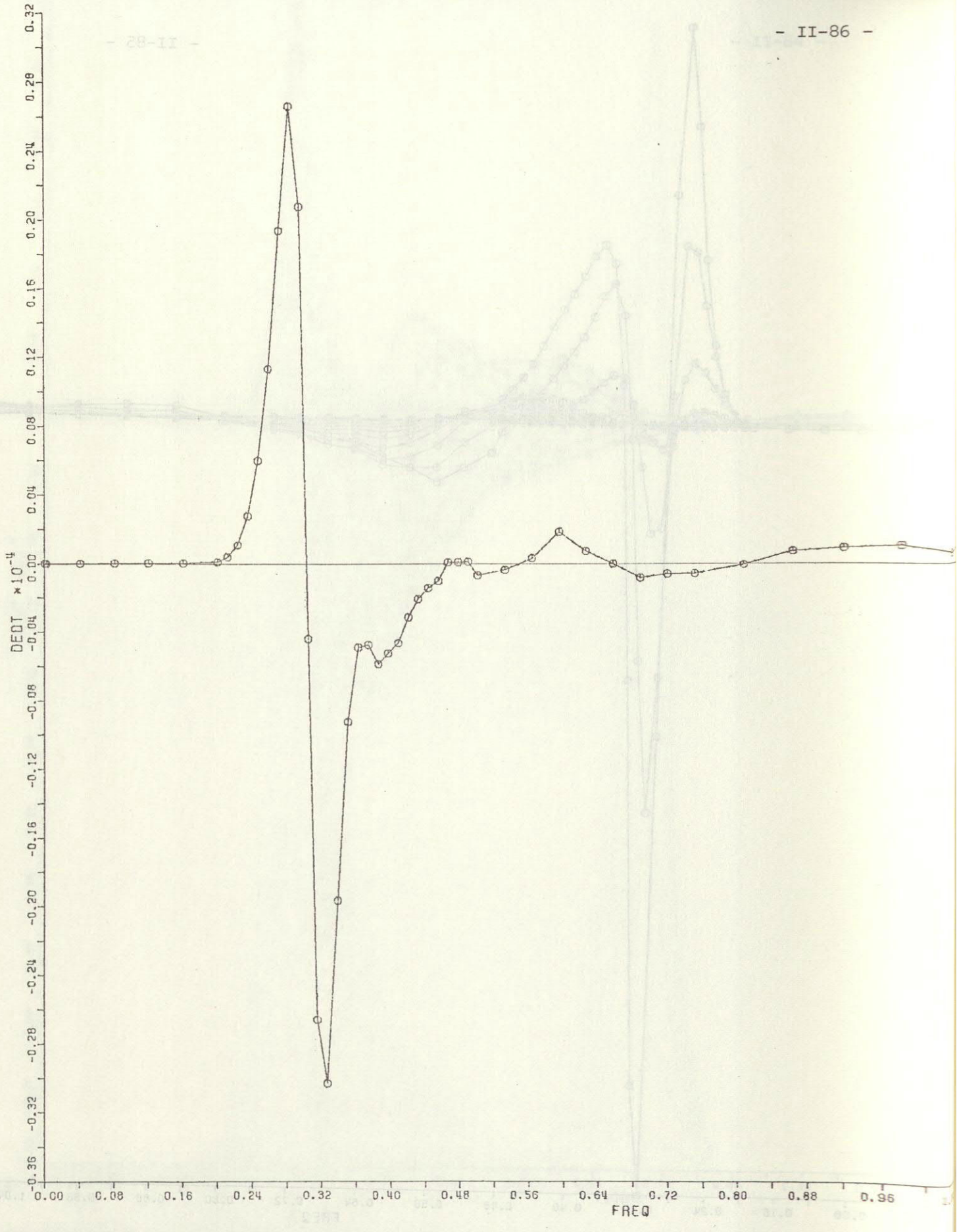

Fig. 25e One-dimensional transfer rate $S_{nl}(f) = \int S_{nl}(f,\Theta)\,d\Theta$.

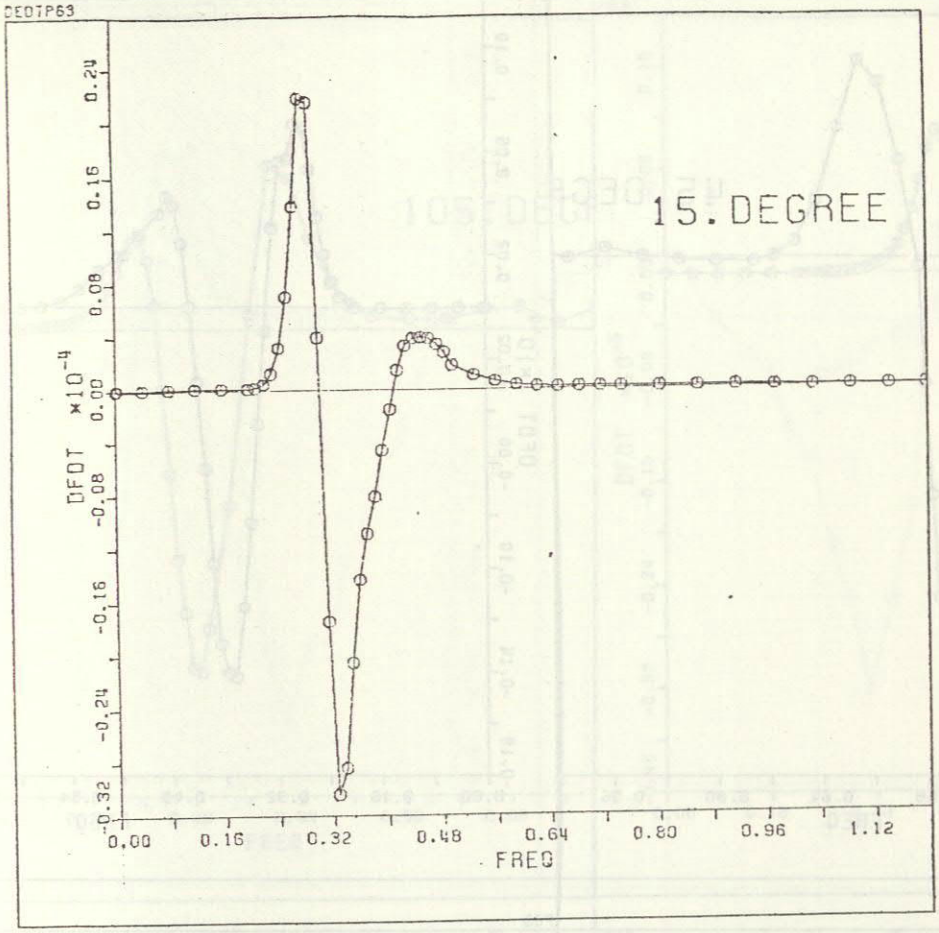

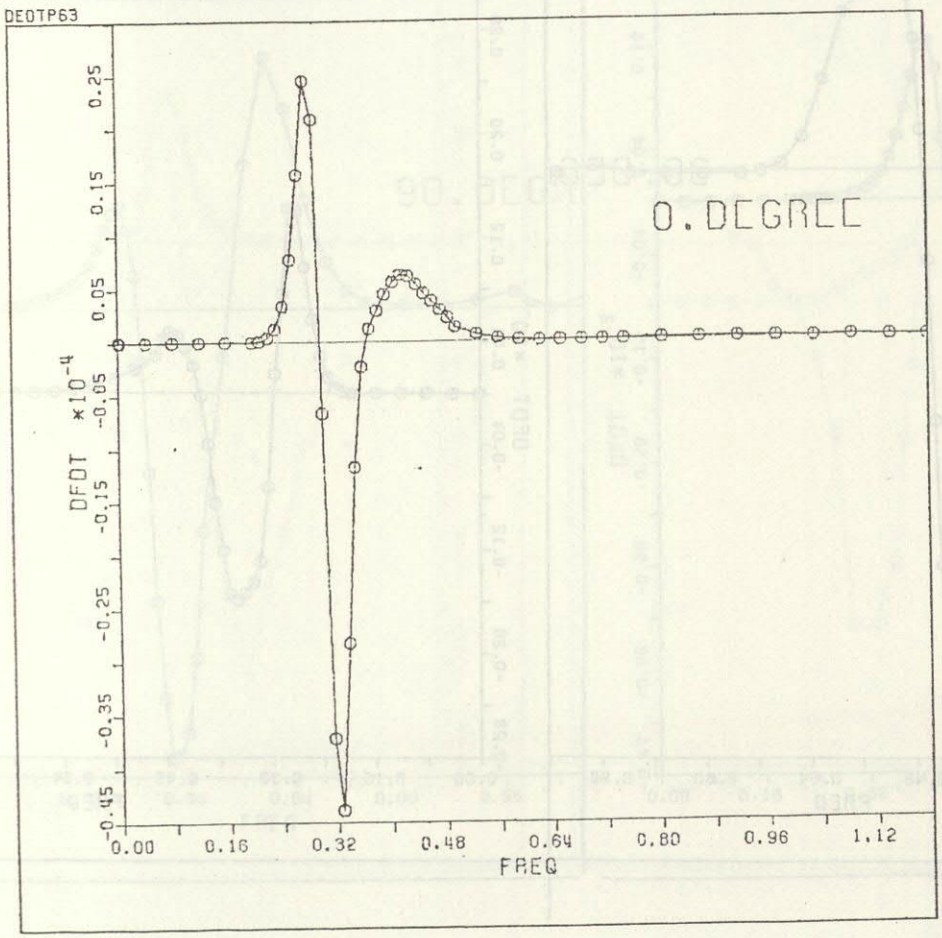

Fig. 25f $S_{nl}(f,\Theta)$

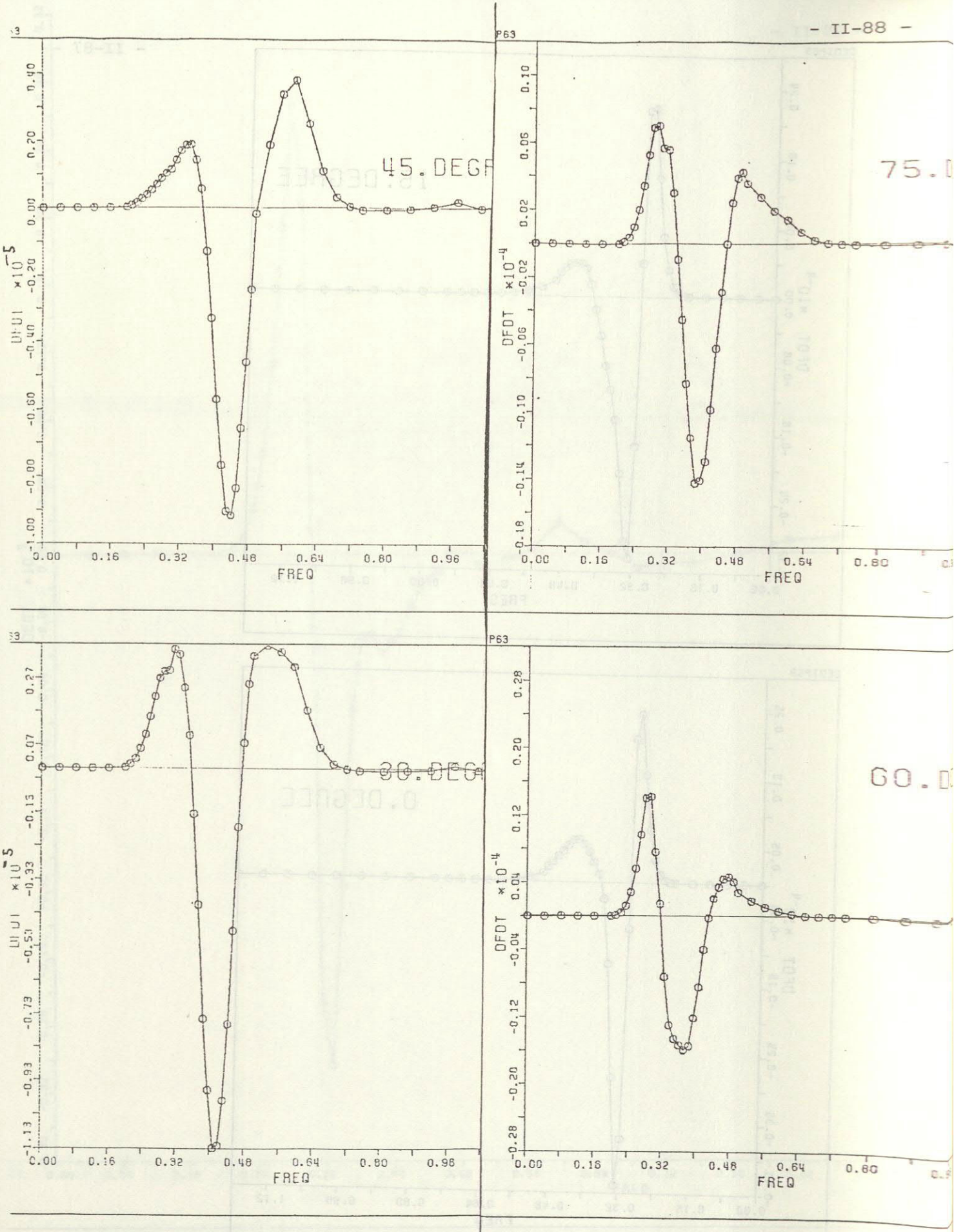

Fig. 25g $S_{nl}(f,\theta)$

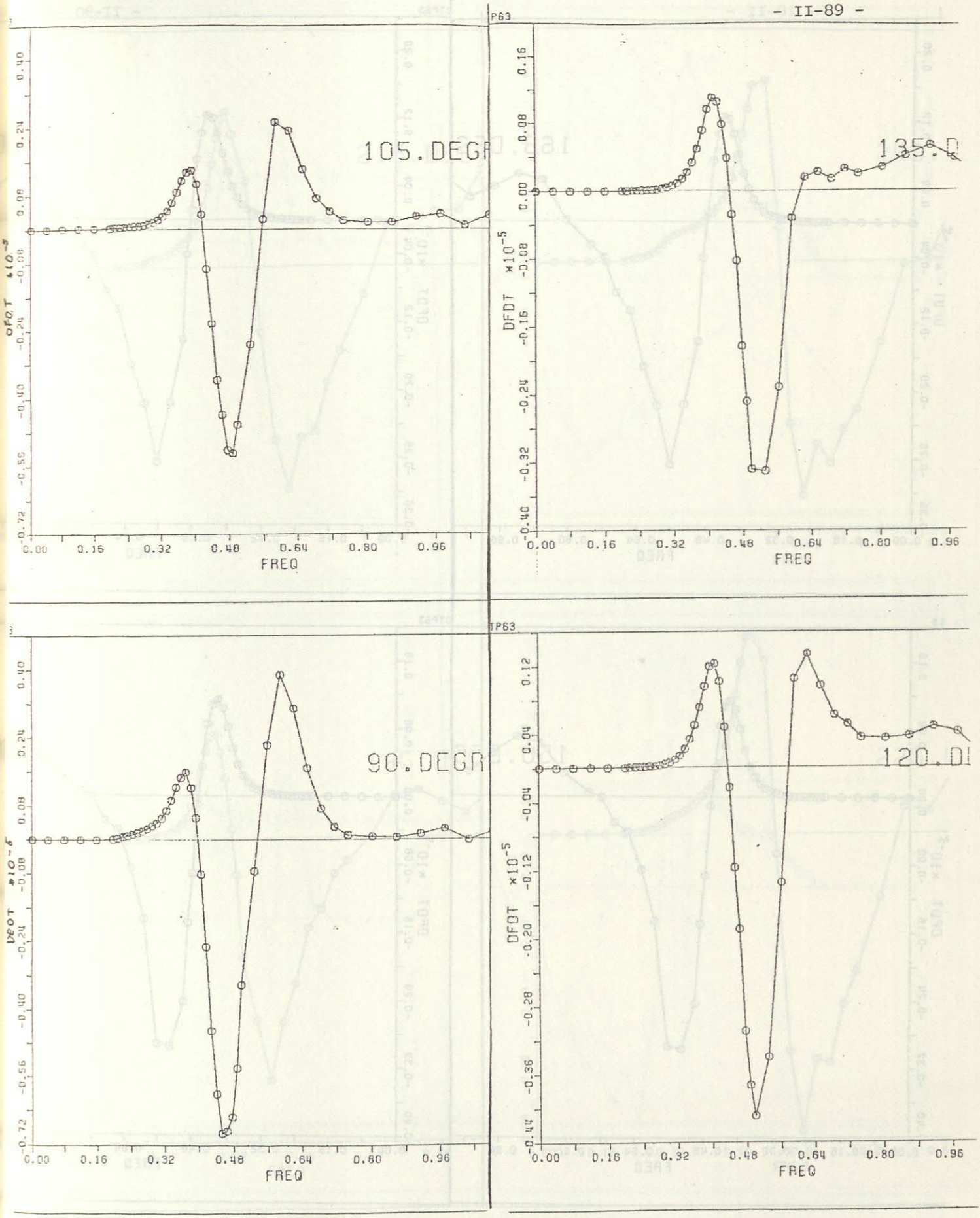

Fig. 25h $S_{nl}(f,\Theta)$

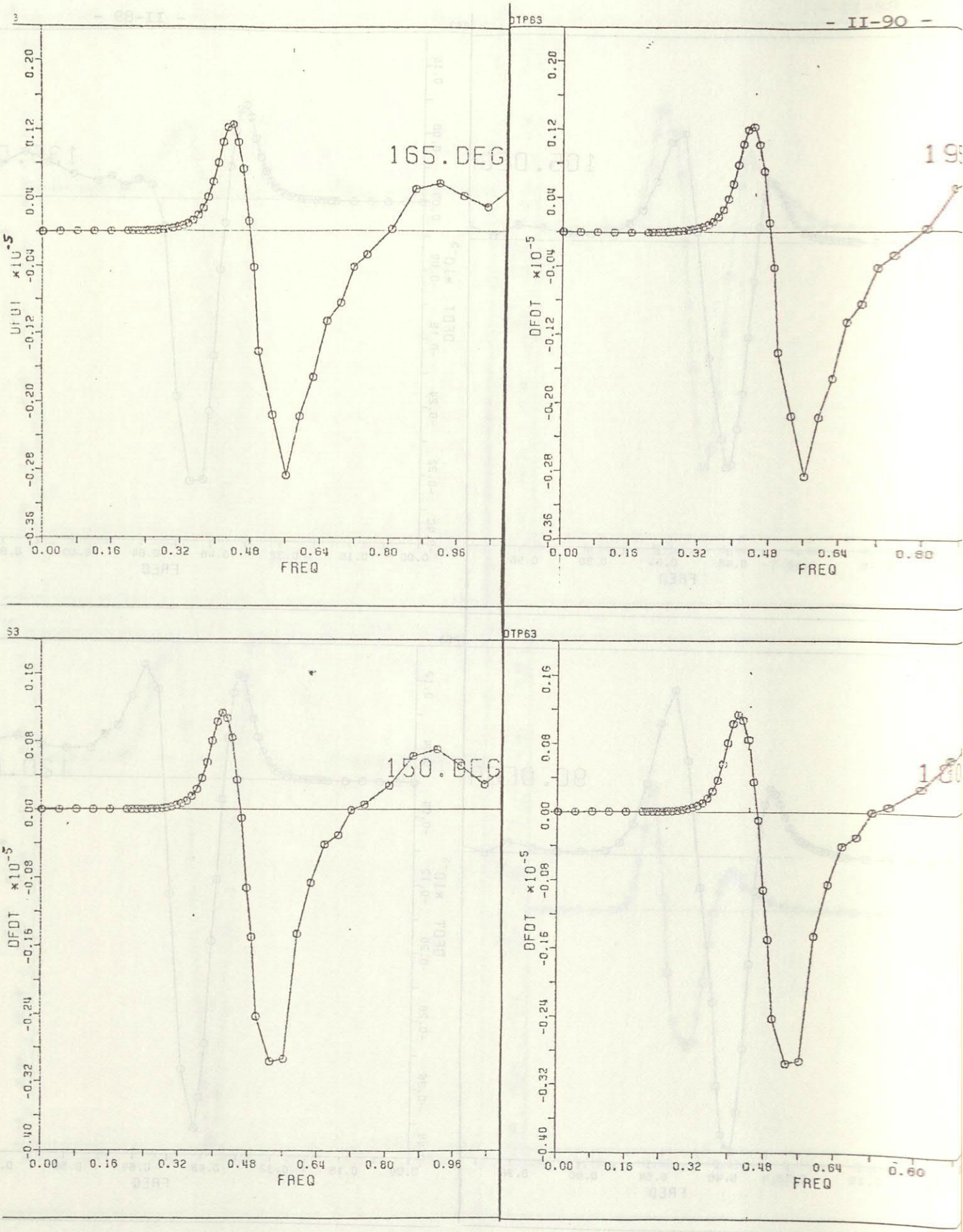

Fig. 25i $S_{nl}(f,\theta)$

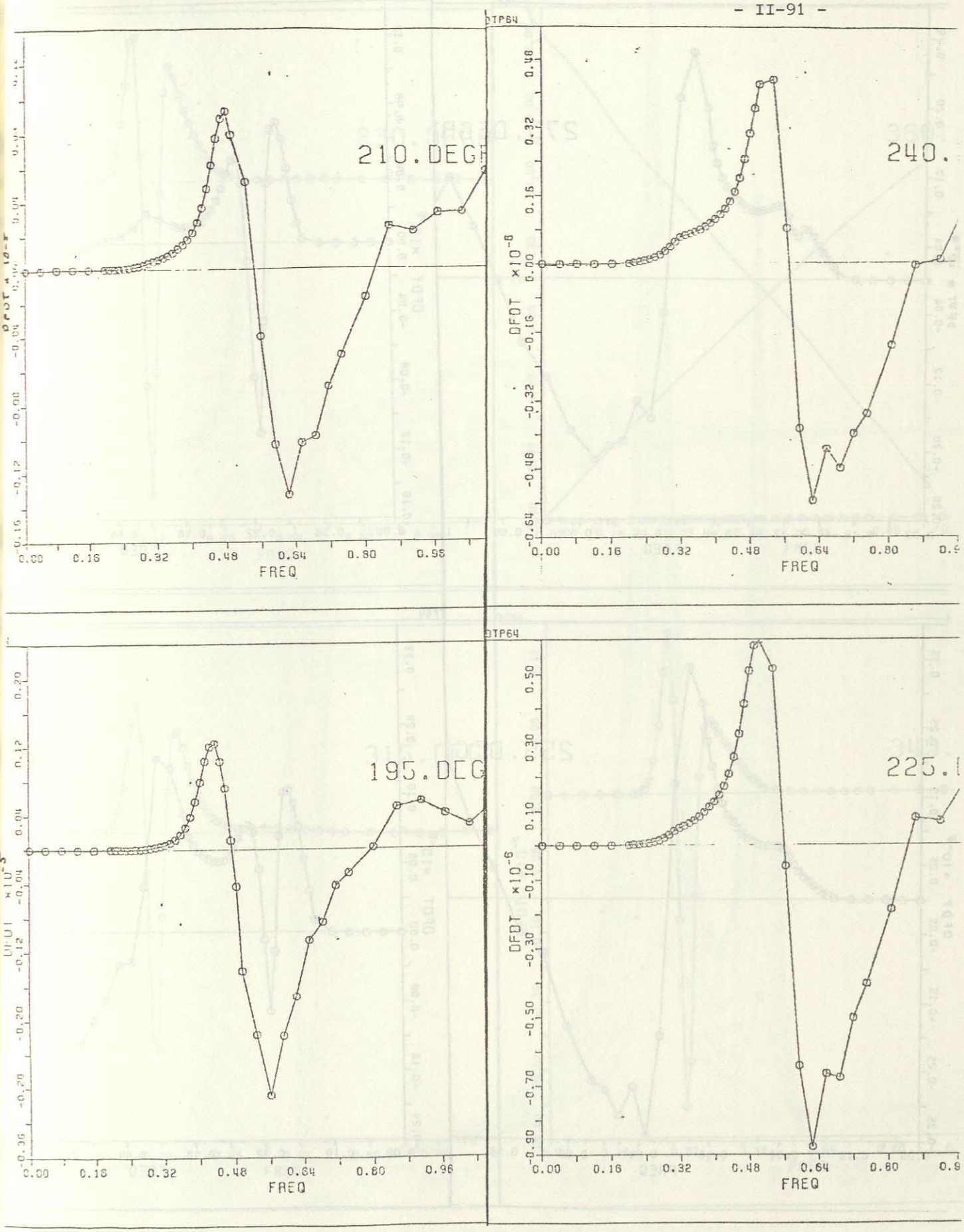

Fig. 25j $S_{nl}(F,\Theta)$

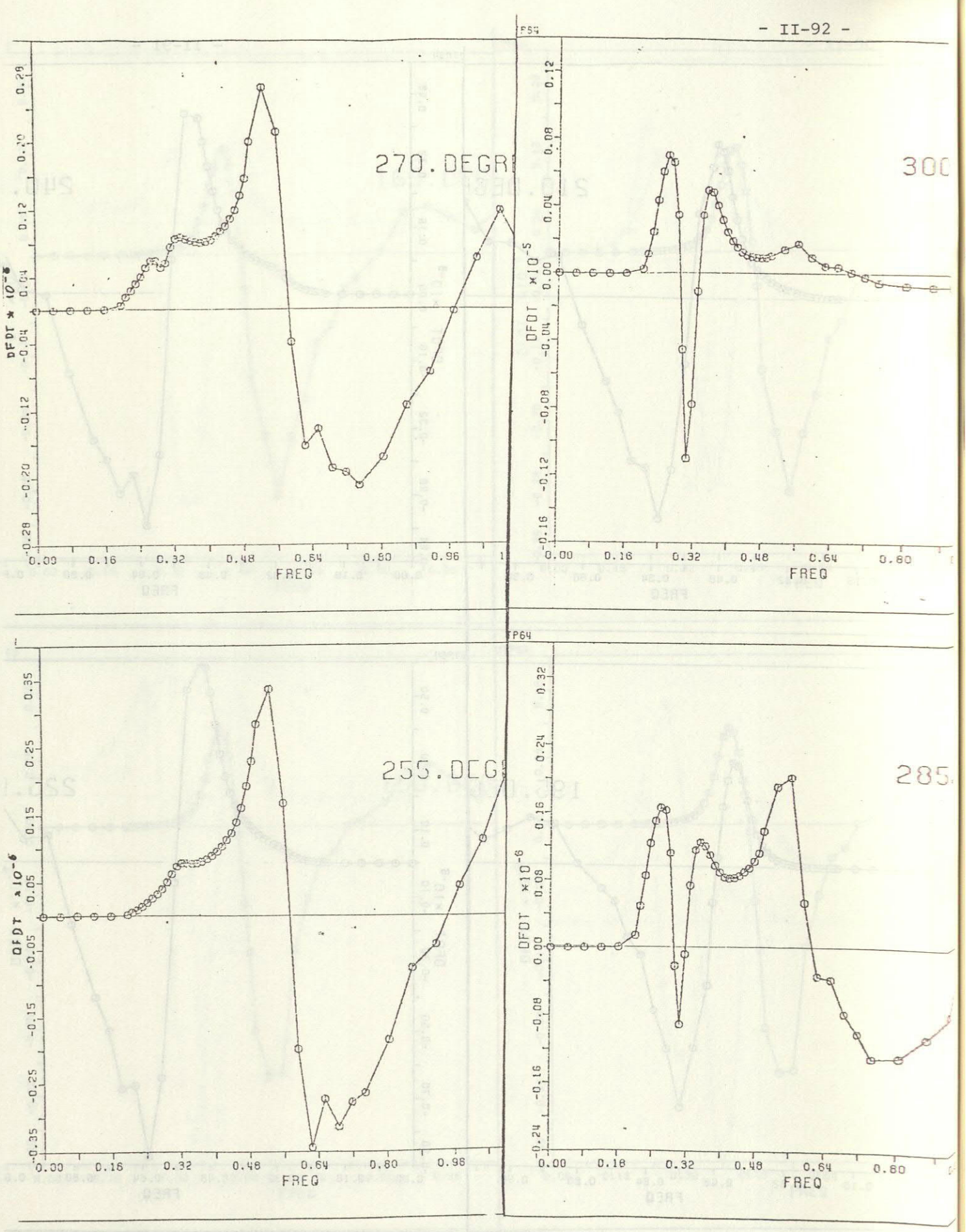

Fig. 25k $S_{nl}(f,\theta)$

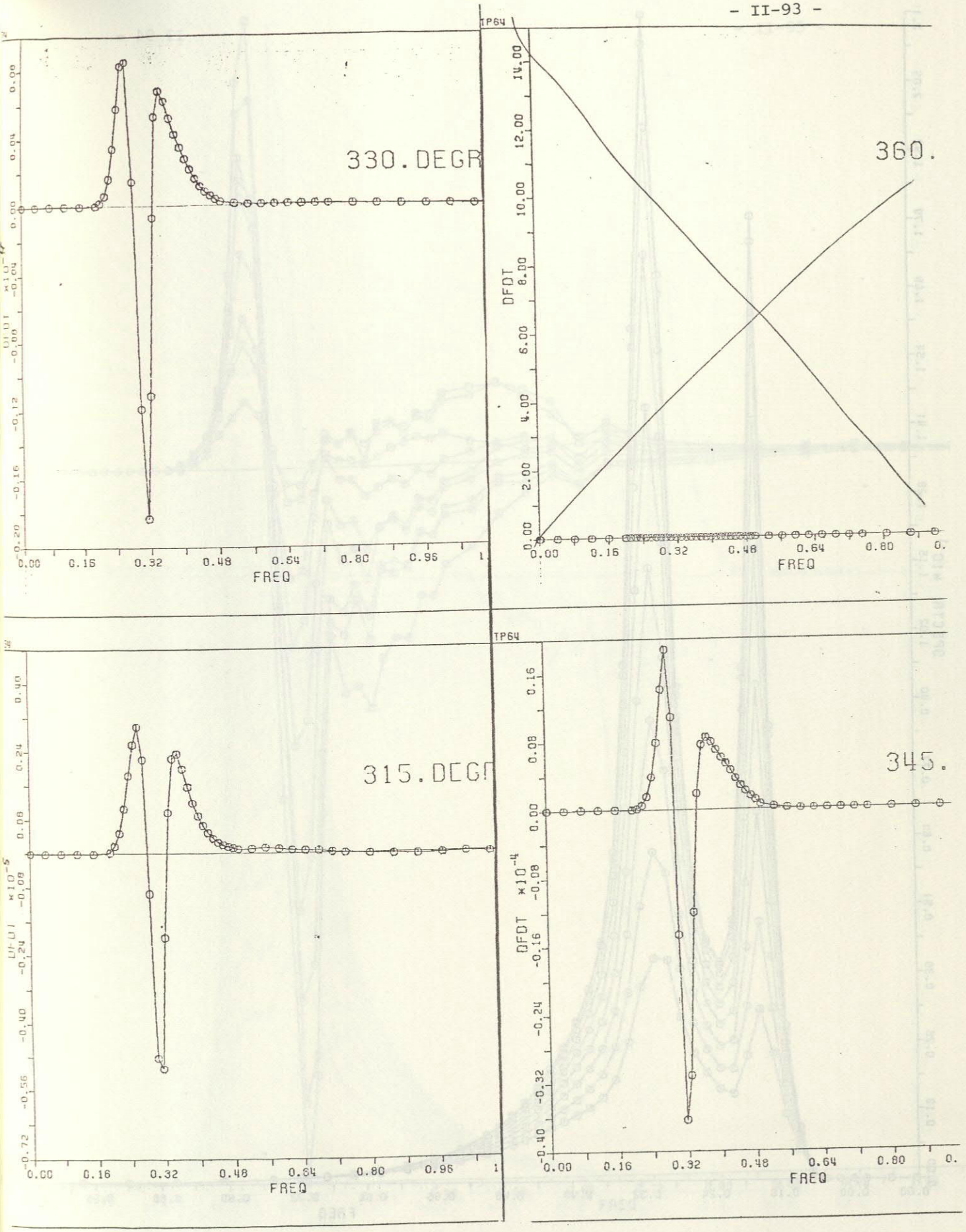

Fig. 25ℓ $S_{nl}(f,\Theta)$

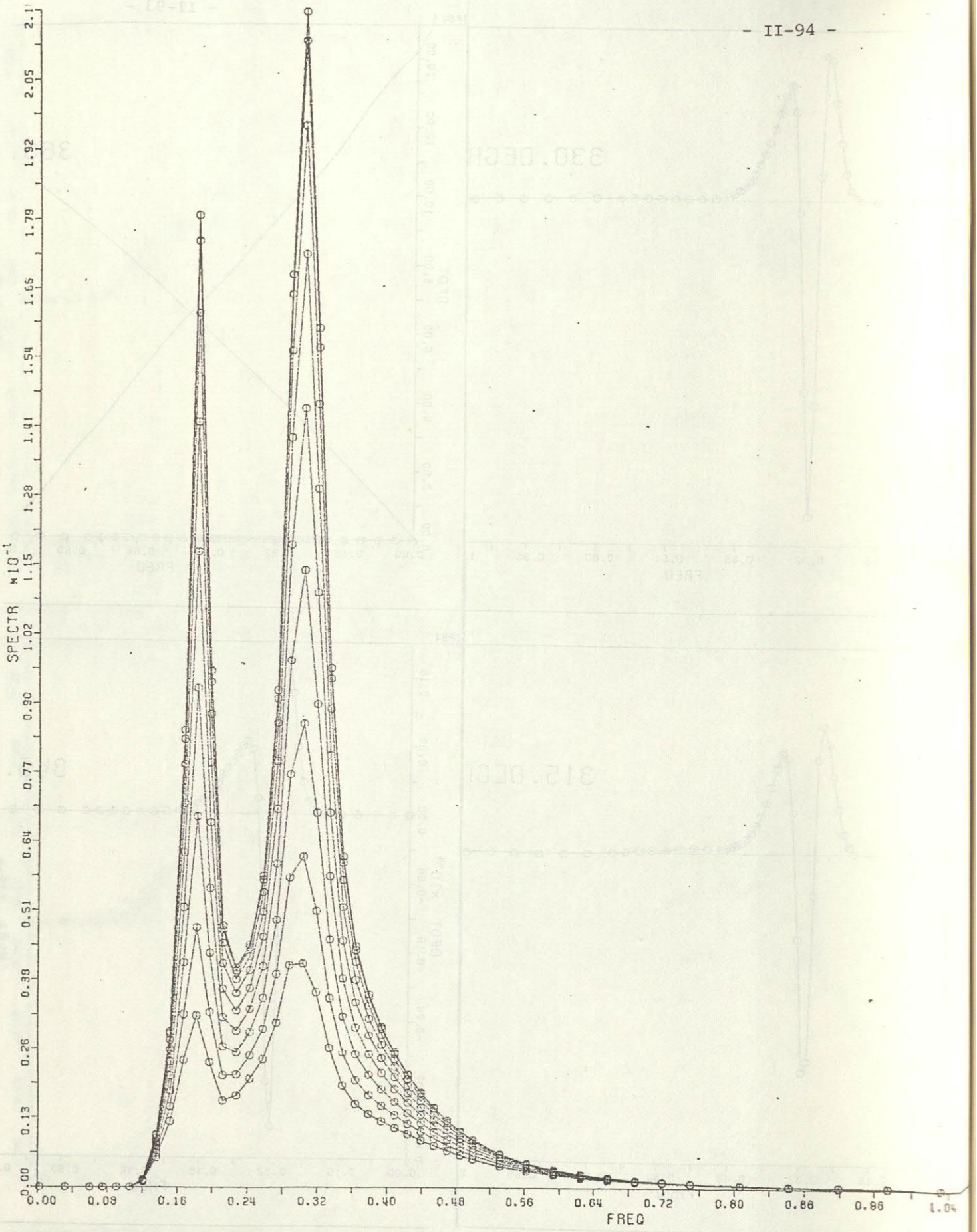

Fig. 26a JONSWAP spectrum, case 1, with superimposed swell. $(f_m)_{sw}/(f_m)_{ws} = 0.6$, $E_{sw}/E_{ws} = 0.5$, $\Theta_{sw} = \Theta_{ws}$. Directional increments are 6°.

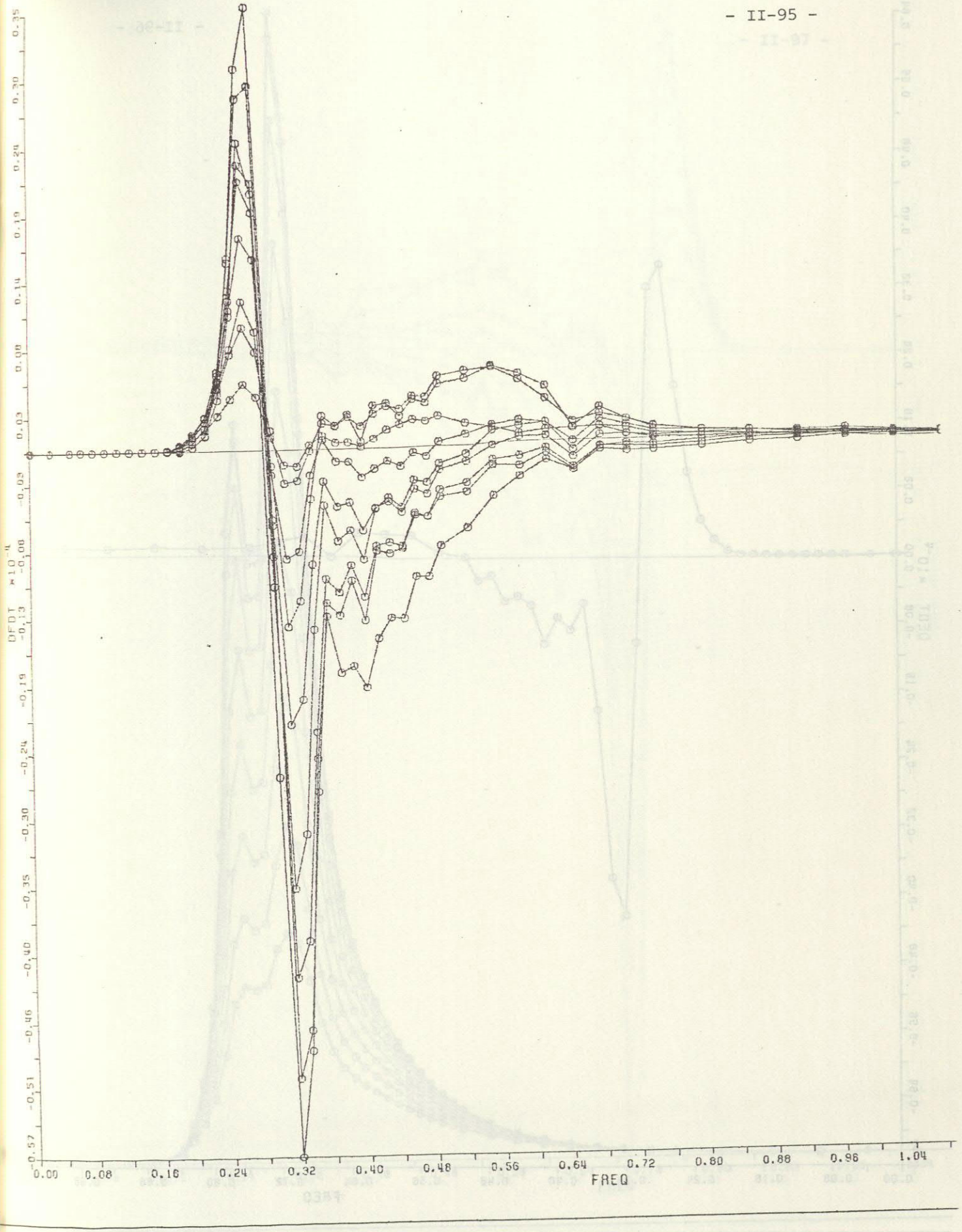

Fig. 26b Two-dimensional nonlinear transfer rate $S_{nl}(f,\Theta)$.

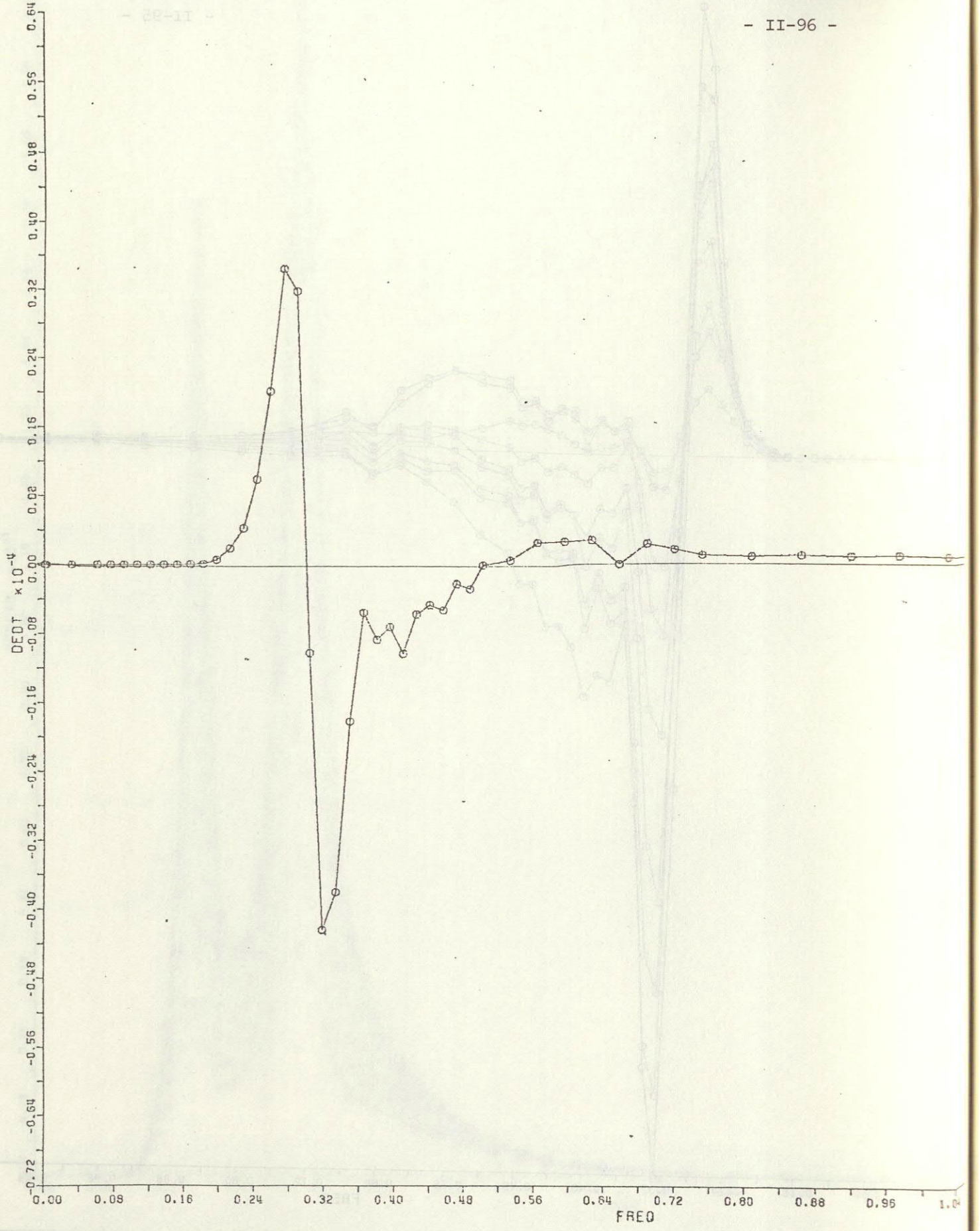

Fig. 26c One-dimensional nonlinear transfer rate $S_{nl}(f) = \int S_{nl}(f,\Theta)\,d\Theta$.

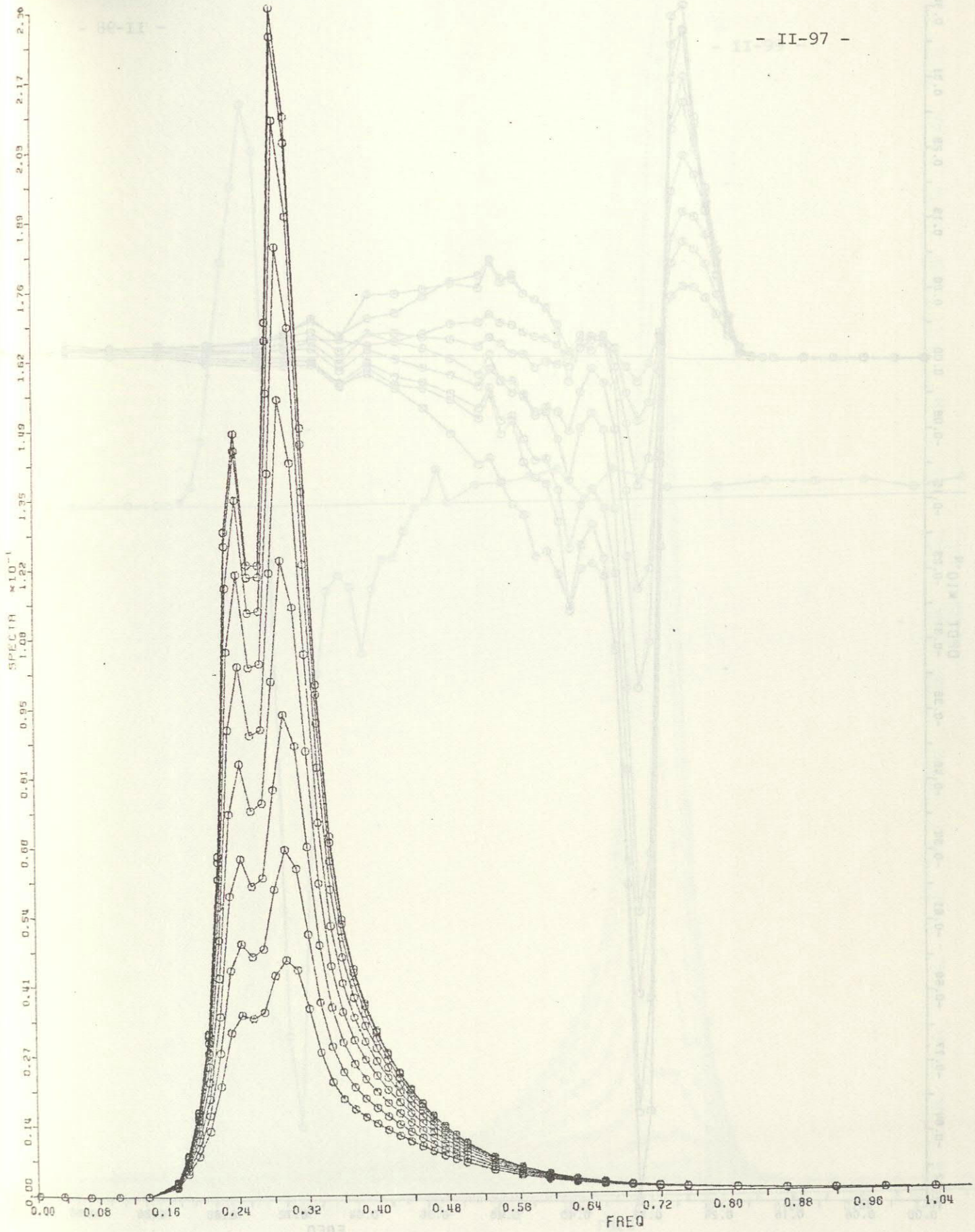

Fig. 27a JONSWAP spectrum, case 1, with superimposed swell $(f_m)_{sw}/(f_m)_{ws} = 0.8$, $E_{sw}/E_{ws} = 0.5$, $\Theta_{sw} = \Theta_{ws}$; directional increments are 6^o.

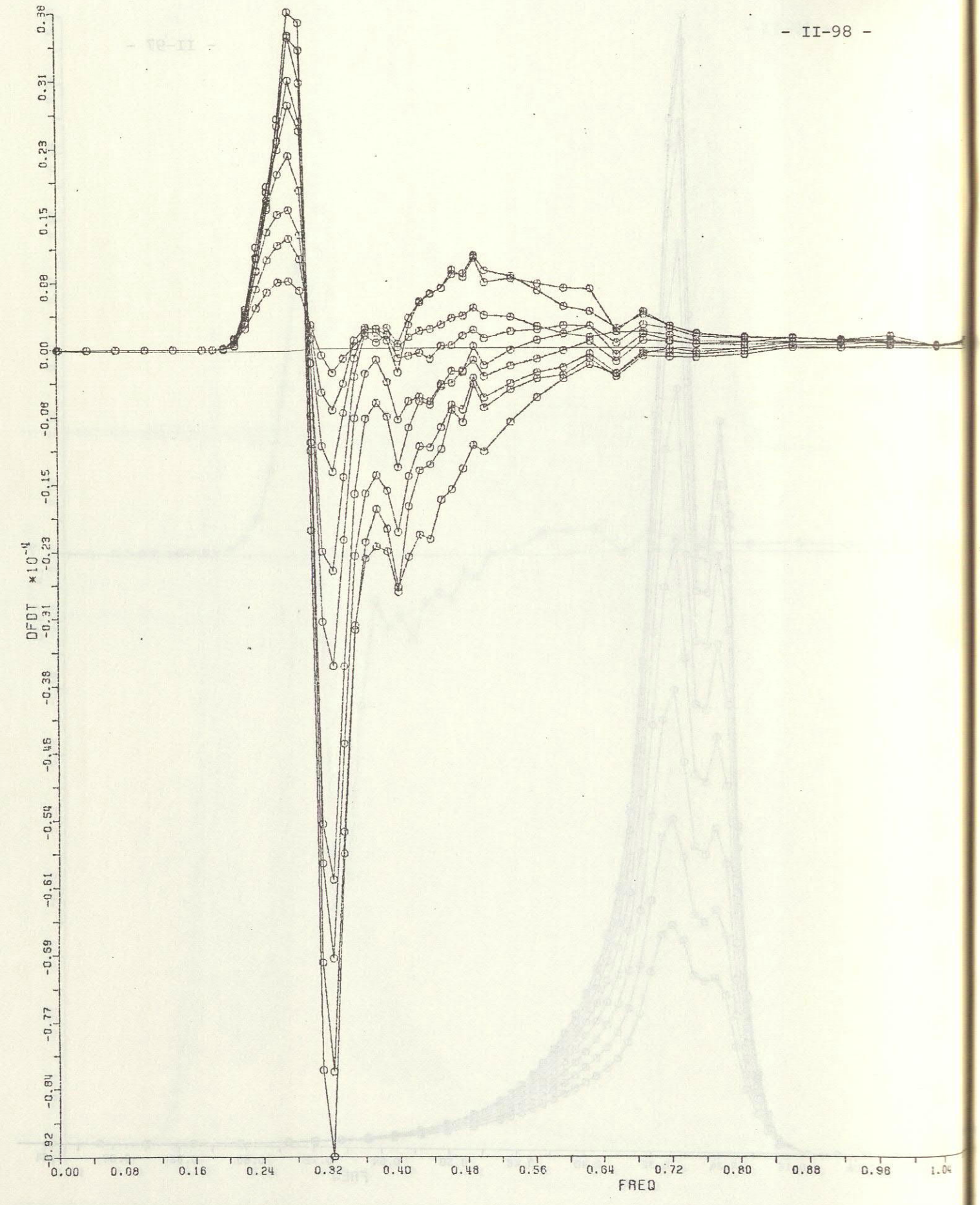

Fig. 27b Two-dimensional nonlinear transfer rate $S_{nl}(f,\Theta)$.

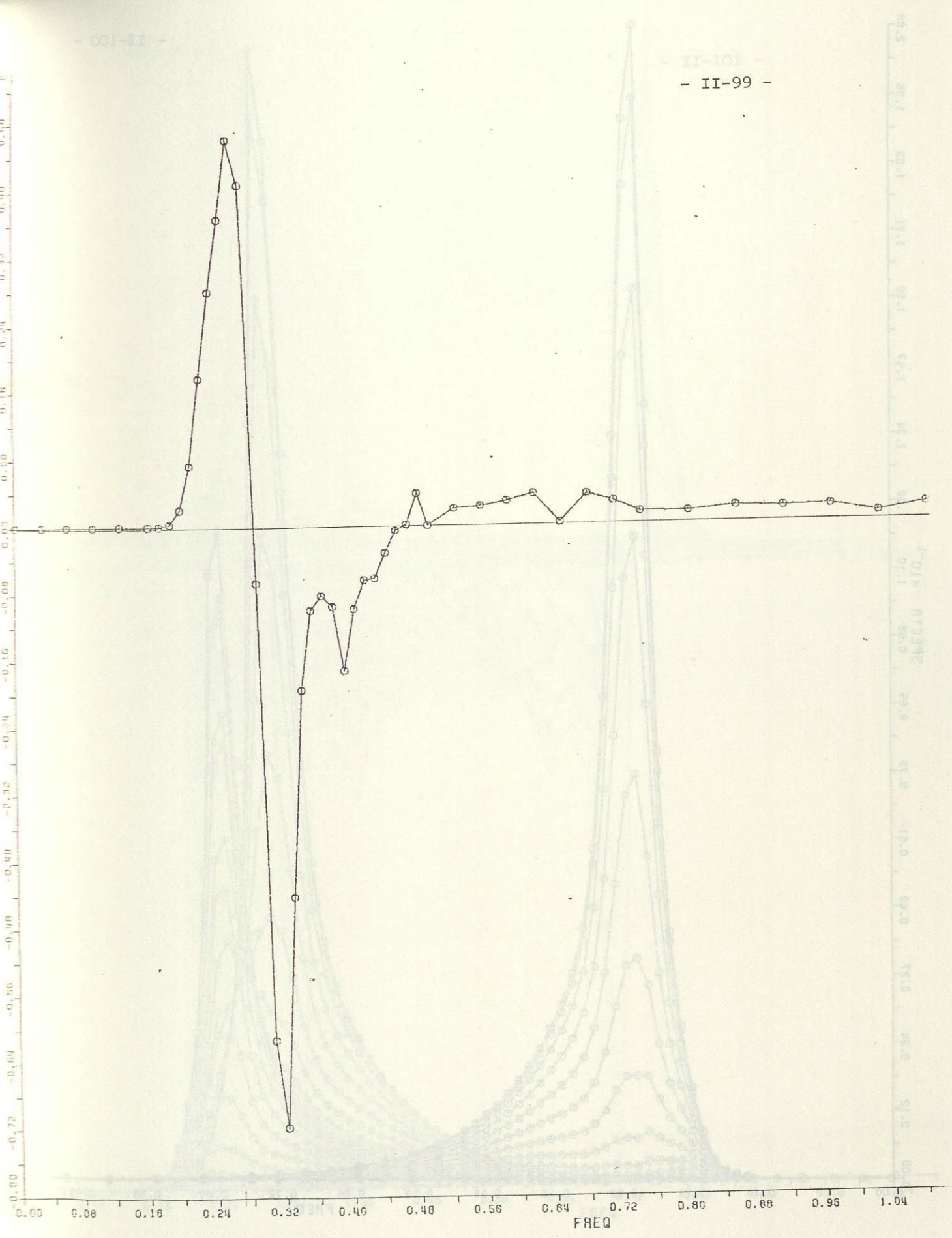

Fig. 27c One-dimensional nonlinear transfer rate $S_{nl}(f) = \int S_{nl}(f,\Theta)d\Theta$.

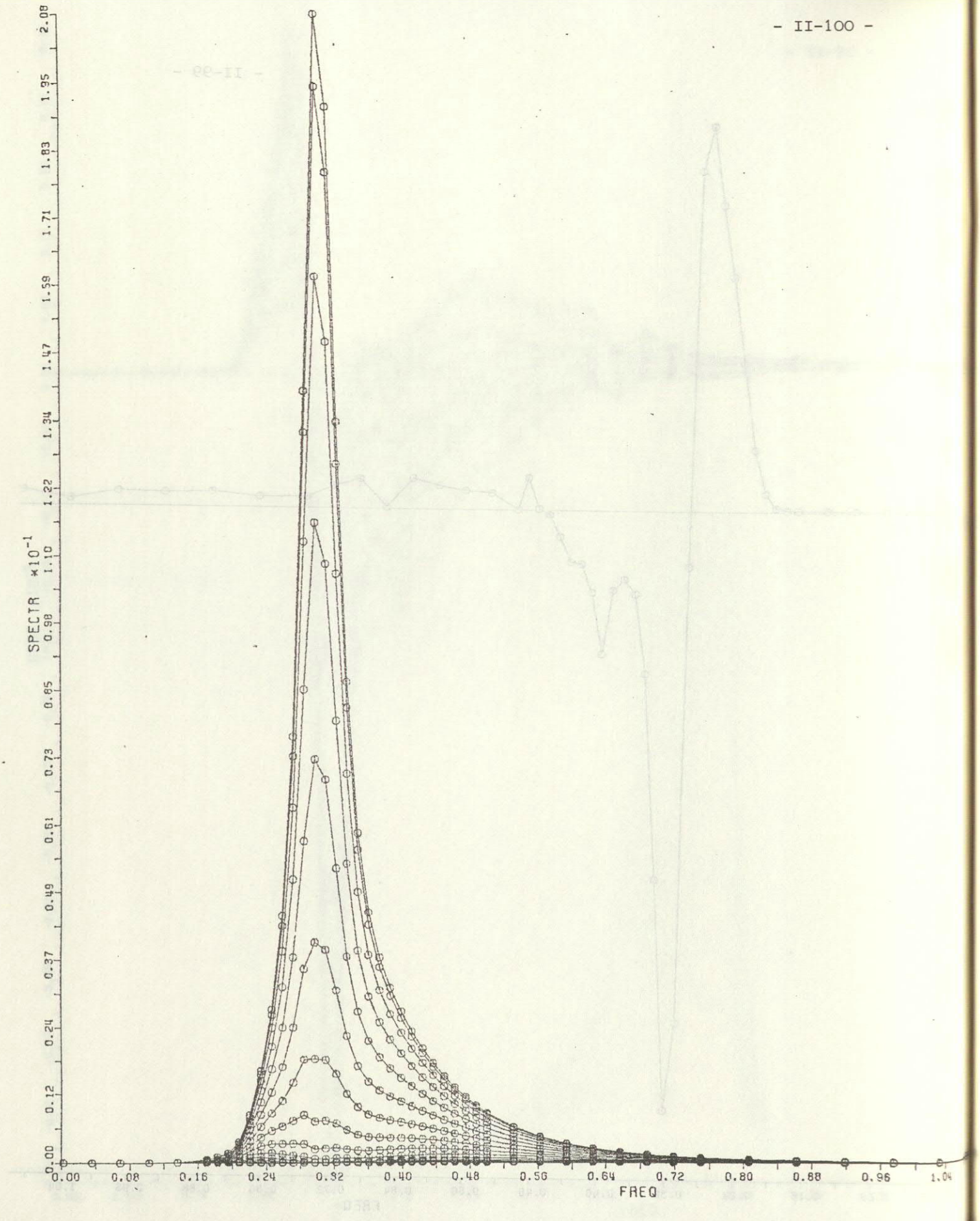

Fig. 28a JONSWAP spectrum, case 1, with superimposed swell.

$(f_m)_{sw}/(f_m)_{ws} = 0.8$, $E_{sw}/E_{ws} = 0.5$, $\theta_{sw} = \theta_{ws} - 90^{\circ}$.

Angles from 0° to 180° in increments of 6°.

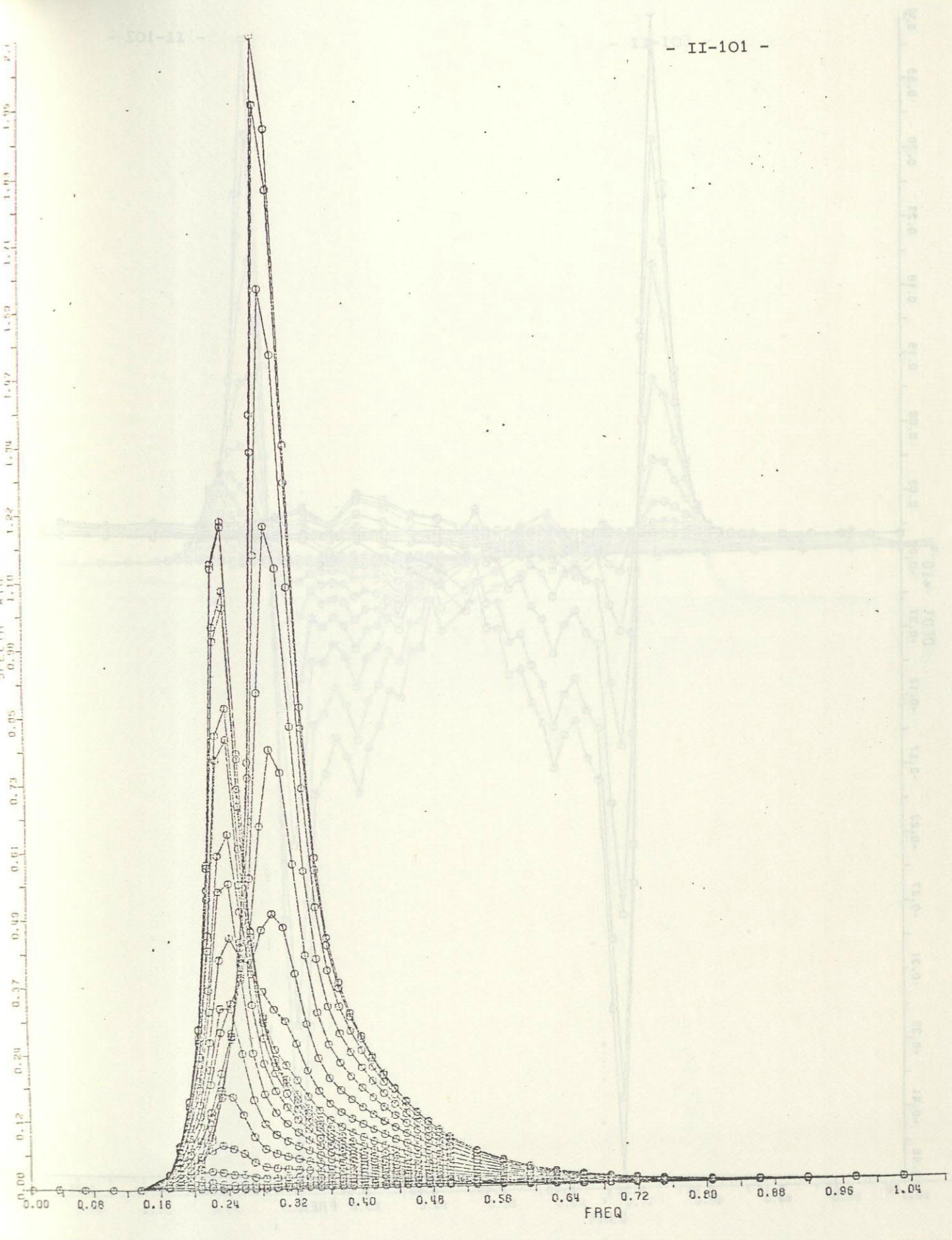

Fig. 28b Same as Fig. 28a, but with angles from 0° to -180° in increments of 6°.

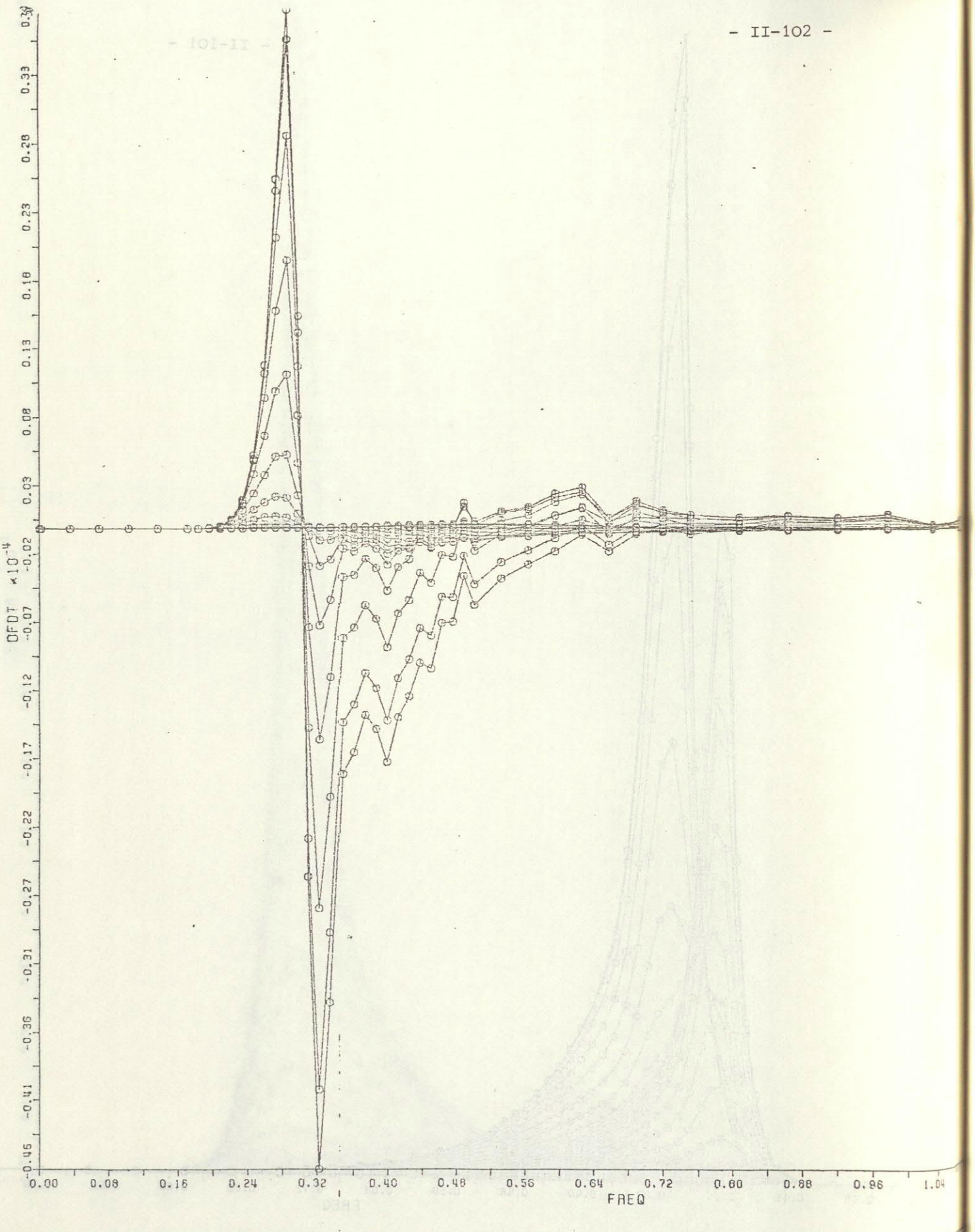

Fig. 28c Two-dimensional nonlinear transfer $S_{nl}(f,\Theta)$ for angles from 0° to 174° in increments of 6°.

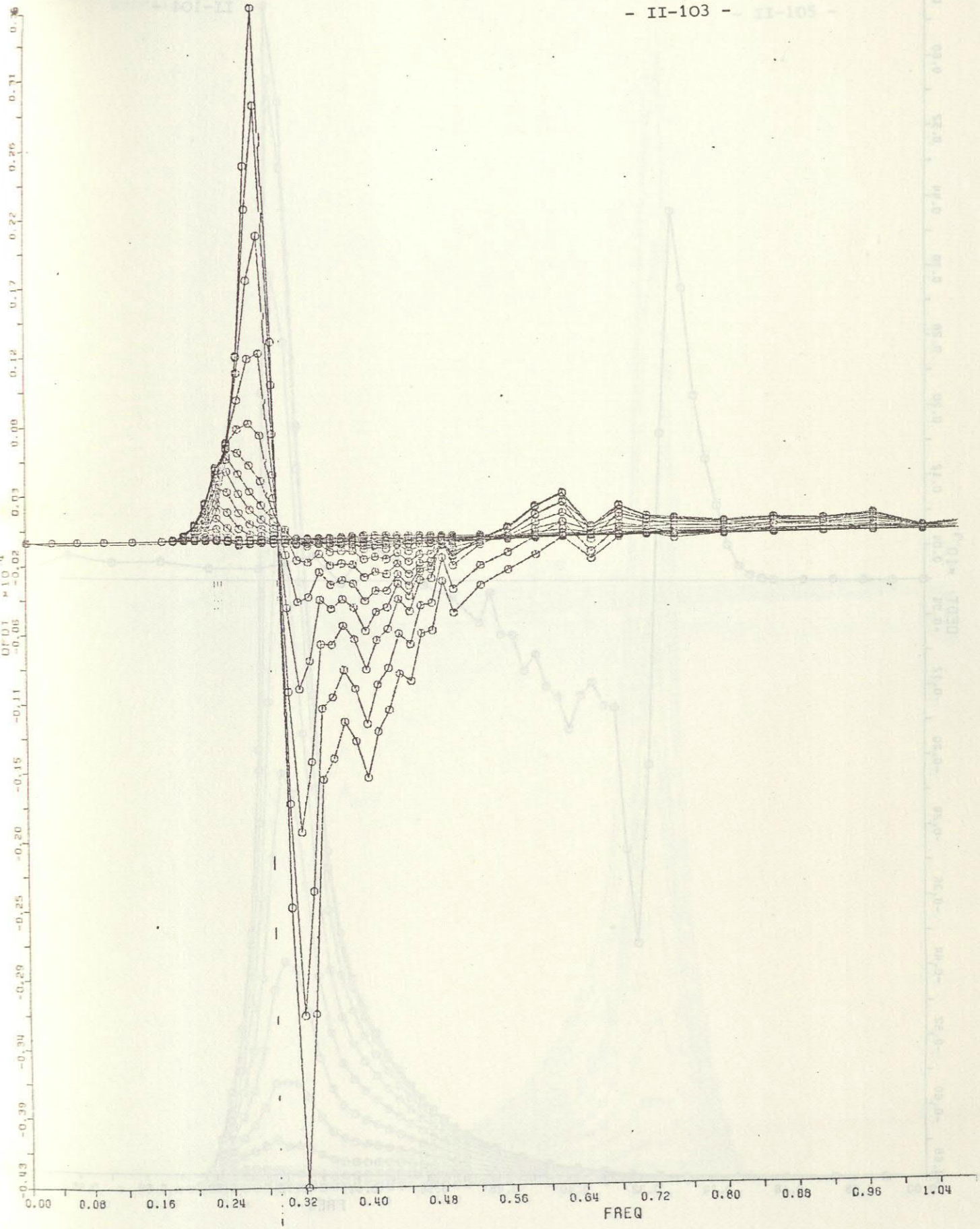

Fig. 28d Two-dimensional nonlinear transfer $S_{nl}(f,\Theta)$ for angles from -6° to -180° in increments of 6°.

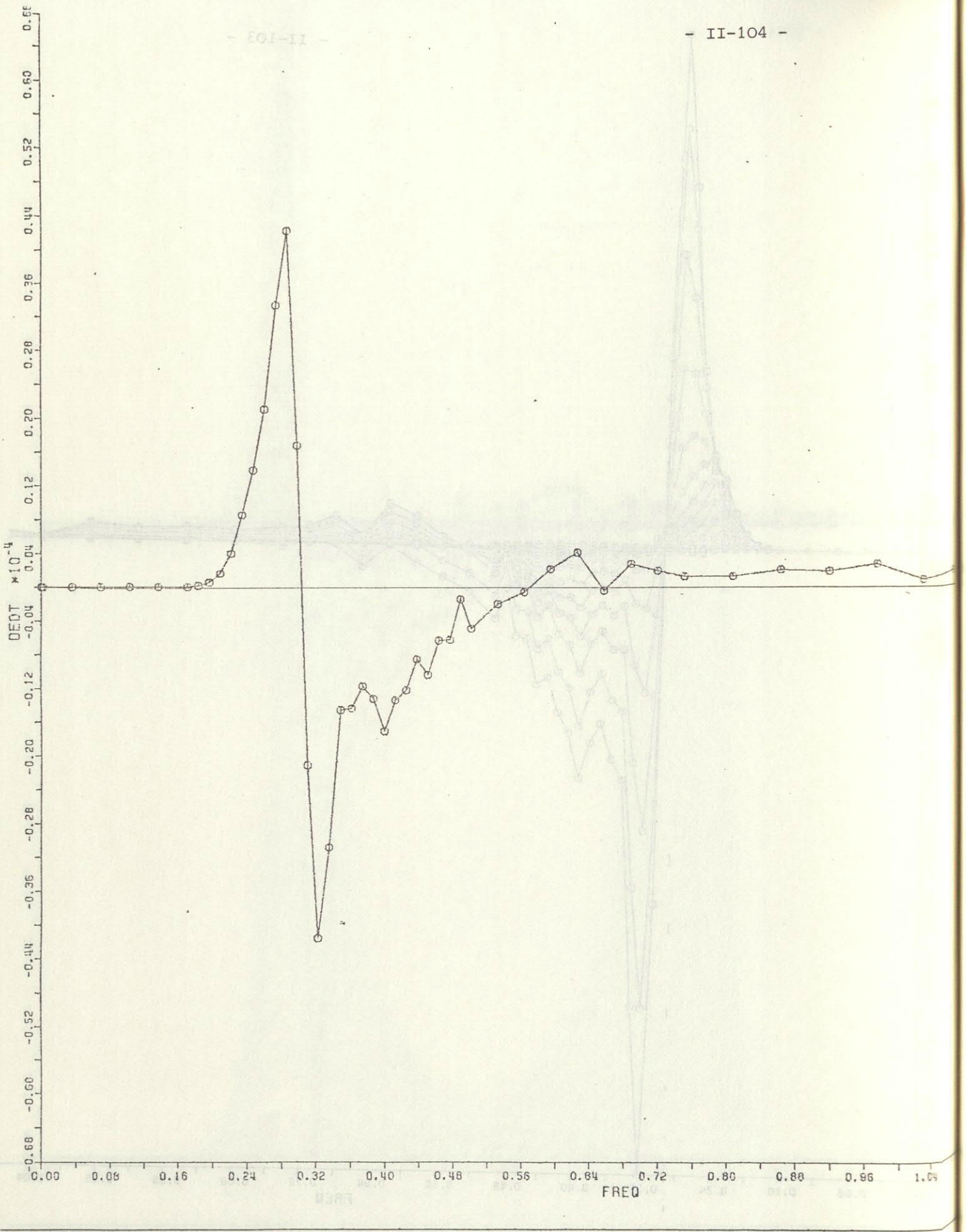

Fig. 28e One-dimensional nonlinear transfer $S_{nl}(f) = \int S_{nl}(f,\theta)\,d\theta$.

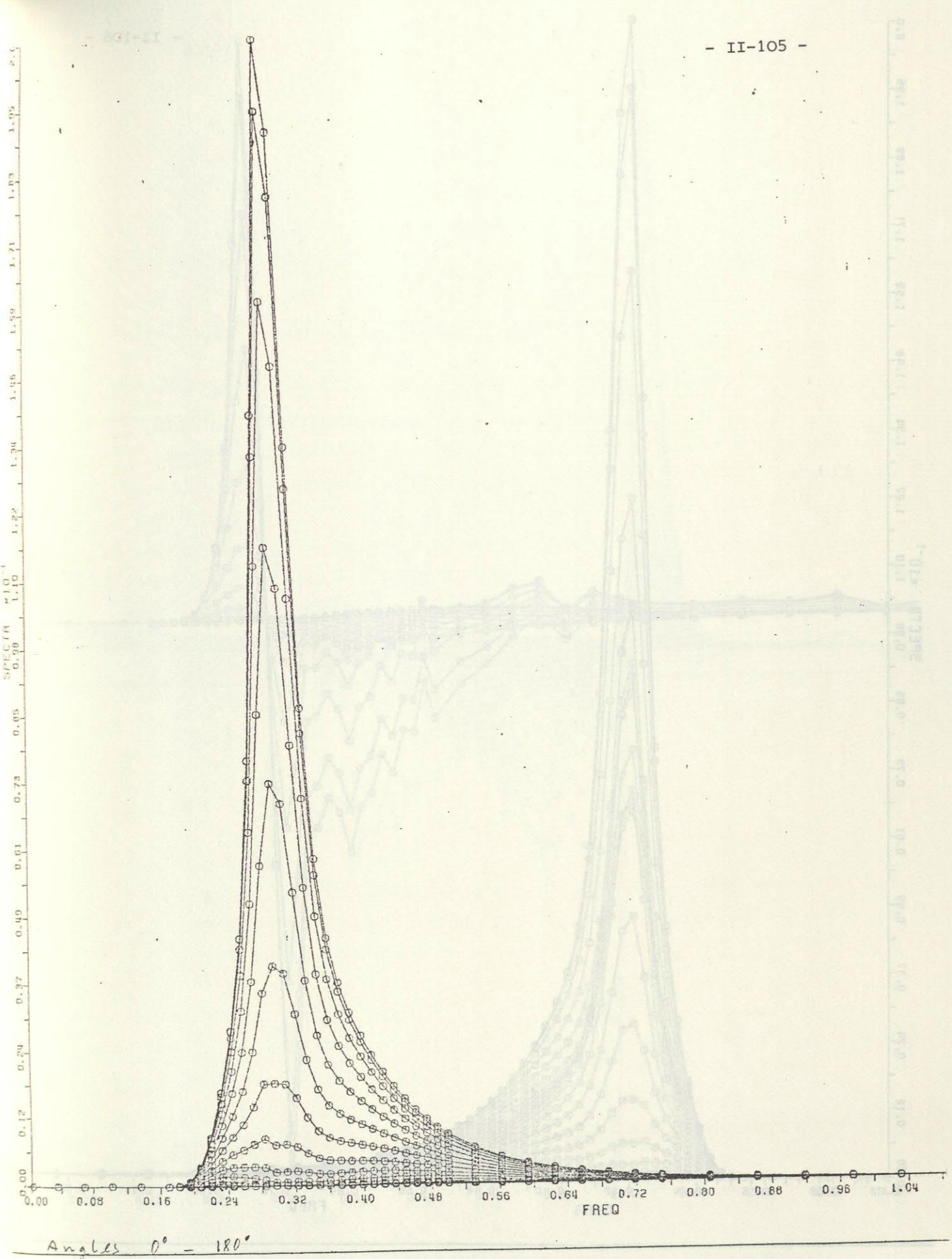

Fig. 29a JONSWAP spectrum, case 1, with superimposed "swell". $(f_m)_{sw} = (f_m)_{ws}$, $E_{sw}/E_{ws} = 0.5$, $\theta_{sw} = \theta_{ws} - 90^{\circ}$. Angles from 0° to 180° in increments of 9.5°.

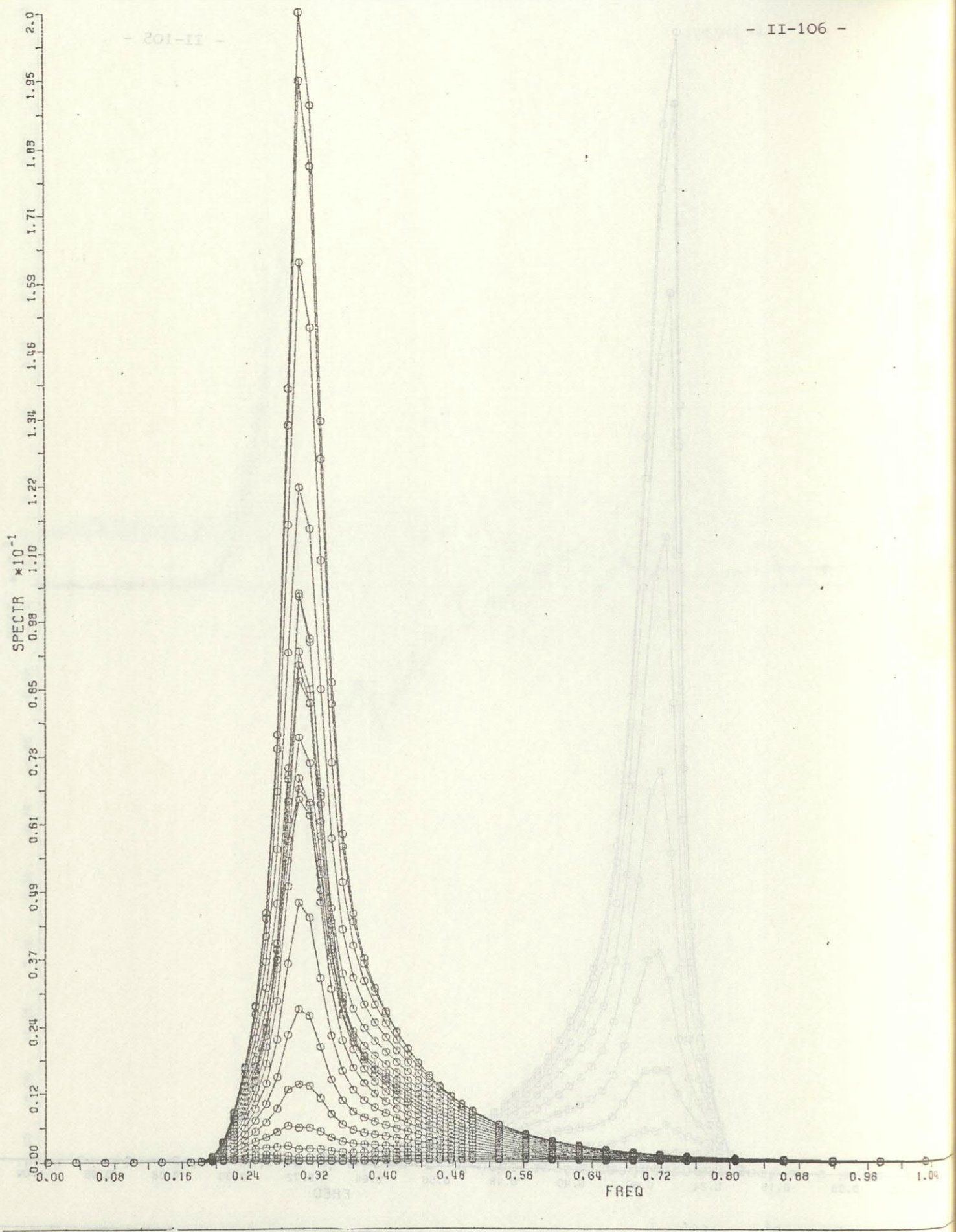

Fig. 29b Same as Fig. 29a with angles from 0° to -180° in increments of 9.5°.

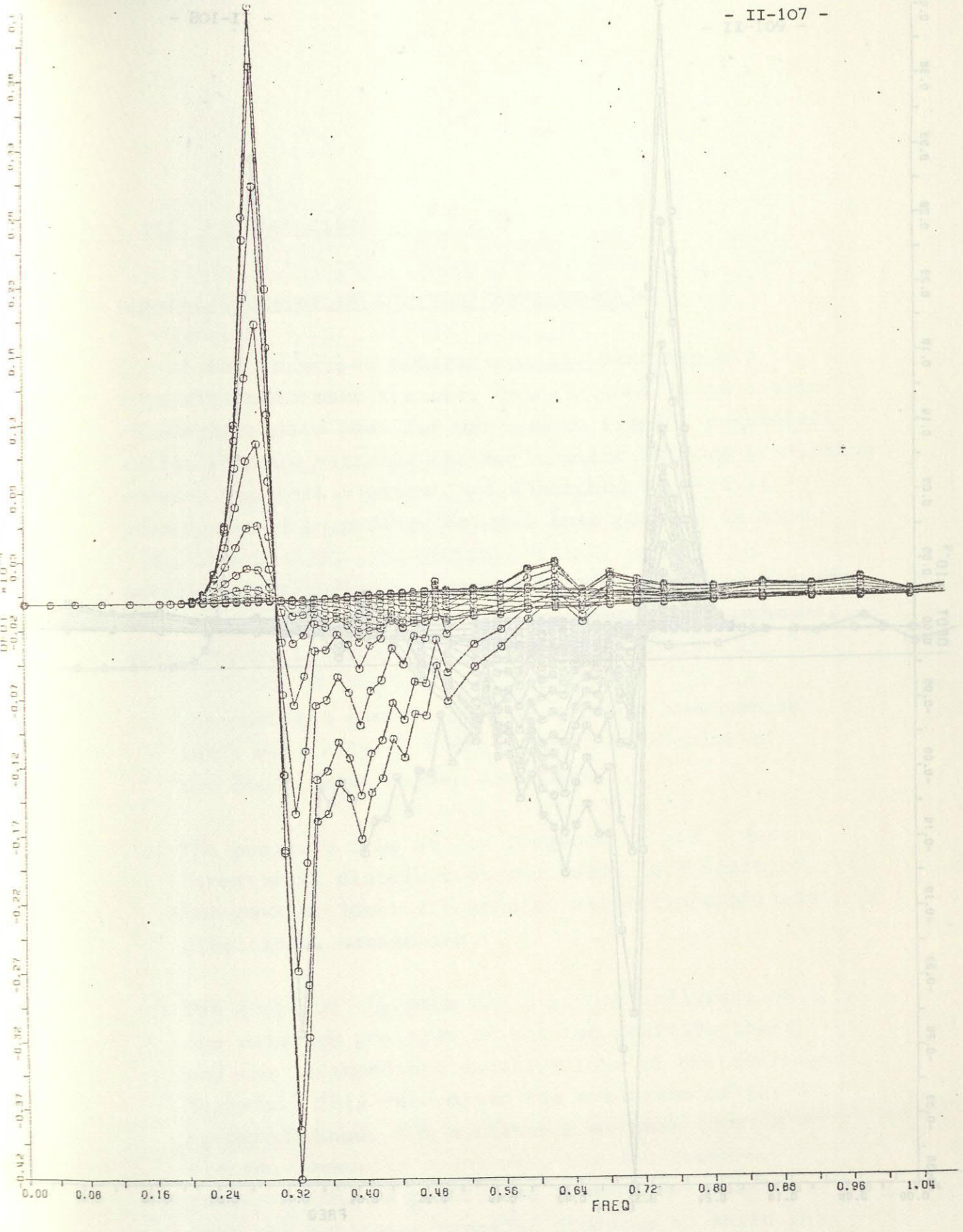

Fig. 29c Two-dimensional nonlinear transfer rate $S_{nl}(f,\theta)$ for angles from 0° to 180° in increments of 9.5°.

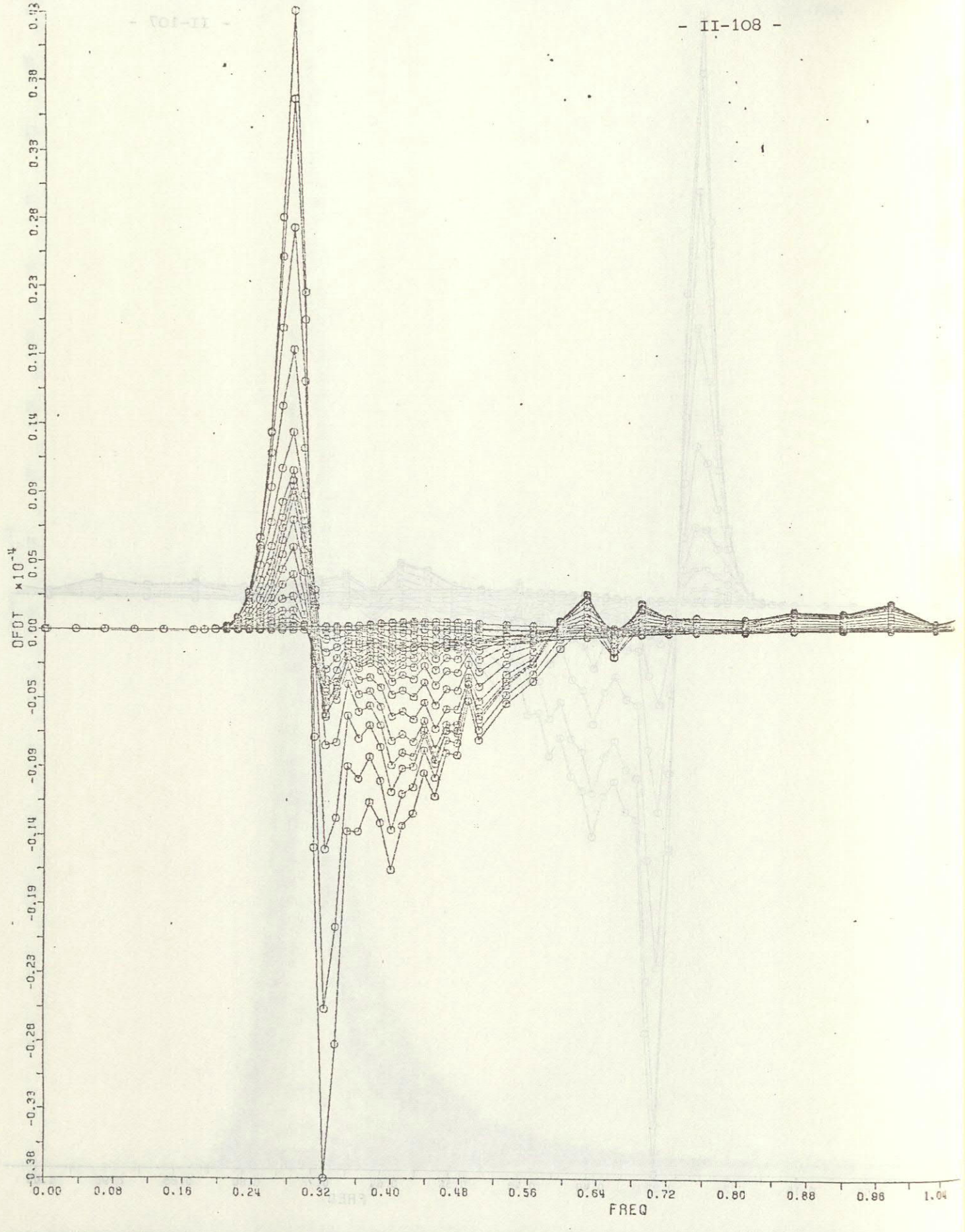

Fig. 29d Two-dimensional nonlinear transfer rate $S_{nl}(f,\theta)$ for angles from -8.5° to -180° in increments of 9.5°.

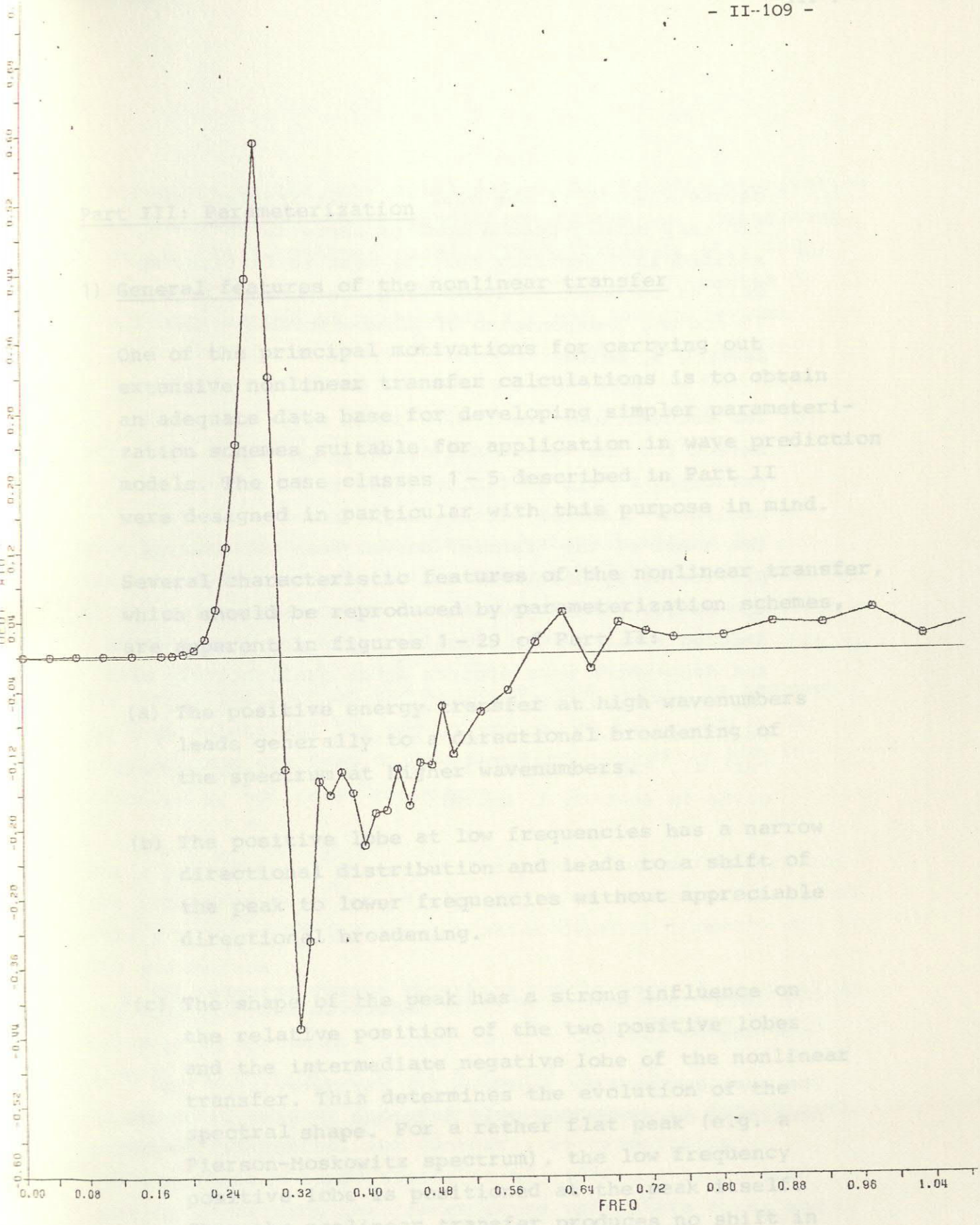

Fig. 29e One-dimensional nonlinear transfer rate $S_{nl}(f) = \int S_{nl}(f,\Theta)d\Theta$.

Part III: Parameterization

1) General features of the nonlinear transfer

One of the principal motivations for carrying out extensive nonlinear transfer calculations is to obtain an adequate data base for developing simpler parameterization schemes suitable for application in wave prediction models. The case classes 1 - 5 described in Part II were designed in particular with this purpose in mind.

Several characteristic features of the nonlinear transfer, which should be reproduced by parameterization schemes, are apparent in figures 1 - 29 of Part II:

(a) The positive energy transfer at high wavenumbers leads generally to a directional broadening of the spectrum at higher wavenumbers.

(b) The positive lobe at low frequencies has a narrow directional distribution and leads to a shift of the peak to lower frequencies without appreciable directional broadening.

(c) The shape of the peak has a strong influence on the relative position of the two positive lobes and the intermediate negative lobe of the nonlinear transfer. This determines the evolution of the spectral shape. For a rather flat peak (e.g. a Pierson-Moskowitz spectrum), the low frequency positive lobe is positioned at the peak itself. Thus the nonlinear transfer produces no shift in the peak, but causes the peak to grow. For highly peaked spectra, on the other hand, the low frequency lobe shifts to the forward face of the spectrum and

causes a shift of the peak to lower frequencies. For very highly peaked spectra there is an additional tendency for the peak to flatten, as well as to shift to lower frequencies (cf. Figs. 7 - 15 and the γ-dependence of parameterization in section 3, below).

(d) The calculations for finite-depth waves show that except for the very small depths, $k_m h = 0.35, 0.5$, the principal effect of finite depth is to enhance the nonlinear transfer without significantly altering the shape of the transfer curve. This was deduced previously by Herterich and Hasselmann (1980) for the narrow peak approximation. The empirically deduced ratio of the transfer rates for finite-depth and deep-water wave spectra agree qualitatively with the theoretical values deduced by Herterich and Hasselmann for narrow peak spectra (cf. Figs. 16 - 24, Part II, Fig. 3, Part III, and the parameterization given in section 4, below).

2) Parameterization of the nonlinear energy transfer for a hybrid wave model

The most appropriate approach for parameterizing the nonlinear energy transfer will depend in general on the

structure of the wave model for which the parameterization is intended. In hybrid prediction models (cf. Hasselmann et al., 1976, Günther et al., 1980, Ewing et al., 1980) the wind-sea part of the wave spectrum is presented by a finite number of parameters a_i, and the space-time evolution of the spectrum is described accordingly by prognostic equations for these parameters in the form

$$\frac{\partial a_i}{\partial t} + \sum_j \underline{D}_{ij} \nabla a_j = S_i \qquad (2.1)$$

where $\underline{D}_{ij}$ represents a propagation velocity matrix and the source function S_i can be represented as a superposition of input, nonlinear and dissipation terms

$$S_i = S_i^{in} + S_i^{nl} + S_i^{ds} \qquad (2.2)$$

The remaining part of the spectrum, the swell, is assumed to have relatively low energy and to be sufficiently decoupled from the rest of the spectrum that it is not influenced by nonlinear processes.

For a hybrid model the natural approach for parameterizing the nonlinear transfer is clearly to construct a functional form for $S_i^{nl} = S_i^{nl}(a_1, a_2 \ldots)$ which depends directly on the parameters a_i.

The hybrid model developed jointly in Hamburg, Wallingford and Wormley is based on the five JONSWAP parameters $a_1 = f_m$, $a_2 = \alpha$, $a_3 = \gamma$, $a_4 = \sigma_a$ and $a_5 = \sigma_b$.

An improved version includes also a prognostic directional parameter. (Rosenthal and Günther , in preparation).

For the NORSWAM study (Ewing et al.,1980), a simplified version containing the first three parameters a_1, a_2 and a_3 was used.

As a first step towards developing a parameterization for hybrid models a five-parameter representation of S_i^{nl} was tested,

$$S_i^{nl} = a_i \cdot \alpha^2 f_m \left[C_i + \sum_{j=3,4,5} M_{ij} \frac{(a_j - a_j^o)}{a_j^o} \right] \quad (i = 1,\ldots 5) \qquad (2.3)$$

where a_j^o (j = 3.4,5) denotes the set of mean JONSWAP shape parameters $a_3^o \equiv \gamma^o = 3.3$, $a_4^o \equiv \sigma_a^o = 0.07$, $a_5^o \equiv \sigma_b^o = 0.09$ and C_i, M_{ij} denote constant coefficients.

The dependence of S_i^{nl} on the scale parameters α and f_m in (2.3) follows from a dimensional analysis of the exact transfer integral expression. The linear dependence of S_i^{nl} on the deviation of the shape parameters from their mean JONSWAP values represents an approximation based on the qualitative observation (cf. Hasselmann et al., 1973, 1976 and part II of this report) that the mean JONSWAP spectrum appears to represent a stable quasi-equilibrium form, small deviations of the spectrum from the mean JONSWAP shape modifying the nonlinear transfer in such a way that the original shape tends to be restored.

To determine the coefficients C_i and M_{ij} the following technique was applied: the nonlinear transfer $S_{nl}(\underline{k})$ for an initial wave spectrum $F(f,\theta)$ characterized by an initial set of parameters a_i at time t was computed, and from this a new spectrum $F'(f,\theta) = F(f,\theta) + \Delta t\, S_{nl}(f,\theta)$ was calculated for the later time $t + \Delta t$. The set of best-fit parameters a_i' to the spectrum F' then determines the change $\Delta a_i = a_i' - a_i$ of the parameters generated by the nonlinear transfer. This defines the nonlinear source function $S_i^{nl} = \Delta a_i / \Delta t$ with respect to the parameter a_i. The functions $S_i^{nl}(a_1,\ldots a_5)$ were calculated in this manner for a set of three shape parameters a_j^o, $a_j^o + \delta a_j$, $a_j^o - \delta a_j$ for each shape parameter a_j, j = 3, 4, 5. The results were then fitted by the linear form (2.3). Figure 1 indicates that for the parameter values of interest a linear fit of the form (2.3) appears an adequate first approximation for most parameters (although a quadratic form would have been more appropriate to describe the dependence on γ). The coefficients are listed in Table 1. In all computations of S_{nl} a $\cos^{2p}(\theta/2)$ spreading function with frequency dependent p as defined in case 1, part 2, was used.

M_{ij}	α	f_m	γ	σ_a	σ_b
γ	5.0685	-0.465	-9.9885	-0.6035	-20.984
σ_a	2.0075	-0.714	-6.559	-18.6205	0.6527
σ_b	2.5315	-0.5925	-2.214	- 9.440	- 21.1820
C_i	-6.5	-0.46	5.3	4.1	2.0

Table 1: MATRIX M_{ij} and coefficiants C_i of equation (2.3)

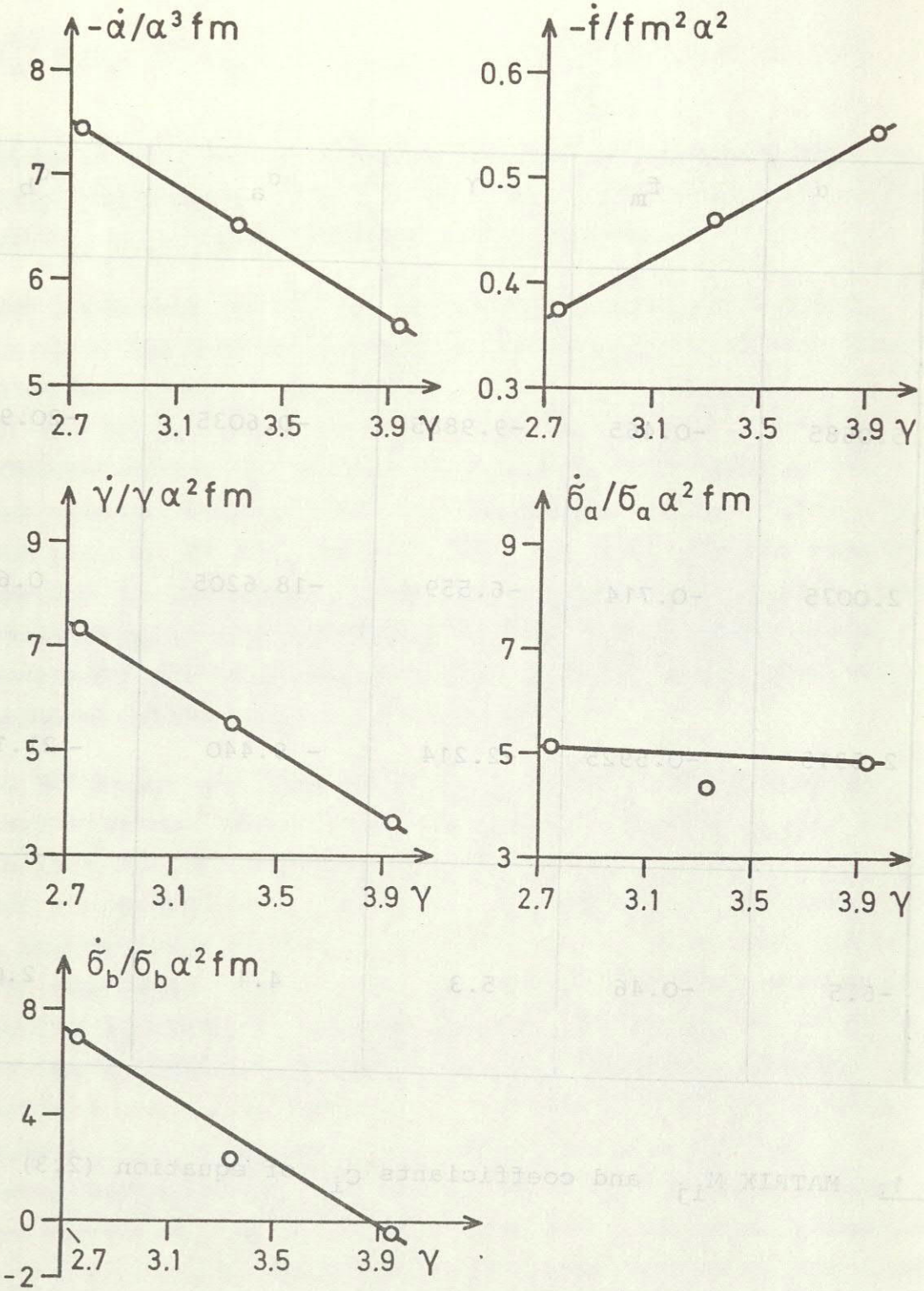

Fig. 1a Dependence of nonlinear parameter source functions on shape parameter γ.

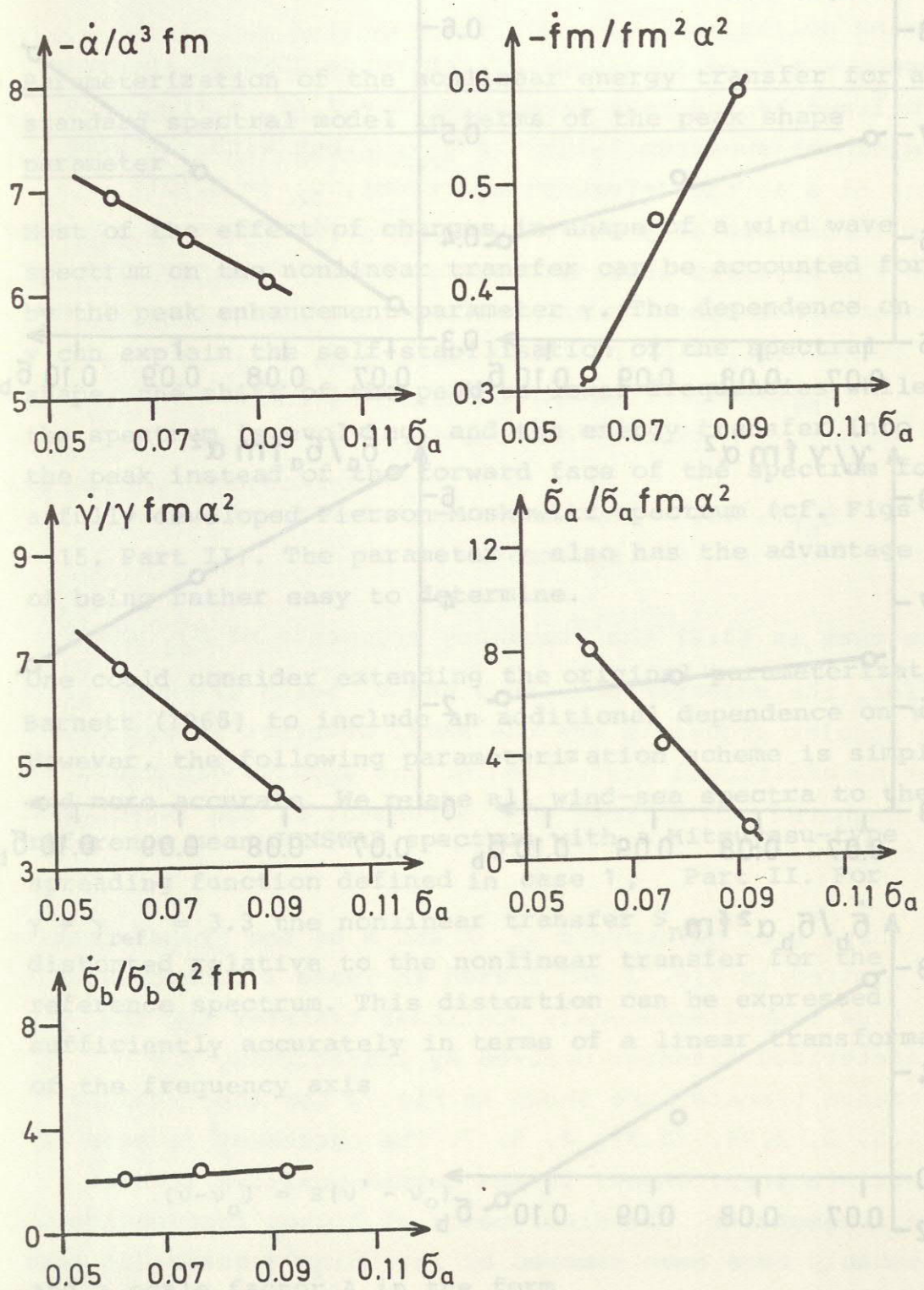

Fig. 1 b Dependence of nonlinear parameter source functions on shape parameter σ_a.

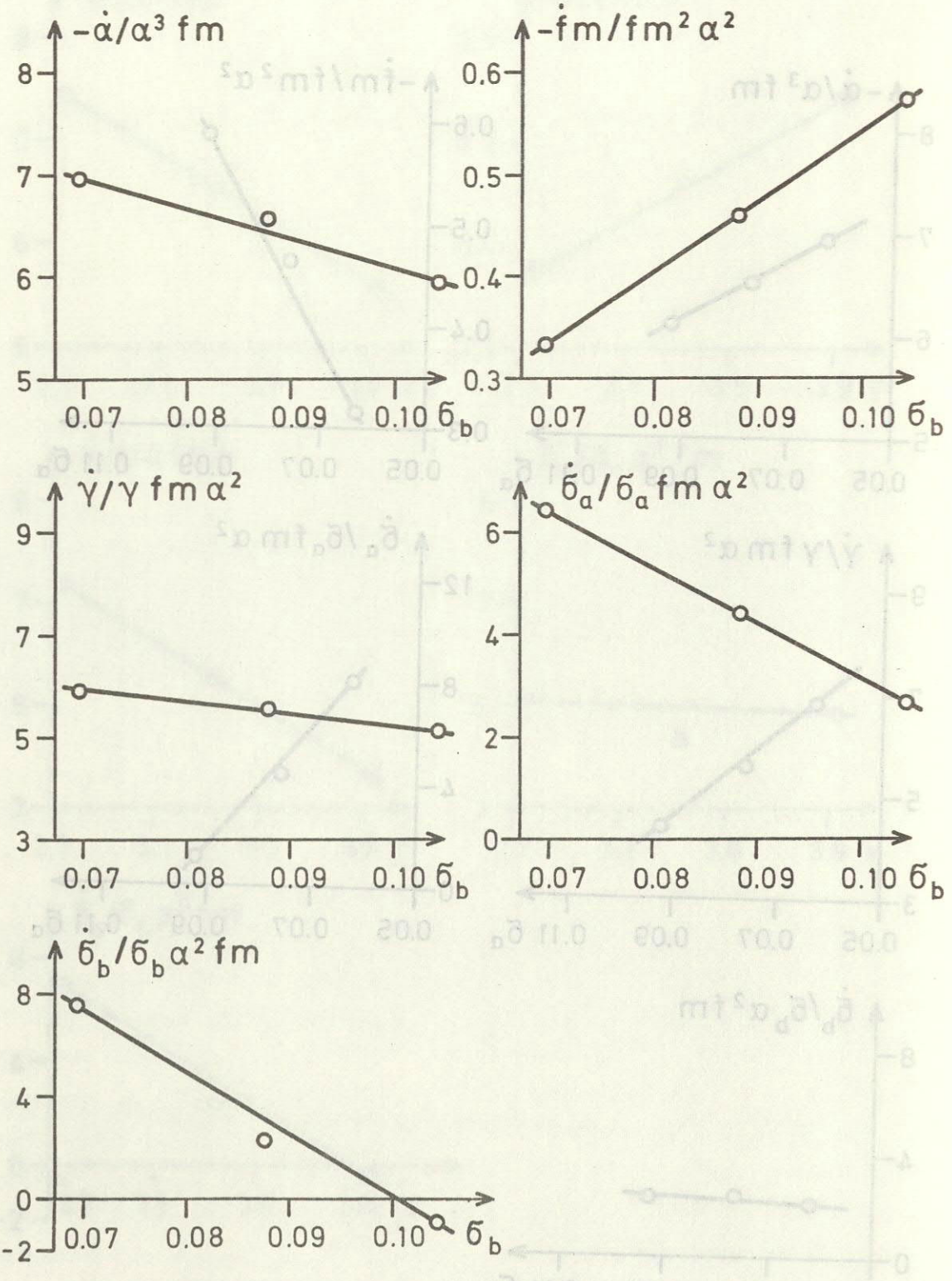

Fig. 1c Dependence of nonlinear parameter source functions on shape parameter σ_b.

3) Parameterization of the nonlinear energy transfer for a standard spectral model in terms of the peak shape parameter γ

Most of the effect of changes in shape of a wind wave spectrum on the nonlinear transfer can be accounted for by the peak enhancement parameter γ. The dependence on γ can explain the self-stabilisation of the spectral shape, the shift of the peak to lower frequencies while the spectrum is evolving, and the energy transfer into the peak instead of the forward face of the spectrum for a fully developed Pierson-Moskowitz spectrum (cf. Figs 7 - 15, Part II). The parameter γ also has the advantage of being rather easy to determine.

One could consider extending the original parameterization of Barnett (1968) to include an additional dependence on γ However, the following parameterization scheme is simpler and more accurate. We relate all wind-sea spectra to the reference mean JONSWAP spectrum with a Mitsuyasu-type spreading function defined in case 1, Part II. For $\gamma \neq \gamma_{ref} = 3.3$ the nonlinear transfer $S_{n\ell}$ is distorted relative to the nonlinear transfer for the reference spectrum. This distortion can be expressed sufficiently accurately in terms of a linear transformation of the frequency axis

$$(\nu - \nu_o) = B(\nu' - \nu_o') \tag{3.1}$$

and a scale factor A in the form

$$S'_{n\ell}(\nu', \theta) = A S_{n\ell}(\nu, \theta) \tag{3.2}$$

where $\nu = f/f_m$ = frequency of reference JONSWAP spectrum, normalised by the peak frequency, $\nu' = f'/f'_m$ = frequency of wind sea spectrum (with $\gamma \neq \gamma_{ref.}$, but with the same value of α as the reference spectrum), ν_o (= 0.101), ν'_o = zero-transfer point between the low frequency positive lobe and negative lobe of the one-dimensional transfer for the reference spectrum and wind-sea spectrum, respectively,

$S_{n\ell}(\nu,\theta)$ = nonlinear transfer of reference JONSWAP spectrum

$S'_{n\ell}(\nu',\theta)$ = nonlinear transfer of wind sea spectrum.

Note that in (3.2) the frequency arguments of $S'_{n\ell}$ and $S_{n\ell}$ differ, the relation between ν and ν' being given by (3.1). The angular arguments are the same, however: it was found that no additional distortion of the angular distribution was required to achieve good agreement of the two-dimensional distributions.

The three free parameters ν'_o, A and B of the transformation are plotted in Fig. 2 and listed in Table 2. Comparisons of the true (one-dimensional) nonlinear transfer and the parameterized transfer derived by transforming the reference transfer are shown in Fig. 3 for the γ-values 1, 1.5, 2, 2.75, (3.3), 4, 5, 7. The agreement is seen to be satisfactory, except in the second positive lobe at high frequencies. The discrepancy at higher frequencies could presumably have been removed by including a quadratic term in the frequency transformation (3.1). This was not done, however, as the precise form of the nonlinear source function at higher frequencies is irrelevant in most wave models. The structure of the source function is normally

determined in the present models by the dissipation term in this frequency range, the dissipation term being tuned to reproduce the observed quasi-equilibrium spectrum independently of the details of the other source functions.

The dependence of ν_o', A and B on γ shown in Fig. 2 summarises rather concisely the principal influence of the spectral shape on the nonlinear transfer discussed in section 1: as γ approaches the fully developed value 1, the nonlinear transfer distribution shifts to higher frequencies (increasing ν_o'), becomes broader (decreasing B) and weaker (decreasing A).

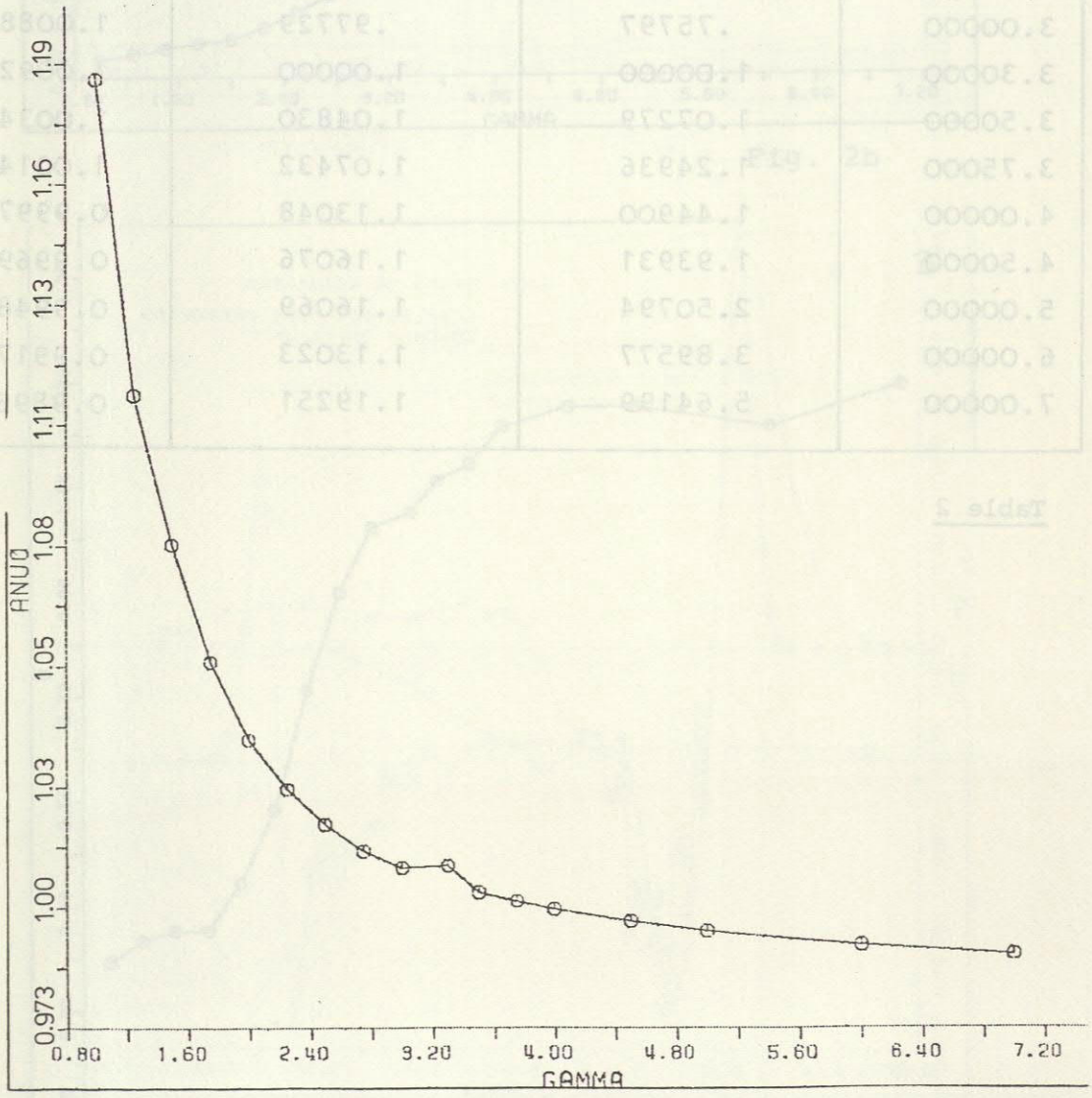

Fig. 2a

γ	A	B	ν_o
1.00000	.14135	.31378	1.1832
1.25000	.17783	.34799	1.1132
1.50000	.21845	.36257	1.0802
1.75000	.26047	.36256	1.0544
2.00000	.28773	.43563	1.0370
2.25000	.37653	.54560	1.0262
2.50000	.49220	.72983	1.0184
2.75000	.61914	.87806	1.0125
3.00000	.75797	.97729	1.0088
3.30000	1.00000	1.00000	1.0092
3.50000	1.07279	1.04830	1.0034
3.75000	1.24936	1.07432	1.0014
4.00000	1.44900	1.13048	0.9997
4.50000	1.93931	1.16076	0.9969
5.00000	2.50794	1.16069	0.9948
6.00000	3.89577	1.13023	0.9917
7.00000	5.64199	1.19251	0.9896

Table 2

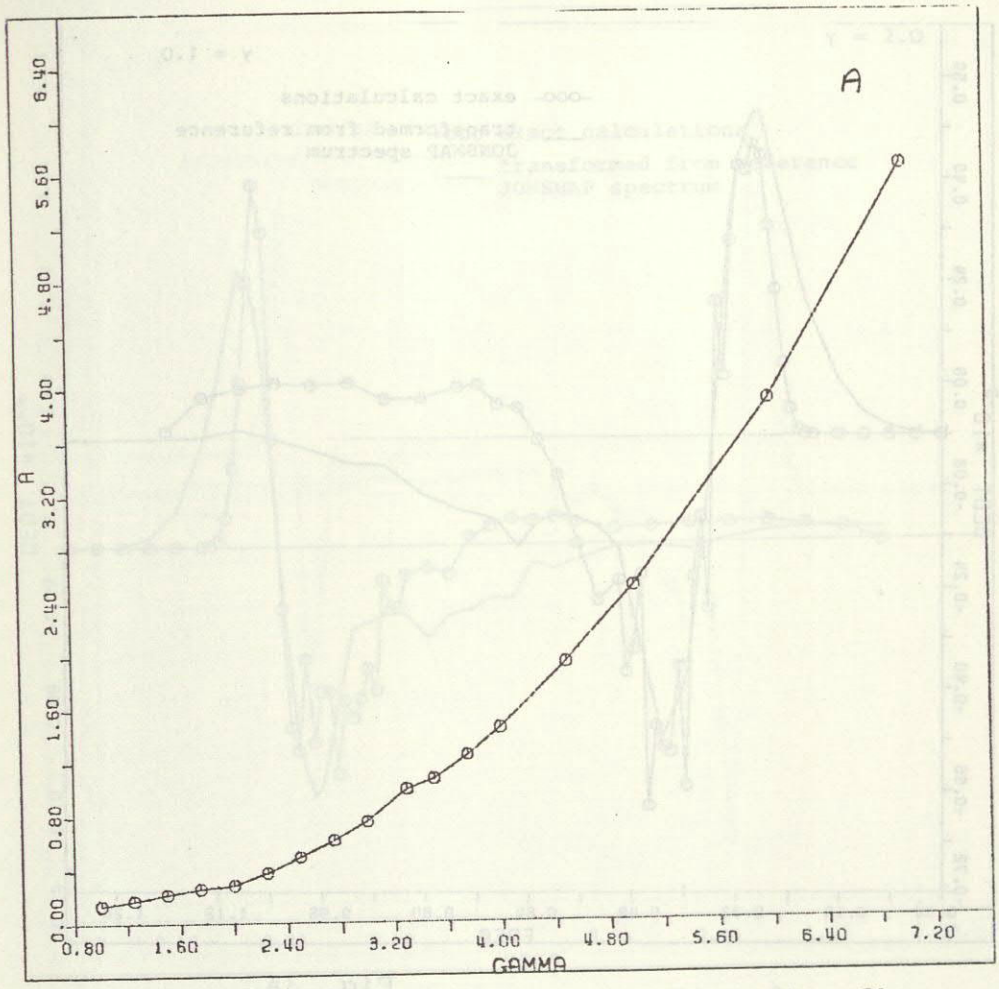
A
A
0.00
0.80
1.60
2.40
3.20
4.00
4.80
5.60
6.40
0.80
1.60
2.40
3.20
4.00
4.80
5.60
6.40
7.20
GAMMA

Fig. 2b

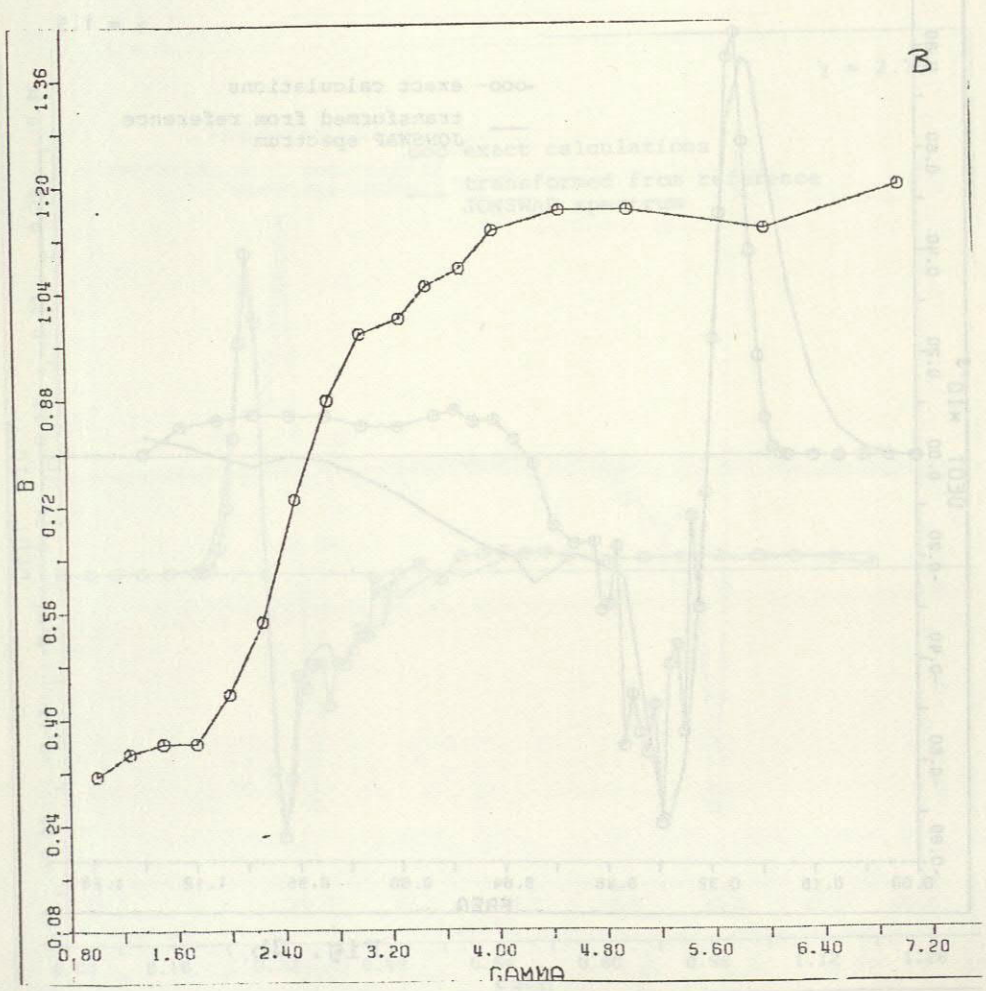
B
B
0.08
0.24
0.40
0.56
0.72
0.88
1.04
1.20
1.36
0.80
1.60
2.40
3.20
4.00
4.80
5.60
6.40
7.20
GAMMA

Fig. 2c

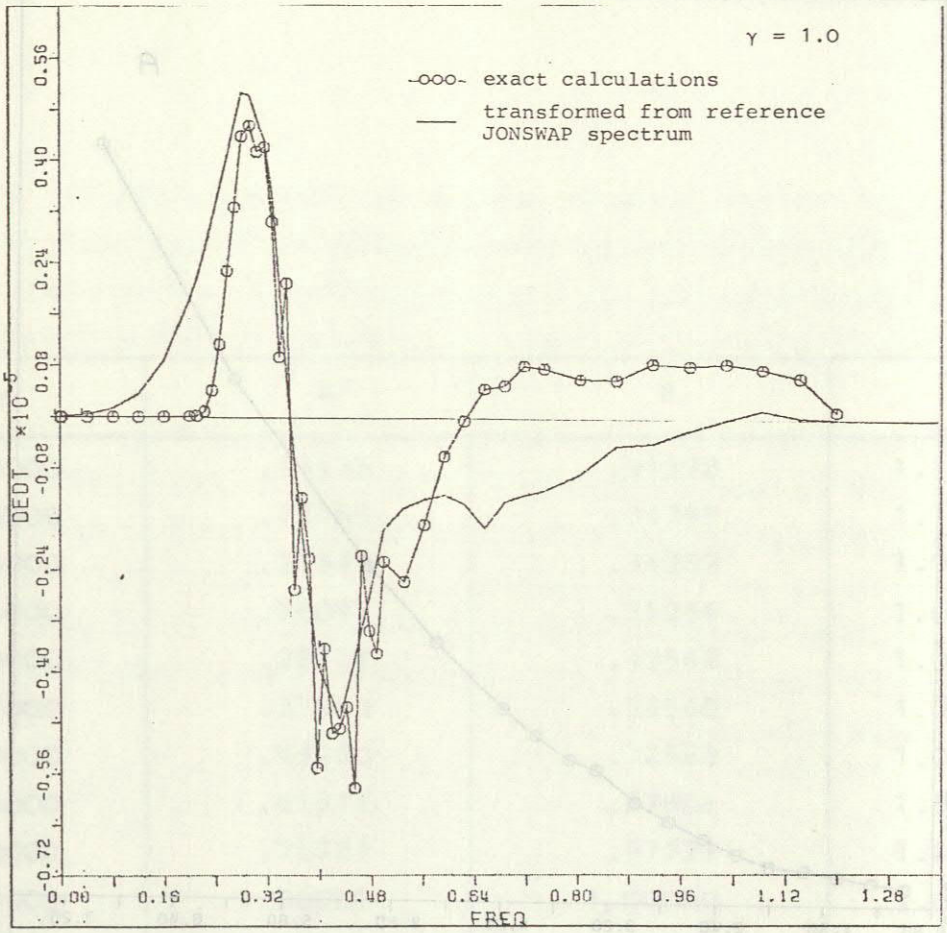
γ = 1.0
-ooo- exact calculations
transformed from reference JONSWAP spectrum
DEDT ×10⁻⁵
0.56
0.40
0.24
0.08
-0.08
-0.24
-0.40
-0.56
-0.72
0.00
0.16
0.32
0.48
0.64
0.80
0.96
1.12
1.28
FREQ

Fig. 3a

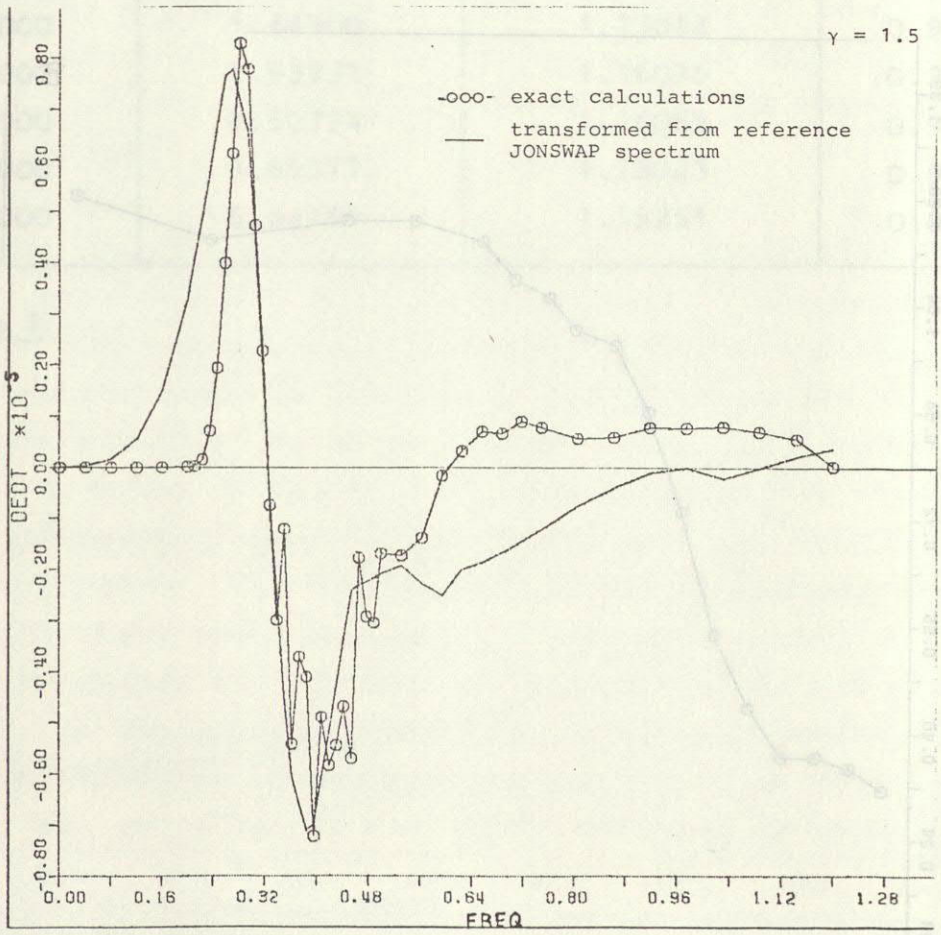
γ = 1.5
-ooo- exact calculations
transformed from reference JONSWAP spectrum
DEDT ×10⁻⁵
0.80
0.60
0.40
0.20
0.00
-0.20
-0.40
-0.60
-0.80
0.00
0.16
0.32
0.48
0.64
0.80
0.96
1.12
1.28
FREQ

Fig. 3b

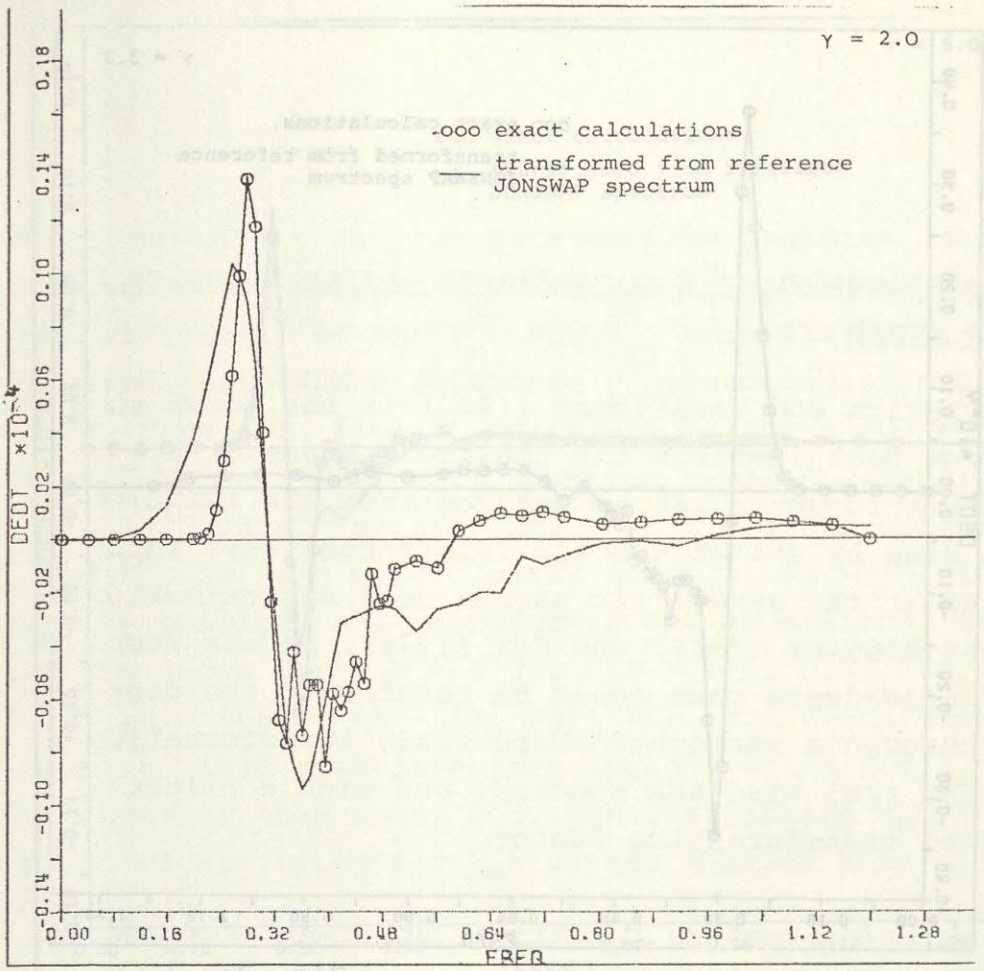
γ = 2.0
ooo exact calculations
transformed from reference JONSWAP spectrum
DEDT ×10⁻⁴
0.18
0.14
0.10
0.06
0.02
-0.02
-0.06
-0.10
-0.14
0.00
0.16
0.32
0.48
0.64
0.80
0.96
1.12
1.28
FREQ

Fig. 3c

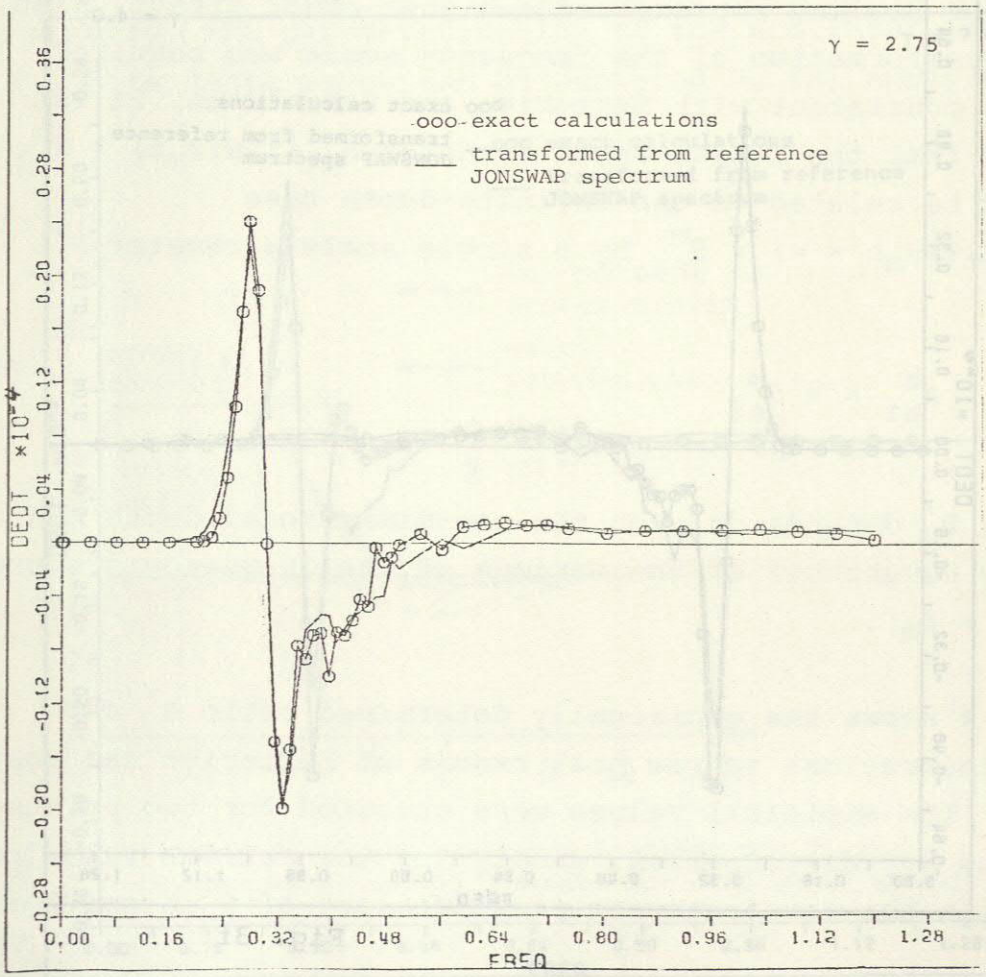
γ = 2.75
ooo exact calculations
transformed from reference JONSWAP spectrum
DEDT ×10⁻⁴
0.36
0.28
0.20
0.12
0.04
-0.04
-0.12
-0.20
-0.28
0.00
0.16
0.32
0.48
0.64
0.80
0.96
1.12
1.28
FREQ

Fig. 3d

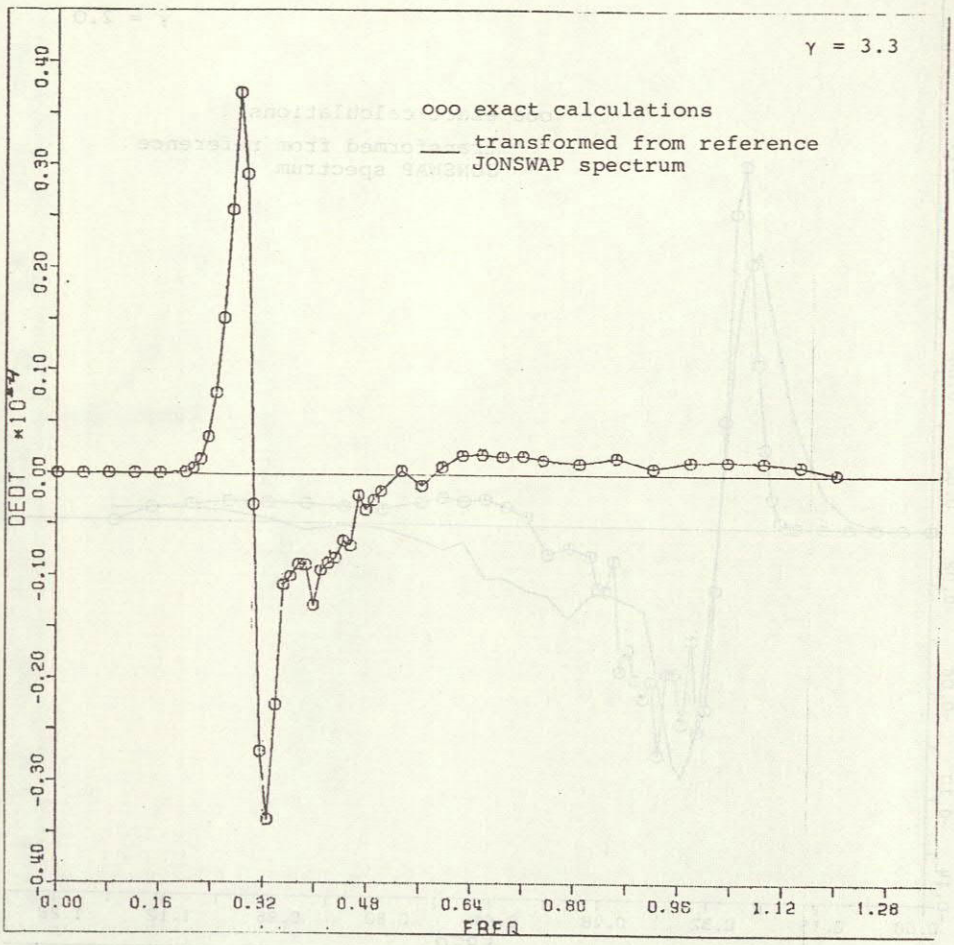
γ = 3.3
ooo exact calculations
transformed from reference JONSWAP spectrum
DEDT ×10**-4
0.40
0.30
0.20
0.10
0.00
-0.10
-0.20
-0.30
-0.40
0.00
0.16
0.32
0.48
0.64
0.80
0.96
1.12
1.28
FREQ

Fig. 3e

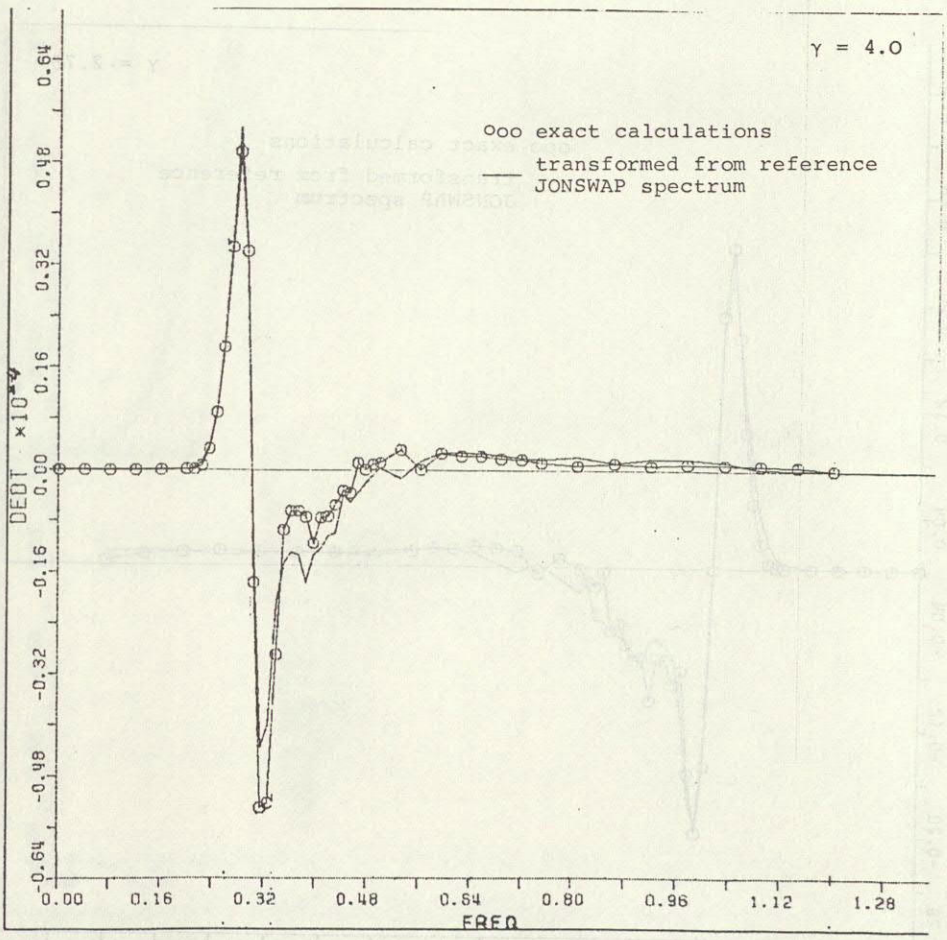
γ = 4.0
ooo exact calculations
transformed from reference JONSWAP spectrum
DEDT ×10**-4
0.64
0.48
0.32
0.16
0.00
-0.16
-0.32
-0.48
-0.64
0.00
0.16
0.32
0.48
0.64
0.80
0.96
1.12
1.28
FREQ

Fig. 3f

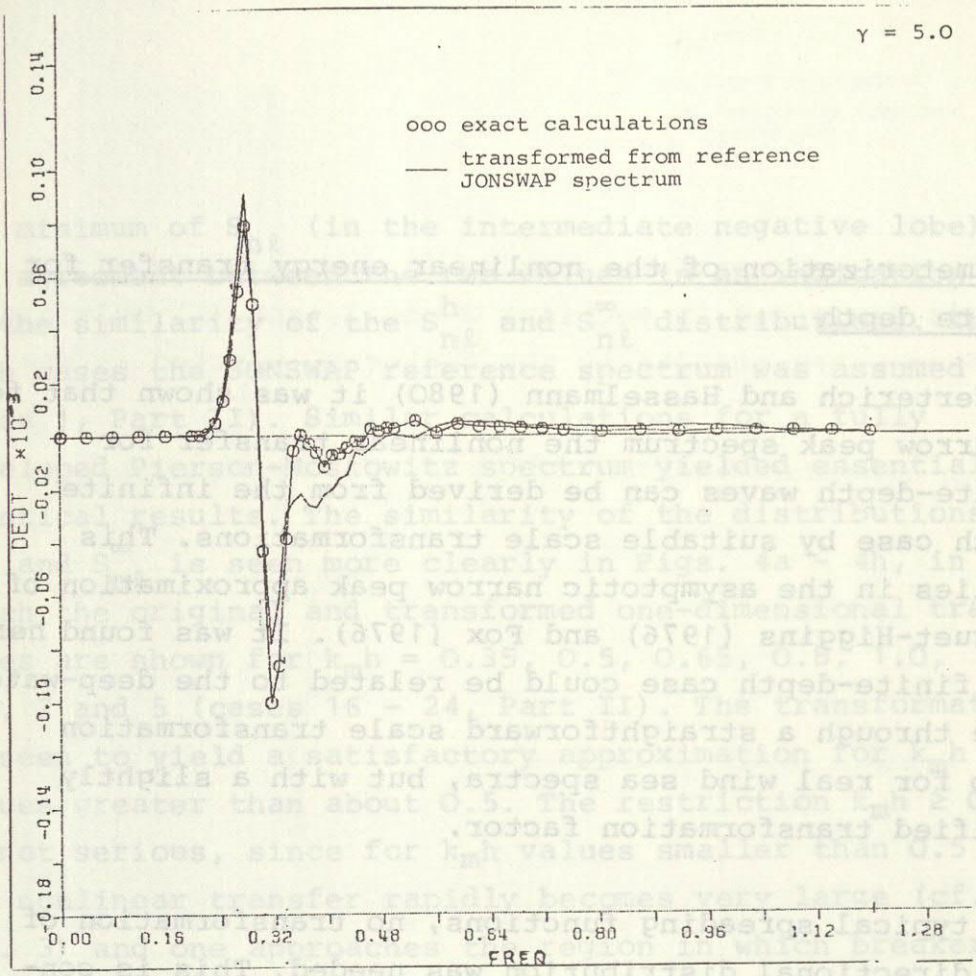
γ = 5.0
ooo exact calculations
___ transformed from reference JONSWAP spectrum
DEDT ×10⁻³
0.14
0.10
0.06
0.02
-0.02
-0.06
-0.10
-0.14
-0.18
0.00
0.16
0.32
0.48
0.64
0.80
0.96
1.12
1.28
FREQ

Fig. 3g

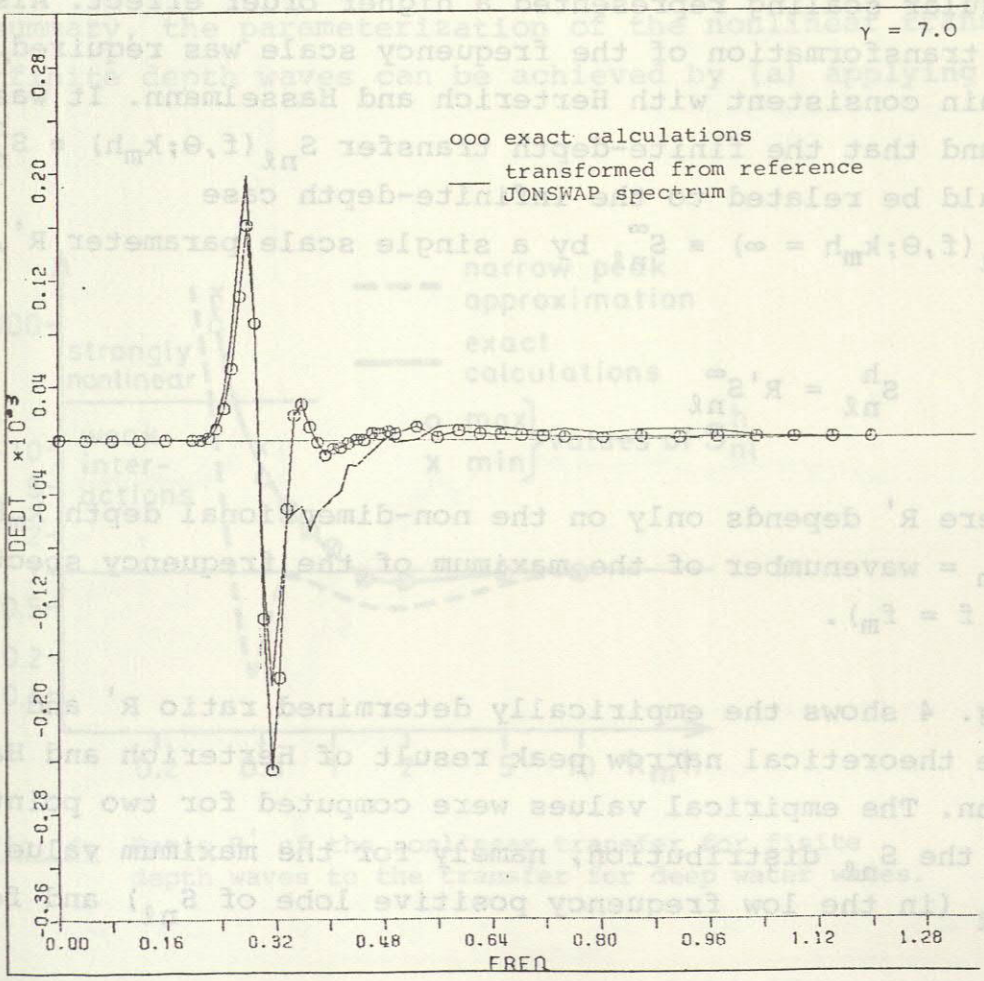
γ = 7.0
ooo exact calculations
___ transformed from reference JONSWAP spectrum
DEDT ×10⁻³
0.28
0.20
0.12
0.04
-0.04
-0.12
-0.20
-0.28
-0.36
0.00
0.16
0.32
0.48
0.64
0.80
0.96
1.12
1.28
FREQ

Fig. 3h

4) Parameterization of the nonlinear energy transfer for finite depth

In Herterich and Hasselmann (1980) it was shown that for a narrow peak spectrum the nonlinear transfer for finite-depth waves can be derived from the infinite depth case by suitable scale transformations. This applies in the asymptotic narrow peak approximation of Longuet-Higgins (1976) and Fox (1976). It was found here that the finite-depth case could be related to the deep-water case through a straightforward scale transformation also for real wind sea spectra, but with a slightly modified transformation factor.

For typical spreading functions, no transformation of the directional distribution was needed. This is consistent with Herterich and Hasselmann, in which the angular scaling represented a higher order effect. Also, no transformation of the frequency scale was required, again consistent with Herterich and Hasselmann. It was found that the finite-depth transfer $S_{n\ell}(f,\Theta;k_m h) \equiv S^h_{n\ell}$ could be related to the infinite-depth case $S_{n\ell}(f,\Theta;k_m h = \infty) \equiv S^\infty_{n\ell}$ by a single scale parameter R',

$$S^h_{n\ell} = R' S^\infty_{n\ell} \tag{4.1}$$

where R' depends only on the non-dimensional depth $k_m h$ (k_m = wavenumber of the maximum of the frequency spectrum at $f = f_m$).

Fig. 4 shows the empirically determined ratio R' and the theoretical narrow peak result of Herterich and Hasselmann. The empirical values were computed for two points of the $S_{n\ell}$ distribution, namely for the maximum value of $S_{n\ell}$ (in the low frequency positive lobe of $S_{n\ell}$) and for

the minimum of $S_{n\ell}$ (in the intermediate negative lobe). The agreement between the two values is an indication of the similarity of the $S^h_{n\ell}$ and $S^\infty_{n\ell}$ distributions. In both cases the JONSWAP reference spectrum was assumed (case 1, Part II). Similar calculations for a fully developed Pierson-Moskowitz spectrum yielded essentially identical results. The similarity of the distributions $S^h_{n\ell}$ and $S^\infty_{n\ell}$ is seen more clearly in Figs. 4a - 4h, in which the original and transformed one-dimensional transfer rates are shown for $k_m h$ = 0.35, 0.5, 0.65, 0.8, 1.0, 1.5, 2 and 5 (cases 16 - 24, Part II). The transformation is seen to yield a satisfactory approximation for $k_m h$ values greater than about 0.5. The restriction $k_m h \geq 0.5$ is not serious, since for $k_m h$ values smaller than 0.5 the nonlinear transfer rapidly becomes very large (cf. Fig. 3) and one approaches the region in which breakers form and weak interaction theory is no longer applicable.

In summary, the parameterization of the nonlinear transfer for finite depth waves can be achieved by (a) applying

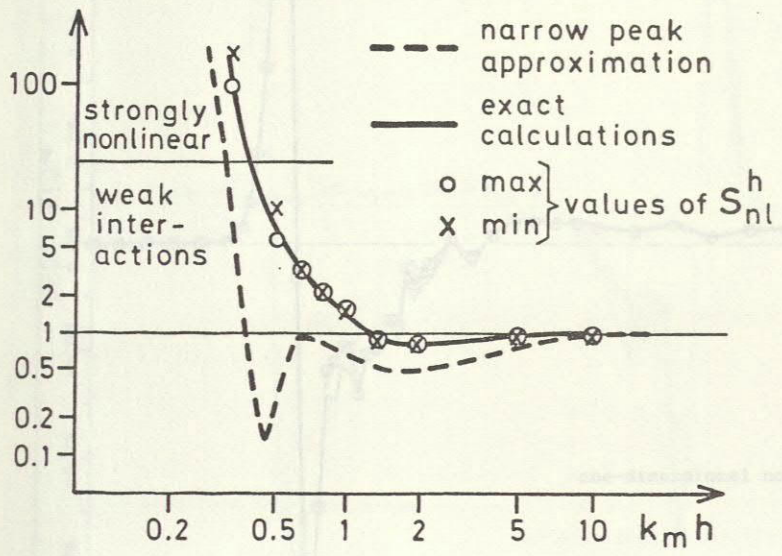

Fig. 4: Ratio R' of the nonlinear transfer for finite depth waves to the transfer for deep water waves.

the deep-water parameterization in accordance with the methods described in sections 2 and 3, and (b) multiplying the deep-water results by the factor R' plotted in Fig. 4.

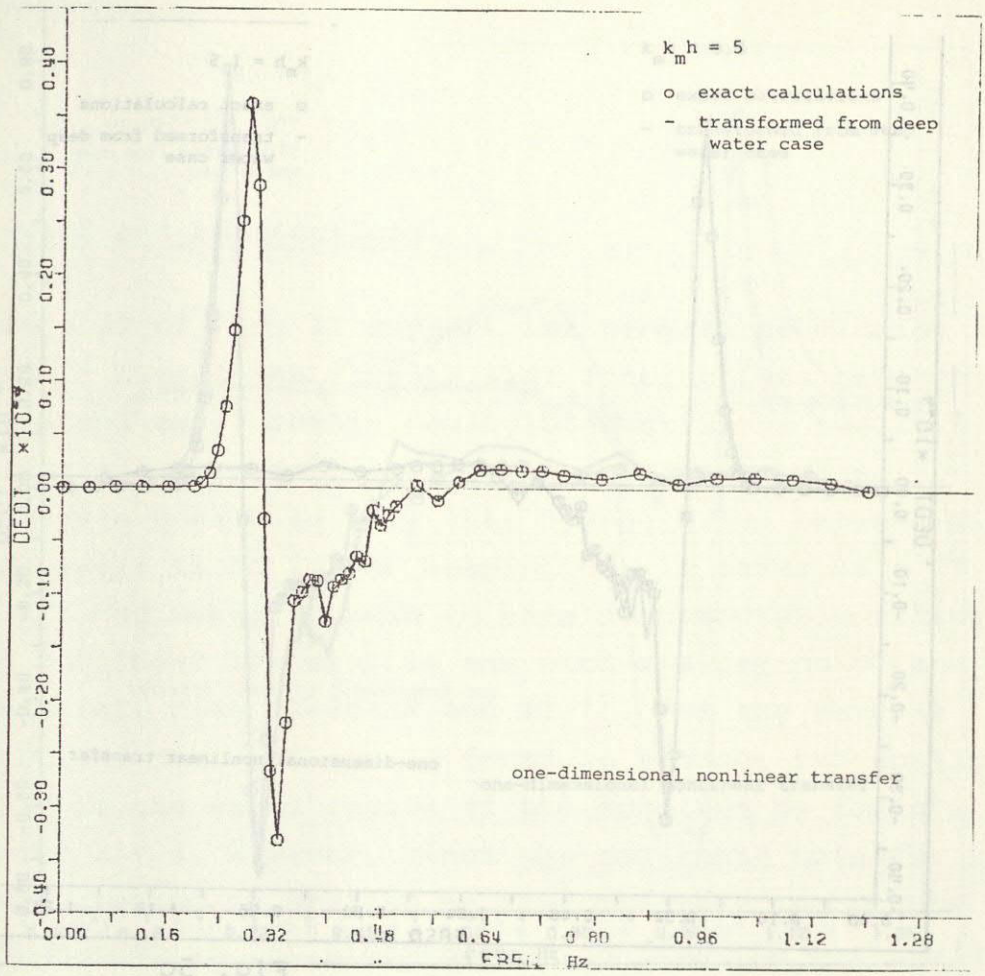
k_m h = 5
o exact calculations
- transformed from deep water case
one-dimensional nonlinear transfer
DEDT ×10⁻⁴
0.40
0.30
0.20
0.10
0.00
-0.10
-0.20
-0.30
-0.40
0.00
0.16
0.32
0.48
0.64
0.80
0.96
1.12
1.28
FREQ Hz

Fig. 5a

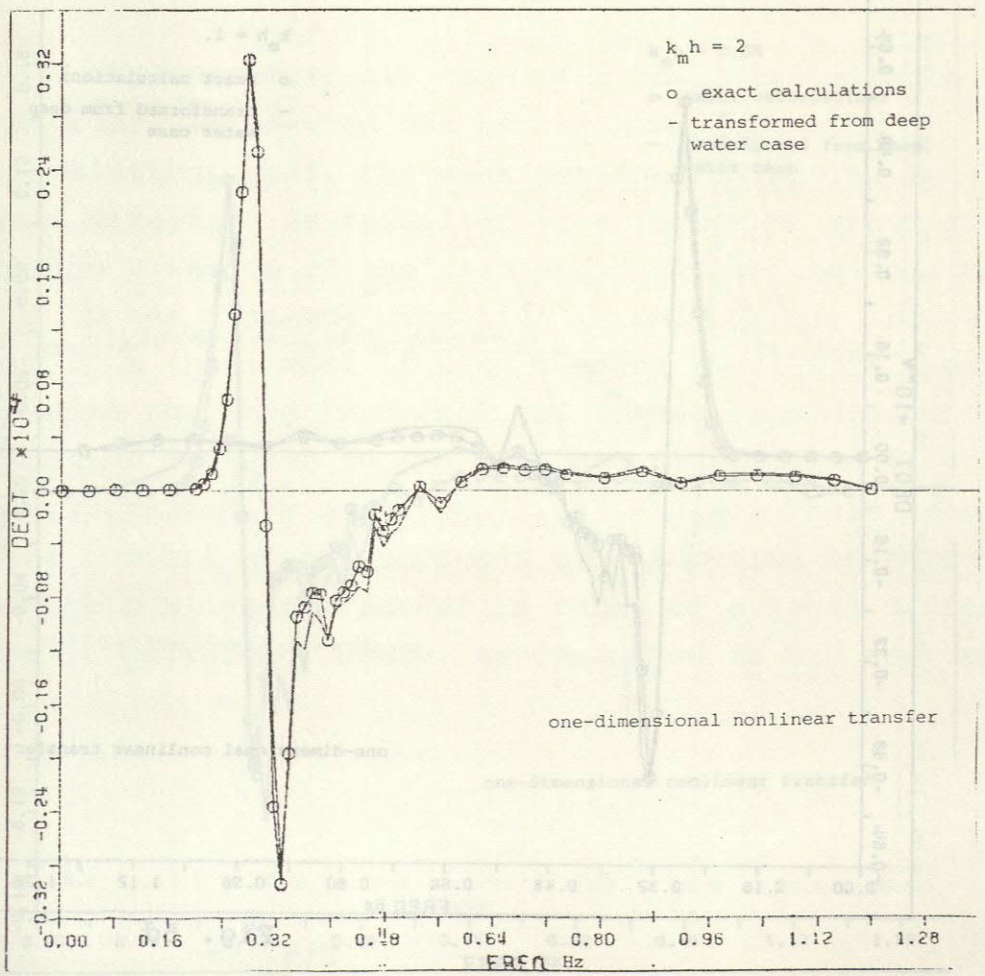
k_m h = 2
o exact calculations
- transformed from deep water case
one-dimensional nonlinear transfer
DEDT ×10⁻⁴
0.32
0.24
0.16
0.08
0.00
-0.08
-0.16
-0.24
-0.32
0.00
0.16
0.32
0.48
0.64
0.80
0.96
1.12
1.28
FREQ Hz

Fig. 5b

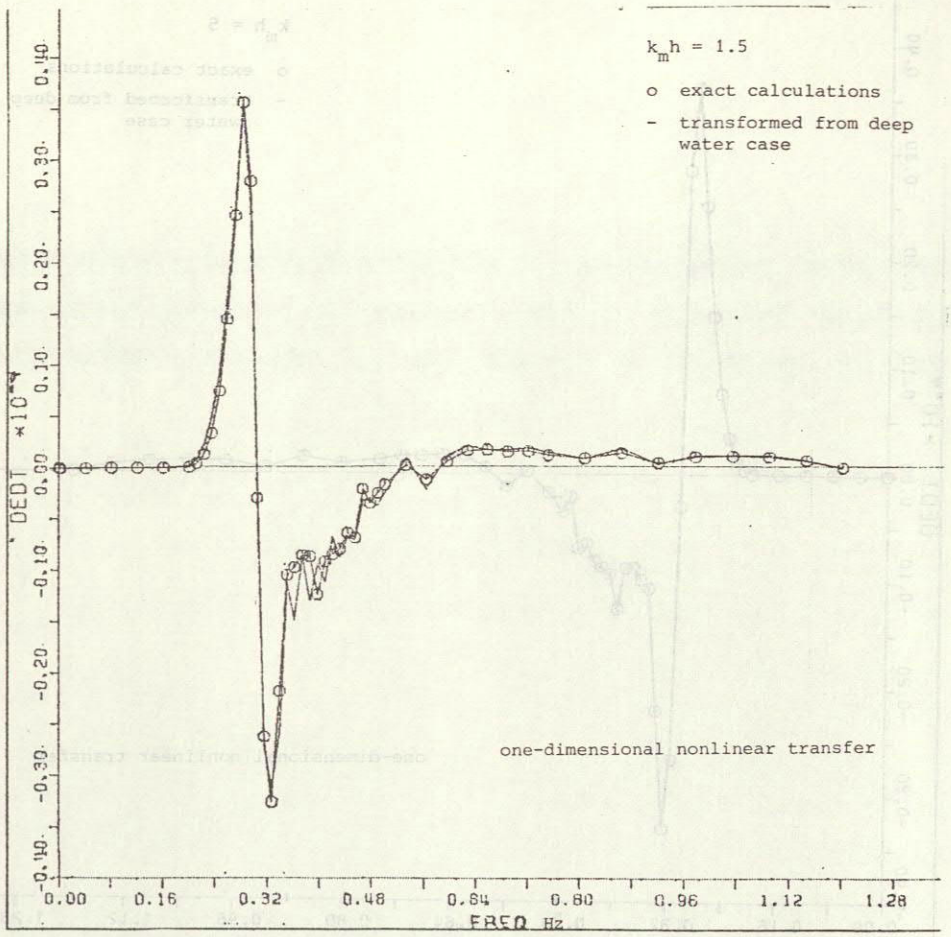
$k_m h$ = 1.5
o exact calculations
- transformed from deep water case
one-dimensional nonlinear transfer
DEDT *10**4
0.40
0.30
0.20
0.10
0.00
-0.10
-0.20
-0.30
-0.40
0.00
0.16
0.32
0.48
0.64
0.80
0.96
1.12
1.28
FREQ Hz

Fig. 5c

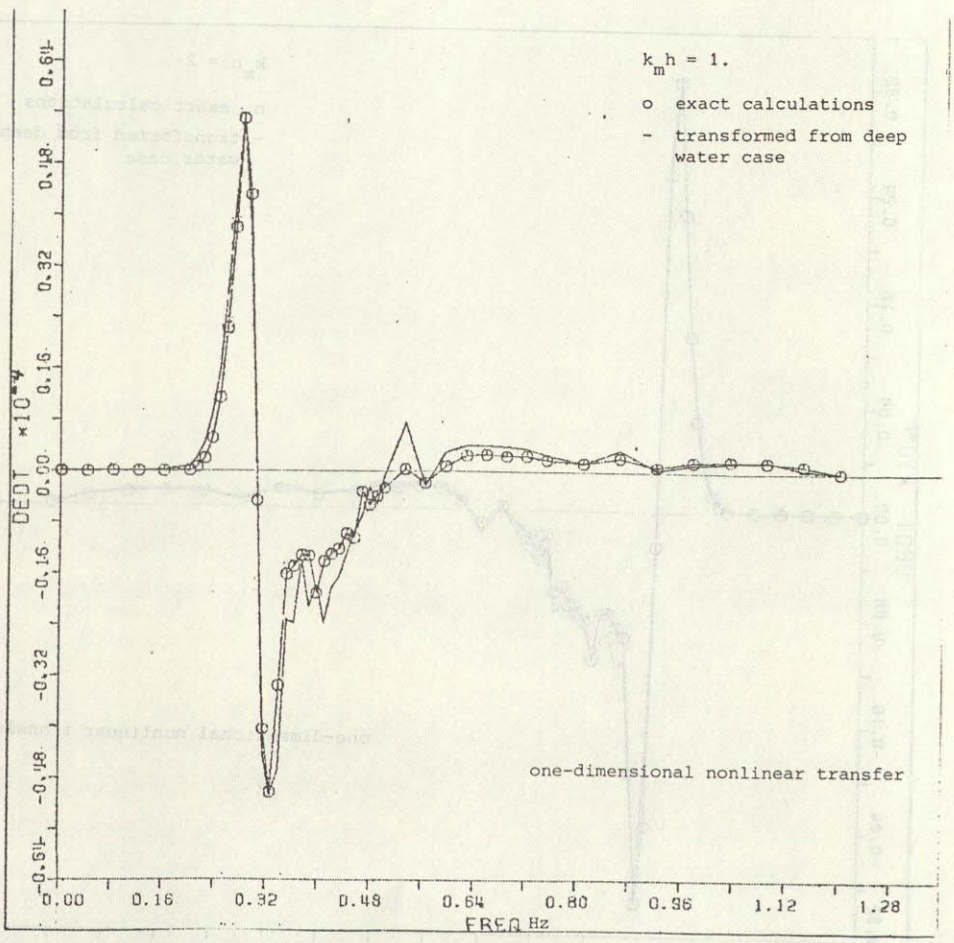
$k_m h$ = 1.
o exact calculations
- transformed from deep water case
one-dimensional nonlinear transfer
DEDT *10**4
0.64
0.48
0.32
0.16
0.00
-0.16
-0.32
-0.48
-0.64
0.00
0.16
0.32
0.48
0.64
0.80
0.96
1.12
1.28
FREQ Hz

Fig. 5d

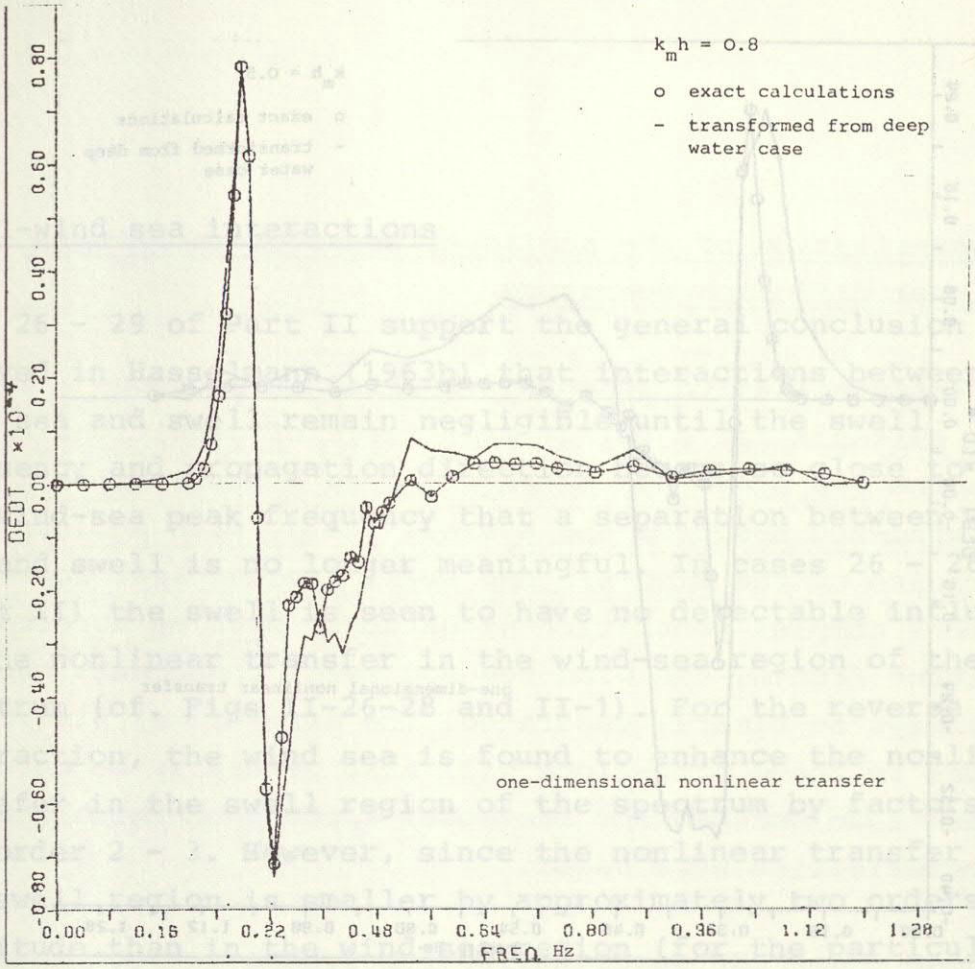
$k_m h$ = 0.8
o exact calculations
- transformed from deep water case
one-dimensional nonlinear transfer
DEDT ×10⁻⁴
0.80
0.60
0.40
0.20
0.00
-0.20
-0.40
-0.60
-0.80
0.00
0.16
0.32
0.48
0.64
0.80
0.96
1.12
1.28
FREQ Hz

Fig. 5e

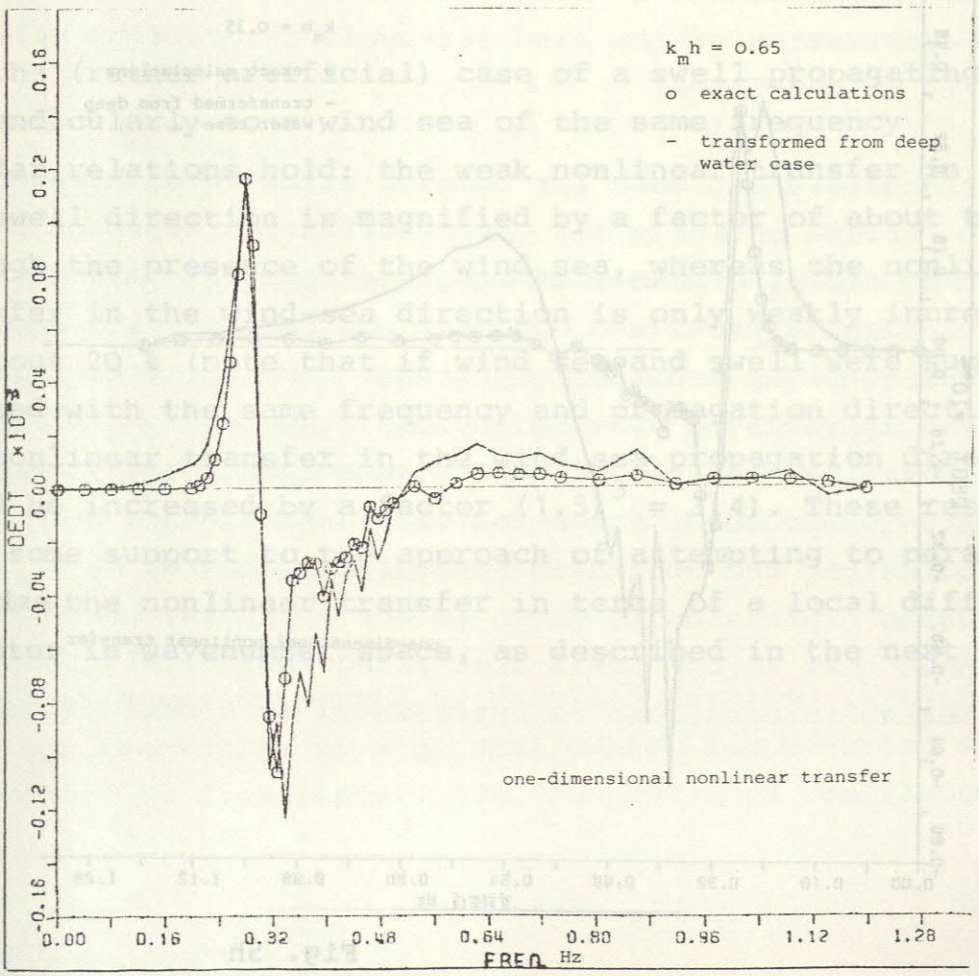
$k_m h$ = 0.65
o exact calculations
- transformed from deep water case
one-dimensional nonlinear transfer
DEDT ×10⁻³
0.16
0.12
0.08
0.04
0.00
-0.04
-0.08
-0.12
-0.16
0.00
0.16
0.32
0.48
0.64
0.80
0.96
1.12
1.28
FREQ Hz

Fig. 5f

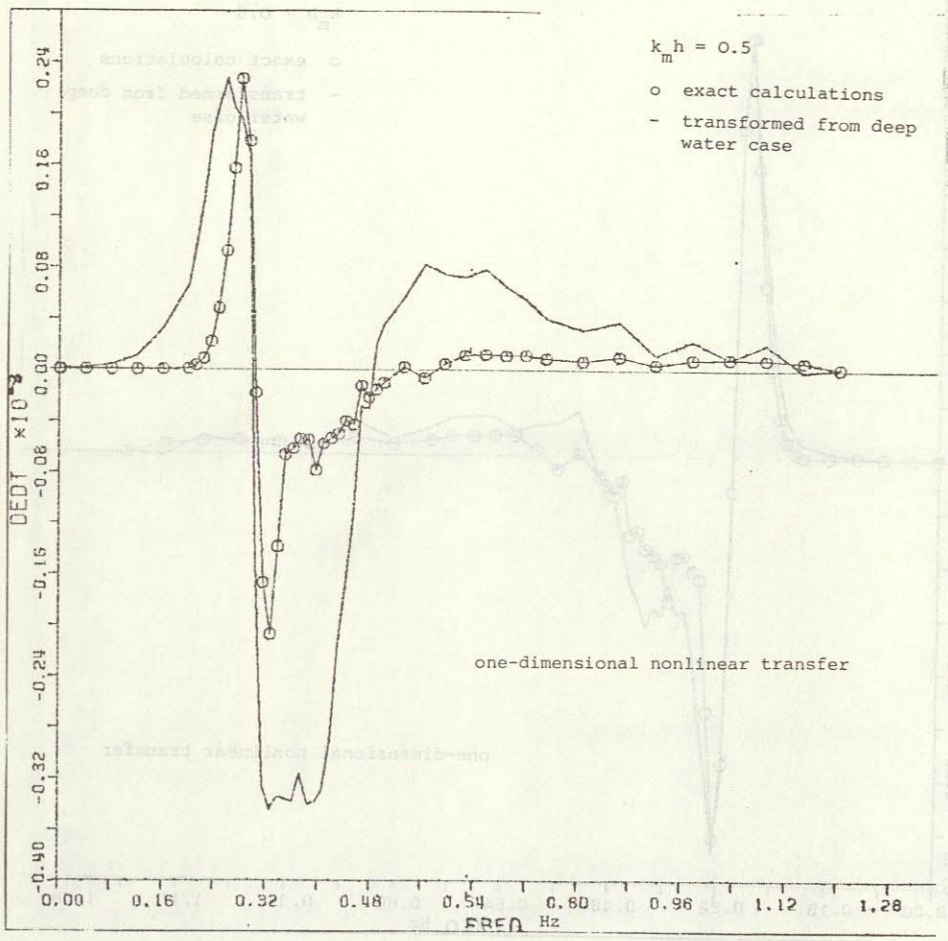
$k_m h$ = 0.5
o exact calculations
- transformed from deep water case
one-dimensional nonlinear transfer
DEDT ×10⁻²
0.24
0.16
0.08
0.00
-0.08
-0.16
-0.24
-0.32
-0.40
0.00
0.16
0.32
0.48
0.54
0.80
0.96
1.12
1.28
FREQ Hz

Fig. 5g

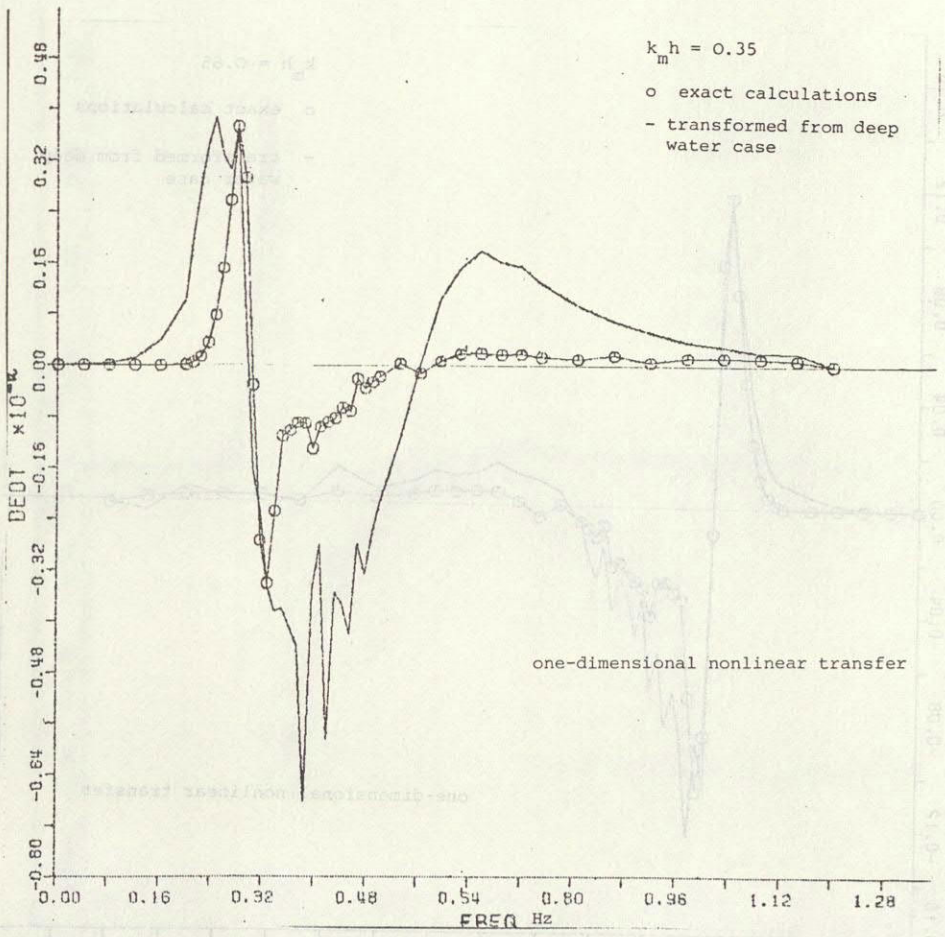
$k_m h$ = 0.35
o exact calculations
- transformed from deep water case
one-dimensional nonlinear transfer
DEDT ×10⁻²
0.48
0.32
0.16
0.00
-0.16
-0.32
-0.48
-0.64
-0.80
0.00
0.16
0.32
0.48
0.54
0.80
0.96
1.12
1.28
FREQ Hz

Fig. 5h

5) Swell-wind sea interactions

Figs 26 - 29 of Part II support the general conclusion derived in Hasselmann (1963b) that interactions between wind sea and swell remain negligible until the swell frequency and propagation direction become so close to the wind-sea peak frequency that a separation between wind sea and swell is no longer meaningful. In cases 26 - 28 (Part II) the swell is seen to have no detectable influence on the nonlinear transfer in the wind-sea region of the spectrum (cf. Figs II-26-28 and II-1). For the reverse interaction, the wind sea is found to enhance the nonlinear transfer in the swell region of the spectrum by factors of the order 2 - 3. However, since the nonlinear transfer in the swell region is smaller by approximately two orders of magnitude than in the wind-sea region (for the particular energy and frequency ratios chosen), this effect is insignificant (and cannot, of course, be detected in the figures).

For the (rather artificial) case of a swell propagating perpendicularly to a wind sea of the same frequency similar relations hold: the weak nonlinear transfer in the swell direction is magnified by a factor of about two through the presence of the wind sea, whereas the nonlinear transfer in the wind-sea direction is only weakly increased by about 20 % (note that if wind sea and swell were superimposed with the same frequency and propagation direction, the nonlinear transfer in the wind sea propagation direction would be increased by a factor $(1.5)^3 = 3.4$). These results give some support to the approach of attempting to parameterize the nonlinear transfer in terms of a local diffusion operator in wavenumber space, as described in the next section.

6) Parameterization of the nonlinear transfer in terms of nonlinear diffusion operators

The parameterization schemes described in sections 2 and 3 are suitable for a fairly wide range of conditions in which the sea state can be regarded as a superposition of a wind-sea spectrum and a swell field, with a clear separation of the wind-sea and swell frequencies. However, for more complex generation situations, such as hurricanes or strong fronts, the wind-sea and swell components can not always be clearly separated. The directional distributions in these situations will also generally be more complex than assumed for the model spectra on which the parameterization were based.

In these cases the parameterization schemes of sections 2 or 3 will need to be generalized. More directional parameters in the wind-sea model will be required and a parameterization of the wind sea-swell interaction will need to be developed.

An alternative approach for complex situations, however, is to replace entirely the parameterization approach in terms of a finite number of discrete spectral parameters by a general approximate operator expression which can be applied to an arbitrary spectrum. Some motivation for such an approach is provided by the computed form of the nonlinear transfer itself, which resembles in many respects a diffusion process. A theoretical justification for approximating the Boltzmann scattering integral by a diffusion expression is given in the appendix, where it is shown that in the small scattering angle limit the scattering integral can be represented as a cubic, fourth

order diffusion operator in wavenumber space. Numerical experiments with various combinations of this fourth order diffusion operator (with suitable choice of the coefficients C_1, C_2, cf. eqn. A-27) were carried out. The experiments were later extended to include an arbitrary superimposed cubic second-order diffusion operator.*) The best fit to the exact integral expressions was obtained with a pure fourth order diffusion operator with $C_1 = 0.019$, $C_2 = 0$, i.e. (cf. eqn. A-26)

$$\left(\frac{dn}{dt}\right)_{nl} = 0.019 \cdot g^{3} \left\{ \left[\nabla^2 + \frac{\partial^2}{\partial k_i \partial k_j} \frac{k_i k_j}{k^2} \right] k^{\frac{27}{2}} \left[n^2 \nabla n^2 - 2n(\nabla n)^2 + \right. \right. \tag{6.1}$$

$$\left. \left. \frac{k_m k_\ell}{k^2} \left(n^2 \frac{\partial^2 n}{\partial k_m \partial k_\ell} - 2n \frac{\partial n}{\partial k_m} \frac{\partial n}{\partial k_\ell} \right) \right] \right\}$$

where $\nabla^2 = \frac{\partial^2}{\partial k_i \partial k_j}$ and $n = F(\underline{k})/\omega$ denote the action (particle) density.

The optimal choice of coefficients depends on the wavenumber (frequency and direction) resolution. The expression (6.1) represents the best fit for a logarithmic frequency discretization with $\Delta f/f = 0.1$ and an angular resolution $\Delta\Theta = 30^{\circ}$. First and second derivatives were obtained in the standard manner using linear combinations of the spectral

---

*) This work was supported by parallel detailed investigations of the properties of a general cubic, second-order diffusion operator by J. Allender, 1980 (unpublished memorandum).

values at three neighbouring points. Higher derivatives were evaluated by successive application of the discretised first and second order derivatives, in accordance with the formal structure of eqn (6.1).

For a higher wavenumber resolution, the differential operators had to be smoothed to obtain a good simulation of the exact expression. This is not unreasonable, since the diffusion expression represents the local interaction limit of a process which is in reality distributed over a finite wavenumber region.

A comparison of the diffusion operator expression (6.1) with the exact integrations is shown in Figs 6 - 8. The coefficients were tuned to give the best fit for a wind-sea type spectrum with $\gamma = 3.3$. Considerable errors are seen to occur in the fit to the nonlinear transfer for a fully developed Pierson-Moskowitz spectrum at $\gamma = 1$, particular in the negative lobe, but this was considered to be less serious, since the nonlinear transfer is reduced by a factor of 10 in this case (see also γ-dependence of transfer rate in Fig. 2b).

The good agreement for both the mean JONSWAP spectrum and the 180^{o}-skewed spectrum of Fig. 7 is encouraging and suggests that the diffusion operator may be applied generally for wind seas with complicated directional distributions. The diffusion operator achieves a computational saving of approximately two orders of magnitude compared with the exact integration (under optimal integration conditions using a pre-filtered integration grid).

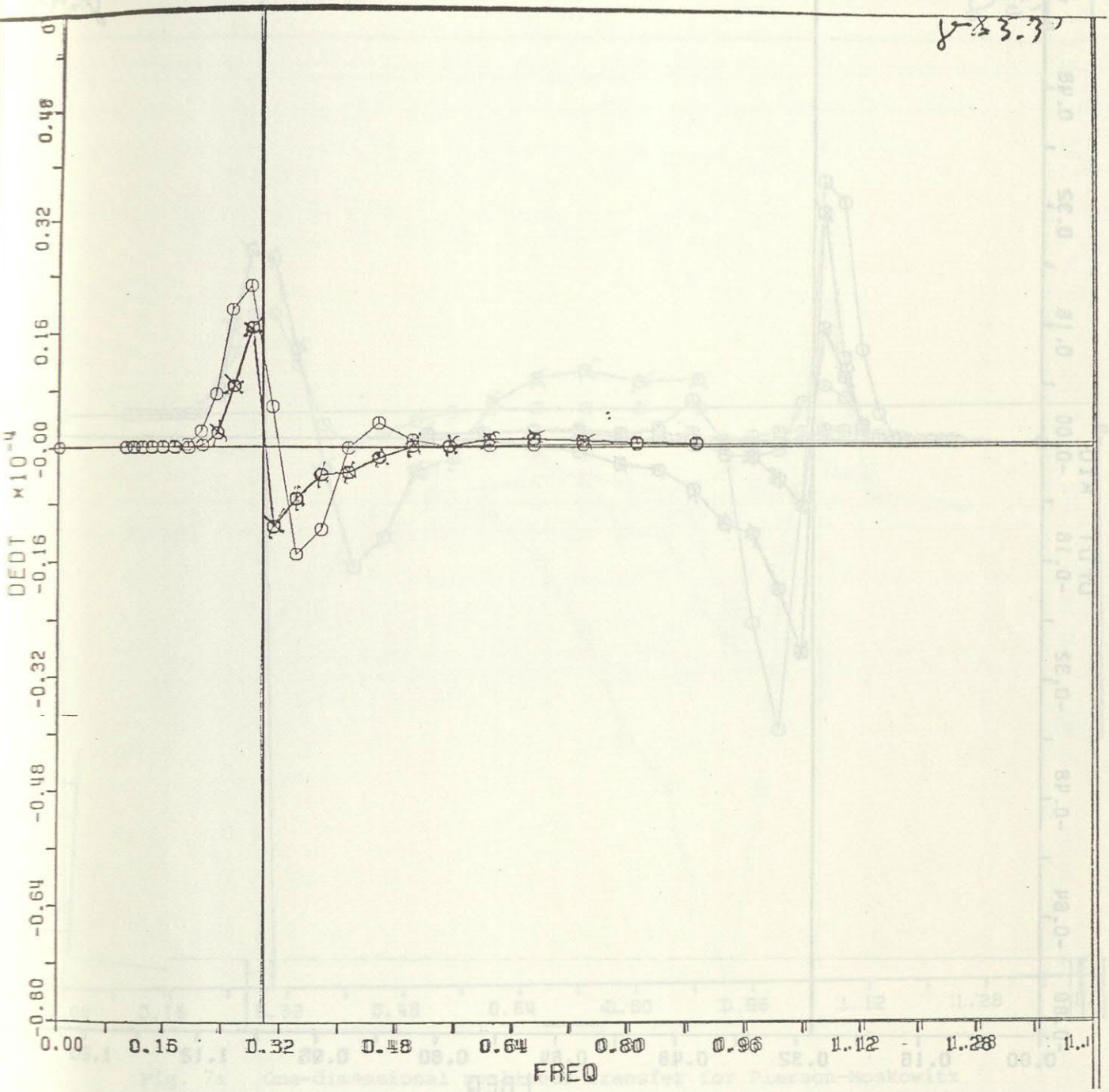

Fig. 6a One-dimensional nonlinear transfer for JONSWAP reference spectrum (Part II, case 1, Fig. 1a) computed using the fourth order diffusion operator, eqn (5.1) (- o -) and by full numerical integration (- x -).

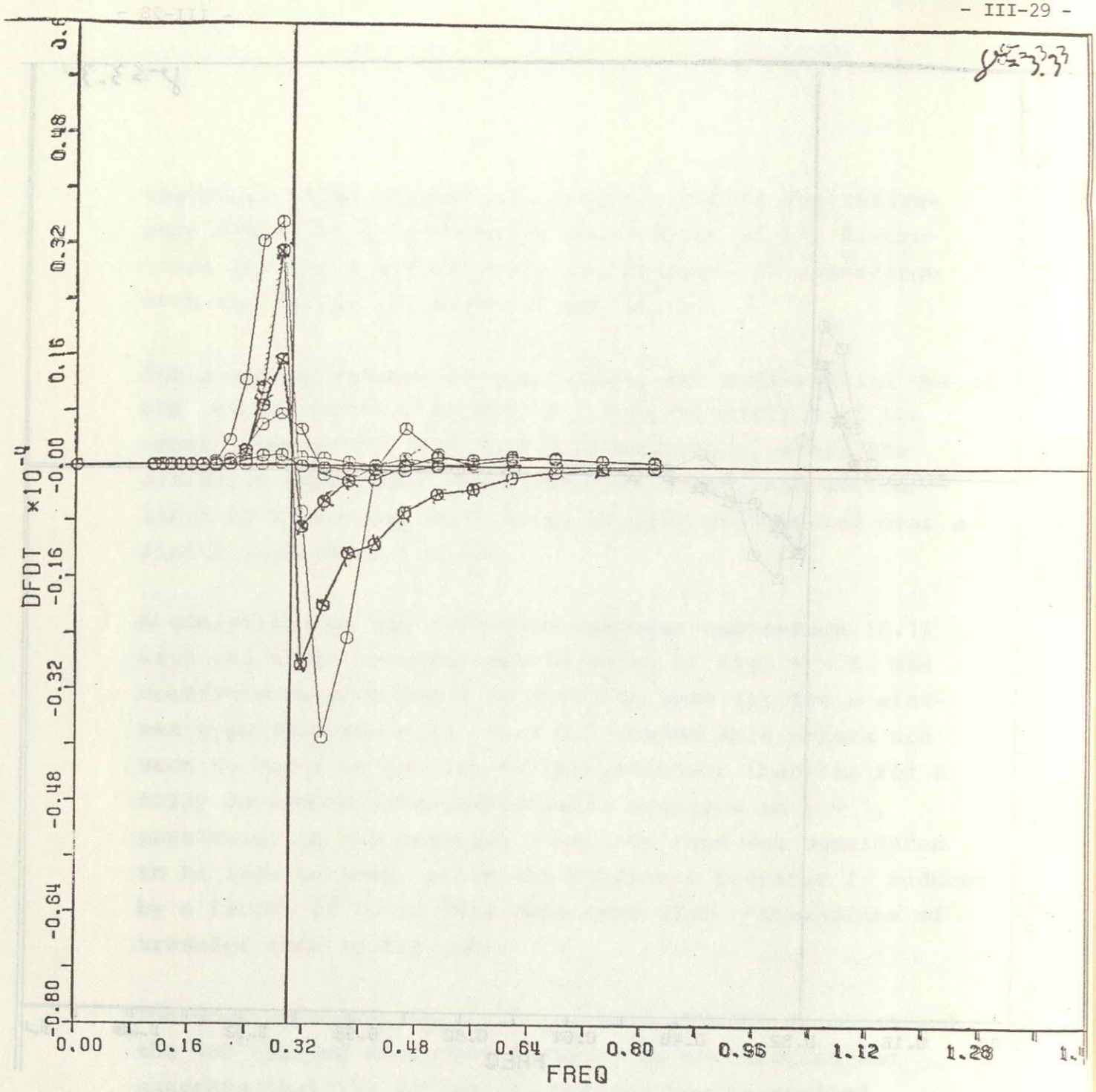

Fig. 6b Two-dimensional nonlinear transfer rates for same case as Fig. 6a, angles $\theta = 0^{\circ}$, 30°, 60°

(- o -) diffusion operator

(- x -) full integration

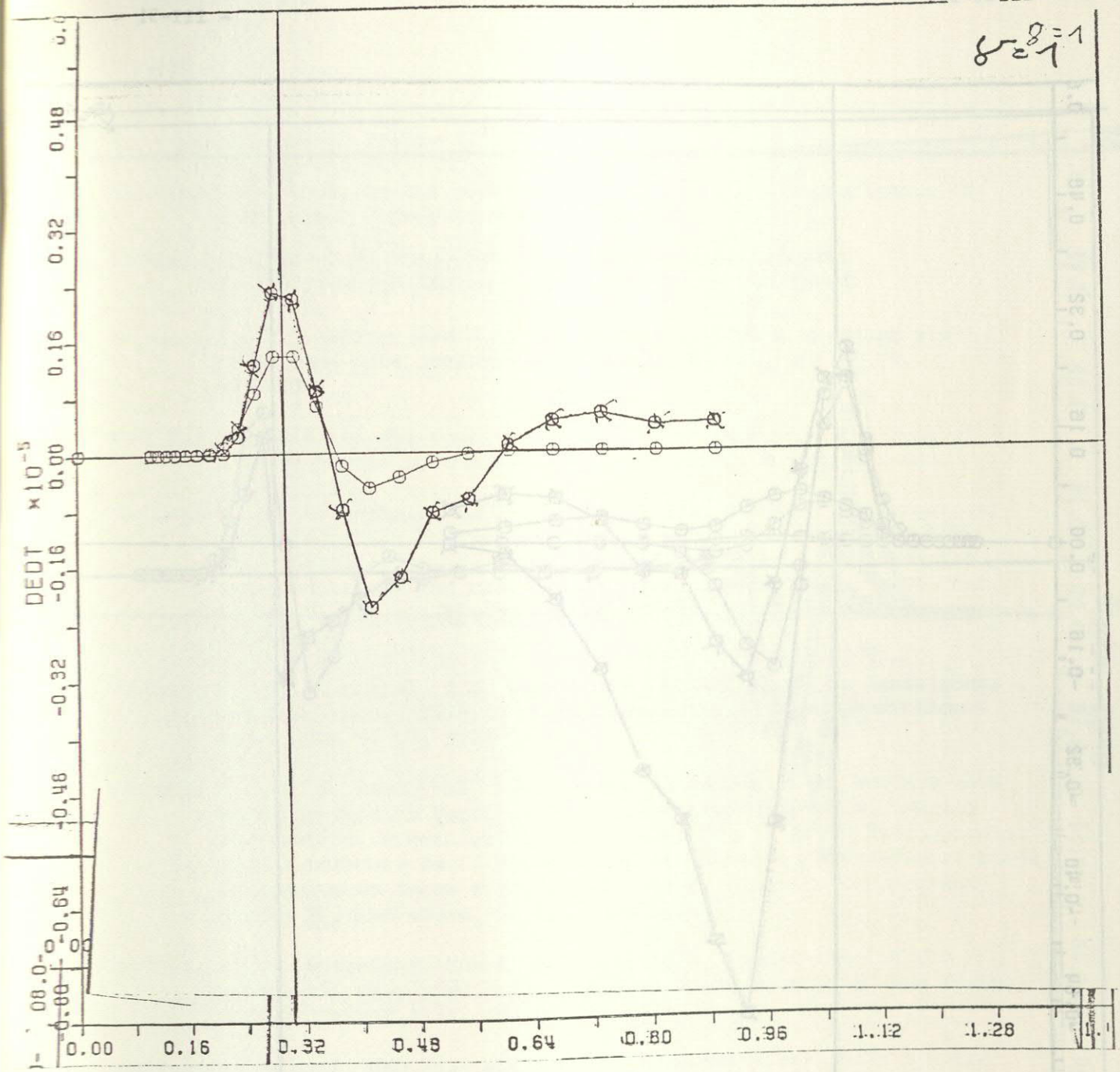

Fig. 7a One-dimensional nonlinear transfer for Pierson-Moskowitz spectrum (Part II, case 13, Fig. 13a) computed using the fourth order diffusion operator, eqn (5.1) (- o -) and by full numerical integration (- x -).

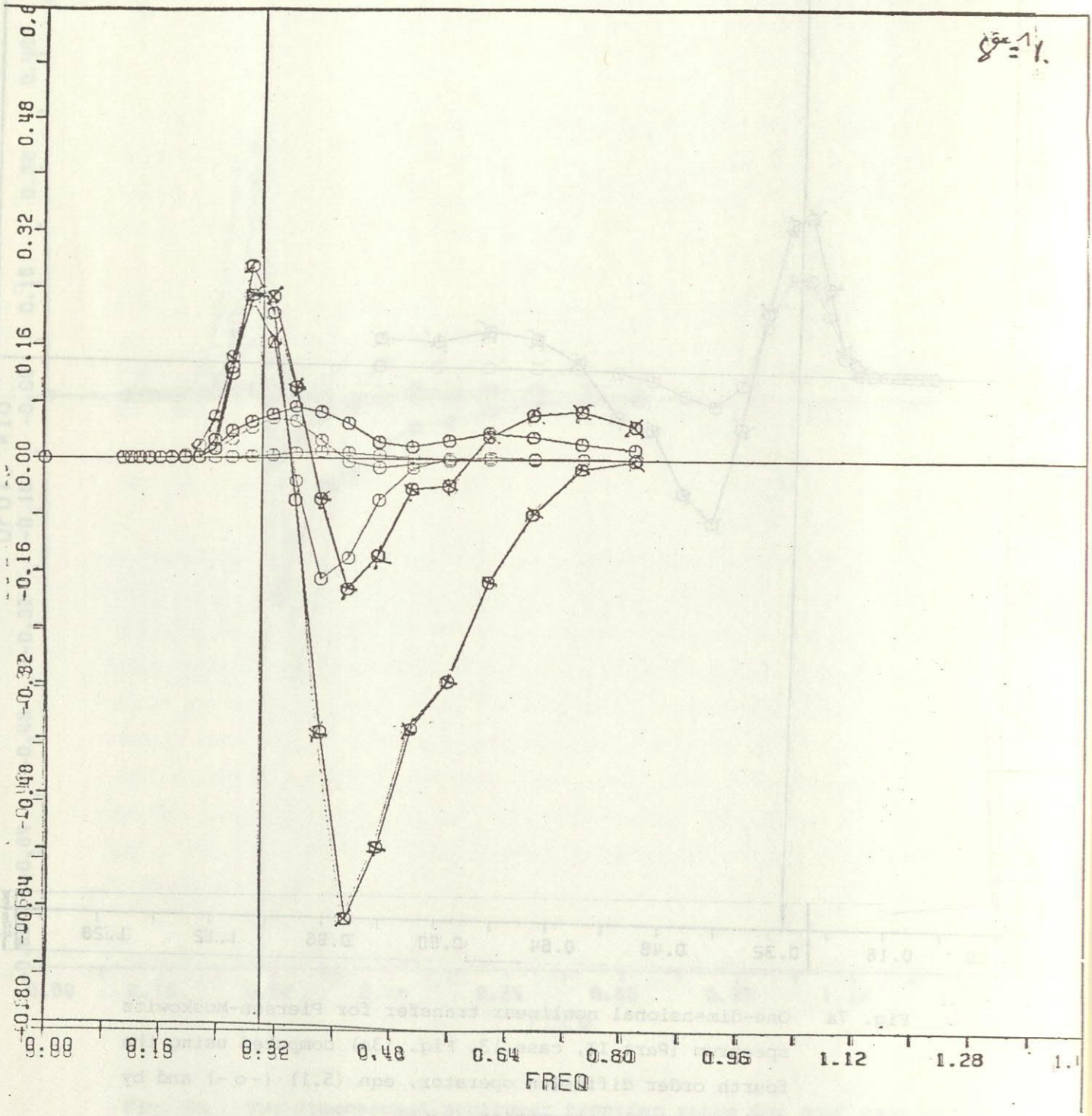

Fig. 7b Two-dimensional nonlinear transfer rates for same case as Fig. 7a, angles $\theta = 0^{\circ}, 30^{\circ}, 60^{\circ}$

(- o -) diffusion operator

(- x -) full integration

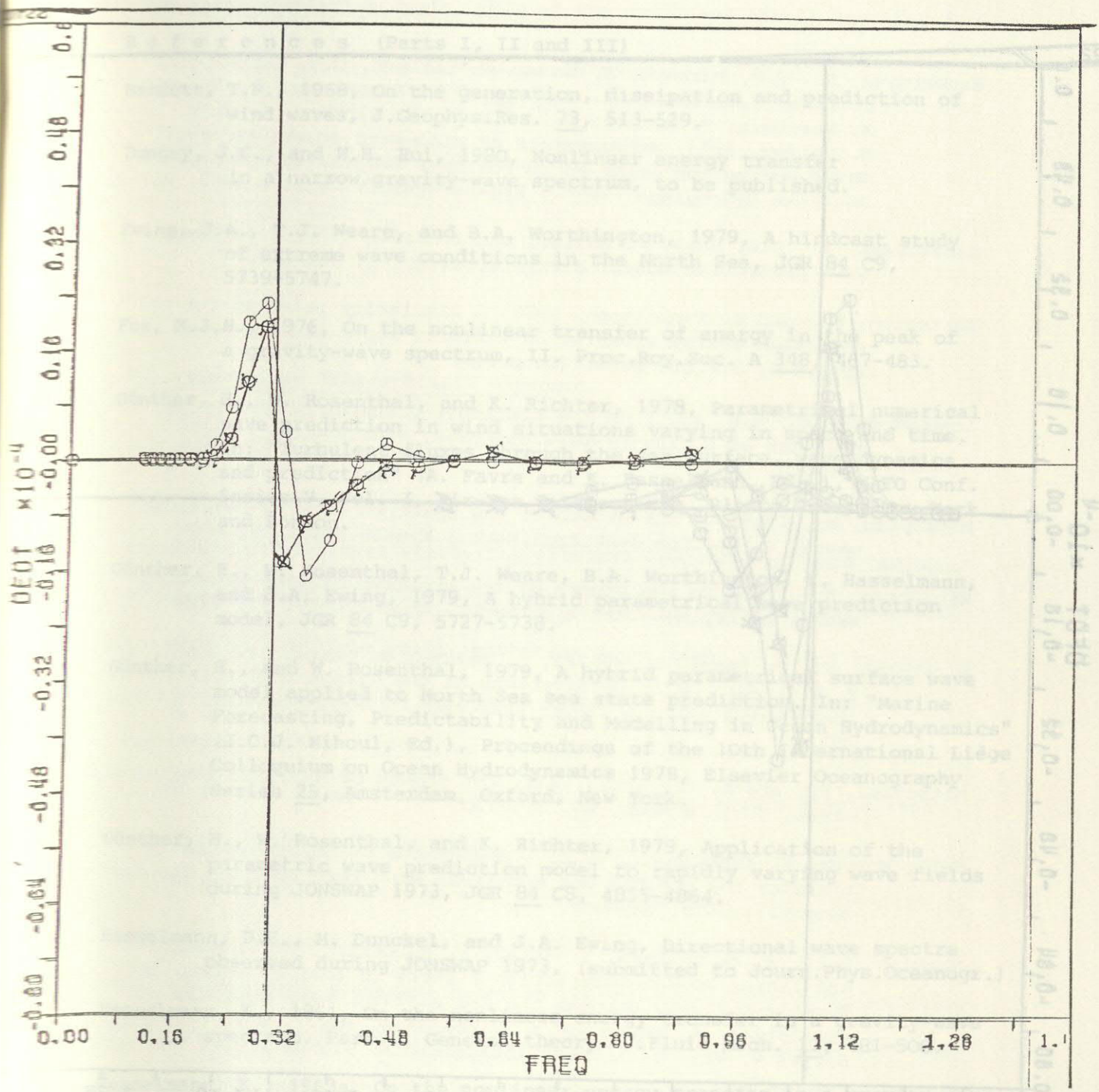

Fig. 8a One-dimensional nonlinear transfer for a JONSWAP spectrum with skewed directional distribution (Part II, case 25, Figs 25a, b) computed using the fourth order diffusion operator, eqn (5.1) (- o -) and by full numerical integration (- x -).

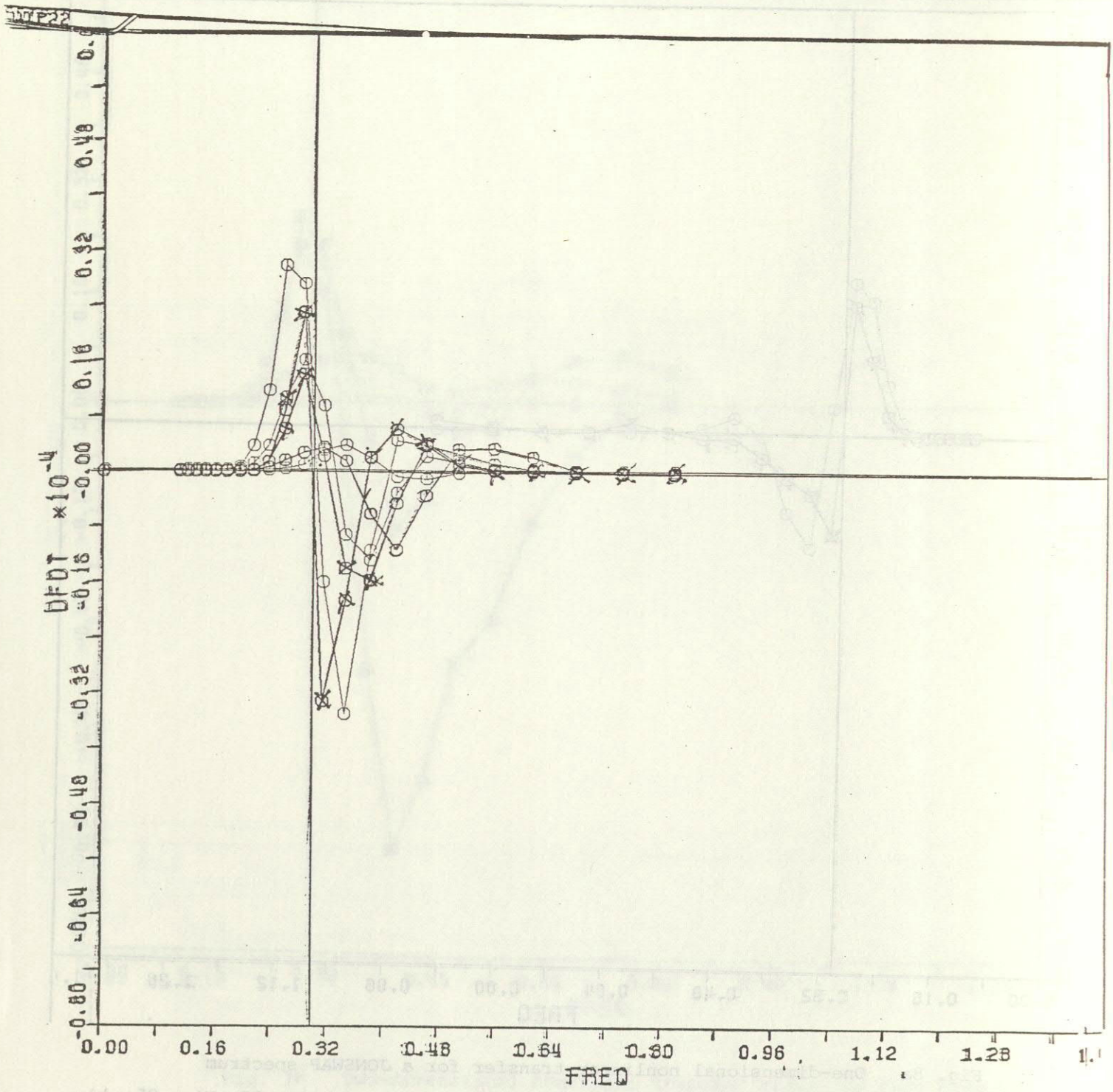

Fig. 8b Two-dimensional nonlinear transfer rates for same case as Fig. 8a, angles $\Theta = 0^{\circ}, 30^{\circ}, 60^{\circ}$

(- o -) diffusion operator

(- x -) full integration

R e f e r e n c e s (Parts I, II and III)

Barnett, T.P., 1968, On the generation, dissipation and prediction of wind waves, J.Geophys.Res. 73, 513-529.

Dungey, J.C., and W.H. Hui, 1980, Nonlinear energy transfer in a narrow gravity-wave spectrum, to be published.

Ewing, J.A., T.J. Weare, and B.A. Worthington, 1979, A hindcast study of extreme wave conditions in the North Sea, JGR 84 C9, 5739-5747.

Fox, M.J.H., 1976, On the nonlinear transfer of energy in the peak of a gravity-wave spectrum, II. Proc.Roy.Soc. A 348, 467-483.

Günther, H., W. Rosenthal, and K. Richter, 1978, Parametrical numerical wave prediction in wind situations varying in space and time. In: "Turbulent fluxes through the sea surface, wave dynamics and prediction" (A. Favre and K. Hasselmann, Eds.), NATO Conf. Series V, Vol. I, Air-Sea Interactions. Plenum Press. New York and London.

Günther, H., W. Rosenthal, T.J. Weare, B.A. Worthington, K. Hasselmann, and J.A. Ewing, 1979, A hybrid parametrical wave prediction model, JGR 84 C9, 5727-5738.

Günther, H., and W. Rosenthal, 1979, A hybrid parametrical surface wave model applied to North Sea sea state prediction. In: "Marine Forecasting, Predictability and Modelling in Ocean Hydrodynamics" (J.C.J. Nihoul, Ed.), Proceedings of the 10th International Liège Colloquium on Ocean Hydrodynamics 1978, Elsevier Oceanography Series 25, Amsterdam, Oxford, New York.

Günther, H., W. Rosenthal, and K. Richter, 1979, Application of the parametric wave prediction model to rapidly varying wave fields during JONSWAP 1973, JGR 84 C8, 4855-4864.

Hasselmann, D.E., M. Dunckel, and J.A. Ewing, Directional wave spectra observed during JONSWAP 1973, (submitted to Journ.Phys.Oceanogr.)

Hasselmann, K., 1961, On the nonlinear energy transfer in a gravity-wave spectrum. Part 1. General theory. J.Fluid Mech. 12, 481-500.

Hasselmann, K., 1963a, On the nonlinear energy transfer in a gravity-wave spectrum, Part 2. Conservation theorems; wave-particle analogy; irreversibility. J.Fluid Mech. 15, 273-281.

Hasselmann, K., 1963b, On the nonlinear energy transfer in a gravity-wave spectrum, Part 3. Evaluation of the energy flux and swell-sea interaction for a Neumann spectrum. J.Fluid Mech. 15, 385-398.

Hasselmann, K., 1966, Feynman diagrams and interaction rules of wave-wave scattering processes. Rev. Geophys. 4, 1-32.

Hasselmann, K., 1968, Weak-interaction theory of ocean waves, basic developments in fluid dynamics (M. Holt, Ed.) New York 2, 117-182.

Hasselmann, K., T.P. Barnett, E. Bouws, H. Carlson, D.E. Cartwright, K. Enke, J.A. Ewing, H. Gienapp, D.E. Hasselmann, P. Kruseman, A. Meerburg, P. Müller, D.J. Olbers, K. Richter, W. Sell, H. Walden, 1973, Measurements of wind-wave growth and swell decay during the Joint North Sea Wave Project (JONSWAP), Deutsche Hydrograph. Zeit., Ergänzungsheft Reihe A (8^{o}), Nr. 12.

Hasselmann, K., D.B. Ross, P. Müller, and W. Sell, 1976, A parametric wave prediction model, J.Phys.Oceanogr. 6, 200-228.

Herterich, K., and K. Hasselmann, 1980, A similarity relation for the nonlinear energy transfer in a finite-depth gravity-wave spectrum, J.Fluid Mech. (in press)

Longuet-Higgins, M.S. 197 , On the nonlinear transfer of energy in the peak of a gravity-wave spectrum, Proc.Roy.Soc. A347, 311-328.

Mitsuyasu, H., 1968, On the growth of the spectrum of wind-generated waves. 1. Rep.Res.Inst.Appl.Mech., Kyushu Univ. 16, 459-

Mitsuyasu, H., 1969, On the growth of the spectrum of wind-generated waves. 2. Rep.Res.Inst.Appl.Mech., Kyushu Univ. 17, 235-

Mitsuyasu, H., F. Tasai, T. Suhara, S. Mizuno, M. Ohkuso, T. Honda, and K. Rikiishi, 1975, Observations of the directional spectrum of ocean waves using a clover leaf buoy, J.Phys.Oceanogr. 5, 750-760.

Mitsuyasu, H., and K. Rikiishi, 1978, The growth of duration limited wind waves, J.Fluid Mech. 85, 705-730.

Sell, W., and K. Hasselmann, 1972, Computations of nonlinear energy transfer for JONSWAP and empirical wind-wave spectra, Rep.Inst. Geophys., Univ. Hamburg.

Shemdin, O.H., K. Hasselmann, V. Hsiao, K. Herterich, 1978, Nonlinear and linear bottom interaction effects in shallow water. In: Turbulent fluxes through the sea surface, wave dynamics and prediction (A. Favre and K. Hasselmann, Eds.), NATO Conference Series V, Vol. I, Air-Sea Interactions. Plenum Press, New York and London.

Webb, D.J., 1978, Nonlinear transfer between sea waves, Deep-Sea Res. 25, 279-298.

Appendix

The small scattering angle limit of the nonlinear energy transfer in a gravity-wave spectrum

1. The generalised Fokker-Planck approach

For small scattering angles the general Boltzman scattering integral for wave-wave interactions reduces to a local differential expression. For linear scattering problems (second-order scattering of incident wave components off another, given disturbance field into a scattered wave) the small scattering angle limit is given by the well-known Fokker-Planck diffusion equation. The corresponding expression for higher order scattering of a field with itself, as in the present case, is more complicated. One obtains a generalised nonlinear, higher-order diffusion expression.

Inspection of exact calculations of the nonlinear energy transfer in a gravity wave spectrum, based on the complete Boltzman integral, shows that the redistribution of energy is rather similar to what may be expected, qualitatively, for a local, diffusive process in wavenumber space: very little energy is transferred into regions in wavenumber space which are far removed from the energy containing regions of the spectrum (weak upwind scattering, small transfer to very low frequencies), and the energy transfer from a pronounced peak is strongest in the immediately adjacent side lobes. It thus appears meaningful to investigate whether the small angle scattering limit is an acceptable approximation

to the exact Boltzman integral expression. If this were the case, it would clearly be of immense value for numerical wave prediction, as a local differential expression in wavenumber space, even if nonlinear and of higher differential order, could probably be incorporated in a routine spectral prediction model, whereas this is out of the question for the exact expression.

It should be noted that the small scattering angle limit is in a sense the complementary case to the narrow-peak approximation considered by Longuet-Higgins and Fox. In their approximation the energy of the spectrum (and thus the expression P in (1)), is assumed to be strongly concentrated in a small region of the wavenumber space near the peak wavenumber $\underline{k}_p$, and the net interaction coefficient a can then be expanded in the neighbourhood of $\underline{k}_p$ ($\underline{k}_1 \simeq \underline{k}_2 \simeq \underline{k}_3 \simeq \underline{k}_4 \simeq \underline{k}_p$). In the present approximation, it is assumed that a is highly concentrated in a subspace $\underline{k}_1 \simeq \underline{k}_2 \simeq \underline{k}_3 \simeq \underline{k}_4$ of the interaction space $\underline{k}_1 \times \underline{k}_2 \times \underline{k}_3 \times \underline{k}_4$ which characterises small angle scattering. In this case the product expression P can be expanded around a central wavenumber. Since the narrow-peak limit yields reasonable approximations under suitable conditions it is not immediately obvious that the small scattering angle limit will also yield an acceptable approximation. However, in addition to the general qualitative features of the computed exact nonlinear transfer expression, the small scattering angle limit also finds some support from the form of the computed net interaction coefficient a, which is indeed found to have a strong peak near the wavenumber combination $\underline{k}_1 = \underline{k}_2 = \underline{k}_3 = \underline{k}_4$. The peak is fairly pronounced, as it arises through a maximum in the coupling coefficients occurring simultaneously with a stationary point in the frequency resonance δ-function (Hasselmann, 1963).

The appropriate expansion for the small scattering angle approximation depends strongly on the symmetry properties of the exact Boltzman integral expression. These are therefore briefly reviewed in the present context in the following section.

2. Symmetry properties

The Boltzman scattering integral for third-order gravity wave interactions is given by

$$\frac{dn_4}{dt} = \iiint a[n_1 n_2 (n_3 + n_4) - n_3 n_4 (n_1 + n_2)] d\underline{k}_1 d\underline{k}_2 d\underline{k}_3 \qquad (1)$$

where the action (number) density spectrum $n_j = n(\underline{k}_j) = F(\underline{k}_j)/\omega_j$, $F(\underline{k}_j)$ = surface displacement variance spectrum, and the net interaction coefficient contains two δ-function factors,

$$a(\underline{k}_1, \underline{k}_2, \underline{k}_3, \underline{k}_4) = a'(\underline{k}_1, \underline{k}_2, \underline{k}_3, \underline{k}_4)\, \delta(\underline{k}_1 + \underline{k}_2 - \underline{k}_3 - \underline{k}_4) \qquad (2)$$

$$= a''(\underline{k}_1, \underline{k}_2, \underline{k}_3, \underline{k}_4)\, \delta(\underline{k}_1 + \underline{k}_2 - \underline{k}_3 - \underline{k}_4)\, \delta(\omega_1 + \omega_2 - \omega_3 - \omega_4) \qquad (2')$$

For the following analysis we note the following symmetry properties: of the expressions appearing in (1) and (2):

a' : symmetrical with respect to all 4 wavenumbers $\underline{k}_j$. It should be noted that associated with each wavenumber $\underline{k}_j$ is a sign s_j, defined by the signs in the resonance conditions

$$\sum_{j=1}^{4} s_j \begin{Bmatrix} \underline{k}_j \\ \omega_j \end{Bmatrix} = 0 \qquad \begin{matrix} (3a) \\ (3b) \end{matrix}$$

When two wavenumbers $\underline{k}_a$ and $\underline{k}_b$ are interchanged in a', the

associated signs s_a and s_b must also be interchanged. The signs s_j are defined only to within a non-specified common sign s_c through the resonance conditions (3a), (3b). The expression a' is independent of s_c.

$\delta(\sum_{j=1}^{4} s_j k_j)$, $\delta(\sum_{j=1}^{4} s_j \omega_j)$: same full symmetry properties as a'.

$P = n_1 n_2 (n_3+n_4) - n_3 n_4 (n_1+n_2)$: symmetrical with respect to interchanges $\underline{k}_1 \leftrightarrow \underline{k}_2$; $k_3 \leftrightarrow k_4$;
antisymmetrical with respect to interchanges of the pair $(\underline{k}_1, \underline{k}_2) \leftrightarrow (\underline{k}_3, k_4)$.

If P is written in the alternative form

$$P = \sum_j \frac{n_1 n_2 n_3 n_4}{s_j n_j} \qquad (5)$$

it is in fact seen to be invariant with respect to any interchange of wavenumbers, provided the associated signs s_j are also interchanged. However, the signs must be defined in (5) such that originally $s_1 = s_2 = -1$, $s_3 = s_4 = +1$; thus the expression (5) is dependent on the common sign s_c and changes sign with a change in the sign s_c.

Thus in summary all factors in (1) are invariant with respect to interchange of any two of the four wavenumbers, provided the associated signs are also interchanged. In addition, all factors except P are invariant with respect to a change of the common sign s_c. However, P changes sign with s_c.

3. Expansion for small scattering angles

In the small scattering angle approximation it is assumed that significant contributions from the Boltzman scattering integral occur only when all four interacting wavenumbers are approximately equal. One could therefore consider expanding the scattering integral around the fixed resultant wavenumber $\underline{k}_4$. However, this expansion is inconvenient as it does not enable one to exploit the symmetry properties listed above. We introduce therefore instead the symmetrical variables

$$\begin{aligned} \hat{\underline{k}} &= \underline{k}_1 + \underline{k}_2 \;,\; \underline{k}' = \underline{k}_1 - \underline{k}_2 \\ \hat{\hat{\underline{k}}} &= \underline{k}_3 + \underline{k}_4 \;,\; \underline{k}'' = \underline{k}_3 - \underline{k}_4 \end{aligned} \tag{6}$$

with

$$\begin{aligned} \underline{k}_1 &= \frac{\hat{\underline{k}} + \underline{k}'}{2} \;,\; \underline{k}_2 = \frac{\hat{\underline{k}} - \underline{k}'}{2} \\ \underline{k}_3 &= \frac{\hat{\hat{\underline{k}}} + \underline{k}''}{2} \;,\; \underline{k}_4 = \frac{\hat{\hat{\underline{k}}} - \underline{k}''}{2} \end{aligned} \tag{7}$$

In terms of these variables equation (1) may be written

$$\frac{d}{dt} n_4 = \frac{d}{dt} n(\underline{k}_4^o) = \int \delta(\underline{k}_4^o - \underline{k}_4) \frac{dn_4(\underline{k}_4)}{dt} d\underline{k}_4 = \iiiint \delta(\underline{k}_4^o - \underline{k}_4)$$

$$a \cdot P \cdot d\underline{k}_1 d\underline{k}_2 d\underline{k}_3 d\underline{k}_4 \tag{8}$$

$$= \iiiint \delta(\underline{k}_4^o - (\frac{\hat{\hat{\underline{k}}} - \underline{k}''}{2})) a \cdot P \cdot (2)^{-8} \, d\hat{\underline{k}} d\hat{\hat{\underline{k}}} d\underline{k}' d\underline{k}''$$

Making use of the δ-function factor $\delta(\underline{k}_1+\underline{k}_2-\underline{k}_3-\underline{k}_4) = \delta(\hat{\underline{k}}-\hat{\underline{\hat{k}}})$ in a, we may write (8) (changing $\underline{k}_4^o$ back to $\underline{k}_4$ again) as

$$\frac{d}{dt}n_4 = \iiint \delta(\underline{k}_4 - (\frac{\hat{\underline{k}} - \underline{k}''}{2}))\cdot a'\cdot P\cdot 2^{-8} d\hat{\underline{k}}d\underline{k}'d\underline{k}'' \qquad (9)$$

where, because of the symmetries listed in section 2, $a' = a'(\hat{\underline{k}},\underline{k}',\underline{k}'')$ is an even function of $\underline{k}'$ and $\underline{k}''$ which is furthermore symmetrical with respect to an interchange of $\underline{k}'$ and $\underline{k}''$.

The small scattering angle approximation assumes in addition that a' has a δ-function-type behaviour with respect to the variables $\underline{k}'$ and $\underline{k}''$ (but not $\hat{\underline{k}}$). The expression P may thus be expanded with respect to these wavenumbers. Writing

$$\left\{\begin{matrix} n(\underline{k}_1) \\ n(\underline{k}_2) \end{matrix}\right\} = n(\hat{\underline{k}}/2) \pm \frac{\partial n}{\partial k_i}(\hat{\underline{k}}/2)\cdot\frac{k_i'}{2} + \frac{1}{2}\frac{\partial^2 n}{\partial k_i \partial k_j}(\hat{\underline{k}}/2)\cdot\frac{k_i'k_j'}{4} + \ldots.$$

$$\left\{\begin{matrix} n(\underline{k}_3) \\ n(\underline{k}_4) \end{matrix}\right\} = n(\hat{\underline{k}}/2) \pm \frac{\partial n}{\partial k_i}(\hat{\underline{k}}/2)\cdot\frac{k_i''}{2} + \frac{1}{2}\frac{\partial n(\hat{\underline{k}}/2)}{\partial k_i \partial k_j}\frac{k_i''k_j''}{4}$$

one obtains

$$P = \left[\frac{n^2}{4}\frac{\partial^2 n}{\partial k_i \partial k_j} - \frac{n}{2}\frac{\partial n}{\partial k_i}\frac{\partial n}{\partial k_j}\right]\left[k_i'k_j' - k_i''k_j''\right] = P(\underline{k}_4;\underline{k}',\underline{k}'') \qquad (10)$$

As next step one must now expand the δ-function term. Integrating equation (9) with respect to $\hat{\underline{k}}$ we obtain

$$\frac{d}{dt}n_4 = 2^{-6}\iint\left[a'P\right]_{\hat{\underline{k}}=2\underline{k}_4+\underline{k}''} d\underline{k}'d\underline{k}'' \qquad (11)$$

Expanding [a'P] = function $(\hat{\underline{k}};\underline{k}',\underline{k}'')$ with respect to $\hat{k}$ about $\hat{\underline{k}} = 2\underline{k}_4$ we may write

$$[a'p]_{\hat{k}=2\underline{k}_4+\underline{k}''} = [a'P]_{\hat{k}=2\underline{k}_4} + \frac{\partial(a'P)}{\partial\hat{k}_i} k_i'' + \frac{1}{2}\frac{\partial^2(a'P)}{\partial\hat{k}_i\partial\hat{k}_j} k_i'' k_j'' \qquad (12)$$

Substituting (10) and (12) into (11) and noting again that a' has a δ-function type character with respect to the variables $\underline{k}'$, $\underline{k}''$ (but not $\hat{\underline{k}}$) and is symmetrical and even in $\underline{k}'$ and $\underline{k}''$, we obtain

$$\boxed{\frac{d}{dt} n_4 = \frac{\partial^2}{\partial k_i \partial k_j} (D_{ij\ell m}[n^2 \frac{\partial^2 n}{\partial k_\ell \partial k_m} - 2n \frac{\partial n}{\partial k_\ell}\frac{\partial n}{\partial k_m}])} \qquad (13)$$

where

$$\boxed{D_{ij\ell m} = 2^{-9} \iint a'(k_\ell' k_m' - k_\ell'' k_m'') k_i'' k_j'' \, d\underline{k}' d\underline{k}''} \quad \text{or} \qquad (14)$$

$$\boxed{D_{ij\ell m} = -2^{-10} \iint a'(k_\ell' k_m' - k_\ell'' k_m'')(k_i' k_j' - k_i'' k_j'') d\underline{k}' d\underline{k}''} \qquad (14')$$

4. Reduction of the diffusion tensor to scalar functions

Of the $2^4 = 16$ component functions contained in the tensor $D_{ijk\ell}(\underline{k})$, only a small number are actually independent, as the tensor is invariant with respect to interchange of the index components i,j and k,ℓ and to interchange of the pairs (i,j), (k,ℓ) and is furthermore isotropic. Application of the usual symmetry theory then yields a tensor which contains 4 apparently independent functions $D_j = D_j(k)$ of the modulus of the wavenumber:

$$D_{ijk\ell} = D_1\delta_{ij}\delta_{k\ell} + \frac{D_2}{2}(\delta_{ik}\delta_{j\ell} + \delta_{jk}\delta_{i\ell}) + D_3\left(\delta_{ij}\frac{k_k k_\ell}{k^2} + \delta_{k\ell}\frac{k_i k_j}{k^2}\right) +$$

$$D_4\frac{k_i k_j k_k k_\ell}{k^4} + \frac{D_5}{4k^2}[\delta_{ik}k_j k_\ell + \delta_{j\ell}k_i k_j + \delta_{i\ell}k_j k_k + \delta_{jk}k_i k_\ell] \qquad (15)$$

$$\equiv \sum_{i=1}^{5} D_i E_i$$

Alternatively, the symmetry properties may be exploited by choosing the coordinate system such that the k_1 axis lies parallel to $\underline{k}$ and the k_2 axis orthogonal to $\underline{k}$. One obtains then only 4 independent non vanishing components, namely D_{1111}, D_{2222}, $D_{1122} = D_{2211}$ and D_{1212} $(= D_{2121} = D_{1221} = D_{2112})$. The apparent discrepancy between this result and (15) is removed by noting that the expressions E_i in (15) are not in fact all independent for vectors in a plane. The relations between the two representations are given by

$$D_{1111} = \sum_{j=1}^{6} D_j$$

$$D_{1122} = D_1 + D_3$$

$$D_{2222} = D_1 + D_2$$

$$D_{1212} = \frac{D_2}{2} + \frac{D_6}{4}$$

From these equations one deduces that the E_j satisfy the identity

$$E_1 - E_2 - 2E_3 + 2E_5 = 0 \tag{16}$$

Thus we may drop, for example, the last term $D_5 E_5$ in (15).

Substituting (15) into (13) we obtain then

$$\frac{dn}{dt} = \left[\nabla^2 D_1 + \frac{\partial^2}{\partial k_i \partial k_j} \cdot \frac{k_i k_j}{k^2} D_3\right]\left[n^2 \nabla^2 n - 2n(\nabla n)^2\right]$$

$$+ \frac{\partial^2}{\partial k_i \partial k_j}\left(D_2\left[n^2 \frac{\partial^2 n}{\partial k_i \partial k_j} - 2n \frac{\partial n}{\partial k_i}\frac{\partial n}{\partial k_j}\right]\right) \tag{17}$$

$$+ \left(\nabla^2 D_3 + \frac{\partial^2}{\partial k_i \partial k_j} D_4 \frac{k_i k_j}{k^2}\right)\left[\frac{k_k k_\ell}{k^2}\left(n^2 \frac{\partial^2 n}{\partial k_k \partial k_\ell} - 2n \frac{\partial^2 n}{\partial k_k \partial k_\ell}\right)\right]$$

where all differential operators refer to the wavenumber space and apply to all the following terms in an expression, including the terms in square parentheses.

A further reduction of (17) can be achieved by invoking the conservation of energy. We note first that (13) already conserves number density, $\int \frac{dn}{dt} = 0$, and momentum, $\int \underline{k} \frac{\partial n}{\partial t} d\underline{k} = 0$. This is to be expected, since the symmetry of a and the asymmetry of the spectral product P with respect to the interchange $(1, 2) \leftrightarrow (3, 4)$, which is responsible for the conservation of number density, and the occurrence of the wavenumber δ-function factor in a, which yields conservation of momentum, were both invoked explicitly in deriving (13). However, no inferences have yet been drawn from the occurrence of the frequency δ-function in a'.

The conservation of energy requires $\int \omega \frac{\partial n}{\partial t}\, d\underline{k} = 0$, which yields, on partial integration of (13),

$$\int \frac{\partial^2 \omega}{\partial k_i \partial k_j} D_{ijk\ell} \left[n^2 \frac{\partial^2 n}{\partial k_k \partial k_\ell} - 2n \frac{\partial n}{\partial k_k} \frac{\partial n}{\partial k_\ell} \right] d\underline{k} = 0 \qquad (18)$$

Returning now to the definition of $D_{ijk\ell}$ in (14'), replacing a' in this expression by the expression (2') containing the frequency δ-function explicitly, and expanding the argument of the δ-function about the point $\underline{k}_j = \frac{\hat{k}}{2}$ with respect to $\underline{k}'$, $\underline{k}''$, $\omega_1 + \omega_2 - \omega_3 - \omega_4 = \frac{1}{4} \frac{\partial^2 \omega}{\partial k_i \partial k_j} (k_i' k_j' - k_i'' k_j'')$, we may write the first two factors of the integrand in (18) as

$$\frac{\partial^2 \omega}{\partial k_i \partial k_j} D_{ijk\ell} = +2^{-12} \int \frac{\partial^2 \omega}{\partial k_i \partial k_j} (k_k' k_\ell' - k_k'' k_\ell'')(k_i'' k_j'' - k_i' k_j') \delta\left(\frac{\partial \omega}{\partial k_\alpha \partial k_\beta} (k_\alpha' k_\beta' - k_\alpha'' k_\beta'') \right) a''\, d\underline{k}'\, d\underline{k}''$$

Since the argument of the δ-function occurs also as a factor in the integrand, it follows that

$$\frac{\partial^2 \omega}{\partial k_i \partial k_j} D_{ijk\ell} = 0 \qquad (19)$$

Substituting (19) into (15) we obtain for the two cases $(k, \ell) = (1, 1)$ and $(k, \ell) = (2, 2)$ (in a coordinate system with the k_1 axis parallel to the vector $\underline{k}$) the two equations

$$\left(\frac{d^2 \omega}{dk^2} + \frac{1}{k} \frac{d\omega}{dk} \right) \left(D_1 + D_3 \right) + \frac{d^2 \omega}{dk^2} \left(D_2 + D_3 + D_4 \right) = 0 \qquad (20)$$

$$\left(\frac{d^2\omega}{dk^2} + \frac{1}{k}\frac{d\omega}{dk}\right) D_1 + \frac{1}{k}\frac{d\omega}{dk} D_2 + \frac{d^2\omega}{dk^2} D_3 = 0 \qquad (21)$$

(The other index combinations $(k, \ell) = (1, 2)$ or $(2, 1)$ vanish by symmetry.)

Subtracting (21) from (20) we may replace (20) by the equation

$$\left(\frac{d^2\omega}{dk^2} + \frac{1}{k}\frac{d\omega}{dk}\right) D_3 + \left(\frac{d^2\omega}{dk^2} - \frac{1}{k}\frac{d\omega}{dk}\right) D_2 + \frac{d^2\omega}{dk^2} D_4 = 0 \qquad (22)$$

Thus of the four functions $D_1, \ldots D_4$ finally only two are independent. For the following we choose these as the functions D_1 and D_2.

5. The deep water case

The equation (13) can be simplified considerably further in the deep water case since the dispersion relation and net interaction coefficient are homogeneous functions of $\underline{k}$. This implies that all coefficients D_j are simple power laws, $D_j = C_j k^p g^q$ where C_j is a dimensionless number. Dimensional analysis (which can be verified by comparison with the original Boltzman integral) then yields

$$D_j = C_j g^{3/2} \cdot k^{27/2} \qquad (23)$$

Substitution of (23) and the dispersion relation $\omega^2 = gk$ into (21) and (22) results in

$$C_1 + 2C_2 = C_3 \qquad (24)$$

and

$$C_3 - 3C_2 = C_4 \tag{25}$$

The small-angle scattering equation (17) reduces finally in this case to

$$\frac{dn}{dt} = \left(C_1\nabla^2 + (C_1 + 2C_2)\,\frac{\partial^2}{\partial k_i \partial k_j} \cdot \frac{k_i k_j}{k^2}\right)\left(g^{3/2} k^{27/2}\right)\left(n^2\nabla^2 n - 2n(\nabla n)^2\right)$$

$$+ \left(C_2\,\frac{\partial^2}{\partial k_i \partial k_j}\right) \cdot g^{3/2} k^{27/2} \cdot \left(n^2 \frac{\partial^2 n}{\partial k_i \partial k_j} - 2n\,\frac{\partial n}{\partial k_i}\,\frac{\partial n}{\partial k_j}\right) \tag{26}$$

$$+ \left((C_1+2C_2)\nabla^2 + (C_1-C_2)\frac{\partial^2}{\partial k_i \partial k_j}\,\frac{k_i k_j}{k^2}\right) g^{3/2} k^{27/2} \left[\frac{k_k k_\ell}{k^2}\left(n^2 \frac{\partial^2 n}{\partial k_k \partial k_\ell} - 2n\,\frac{\partial n}{\partial k_k}\,\frac{\partial n}{\partial k_\ell}\right)\right]$$

or, separated with respect to the two coefficients C_1, C_2:

$$\frac{dn}{dt} = C_1 \cdot \{(\nabla^2 + \frac{\partial^2}{\partial k_i \partial k_j}\,\frac{k_i k_j}{k^2})\,A + (\nabla^2 + \frac{\partial^2}{\partial k_i \partial k_j}\,\frac{k_i k_j}{k^2})\,D\} +$$

$$C_2 \cdot \{(2 \cdot \frac{\partial^2}{\partial k_i \partial k_j}\,\frac{k_i k_j}{k^2})\,A + \frac{\partial^2}{\partial k_i \partial k_j} B + (2\nabla^2 - \frac{\partial^2}{\partial k_i \partial k_j}\,\frac{k_i k_j}{k^2})\,D\} \tag{27}$$

where $A = g^{3/2} \cdot k^{27/2} \cdot (n^2\nabla^2 n - 2n(\nabla n)^2)$

$$B = g^{3/2} \cdot k^{27/2} \cdot (n^2\,\frac{\partial^2 n}{\partial k_i \partial k_j} - 2n\,\frac{\partial n}{\partial k_i}\,\frac{\partial n}{\partial k_j})$$

$$D = g^{3/2} \cdot k^{27/2} \cdot \left\{\frac{k_k k_\ell}{k^2}\,(n^2\frac{\partial^2 n}{\partial k_k \partial k_\ell} - 2n\frac{\partial n}{\partial k_k} \cdot \frac{\partial n}{\partial k_\ell})\right\}$$